KERNFORSCHUNGSZENTRUM

KARLSRUHE

September 1970

KFK 969
EANDC(E)-118"U"

Institut für Neutronenphysik und Reaktortechnik
Projekt Schneller Brüter

Evaluation of Fast Critical Experiments Using Recent Methods and Data

Compiled by
E. Kiefhaber, J.J. Schmidt

GESELLSCHAFT FÜR KERNFORSCHUNG M.B.H.
KARLSRUHE

KERNFORSCHUNGSZENTRUM KARLSRUHE

September 1970

KFK 969
EANDC(E)-118"U"

Institut für Neutronenphysik und Reaktortechnik

Projekt Schneller Brüter

Evaluation of Fast Critical Experiments Using Recent Methods and Data

compiled by

E. Kiefhaber and J.J. Schmidt

with contributions from

H. Bachmann, B. Hinkelmann, B. Krieg
I. Siep, E. Stein, D. Thiem, and K. Wagner

Gesellschaft für Kernforschung m.b.H., Karlsruhe

Abstract

In this work we study systematically the influence of changes in nuclear data on the calculated values for the criticality and other important parameters of critical assemblies. The analysis is done for a variety of assemblies which differ in geometry, material composition, and energy distribution of the normal and adjoint flux. The primary objective is:

(a) to detect deficiencies in nuclear data and calculational methods,
(b) to get first preliminary improvements and
(c) to get indications in which respect and in which way further long-range improvements should be carried on.

The long-range aim of this kind of investigations is to provide or establish satisfactory nuclear data and calculational methods which can reliably be applied to the calculation of fast critical assemblies and of large fast power reactors. In the present investigation the differences between calculated and measured results for the critical assemblies studied are not yet reduced to a satisfactory level. Therefore this study must be considered as one step in the desired direction but further investigations along the same line will be necessary.

Zusammenfassung

In dieser Arbeit wird systematisch der Einfluß von Änderungen in den nuklearen Daten auf berechnete Werte für die Kritikalität und andere wichtige Parameter kritischer Anordnungen untersucht. Eine Reihe von Anordnungen, die sich in ihrem geometrischen Aufbau und in ihrer Materialzusammensetzung und daher auch in der Energieverteilung des normalen und adjungierten Neutronenflusses erheblich unterscheiden, bildet die Basis der Untersuchungen. Das Hauptziel ist:

(a) Mängel in den nuklearen Daten und Berechnungsverfahren herauszufinden,

(b) erste vorläufige Verbesserungen zu erreichen und

(c) Hinweise zu erhalten, in welcher Richtung langfristige und langwierige Verbesserungen durchgeführt werden sollen.

Das Endziel dieser Art von Untersuchungen besteht darin, für die Berechnung von schnellen kritischen Anordnungen und großen schnellen Leistungsreaktoren genügend gute und verläßliche nukleare Daten und Rechenmethoden zur Verfügung zu stellen. Beim gegenwärtigen Stand der Untersuchungen konnten die Differenzen zwischen gemessenen und berechneten Werten für wichtige Parameter von kritischen Anordnungen noch nicht auf ein genügend kleines Maß verringert werden. Diese Arbeit muß daher als ein erster Schritt in die gewünschte Richtung angesehen werden. Weitere Schritte werden jedoch notwendig sein, um das langfristige Ziel zu erreichen.

Contents

I. INTRODUCTION

The aim of the present report is twofold:

(i) the results of this study are presented in more detail than it was possible in the paper [1] presented at the BNES Fast Reactor Physics Conference in 1969,

(ii) the group constants which have been prepared during this work, the data used in the calculations and the comparisons between theory and experiment are documented as a reference for further studies.

In this paper we study systemically the influence of changes in nuclear data on the calculated values for the criticality and other important parameters of critical assemblies. As in the preceding work [2] the analysis is done for a variety of assemblies which differ in geometry, material composition, and energy distribution of the normal and adjoint neutron flux (see table 1).

The primary objective and short range aim of our work is

(a) to detect deficiencies in nuclear data and/or calculational methods,

(b) to get first improvements in the data and/or methods as far as possible,

(c) to get indications in which respect and in which way further improvements which need longer time should be carried on.

In the present investigation the differences between the calculated and measured results for the critical assemblies studied are still not reduced to a satisfactory level. This study is only intended as a step in this direction, and further investigations along the same line will be necessary.

The long range aim of our investigation is to establish satisfactory nuclear data and calculational methods which can be reliably used for the calculation of fast critical assemblies and of large fast power reactors, and to try

---

Zum Druck eingereicht am 14.9.70

to obtain a more and more precise judgement of the reliability and confidence level of predicitions of the nuclear characteristics of fast reactors. The necessity and importance of such a study is illustrated e.g. in [36] which shows to which extent the economics of large fast breeders are influenced by variations in the basic nuclear data.

In comparing the measured results for critical assemblies with the corresponding calculated results one should be aware of the possible sources of errors. These may lie in

(i) The microscopic nuclear data and the theoretical methods used for their determination.
(ii) The method and model used to analyse the integral measurement and the accuracy of the experimental results.

To check the reliability of the predictions only those integral experimental quantities should be used for the comparison

(a) which are(or at least seem to be) free of systematic errors,
(b) for which the experimental uncertainty limit is rather small,
(c) for which the calculational model is (or at least seems to be) most adequate.

In this respect the criticality of the system is supposed to be the most suitable and most reliable quantity. This is the reason why primarily we are comparing our calculated value for the criticality factor k_{eff} with the measured one. A disagreement in this value is a strong indication that there are remarkable deficiencies in the nuclear data or the calculational methods or even in both. Because of possibly compensating effects present in the determination of criticality we are further comparing some calculated quantities which may be more instructive with respect to special aspects with the corresponding experimental results. Such quantities are e.g. reaction rate ratios, spatial reaction rate distributions, ratios of material worths and the neutron energy distribution.
We use this additional information as supplementary indications to necessary improvements in data and/or methods.

The changes in microscopic nuclear data and consequent changes in the group constants which have been performed for the present investigations are outlined in section II.

Section III contains a description of the critical assemblies studied.

In section IV the calculational methods used are discussed in some detail.

The detailed results of the present study are given in section V.

The general discussion and the conclusions drawn are presented in section VI.

Appendix I contains the complete documentation of the new group constants and Appendix II the documentation of the additional data used in the calculations.

II. MICROSCOPIC NUCLEAR DATA BASIS

II.1. KFK-SNEAK Set

The group constant set used as reference set is the KFK-SNEAK set often abbreviated as SNEAK-set. Almost all of its physical basis is outlined extensively in the report KFK 120/part I, the pertinent microscopic energy dependent data are tabulated in reference [27]. The generation of the KFK-SNEAK set is described in reference [3]; tables with the corresponding group constants are given in reference [4]. For convenience the most important characteristics of this set for the heavy fertile and fissionable nuclei (see als [26]) are repeated here.

U^{235}

The fission cross section values below 20keV down to the eV range are based on the data of Michaudon et al. [5] from Saclay. Between 20keV and 1MeV the data of White [6] and of Perkin et al. [7] were used. Above 3MeV the old Los Alamos data [8] were used still without the recent corrections for the long counter efficiency. Between 1 and 3 MeV an eye-guide curve through rather scattering data was chosen.

The α values used below 10keV correspond to an unweighted arithmetic average of direct measurements by de Saussure et al. [9]. Wang-Shi-di et al. [10] and estimates by Uttley [11] from measured (σ_T: Uttley [11]; σ_f: Michaudon et al. [5]) and calculated (σ_n: measured σ_{pot} = 11.7 b [11] plus calculated constant average resonance scattering cross section contribution of 0.6 barn) cross sections. Between 10 keV and 1 MeV the highest weight was given to the rather well agreeing liquid scintillator results of Diven et al. [12] and Weston et al. [13]. Below 1MeV the capture cross sections wer obtained as the product of α and the fission cross sections. Above 1MeV, where no measurements are available, α was rather arbitrarily smoothly extrapolated to 10MeV such as to correspond rather closely to a 1/E dependence of σ_γ.

Concerning $\bar{\nu}$ the thermal value was taken from the careful evaluation of

Westcott et al. [14]. At higher energies all measurements available up to mid 1966 were renormalized to the following basic standards

$\bar{\nu}$(2200 m/sec) (U^{235}) = 2.430 ± 0.008
(Westcott value [14])

$\bar{\nu}_p$(2200 m/sec) (U^{235}) = 2.414 ± 0.008

($\bar{\nu}_d$(2200 m/sec)(U^{235}) = 0.016)

$\bar{\nu}_{spont.}$ (Cf^{252}) = 3.773 ± 0.012

$\bar{\nu}^p_{spont.}$ (Cf^{252}) = 3.764 ± 0.012

($\bar{\nu}^d_{spont.}$(Cf^{252}) = 0.009)

and fitted to straight line segments (see extensive description and documentation in reference [15]). Below 2.5MeV down to thermal, i.e. for the most important energies, $\bar{\nu}(E)$ is represented by

$$\bar{\nu}_{25}(E) = 2.430 + 0.106E \qquad (E \text{ in MeV})$$

U^{238}

Below 40keV the capture cross section is composed by contributions only from s and p wave neutrons without inelastic scattering competition. In this range σ_γ was calculated from average s and p wave resonance parameters and statistical distributions, viz.

$\bar{\Gamma}_\gamma$ = 2.48 ± 5.6 (meV)
independent of l and J

S_o = $(0.90 \pm 0.10)\cdot 10^{-4}$

S_1 = $(2.5 \pm 0.5)\cdot 10^{-4}$
independent of J

$\bar{D}_{J=1/2}$ = 20.8 ± 2.0 (eV)
independent of l

$\bar{D}_{J=3/2}$ = 11.4 ± 1.1 (eV)

ν_n = 1 for all l and J

ν_γ = ∞ for all l and J

R = 9.18 ± 0.13 (f)

Corresponding to a potential scattering cross section

σ_{pot} = 10.6 ± 0.2 (b)

where

l = neutron orbital angular momentum,

J = total compound nucleus angular momentum,

ν_x = number of degrees of freedom in a χ^2 type distribution for process x (x=n;γ; n=scattering, γ=capture)

The statistical formula used is an energy and half width distribution average of single level Breit-Wigner resonance terms. The derivation of the statistical data listed above is to be found in reference [16]. In the SNEAK set there is still some inconsistency in σ_γ (U238) in the groups 13 and 14 (1.0 - 4.65 keV). In the whole group 14 and part of the group 13 σ_γ was calculated from resolved resonance parameters (1.0 - 3.9keV) as contained in the KEDAK file [16]. The number of p wave resonances analysed and considered in this range and therefore the calculated σ_γ values are too small compared to σ_γ values calculated from the above statistical parameters which actually take all p wave resonances into account.

Above 130keV the measurements by Barry et al. [17] were used up to 10 MeV. As Barry uses the same detector for the neutron flux measurements as White [6] in his fission cross section measurements, this choice is consistent with the choice of White's $\sigma_f(U^{235})$ data.

Between 40 and 130 keV the σ_γ values were obtained by smooth interpolation beteween the statistical theory estimates and Barry's data.

The inelastic scattering cross sections for the important energies below 2MeV were obtained by a careful analysis of all available excitation and other inelastic scattering data; this is extensively described in reference [18]. Among more recent experiments the highest weight was given to the comprehensive excitation cross section measurements by Barnard et al. [19]. These give about 20% larger inelastic scattering cross sections between 1.0 and 1.6MeV than obtained in earlier evaluations. The inelastic scattering probabilities were still taken throughout from the Russian ABN set [20].

The fission cross section values between threshold and 3MeV are based on the results of Lamphere [21] and between 3 and 10MeV on the old Los Alamos data [8] also still without the recent corrections for the long counter efficiency.

A weighted least squares fit to the available renormalized experimental $\bar{\nu}$ values led to the following linear relationship for $\bar{\nu}(E)$ valid between threshold and 15MeV (see reference [18])

$$\bar{\nu}(E) = 2.3576 + 0.1557E \qquad (E \text{ in MeV})$$

Pu^{239}

The fission cross section values below 20keV are based on the experimental data of Bollinger et al. [22]. Consistently with U^{235} the measurements of White et al. [6, 7] were used between 20keV and 1MeV. Between 1 and 3MeV we relied on two rather dense and compatible Russian measurement series [28, 29]. Between 3 and 10MeV as for U^{235} the (still uncorrected) Los Alamos fission data [8] were used.

Below 30keV the α values are based on the old KAPL integral measurements [23]. Between 30keV and 1MeV the rather well agreeing Oak Ridge [24] and Los Alamos [25] liquid scintillator values were used. As for U^{235} below 1MeV the capture cross sections were obtained as the product of α and the fission cross sections. Above 1MeV no measurements are available and, as for U^{235}, α was rather arbitrarily extrapolated to 10MeV in rather close correspondence to a 1/E behaviour of σ_γ.

Concerning $\bar{\nu}$ the thermal value was obtained as a weighted least squares average of all measurements available up to mid 1966 after renormalization to the U^{235} and Cf^{252} $\bar{\nu}$ standard values listed in the U^{235} section above; the result was

$$\bar{\nu}\ (2200\ \text{m/sec})(Pu^{239}) = 2.892$$
$$\bar{\nu}_p\ (2200\ \text{m/sec})(Pu^{239}) = 2.886$$
$$(\bar{\nu}_d\ (2200\ \text{m/sec})(Pu^{239}) = 0.006)$$

Using the same procedures as for U^{235} the energy dependence of $\bar{\nu}$ for Pu^{239} was obtained to

$$\bar{\nu}_{49}(E) = 289200 + 0.12791E + 0.00189E^2 - 0.00010E^3 \qquad (E \text{ in MeV})$$

Extensive documentation of these evaluations is to be found in reference [26].

Starting from the KFK-SNEAK set improvements are now introduced by the successive replacement of older data by more recent, more reliable data (see also reference [2]). The changes in basic data leading to partly important modifications in the KFK-SNEAK group cross sections are discussed in the following. In generating modified group cross sections the same collision density weighting spectrum as for the KFK-SNEAK set was used (see reference [4], figure 1).

II.2. SNEAPM, SNEPMB Sets

The SNEAPM set differs from the KFK-SNEAK set only in that in the range 10 to 500keV the $\sigma_\gamma(U^{238})$ values are replaced by the experimental results obtained by Pönitz et al. [30] and by Menlove and Pönitz [31]. This lowers the group σ_γ^{28} values in the groups 6 to 11 (10-800keV) by up to 13.5%.

In the SNEPMB set, in addition to these changes for U^{238}, σ_f and σ_γ of U^{235} (α is kept konstant) are lowered in group 7 to 10 (21.5-400keV) according to a $\sigma_f^{25}(E)$ curve proposed by Beckurts [32]. This curve was obtained by multiplying measured $\sigma_f^{25}/\sigma_\gamma(Au)$ ratios with the $\sigma_\gamma(Au)$ shape measurements normalized to an absolute determination of $\sigma_\gamma(Au)$ at 30keV by Pönitz et al [30, 33] in the range 25 to 500keV and subsequent averaging. The corresponding modified σ_γ^{28}, σ_f^{25} and σ_γ^{25} group cross section values are given in **tables AI-1 and AI-2.**

II.3. PU9SCP Set

In this set the SNEAK set $\alpha(Pu^{239})$ values in the group 11-15 (465eV to 21.5keV) based on the old KAPL measurements are replaced by values based on the first results of the linear accelerator $\alpha(Pu^{239})$ measurements by Gwin et al. [34]. The σ_γ values are correspondingly changed for σ_f kept constant. Among the more recent experimental α_{49} data available at the

time where the PU9SCP set was established Gwin's data were considered to be the most reliable ones by the following reasons. From the available measurements Gwin's results were assigned the smallest errors (on the average about ± 15% in α). The independent α estimates by Pitterle et al. [35] and Ribon et al. [36] from evaluated measured total and fission cross sections and calculated scattering cross sections agree best with Gwin's data among the available experimental α_{49} results. The latest available results obtained by Schomberg et al. [37] in measurements with considerably improved pulse shape discrimination, background determination and electronics are partly substantially lower than the first preliminary results reported in 1967 [38]. Below 4keV Schomberg's more recent data [37] are in good agreement with Gwin's values, above 4keV they are closer to Gwin than Schomberg's first preliminary data, but there are still discrepancies between Schomberg's and Gwin's results particularly in the regions 4-7keV and 10-30keV, which might partly be due to different normalizations. First α_{49} measurements of Ryabov et al. [39] with the fast pulsed reactor IBR as neutron source are compatible with Gwin's and Schomberg's measurements below 2 keV, but are even below the KAPL measurements above 2keV. Extensive discussions at the Anglo-Russian Seminar at Dubna in June 1968 clarified this discrepancy. Compared to the other more recent measurements Ryabov et al. overestimated the fission rates and underestimated the capture rates by applying too large corrections for neutron scattering before capture. First corrections for both errors led to a considerable enlargement of Ryabov's α values with results coming close to those of Gwin. More details can be found in reference [40]. The new α and σ_γ values for Pu^{239} in the groups 11-15 are given in table AI-3.

II.4. SCTALØ Set

The inelastic scattering probabilities contained in the ABN set [20] used in the SNEAK set are replaced by Karlsruhe data. In the range of resolved residual nucleus levels excitation cross sections evaluated and documented in various sections of the report KFK 120/part I are taken from the KEDAK file [27]. In the "continuum" range of residual nucleus levels the Weißkopf evaporation model [41] is used with nuclear temperatures as recommended by Swarcbaum et al. [42]. The materials concerned are C, O, Na, Al, Cr,

Fe, Ni, U^{235}, U^{238} and Pu^{239}, Pu^{240}, Pu^{241}, Pu^{242}. For the most important nuclide U^{238} the new inelastic scattering spectra turn out to be somewhat softer than the ABN set spectra.

The new inelastic scattering matrices are given in table AI-7. The calculation of the inelastic scattering matrices and their comparison with the ABN set matrices are more extensively described in appendix AI.

II.5. UPUCØR Set

In this set the SNEAK set fission data in the group 1 - 3 (2.5 - 10.5MeV) for U^{235} and Pu^{239} and in the groups 1 and 2 (4.0-10.5MeV) for U^{238} based on the old Los Alamos measurements by Smith et al. [8] were downgraded by up to about 10% in accord with recent efficiency corrections for the long counter used in the above measurements [43].

Recently comprehensive $\bar{\nu}(Pu^{239})$ results became available by measurements of Fréhaut et al. [44] in the range 1.5 to 15 MeV and Condé et al. [45] in the range 4 to 15 MeV. Both measurements show very good agreement and close a gap in the higher MeV range. Below 4MeV they are in agreement with the scattered earlier measurements. From 4MeV upwards they show differences up to +4% at 15MeV from the former evaluated curve [26] which forms the basis of the SNEAK set $\bar{\nu}$ data.

The new σ_f and $\bar{\nu}$ data are given in table AI-4.

II.6. PUO2RE Set

For the higher stable Pu isotopes Pu^{240}, Pu^{241} and Pu^{242} the SNEAK set so far contained the group cross sections and shielding factors as given in the ABN set [20]. They were completely replaced by group cross sections and shielding factors calculated from the recently evaluated microscopic cross sections of Yiftah et al. [46]. After the publication of the evaluation of Yiftah et al. the very comprehensive resonance total and partial cross section measurements for Pu^{240} by the linear accelerator group of the BCMN Geel [47] became available. They showed in particular that the average s wave capture width (32meV) and the s wave strength function ($1.37 \cdot 10^{-4}$) as assumed by Yiftah et al. in their calculations of $\langle\sigma_\gamma\rangle(E)$

for Pu^{240} on the basis of previous much less comprehensive measurements had to be replaced by the lower values $\bar{\Gamma}_\gamma$ = 23.2meV and $S_o = 1.05 \cdot 10^{-4}$. With these values and a (probably somewhat too low) p wave strength function $S_1 = 1.5 \cdot 10^{-4}$ the capture cross sections of Pu^{240} were recalculated in the range of predominant s and p wave capture above 1keV and extrapolated to higher energies so as to join smoothly the curve of Yiftah et al. at about 800keV. These lower σ_γ^{40} values were taken into account in the PU02RE set. Integral substitution measurements performed by Oosterkamp [48] in SNEAK assemblies, viz. measurements of reactivity differences due to substituion of a PuO_2/UO_2 mixture containing 8% Pu^{240} by another one containing 22% Pu^{240} were well reproduced by theoretical calculations using the improved capture data for Pu^{240} mentioned above (see more extensive discussion in reference [40]).

The much more comprehensive and accurate experimental information used in the evaluation of Yiftah , Schmidt et al. leads to striking differences of the present to the ABN group cross sections particularly for Pu^{240}. The capture data for Pu^{240} are about a factor 2 lower than the ABN set values in the energy range 1keV to 1MeV. The fission cross sections for Pu^{240} in the ABN set drop to zero in the keV range with decreasing energy, whereas according to the Gee [47] and the Los Alamos bomb shot measurements [49], as a consequence of the phenomenon of intermediate subthreshold fission, σ_f^{40} on the average over many resonances resp. fission resonance clusters is of the order of 100 mb and higher all the way down to the resolved resonance range.

The new group cross sections, shielding factors and inelastic scattering matrices for Pu^{240}, Pu^{241} and Pu^{242} are given in table AI-5.

II.7. MØX911, MØXTØT Sets

Finally, as trial data the recent measurements of $\sigma_\gamma(U^{238})$ by Moxon et al [50] in the range 500eV to 100keV were used to replace the SNEAK and SNEAPM set U^{238} capture data in the groups 9 to 11 (10-100keV, MØX911 set) and in the whole range, groups 9-15 (465eV-100keV, MØXTØT set). The

results of these measurements are nearly equal to those of the previous measurements of Moxon et al. [51], in particular the former $B^{10}(n,\alpha)$ normalization was once again carefully checked. The Moxon data are on the average about 20% smaller than the SNEAK set data and of the order of 10% smaller than Pönitz's values in the common energy range 25-100keV. The difference between Moxon and Pönitz is still unexplained. Furthermore the apparent discrepancies between Moxon's results and the average of a number of absolute and relative determinations at selected energies (24; 30; 65keV) have still to be resolved.

The modified capture data for U^{238} are given in table AI-6.

III. THE CRITICAL ASSEMBLIES STUDIED

In this chapter we will briefly describe the critical assemblies considered for the present study. A more detailed documentation of the assembly characteristics used in the calculations and of the integral data used for comparison between theory and experiment will be given in Appendix II.

Basically we studied 12 fast critical assemblies: SUAK U1B, SUAK UH1B, ZPR III-10, ZPR III-25, ZPR III-48, ZPR III-48B, ZEBRA 6A, SNEAK 3A1, SNEAK 3A2, SNEAK 3B2, SNEAK 5C, ZPR III-55. Six of these assemblies are fuelled with U235, five with Pu239, and one (SNEAK 3B2) with a two-zoned core, the inner zone containing Pu239 and the driver zone U235. Some characteristics of the assemblies are given in table 1.

All criticals are of medium or large size, the smallestone, SUAK U1B, having a core volume of about 40 liters. We have not included very small assemblies like GODIVA or JEZEBEL in our studies because the high energy cross sections of those materials which could be checked by these assemblies are not very much uncertain und are not so important for the physics prediction of large fast power reactors.

The hardness of the neutron energy spectrum veries considerably as can be seen e.g. from the median fission energy, the neutron lifetime, and the ratio $\sigma_f(U238)/\sigma_c(U238)$ given in table 1. The migration area M^2 of the core varies considerably between the lowest value for SUAK UH1B and the higher values for the more dilute assemblies ZPR III48, ZEBRA 6A, and SNEAK 3A1. Apart from the k_∞-experiments SNEAK 5C and ZPR III55 there is also a large span in the geometric configuration characterized by the geometric buckling B^2 and the core volume between the small unreflected SUAK-assemblies and the larger well reflected assemblies ZPR III-25, ZPR III-48, ZEBRA 6A and the three SNEAK criticals, the small but reflected assembly ZPR III-10 ranging in between. The leakage probability and the probability for the most important reaction ratios in the core are also given in table 1.

SUAK U1B is a metal fuelled uranium assembly with 20% enrichment of about 30 cm length in each direction of the cube.

SUAK UH1B is similar to SUAK U1B. It is also a metal fuelled uranium assembly with 20% enrichment but containing a relatively large amount of hydrogen in foils of polyethylene. The hydrogen to uranium atom ratio is about 0.5.

ZPR III-10 is a metal fuelled uranium assembly with a rather small core of about 17% enrichment surrounded by a relatively large reflector of depleted uranium.

ZPR III-25 has a larger core. The uranium metal fuel has an enrichment of about 9%. The core is surrounded also by a relatively large reflector of depleted uranium.

ZPR III-48 is a well known assembly with plutonium as fissionable material. The fuel enrichment is about 18%. In order to simulate the neutron energy spectrum of a sodium cooled fast reactor with ceramic fuel, Na and C have been added to the core composition to soften the spectrum. The reflector of about 30 cm thickness consists of depleted uranium metal.

ZPR III-48B is very similar to ZPR III-48. The essential difference is the inner core zone which has a higher content of Pu^{240} compared to ZPR III-48.

ZEBRA 6A is a somewhat smaller plutonium assembly with a fuel enrichment of about 24%. Na and C are also added to influence the neutron energy spectrum in the desired manner. The reflector of about 30 cm thickness consists of natural uranium and graphite.

SNEAK 3A1 was built to simulate the core of a fast steam cooled power reactor. The enrichment of the uranium-metal fuel is about 20%. The polyethylene foils used to simulate the coolant are contained in stainless steel canned platelets. The hydrogen concentration of SNEAK 3A1 is about half that considered for a typical steam cooled power reactor characterized by a coolant pressure of about 170 atm and a relatively small coolant

volume fraction of the core. Within the unit cell one Al- and one Al_2O_3-platelet are used together with the fuel- and stainless steel canned polyethylene-platelet to influence the neutron energy spectrum in the desired manner.

SNEAK 3A2 is slightly smaller in core volume than SNEAK 3A1 but has still a relatively large core zone. By adjusting the thickness of the polyethylene foil one obtained in SNEAK 3A2 a hydrogen concentration which corresponds to that of a future steam-cooled power reactor with the characteristics mentioned before. Besides the thickness of the polyethylene foil the composition is almost identical to SNEAK 3A1.

SNEAK 3B2 has an inner core zone which contains plutonium instead of uranium as fissile material. Otherwise the composition of this two-zoned core assembly is equivalent to SNEAK 3A2.

SNEAK 5C is a so-called k_∞-experiment. It consists of an inner plutonium zone of about 300 liters and an outer uranium driver zone. By adjusting the compositions of both zones in the appropriate manner one aims at a flat distribution of the normal and adjoint fluxes across the inner test zone and to bring the k_∞ of the test zone close to 1. The atom ratio C/U238 in SNEAK 5C is rather large, about 12, which leads to a "soft" neutron energy spectrum.

ZPR III-55 is also a k_∞-experiment for a plutonium composition from which one tries to get information on the α-value of Pu239 in the energy range from 0.5 to 20keV ($\alpha=\sigma_c/\sigma_f$). Because of the smaller C/U238 atom ratio of about 2.4 the neutron spectrum is not as "soft" as that of SNEAK 5C.

In addition to these assemblies we consider also the measurements concerning the steam density- and steam void-coefficient which have been performed during the so-called SNEAK-3A-series. They are described in [57] and include besides the assemblies SNEAK 3A1 and SNEAK 3A2, mentioned before, two other assemblies SNEAK 3A0 and SNEAK 3A3 which contained no hydrogen and twice the hydrogen concentration of SNEAK 3A2, respectively.

Apart from the leakage the small and "clean" assemblies SUAK-U1B and SUAK-UH1B provide checks for the higher energy data of U235 and U238. Because of the increased moderation SUAK UH1B is more sensitive than SUAK U1B to the capture data of U238 and U235 since there is a rapid increase of the capture cross sections to lower energies. For ZPR III-10 the importance of the leakage is reduced compared to SUAK U1B and the importance of the U235 and U238 data in the hundred keV region is increased. The same tendencies but still more pronounced are valid for ZPR III-25. The larger and well reflected assemblies SNEAK 3A1 and SNEAK 3A2 will give additional information on the uranium data in the lower keV region. The somewhat similar plutonium assemblies ZPR III-48 and ZEBRA 6A are both included in the analysis since the information on plutonium assemblies is not very extensive. ZPR III-48B is of interest because of its higher Pu240 concentration in the inner core zone compared to the usually available plutonium isotopic composition. The k_∞-experiments SNEAK 5C and ZPR III-55 provide a check of the low energy capture data of U238 and, hopefully, of the capture and fission data of Pu239 in the keV region. SNEAK 3B2 has been included in the analysis as the first fast critical at Karlsruhe containing plutonium.

With this selection of critical assemblies we are confident to obtain essential information on the reliability of data and methods for the energy range of interest in fast reactor analysis.

IV. THE CALCULATIONAL METHODS USED

IV.1. General Approach

In this study we want to determine the effect of each change in the nuclear data for the whole variety of criticals. The reason is two-fold:

1. we want to get an insight into the uncertainty of the calculation of characteristic quantities for these assemblies,
2. we want to obtain information on the sensitivity of the quantities studied on various changes of the nuclear data of several materials in different energy regions.

Doing this in the most correct way would consume a large amount of computer time since one has to perform e.g. two-dimensional calculations and has to apply corrections as mentioned later e.g. for heterogeneity etc. which in a strict sense would have to be recalculated for each change in the nuclear data. In order to avoid this we treated the problem in the following approximate manner: For each assembly which has not essentially a two-zoned core, we determined with our reference group set, the so-called SNEAK set [3], [4], the bucklings in each one-dimensional direction (i.e. B_x^2, B_y^2, B_z^2 respectively B_r^2, B_z^2) by comparing one-dimensional results for the criticality with the corresponding ones of fundamental mode calculations. These adjusted bucklings have then been used throughout the study in the fundamental mode calculations for the modified group sets. The adequacy of this procedure has been proved by some two-dimensional diffusion calculations with 11 energy groups especially for those changes in the nuclear data which caused major changes in the calculated criticality. The 11 group constants are condensed from the original 26 group constants using as weighting spectrum that of a one-dimensional diffusion calculation in spherical geometry for each modified group set. These two-dimensional results of course have to be considered as the basic ones. The fundamental mode results are used only to obtain the criticality difference of those changes in the nuclear data which lead to relatively small changes in criticality.

IV.2. Corrections

To get the final results (best available values of table V-4) some corrections which are partially calculated by ourselves and partially taken from the literature have to be applied if necessary: (a) the heterogeneity correction using the ZERA-code [58], (b) the transport correction using a one-dimensional SN-code, (c) the so-called REMO-correction which arises from a more elaborate treatment of the elastic slowing down [3], [2], (d) a correction for the transport cross section which takes into account the anisotropic down-scattering of hydrogen especially for SUAK UH1B [3], [59]. In the cases where these corrections are calculated by ourselves they were determined once with the SNEAK-reference set and are then assumed to be only weakly dependent on changes in the nuclear data and therefore are taken the same for the modified group sets.

IV.3. Comment on the Fission Spectrum

With respect to the calculational methods we should mention that the standard fission spectrum χ in our group sets is that belonging to $\nu=2.8$ of the Russian ABN-set [20]. In reality χ depends on the energy of the fissioning neutron and the type of the fissionable isotope; these dependences cannot routinely be taken into account in our calculations. We studied the magnitude of the effects which can be attributed to changes in the fission spectrum in an approximate manner. The main results are (see table 2): for U235-fuelled assemblies a reduction of the criticality between 0.001-0.003 and a decrease of the neutron spectrum by about 6% only in the energy range from 6.5-10.5MeV if $\chi(\nu=2.6)$ is used instead of $\chi(\nu=2.8)$; for Pu239 fuelled assemblies a slight increase in criticality (about 0.001) and an increase of the neutron spectrum by 11% in the energy range mentioned, if $\chi(\nu=3.0)$ is used instead of $\chi(\nu=2.8)$. The average ν of U235 fuelled assemblies is in the range 2.5 - 2.6, that of Pu239 fuelled assemblies in the range 2.9 - 3.0. One should mention that the fission ratio $\sigma_f(U238)/\sigma_f(U235)$ is only changed by 1-2% by the changes of the fission spectrum mentioned above.

IV.4. Accuracy of the Two-Dimensional Diffusion Results *)

Since the two-dimensional diffusion results obtained with the DIXY-program form the basis of our best available criticality predictions, it was necessary to check the validity of the approximations made in deriving these results. The first approximation is the condensation from 26 to 11 groups. Comparing the usual 11-group result with that of one 26-group two-dimensional check calculation for SNEAK 3A1 using the same spatial mesh (1600 meshpoints) we observed a difference in k_{eff} of 0.0001 which was far less than the accuracy of 0.001 required for each calculation. The second approximation concerns the distance between the meshpoints for the calculation of the space dependence of the neutron flux. This problem has been studied for an assembly similar to SNEAK 3A1 by two-dimensional calculations using 26 groups. The results are presented in the following table.

Dependence of k_{eff} on the spatial mesh

		case 1	case 2	case 3
Radial direction	number of mesh points	20	40	68
	number of mesh intervals in the core per transport mean free path	1.04	2.16	3.64
Axial direction	number of mesh points	20	40	60
	number of mesh intervals in the core per transport mean free path	1.1	2.2	3.74
Total number of mesh points		400	1600	4080
k_{eff}		0.98600	0.98746	0.98744

From this table one concludes that 2 mesh intervals per transport mean free path is sufficient for the two-dimensional calculations if an accuracy of 0.001 in k_{eff} is desired.

*) All results quoted in this paragraph have been provided by W. Höbel (Karlsruhe).

IV.5. Approximate Treatment of the Anisotropic Scattering of Hydrogen in SUAK UH1B

Usually we use the diffusion equation for the determination of the criticality of the assemblies studied. In deriving the cross sections respectively group constants which are needed in this equation the usual transport approximation is applied. It is very probable that this approximation is not sufficient for the anisotropic scattering of hydrogen and leads to errors in the transport cross section and the diffusion constant and therefore also to errors in the leakage probability. Among the hydrogen containing assemblies the leakage probability is most important for SUAK UH1B. Therefore an improved but still approximate treatment of the problem has been applied for this assembly [3] which is indicated in the following.

From the P1-equations the following relation can be derived:

$$(IV.1)\quad \sigma_{tr}^{i} = \sigma_{t}^{i} - \sum_{j \leq i} \sigma_{1}^{j \to i} \frac{J_j}{J_i}$$

where $\sigma_1^{j\to i} = \sigma_o^{j\to i}\,\mu^{j\to i}$ is the second moment of the scattering matrix and J_j is the net current in the energy group j. For the isotopes with higher atomic weight than 10, the second term on the right hand side of the above equation (IV.1) can be approximated by $\sigma_e^i \mu^i$. σ_e^i is the elastic scattering cross section in group i and μ^i the average cosine of the scattering angle. This approximation is of course not adequate for hydrogen. Improvements compared to this average cosine concept have been made for hydrogen in two steps: in the first step it was assumed that the currents are weakly energy-dependent so the ratio J_j/J_i in equation (IV.1) is set equal to unity, in the second step the group dependent currents of the SUAK UH1B assembly have been used to determine the transport cross section of hydrogen. Since the group dependence varies with space coordinates the group currents have been taken at two space points, located at distances of 6.5 cm and 13.3 cm from the core boundary. The resulting transport cross sections of hydrogen

have been used in the appropriate core regions in the criticality calculations. The influence of these two steps of improvements on the criticality has been studied for SUAK UH1B in diffusion approximation using a spherical model for the assembly. The following changes Δk have been obtained for the ABNSET: the first step gives $k=0.011$, the second step $k=0.0022$ compared to the usual average cosine concept. The reason for these different results is that in the second step the transport cross section of hydrogen is increased in the high energy region even slightly more than in the first step since J_j/J_i is smaller than one. But below 0.5MeV this tendency in reversed and the transport cross section is calculated even smaller than with the average cosine concept. Since the transport cross section is also used in the boundary condition of the diffusion calculations the calculated change in criticality may also depend on the geometrical model used for the assembly because in spherical geometry only one external boundary has to be considered whereas in the real cubic arrangement three boundaries have to be taken into account.

It seems to us that the magnitude of this correction is still uncertain. We have applied in the present evaluation a value of 0.007 for this correction which is taken from the literature [59] and is in between of the two extreme values mentioned before in this paragraph.

We will study the effect of the anisotropic scattering of hydrogen once again using the appropriate recently established improved version of the DTK-S_N-code.

IV.6. Weighting Spectrum and σ_o-Concept

The effect of the weighting spectrum on criticality has been studied using the REMØ-concept for the direct calculation of the elastic removal group constants. The results are discussed in [2]. In all cases studied there the differences have been smaller than 0.005 in k. For the neutron spectrum the REMØ-procedure generally leads to better agreement of calculations with experiments.

It should be mentioned, however, that the REMØ-concept is used only for those isotopes which scatter only into the next group of the 26-group set with the ABN-group structure. The REMØ-concept is not well suited for

hydrogen because the correction is applied only to the elements $\Sigma_{I \to I+1}$ of the scattering matrix. Comparing the scattering cross sections of hydrogen in the ABH- and SNEAK-set one notices considerable differences which most probably are due to the weighting spectrum used because the basic nuclear data are well known. In the SNEAK-set the weighting spectrum corresponds to that of the SNEAK 3A2 assembly. Therefore one may obtain changes in criticality and neutron spectrum for the SUAK UH1B assembly if the appropriate weighting spectrum is used for the determination of the scattering cross sections of hydrogen.

One should mention also that the REMØ-correction is applied only for neutron energies above 1keV (group 1-14). The extension to lower energies will probably bring about some influence on the results for the criticality of assemblies with rather soft neutron spectra like ZPR III-55 and especially SNEAK 5C.

In reactor calculations we normally use an average background cross section σ_o for the determination of resonance self-shielding (σ_o-concept, see [20], [4]). The determination of σ_o in each group is normally done with the infinite dilute total cross section with the exception of U238 (see [3], [4]). For the test calculations σ_o has been determined in a different way using the effective total cross section with the strongest resonance self shielding (see [2]). Because these two methods are extreme approximations to the true situation a possible error of 0.002 may arise when using the σ_o-concept at least for assemblies with a not too "soft" neutron spectrum because the difference increases as the importance of the low energy end of the spectrum increases.

IV.7. Accuracy of the Calculated Material Worths and Reaction Rates

a) Comparison of one- and two-dimensional results

In order to save computer time the material worths and the reaction rates in the core center have been calculated in spherical geometry using 26 energy groups. This procedure has been adopted because it seems more important to us to take into account all energy groups and to approximate

the geometry than to perform calculations for the real geometry but with a reduced number of energy groups. Taking into account the real geometry and the whole number of groups would necessitate rather large computer times. We expected that the desired quantities can be calculated well enough with the procedure mentioned and checked this by two-dimensional calculations for SNEAK-3A1 and SNEAK-3A2 with 4 and 11 groups. The results given in table 3 indicate that for predominantly scattering materials like C, H, O, Mg the agreement between the various results is very poor as has been expected. This is essentially due to the influence of group collapsing as is already known in the literature (see e.g. [60]). Therefore even the 26-groups results may be doubtful. For the other materials the agreement is rather good: for the case with 11 groups the differences amount to about 5%. This indicates that there is no systematic deviation between the results for spherical geometry and the two-dimensional ones as could e.g. arise from differences in the normalization integral. This has also been found by Pitterle et al. [35]. For the same assemblies SNEAK 3A1 and SNEAK 3A2 in the central region of the core the microscopic reaction rate per unit flux and per atom of U235, this means the effective group averaged cross section, agrees within 0.15% and the important reaction rate ratios U238(n,γ)/U235(n,f) U235(n,γ)/U235(n,f) and U238(n,f)/U235(n,f) also within 0.15% comparing one-dimensional 26 group results with two-dimensional 4- and 11-group results.

The results mentioned so far have been obtained using the SNEAK set but it is expected that they are valid for other group sets and other assemblies as well. Calculations for the two assemblies SNEAK 3A1 and SNEAK 3A2 using the MOXTOT-set indeed showed practically the same results as obtained for the SNEAK set. Therefore, it seems very probable that the one-dimensional results for the central material worth and the central reaction rate are not subject to systematic calculational errors.

b) Comparison of results with and without REMØ-correction

As stated two paragraphs before the REMØ-correction generally leads to a better agreement between calculations and experiment for the energy-dependent neutron flux. The differences between the spectrum calculated in the

usual way and that calculated with the REMO-correction are quite appreciable. For the assembly SNEAK 3A1 e.g. they amount to about ±15% in some energy groups. The question arises wether such changes in the energy dependence of the neutron spectrum affect the calculated material worths to a remarkable extent or not.

The REMO-correction is based essentially on a correction of the macroscopic elastic and total removal cross section elements of the scattering matrix and is appropriate for the calculation of the neutron flux. The question if the REMO-correction is also an adequate procedure for the calculation of the adjoint flux will not be considered here although we adopted this assumption in the present study.

In the following lists we compare the results for the calculated material worths using two different methods:

method a): The normal and adjoint fluxes used in the perturbation calculations have been obtained using REMO-corrected group constants.

method b): The normal and adjoint fluxes used are calculated in the usual manner without the REMO-correction for the group constants.

In both methods we used perturbation cross sections which have been calculated in the usual way without any REMO-correction. For a rigorous comparison of the influence of the REMO-correction one should apply in method a) the REMO-correction to the perturbation cross sections too. This has not been done here because it would have caused inconveniences in handling the programme for the REMO-correction and because we think that the effect is almost negligible for the perturbation calculations of the material worths.

This assumption seems to be reasonable because the REMO-correction has to be applied both to the normal and pertubed core composition and these two compositions are almost identical apart from the relatively small addition of the special material or isotope considered. The amount of material added to the normal mixture is in our cases 10^{20} atoms which means for most materials about 1-10% of the amount which is normally present in the

Results for Assembly ZPR III-48 using the SNEAK-set

Material	AL	B10	C	CR	FE	MO	NA	NI	Pu239	Pu240	U235	U238
Material worth method a) / Material worth method b)	0.939	1.050	0.738	0.969	1.002	1.043	0.937	1.020	0.984	0.967	0.980	0.976

Results for Assembly SNEAK 3A1 using SNEAK-set

Material	AL	B10	C	CR	FE	H	MO	NI	O	Pu239	U235	U238
Material worth method a) / Material worth method b)	0.867	1.019	1.174	0.988	0.976	0.992	1.021	1.029	1.263	0.996	0.993	0.997

Results for Assembly SNEAK 3A2 using SNEAK-set

Material	AL	B10	C	CR	FE	H	MO	NI	O	Pu239	U235	U238
Material worth method a) / Material worth method b)	0.851	1.006	1.094	0.991	0.976	0.980	1.006	1.015	1.182	1.000	0.994	0.985

mixture. Therefore we expect that the influence of the REMO-correction on the cross sections of both mixtures will be almost identical and the net effect on the perturbation cross sections will be practically zero because of a compensation effect since the perturbation cross sections are determined as differences between the cross sections of both compositions which show almost identical REMO-corrections.

It can be seen from this list that for the fertile and fissile isotopes the influence of the REMO-correction on the calculated material worth is generally smaller than 3% and for the predominantly absorbing materials generally smaller than 5% which is not too much compared to the existing discrepancies between calculation and experiment. However, one should have this in mind when in the future these discrepancies come down to comparable magnitude. For predominantly scattering materials, as expected, the influence of the REMO-correction is larger - up to 30% - . But for these materials all 26-group results either with or without REMO-correction are somewhat doubtful as indicated in the preceding paragraph.

V. RESULTS AND DISCUSSION

V.1. Results of Fundamental Mode Calculations for k_{eff}

The results of the fundamental mode diffusion calculations for k_{eff} are given in table V-1. The values given refer to the homogenized core composition. For an easy comparison with the measured values the calculated criticality values for the SNEAK-series have been normalized in such a way that the normalized value for k_{eff} of SNEAK 3A2 is equal to unity for all sets of group constants.

In the figures AII-1 to AII-36 the neutron flux, the adjoint neutron flux and the collision density are shown for 12 assemblies. For an easy intercomparison of corresponding curves for different assemblies we have taken the same scale in the corresponding figures for the different assemblies. The curves have been obtained from the group values using a program which produces a smooth curve through the group values [61].

Except for the two-zoned cores SNEAK 3B2 and ZPR III-48B the values for the normal and adjoint fluxes have been taken from fundamental mode calculation. The normalization is

$$\int_0^\infty \nu\Sigma_f(E)\ \phi(E)dE = 1$$

for the flux density and

$$\int_0^\infty \chi(E)\ \phi^+(E)dE = 1$$

for the adjoint flux. For the two exceptions SNEAK 3B2 and ZPR III-48B the normal and adjoint fluxes at the core center have been taken from one-dimensional calculations. The corresponding curves therefore have been drawn with an arbitrary normalization. For the adjoint flux the arbitrary normalization has been done in the following way: for SNEAK 3B2 the curve has been normalized to agree in the relatively flat region between 50 - 100 keV with the corresponding curve of SNEAK 3A2; for ZPR III-48B the normalization has been done in the energy range from 0.4 - 0.8 keV to give agreement with the similar curve of ZPR III-48 which is also flat in this energy range.

All results for the collision densities have been taken from one-dimensional calculations. This has been done because the programs involved in these calculations can handle only the results of one-dimensional calculations in the appropriate way. Therefore it would have been very inconvenient

to use the results of the fundamental mode calculation in order to get the corresponding collision density. The curves given always belong to the inner core zone, sometimes to an even smaller artificial zone around the core center. The normalization for all collision density curves is arbitrary.

All results for the figures AII-1 to AII-36 have been obtained using the SNEAK-set.

In the following we will indicate the sensitivity of the criticality of the various assemblies studied to changes in the nuclear data. This will be done for each assembly by giving the criticality changes for the most important changes of the group constant sets.

SUAK U1B: SNEAK → SNEPMB: $\Delta k = -0.015$
SNEPMB → SNEAPM: $\Delta k = +0.021$

This small assembly with a relatively hard neutron spectrum is very sensitive to the reduction of the U235 fission cross section which is implied in the first step and is omitted in the second step. The reduction of the U^{238} capture data causes a criticality increase of $+0.006 = 0.021-0.015$.

SUAK UH1B: SNEPMB → SNEAPM: $\Delta k = +0.008$
PU9SCP → SCTALO: $\Delta k = +0.003$
MOX911 → MOXTOT: $\Delta k = +0.004$

Due to the much softer neutron spectrum of this assembly compared to SUAK U1B changes in the high energy data are less important. The omission of the reduction of the U^{235} fission cross section gives rise to a criticality increase which is only 1/3 of that obtained for SUAK U1B. Taking into account the lower U^{238} capture cross section of MOXON in the keV-region causes an increase of criticality which is not negligible for this assembly. The increase of criticality obtained with the new scattering probabilites for the inelastic scattering probabilities for the inelastic scattering is due to the special energy dependence of the neutron importance for this assembly which increases considerably below 1 MeV with decreasing energy.

ZPR III-10: SNEAK → SNEPMB: -0.015
SNEPMB → SNEAPM: +0.026

The results for this assembly with a relatively hard neutron spectrum are very similar to that obtained for SUAK U1B.

ZPR III-25: SNEAK → SNEPMB: -0.010
SNEPMB → SNEAPM: +0.029
PU9SCP → SCTALØ: -0.011
PUO2RE → MOX911: +0.013

Apart from the results similar to ZPR III-10 the new inelastic scattering data cause a remarkable reduction of criticality which is due to the special form of the energy dependence of the neutron adjoint which decreases below 1 MeV with decreasing energy contrary to the behaviour for most of the other assemblies. The reduction of the U^{238} capture data in the 10 - 100 keV region to the low MOXON-values shows a remarkable effect on the criticality of this assembly because the enrichment is lower and the neutron spectrum somewhat softer than that of the assemblies considered in the preceding paragraphs. The higher sensitivity to the U^{238} capture data in this energy region is also indicated by the difference between the first two steps which amounts to +0.019=0.029-0.010 and is considerably larger than the corresponding data for the SUAK assemblies and for ZPRIII-10.

ZPR III-48: SNEAK → SNEPMB: +0.009
SNEAPM → PU9SCP: -0.009
PUO2RE → MOX911: +0.008

This assembly is rather sensitive to the U^{238} capture data below about 100 keV which have been changed for the sets SNEPMB and MOX911. The new α-values for Pu^{239} of GWIN used in the PU9SCP-set cause a criticality reduction which is not as large as that of -0.016 reported previously [2] where lower limits of the first preliminary α-values of SCHOMBERG had been used.

ZEBRA 6A: SNEAK → SNEPMB: +0.006
SNEPMB → PU9SCP: -0.010
PUO2RE → MOX911: +0.006

As expected this assembly shows a behaviour similar to that observed for ZPR III-48.

SNEAK-Series: The criticality of the assemblies considered within the SNEAK-3A-series reacts most sensitive to the first two steps of changes in the group cross section sets. The fact that the absolute values of the criticality differences for the first two steps are of the same magnitude indicates that the steam density coefficient is much more sensitive to changes in the U^{235} fission cross section than to those in the U^{238} capture cross section in the energy region considered (i.e. between about 20 - 500 keV). One should of course always have in mind that the criticality values for the SNEAK-series are normalized in such a way as to give a k_{eff} equal to unity for SNEAK 3A2.

SNEAK 3A1:	SNEAK → SNEPMB:	-0.009
	SNEPMB → SNEAPM:	+0.018
	PUO2RE → MOX911:	+0.009
	MOX911 → MOXTOT:	+0.006

The criticality change corresponding only to the reduction of the U^{238} capture cross section in the first step amounts to +0.009. It is overcompensated by the effect of the reduction of the U^{235} fission cross section which is twice as large as can be seen from the second step leading from a criticality change of -0.009 for the first step to a total criticality change of +0.009 for the first two steps. From the last two steps it can be seen that for SNEAK 3A1 the changes caused by the MOXON data are more important in the 10 - 100 keV region than in the energy region below 10 keV.

SNEAK 3A2:	SNEAK SNEPMB:	-0.006
	SNEPMB SNEAPM:	+0.013
	PUO2RE MOX911:	+0.007
	MOX911 MOXTOT:	+0.007

For SNEAK 3A2 the results are qualitatively similar to those for SNEAK 3A1. The last two steps cause nearly equal criticality changes. This means that for this assembly with respect to criticality the influence of the change to the MOXON data is of equal importance for the energy region below 10 keV as for the 10 - 100 keV region. This fact gives direct evidence of the softer neutron spectrum of SNEAK 3A2 compared to that of SNEAK 3A1.

SNEAK 5C: SNEAK → SNEPMB: +0.008
SNEAPM → PU9SCP: -0.015
PUO2RE → MOX911: +0.008
MOX911 → MOXTOT: +0.014

The largest criticality change for this assembly is caused by the change to the Pu^{239} α-values of GWIN (SNEAPM→PU9SCP). The reduction of the U^{238} capture cross section to the PÖNITZ-data in the first step produces nearly the same criticality increase as that of the subsequent inclusion of the MOXON-data in the 10-100 keV region (PUO2RE→MOX911). The criticality effect of the change to the MOXON U^{238} capture data in the whole energy region concerned overcompensates that of the change to the GWIN α-data. A comparison of the two last steps illustrates the importance of the energy region below 10 keV for this assembly compared to e.g. SNEAK 3A2 which already has a relatively soft neutron spectrum.

ZPR III-55: SNEAK → SNEPMB: +0.018
SNEAPM → PU9SCP: -0.011
PU9SCP → SCTALO: -0.013
PUO2RE → MOK911: +0.017
MOX911 → MOXTOT: +0.017

For this assembly relatively large criticality changes have been obtained. Qualitatively the results are similar to that for SNEAK 5C or even to SNEAK 3A2 with the exception of the importance of the inelastic scattering data for this assembly which is due to the special neutron adjoint as has been discussed for ZPR III-25. For a quantitiative understanding of the effects one should have in mind that the atomic number density of U^{238} is considerably larger than that e.g. for SNEAK 5C and SNEAK 3A2 and that the neutron spectrum is considerably harder than that of SNEAK 5C. This fact is for both assemblies illustrated for example by the different criticality changes cased by the two last changes in the group cross section sets.

At the end of this chapter we will discuss briefly which assemblies are most sensitive to the changes in the nuclear data which have been performed during this study.

SNEAK → SNEPMB:	ZPR III-55	: +0.018
	SNEAK 5C	: +0.008
	SUAK U1B	: -0.015
	ZPR III-10	: -0.015
	ZPR III-25	: -0.010

This change actually consists of two different changes:

a) the reduction of the U^{238} capture cross section

b) the reduction of the U^{235} fission and capture cross section.

The second part has no influence on the Pu-fuelled assemblies. These assemblies show the effect of the first part only and therefore a criticality increase is observed. For all U-fuelled assemblies the effect of the first part is more than compensated by the effect of the second part and therefore we obtained a decrease of criticality for these assemblies. Since in the next step (SNEPMB→SNEAPM) the second part has been cancelled the effect of the first part can be determined separately (assuming additivity for the criticality changes of the two parts). This leads to the result that the criticality effect of the first part for the assemblies ZPR III-25 and ZPR III-10 is of comparable magnitude as the corresponding values for ZPR III-55 and SNEAK 5C.

SNEPMB → SNEAPM:	ZPR III-25	: +0.029
	ZPR III-10	: +0.026
	SUAK U1B	: +0.021
	SNEAK 3A1	: +0.018

This step corresponds to the cancelling of the second part mentioned for the step before i.e. going back from the reduced U^{235} fission cross sections to the previously used values in the 25 - 500 keV region. It produces rather large criticality changes, of course only for the U-fuelled systems.

SNEAPM → PU9SCP:	SNEAK 5C	: -0.015
	ZPR III-55	: -0.011
	ZPR III-48	: -0.010

The inclusion of the Pu^{239} α-values of GWIN results in a criticality reduction of about -0.01 for the usual Pu-fuelled assemblies. The reduction becomes even larger if the neutron energy spectrum becomes softer. SNEAK 5C seems

to be at the lower end of the "soft" assemblies because its median fission energy of 1.2 keV is rather low. This has been demonstrated in our study because a reduction of 0.016 has been obtained in the present study for the somewhat "harder" assembly SNEAK 5B which is described in [62] and has a median fission energy of about 3 keV.

PU9SCP → SCTALO: ZPR III-55: -0.013
ZPR III-25: -0.011

The new inelastic scattering probabilities generally have only a small effect on the criticality. The two exceptions given above are caused by the special form of the energy dependence of the adjoint flux as mentioned before.

SCTALO → UPUCOR: SUAK U1B: -0.006
ZPR III-10: -0.005
SUAK UH1B: -0.004

The reduction of the fission cross sections in the energy region above 2 MeV causes only relatively small criticality changes for the assemblies considered in the present study. For smaller assemblies with even harder neutron spectra more marked effects are to be expected.

UPUCOR → PUO2RE: SNEAK 5C : +0.004
ZEBRA 6A : +0.004

Because of the relatively small concentration of higher plutonium isotopes in the presently available assemblies the effect of rather drastic changes in the nuclear data for the higher plutonium isotopes is not very pronounced.

PUO2RE → MOX911: ZPRIII-55: +0.017
ZPRIII-25: +0.013

Because of the large U^{238} atomic number densities present in both assemblies and because of their energy distributions of the neutron flux which give considerable weight to the energy region between 10 - 100 keV these two assem-

blies show the largest effects of the reduction of the U^{238} capture data from the PÖNITZ-values to the MOXON-values in this energy range.

MOX911 → MOXTOT:	ZPR III-55:	+0.017
	SNEAK 5C :	+0.014
	SNEAK 3A2 :	+0.007

This step gives only a marked criticality effect for assemblies with soft neutron spectra. The effect is most pronounced for ZPR III-55 with its relatively large U^{238} concentration.

V.2. Results for k_{eff} from One- and Two-Dimensional Calculations

The results for the criticality of the various assemblies obtained in one- and two-dimensional diffusion calculations using different sets of group constants are given in table V-2. These results essentially confirm the results obtained by the fundamental mode calculations and thus provide a check that our general approach is correct which assumes that if no two-dimensional results are available for the criticality differences when going from one group set to the other the corresponding fundamental mode criticality differences can be used. This assumption is valid if the criticality differences are not too large.
Its validity is reduced to some extent if the properties of the blankets or reflectors are changed by changes in the group constants. This is expecially true of the reductions in the capture cross section of U^{238} and to a smaller degree of the reduction in the high energy fission cross sections of all materials (SCTALO→UPUCOR).

V.3. Results for the Best Available Values of the Criticality

In this section we have to compare our calculated criticality values for the various assemblies with the corresponding measured values. The calculated values are based on the results of two-dimensional diffusion calculations. If necessary the criticality differences obtained by fundamental mode calculations for successive changes in the group constant sets have been used to determine in an approximate manner criticality values for the

modified data sets which are equivalent to two-dimensional results. In order to establish the best theoretical values for k_{eff} some corrections have to be applied as outlined in chapter IV-2. The numerical values of these corrections for the various assemblies are given in table V-3. The origin of the data is described in Appendix II for each assembly separately.

The corrections have been assumed to be the same for the different sets of group constants used in this study. They have been applied to the exactly or approximately determined criticality values which correspond to two-dimensional diffusion calculations. In this way the best available criticality values of the various assemblies have been determined for the different sets of group constants. They are given in table V-4 together with the experimental results. These results will be discussed in a subsequent chapter.

V.4. Results for Material Worth Ratios and Central Reaction Rate Ratios

The information on the material worth and reaction rate of various materials is considered in our study as complementary to the information provided by the criticality. The normalization of the material worths relative to that of U^{235} which is used generally in this study brings the advantage to avoid the trouble with the well known discrepancies in the absolute magnitude of the measured and calculated material worths or reactivity coefficients [63]. Furthermore the calculated values are independent of the so-called normalization integral which may perhaps be in error at least for one-dimensional models of the real two- or three-dimensional problems because the geometry is not taken into account properly although our results mentioned in chapter IV-7 seem to indicate that this is not the case. The reaction rates are usually normalized in the experiments to the number of fissions of U^{235}. For an easy comparison with the experimental results this normalization has also been done for the theoretical results.

The theoretical results presented for the central material worth ratios have been obtained by first order perturbation theory using the normal and adjoint fluxes of homogeneous diffusion calculations. In the interpretation of discrepancies between theory and experiment one should be

very cautious because in the calculations the effects of sample size (see e.g. [64]) and sample environment have not been taken into account. For those materials which show a large contribution to the material worth by the so-called scattering- or degradation-term the theoretical results can not be considered as very reliable as has been explained in chapter IV-7. Further but perhaps less severe doubts on the reliability of the calculated material worths arise from the fact that the group constants usually used in the adjoint flux- and perturbation calculations are the same as that used for the normal flux calculations, i.e. group constants which have generally been obtained by a flux averaging procedure within the groups (see e.g. [60]).

The theoretical results for the central reaction rate ratios have been obtained also by homogeneous diffusion calculations. In comparing them with experimental results one should examine quite carefully if the experimental situation corresponds to this assumption of homogeneity. It is known that the so-called chamber-measurements for the determination of reaction rates do not correspond to the assumption of homogeneity made in the calculations. On the other hand the reaction rates measured with foils (see e.g. [65]) often can be adequately treated theoretically only by heterogeneous calculations.

Some theoretical results from spherical calculations for SNEAK 3A1 and SNEAK 3A2 are given in table V-5. For the same assemblies the reaction rate ratios $\sigma_f U^{238}/\sigma_f U^{238}$ and $\sigma_c U^{238}/\sigma_f U^{235}$ obtained from fundamental mode homogeneous calculations with the various group sets are given in table V-6. Corresponding experimental results are presented in [65], [66] and [67]. In comparing them with our theoretical results one should be aware of the effect of sample size for the material worth [64] and the fact that the experimental results for reaction rates measured with chambers and foils are sometimes quite different [65]. Therefore from the tables V-5 and V-6 only the tendencies with the different group sets can be deduced but no final conclusions can be drawn by the direct comparison with the experimental results.

The theoretical results for the central material worth ratios and central reaction rate ratios for ZPR III-48 are given in table V-7. Generally the agreement between theory and experiment is not too bad. Perhaps a certain amount of the disagreement for the material worth of B^{10}, Fe, Cr, Ni, Mo may be due to the sample size effect. This seems at least to be

possible considering the results shown in [64] for most of these materials. The calculated worth for sodium seems to be doubtful since it is a predominantly scattering material.

The theoretical result for the worth of Pu^{240} shows a marked improvement compared to the experimental result when the PUO2RE-set is used i.e. when the updated data for the higher plutonium isotopes are included.

The theoretical result for the reaction rate ratio $\sigma_f Pu^{239}/\sigma_f U^{235}$ is consistently lower than the measured one. This gives - togetherwith the material worth ratio - an indication that Pu^{239} is underreactive in the group sets used in this study.

In table V-8 the central reaction rate ratios obtained from fundamental mode homogeneous diffusion calculations with various group sets are given.

Table V-9 shows the theoretical results for the central material worth ratios and central reaction rate ratios for assembly ZPR III-48B. The results are essentially the same as those for the assembly ZPR III-48. Therefore no additional or more precise conclusions can be drawn from a comparison of the theoretical and experimental results than those already obtained for the assembly ZPR III-48. Especially no specific results with respect to Pu^{240} can be deduced by comparing theory and measurement for ZPR III-48B.

It has been checked for assembly SNEAK 3A2 that the energy dependence of the neutron flux in the core center is practically the same for the diffusion and S_N-calculations. Therefore the central reaction rates are nearly the same in both calculations. The very small deviations are unimportant compared to the discrepancies which still exist between theory and experiment.

V.5. Results for Reaction Rate Traverses

The only experimental results for reaction rate traverses considered for a comparison between theory and measurement are those for SNEAK-3A2 [65] and [67]. Earlier measurements have most times been performed using chambers. These measurements are not considered very reliable. Furthermore it is argued that streaming effects sometimes may lead to erroneous results in the experiments (see [67] p. 42) . The presently available foil experiments are considered more reliable (see [67] p. 42). Foil ex-

periments which can with some confidence be compared with calculated results are only the measurements of BÖHME and SEUFERT in SNEAK 3A2 described in [65] and also in [67]. These experiments show discrepancies to the chamber measurements, which are attributed to the streaming effect, and discrepancies to the theory especially in the blanket region near the core which are considered as "not yet understood" in [67].
In the core region the calculated traverses for $\sigma_f(U^{235})$, $\sigma_f(U^{238})$, $\sigma_c(U^{238})$ show a steeper descent to the core-blanket interface than the experimental ones. This effect is less strong for $\sigma_f(U^{238})$. In the blanket region near the core all three traverses show an increase of the ratio of the theoretical to the experimental result which is most pronounced for $\sigma_f(U^{238})$.
The three reaction rate traverses mentioned have been calculated for SNEAK-3A2 with the SNEAK-set as the basis of our study and the MOXTOT-set as the final group set of our present study. The ratio of the results obtained with the MOXTOT-set to the corresponding results with the SNEAK-set are shown in fig. 1. All results have been obtained for the axial direction using one-dimensional diffusion theory for the homogeneous case. The radial leakage has been taken into account by a global buckling. For the capture rate in U^{238} and the fission rate in U^{235} the traverses calculated using the MOXTOT-set are larger in the outer core region and especially in the blanket than the traverses calculated using the SNEAK-set. Both traverses are normalized at the core center. The fission rate traverse for U^{238} remains essentially unchanged within the core region. In the blanket region, however, the MOXTOT-set-results are considerably smaller than the SNEAK-set-results. From the results of fig. 1 it can be concluded that all three traverses now show nearly the same tendency within the core region when the MOXTOT-set-results are compared with the experimental results. The agreement between theory and experiment is improved for the core region when the MOXTOT-set is used compared to the SNEAK-set results which have been used for fig. 19 of [65] respectively fig. 29 of [67] which is reproduced as fig. 3 in this report for sake of an easy comparison. It seems probable that the calculations will give a slightly steeper descent of the traverses to the core boundary than the experiments, but the differences will become rather small in the core region using the MOXTOT-set.

In the blanket region the peak within the first 5 cm of the blanket near the core which is already observed when comparing the calculated to measured ratio for the traverses for the SNEAK-set in fig. 3 is increased by about 5% for $\sigma_c(U^{238})$ and $\sigma_f(U^{235})$ when the MOXTOT set is used. This leads to an overall deviation between theory and experiment of about 10% at a distance of about 5 cm from the core-blanket interface for both reaction rate traverses when the MOXTOT-set is used. For the fission rate in U^{238} the situation is reversed. Using the MOXTOT-set reduces the deviation observed between theory and experiment when the SNEAK-set is used. However, one should have in mind that this deviation for $\sigma_f(U^{238})$ is the most pronounced one of all the three reaction rate traverses studied. Even when the MOXTOT-set is used a deviation of about 15% will remain between theory and experiment for the $\sigma_f(U^{238})$ traverse at a distance of about 5 cm from the core-blanket interface. This leads to the result that with the MOXTOT-set all the three reaction rate traverses $\sigma_c(U^{238})$, $\sigma_f(U^{238})$, $\sigma_f(U^{235})$, can be rather well predicted within the core region but are overestimated by 10 to 15% in the blanket at a distance of about 5 cm from the core-blanket interface using the usual diffusion theory results. Since this overestimation appears for all three reaction rates it is not very probable that it is due to spatial resonance self-shielding which cannot be taken into account by the presently used σ_o-concept for the homogeneous mixtures. If the neglect of the spatial resonance shielding should be responsible for the deviation between theory and experiment in the core-blanket transition region one would expect that the reaction rate traverses $\sigma_c(U^{238})$ and $\sigma_f(U^{235})$ would show opposite tendencies since the atomic number density of U^{238} is increased that of U^{235} is decreased when going from the core to the blanket region.

Therefore we tried to check whether a transport effect could be responsible for the observed deviations between experiment and diffusion theory result. Unfortunately at the time of this study no code was available to evaluate reaction rate traverses using the fluxes calculated by an S_N-code. Therefore we used the fission source traverse instead of the reaction rate traverses. Fig. 2 shows a comparison of the one-dimensional S_6- and diffusion theory fission source traverses. Both are normalized to give one source neutron in the whole reactor. For the calculations 35 mesh-intervals in the core and 20 mesh-intervals in the blanket have been used. The desired accuracy in k_{eff} was 10^{-4} in both calculations and a source accuracy of 10^{-3} was

required in the diffusion calculation. The results shown in fig. 2 have been confirmed by doubling the number of mesh-intervals and requiring a ten times higher accuracy. Fig. 2 clearly demonstrates that by using transport theory the fission source distribution in the blanket is changed by about 10% compared to the diffusion theory result. This means that at least the fission rate of U^{238} will be changed by about the same amount.

The dip of the curve in fig. 2 at a distance of about 5 cm from the core-blanket interface has just about the same magnitude (about 10%) as the peak discussed just before which will be obtained practically at the same position when the MOXTOT-set-results are compared with the experimental results for the reaction rate traverses. The peak shown in fig. 2 in the outer blanket region cannot clearly be verified experimentally because the measurements do not have the necessary accuracy in this region because of bad statistics.

For the inner blanket region, however, fig. 2 strongly indicates that the reaction rate traverses should be evaluated using transport theory results if an accuracy of better than 10% is required. It can be expected from the preceding results that doing this and using the MOXTOT-set the deviations between theory an experiment for the reaction rate traverses will become rather small in such regions of the core where the experiments can be considered as reliable.

V.6. Results for the Neutron Importance

The results for the neutron importance for the assembly SNEAK 3A2 reported in [67] table 10 and [67] fig. 26 and in [68] show no drastic disagreement between theory and experiment. The most pronounced deviation of about 5% has been observed for the Sb/Be source with an energy of 24 keV.

We studied whether the new groups sets would bring about certain improvements. We found that in the energy region of interest the neutron importance shows a smaller energy slope with the MOXTOT-set compared to the results with the SNEAK-set. The changes are small, of the order of 2% or less. They tend to decrease the differences between theory and experiment reported in table 10 of [67] but for the low-energy Sb/Be source the difference between the measured and calculated result is still larger than the experimental uncertainty.

We wanted to study if the REMO-correction for the elastic removal group constants causes changes in the calculated neutron importance. We excluded the problem whether the REMO-correction is an appropriate method when applied to the adjoint flux or importance calculation. A calculation with REMO-corrected group constants resulted in an additional small decrease of the difference between theory and experiment of about 1% for the Sb/Be source but even then the remaining discrepancy is larger than the experimental uncertainty.
The influence of using heterogeneity-corrected cross sections for the adjoint flux calculations has not been studied in this work.
A more principal uncertainty in the adjoint flux calculation mentioned e.g in [60] is caused by the use of flux-weighted group constants for the calculation of the adjoint group fluxes.

V.7. Heterogeneity Calculations

V.7.1. Introduction

As has been shown e.g. in [58], [65], [66], [67], [69] heterogeneity calculations are helpful and sometimes necessary to control and improve the accuracy of nuclear data. Beside the calculations which are performed to obtain criticality corrections for most of the assemblies studied in this report using always the SNEAK-set, we started a few investigations to determine the influence of different group sets on the heterogeneity correction of k_{eff} and to check the method applied.
Furthermore we calculated reaction rate distributions within the unit cells and within the fuel platelets itself again for different group sets. On the one hand we wanted to see of what use these data are for the improvement of special cross sections, on the other hand we wanted to get more theoretical data concerning some experiments referred to in [58], [65], [66], [67]. Up to now a part of the reported experimental data could not be verified by calculations. The authors supposed that these differencies may be caused by inexact cross sections as well as by insufficient calculational methods.
Our own ivestigations did have the aim to clear some of these discrepancies.

V.7.2.1. Codes, Cross Section Sets, Assemblies Investigated and Their Geometric and Material Data

All heterogeneity calculations were performed with the code ZERA, described in [69] and [58]. ZERA is part of the NUSYS-system and contains evaluation routines to calculate reaction rates and to produce heterogeneity corrected cross sections for the homogenized unit cells.

For our comparison-calculations we used the old ABN-set and the more recently established sets, called SNEAK, SNEPMB and MOXTOT, presented in [3] and in this report.

We investigated the two critical SNEAK assemblies 3A1 and 3A2. Both facilities have two uranium fuelled core zones with about the same homogenized composition in each zone, but with differing structure of the unit cells. The detailed description of both facilities, of their macroscopic geometry and dimensions of their homogenized compositions as well as the microscopic structure of their unit cells and the atom densities of the single platelets are given in ref. [66] (3A1) and in ref. [65] (3A2). We have taken the necessary data exactly from these reports.

The atom densities of the 35% enriched uranium platelet used in the unit cell of core zone II are taken from ref. [67], while the atom densities of the natural uranium platelet has been determined in such a manner that the homogenized uranium densities in the unit cell of core zone II are identical with that used in core zone I. To explain it in more detail: The unit cell of core zone I has four platelets, one of them is a 20% enriched uranium platelet, the unit cell of core zone II has 36 platelets, five of them are 35% enriched uranium platelets and four of them are natural uranium platelets.

For all ZERA-calculations we used the following total bucklings: Assembly 3A1: $B^2 = 22.01 \times 10^{-4} cm^{-2}$, Assembly 3A2: $B^2 = 25.55 \times 10^{-4} cm^{-2}$.

For the one-dimensional radial diffusion calculation for SNEAK 3A1 we used the buckling $B^2 axial = 8.47 \times 10^{-4} cm^2$.

V.7.2.2. Cell Structures, Modifications and Notations

All SNEAK 3A platelets have the same thickness of 0.314 cm. Within a single zone the platelets are arranged in periodic sequences. Such sequence is defined as the normal unit cell. In order to enlarge the effect of heterogeneity one can re-arrange the platelets as is done in the bunching experiments. Single bunched cells are built from two normal cells, double bunched cells from four normal cells. The thickness of a single material zone (two identical platelets) amounts to 0.628 cm for the single bunched cell and to 1.256 cm for the double bunched cell (four identical platelets).

V.7.3. Influence of Heterogeneity on k_{eff}

In order to get the effect of heterogeneity by means of ZERA-calculations it is necessary to compare with results from the homogenized cells. We obtain the heterogeneity correction if we reduce the platelet-thickness by a factor large enough to avoid spatial self-shielding effects. We have chosen in our calculations a factor of 1000. (To avoid numerical difficulties perhaps a factor of 100 is more appropriate.) We denote such a cell as quasihomogeneous.

Now we define the heterogeneity effect of k_{eff} as difference Δk_{eff} between the ZERA-calculated multiplication factors of the heterogeneous and the quasihomogeneous cells.

Implicitly the ZERA-code relies on the assumption that the source distribution is flat within a single zone. For this reason we divided the uranium zone in five subregions with the following thicknesses: 0.02, 0.03, 0.214, 0.03, 0.02 cm. In case of bunched cells these thicknesses are duplicated or multiplied by four.

This is valid for the unit cells of core zone I.

V.7.3.1. Zera-Calculated Δk_{eff} for Different Cross Section Sets

These calculations are performed using the normal unit cell of core zone I.

The results are given in the following table.

Δk_{eff}(ZERA-calc.) /in units 10^{-3}/

Group Set	Assembly 3A1	3A2
ABN	-1.54	-1.32
SNEAK	+1.14	+2.53
SNEPMB	+1.20	+2.56
MØXTØT	+0.90	+2.22

The table shows at first sight the very strong difference between the results of the ABN-set on the one hand and the results of the SNEAK-set and the succeeding ones on the other hand.
The variations within the results of the new SNEAK-sets are comparative small.

V.7.3.2. The differences between ABN and SNEAK results increase strongly with increasing heterogeneity. This is apparent from the next table, which contains the results for different degrees of bunching. *)

Δk_{eff} (ZERA-calc.) /in units 10^{-3}/ for different degrees of bunching (Zone I)

Assembly	3A1			3A2		
Group Set	normal	single	double	normal	single	double
ABN	-1.54	-4.24	-9.21	-1.32	-3.98	-10.51
SNEAK	+1.14	+0.83	-0.10	+2.53	+3.03	+2.35

*) Meanwhile it has been found that the main reason for this discrepancy between the results for this two cross section sets comes from the fact that in the SNEAK-set and the succeeding ones the cross section U^{238} used for the determination of the background cross section σ_o -necessary for the calculation of the resonance-self-shielding- has been set equal to the potential cross section of 10.6 barns in the groups 10-21 whereas in the ABN-set the total cross sections are used for the corresponding values.

V.7.3.3. One-Dimensional Diffusion Calculations with Heterogeneity Corrected Cross Sections for two Core Zones

The ZERA-calculated Δk_{eff} of the central core-zone I is generally used for the correction of one-dimensional diffusion theory results. This method is justified, if the assembly may be well described by applying a fundamental mode calculation. A better approximation is the one-dimensional calculation of Δk_{eff} with ZERA-corrected cross sections. In our case the two zones have practically the same homogeneous composition, but a different structure of the unit cells. Therefore it seems to be interesting to check the ZERA-correction Δk_{eff} by calculating the same quantity in one-dimensional diffusion theory with ZERA-corrected cross sections for both core zones. Doing this a certain difficulty arises: The unit cell of core zone II is built by 36 platelets. A further splitting in subregions has become a question of calculation-time. Therefore we kept the normal structure using the actual platelet thickness for each region. We have justified this procedure by a test calculation in core zone I. Only a negligible change in Δk_{eff} of about $1 \cdot 10^{-5}$ which is within the accuracy limit was obtained changing from five subregions to one single region per platelet. Of course, this is valid only for the normal unit cell but not for bunching experiments.
In the following table the ZERA-results for each core zone and the one-dimensional radial diffusion result for the whole assembly are given.

SNEAK 3A1 Δk_{eff} [in units of 10^{-3}]

$B^2_{total} = 22.01 \cdot 10^{-4}$ cm^{-2}, $B^2_{axial} = 8.47 \cdot 10^{-4}$ cm^{-2}, SNEAK-set

ZERA-calc. Zone I	+1.14
ZERA-calc. Zone II	-0.06
Diff.-calc. whole assembly with ZERA-corrected cross sections in both core zones	+1.80

The differing ZERA-results for the two core zones demonstrate the necessity to determine Δk_{eff} at least by a real one-dimensional calculation using the ZERA-corrected cross sections for the two zones of different cell structure.

The somewhat surprising results of the preceding table are probably due to the fact that using the heterogeneity-corrected cross section the flux shape is slightly modified which is equivalent to a slight correction of the buckling for the ZERA-calculations.

Generally it will be not sufficient to take only ZERA-results for a central unit cell as heterogeneity correction for a one-dimensional k_{eff}.

V.7.4. Reaction Rate Ratios of Uranium for a Central Unit Cell of SNEAK 3A2 and their Dependence on the Degree of Bunching. Comparison with Experiments

The experimental data are reported in [65] Fig. 15 and [67] Fig. 15, Table 11. Some theoretical data are given there too, but they did not agree well with the experimental values.

In order to check the theoretical values and to get a deeper insight into the effect of the different nuclear data we re-determined these quantities by ZERA-calculations. The results of these calculations can be considered as representative for central reaction rate ratios, because in the middle of the core the macroscopic flux spectrum of diffusion calculations is in good agreement with the fundamental mode spectrum using a suitable buckling. Fig. 4 is presented in the same manner as has been done in [65] Fig. 15. We have only replaced the theoretical data.

In case of the $\sigma_f^{28}/\sigma_f^{25}$ ratio neither the ABN nor the SNEAK set are able to represent the experimental data. Both sets are completely unable to verify the dependence of the degree shown by the experiments. This leads us to the suspicion that the given experimental data are erroneous.

In case of the $\sigma_c^{29}/\sigma_f^{25}$ ratio the SNEAK set represents the experimental data better, although the theoretical points do not lie completely within the experimental errors.

A lowering of σ_f^{25} by about 6% for the normal cell or an increase by about the same amount for the bunched cells would result in a rather good agreement for these ratios between theory and experiment considering only the dependence on the degree of bunching.

V.7.5. Fine Structure of Reaction Rates

The comparison between ZERA-calculated data and the measured spatial distribution of reaction rates within a single platelet is suggested in the above mentioned references as a suitable method to check and improve the accuracy of cross sections. It was our aim to apply this method to the new group sets. Therefore we investigated the influence of various cross section sets on the rate distributions within the 20% enriched uranium platelet of 3A2 unit cell (zone I).

The results are given in Fig. 5A and Fig. 5B. All rates are normalized to one in the central subregion of the uranium platelets.

The most essential results and conclusions are the following ones:

a) For the new group sets all reaction rate cell traverses for U^{238} and U^{235} lie close together. But for U^{235} a large difference exists between these curves and that calculated using the ABN set. This is valid for fission rates as well as for capture rates of U^{235}.

b) The U^{235} reaction rate distributions calculated with the new group sets show so small differences, that a significant conclusion concerning the accuracy of cross sections seems to be impossible.

c) We feel that the differences in the normalized cell traverses for U^{238} are not so significant between the various group sets that definite conclusions can be drawn by comparing them with the experiment. Especially not because the shape of the curve is influenced by the two quantities, the infinite dilute cross section (σ_c^{∞}) and the resonance-self-shielding factors (f-factors). However, it seems to us that precise and reliable measurements of the central reaction rate ratio $\sigma_c^{28}/\sigma_f^{25}$ will give information on the correctness of the U^{238} capture data as can be seen from Fig. 4. This information will be additional and more unique than the information which can be obtained from a comparison of k_{eff} between theory and experiment.

V.7.6. General Conclusions

The most striking result of our investigations is the very large discrepancy between ZERA-calculated data using the ABN set on the one hand and using the more recently established sets on the other hand. Compared to this discrepancy the differences within the results of the new group sets are small, although considerable changes of cross sections exist between them. Therefore there seems to exist a fundamental difference between the old ABN- and the new sets and/or the treatment of these data by the ZERA-code.

Furthermore it seems to be impossible to come to a definite conclusion on cross section accuracy by evaluating the fine structure of reaction rates within normal, single or double bunched cell-regions. More information may become available by enlarging the heterogeneity and probably by considering in more detail the energy dependence of the neutron flux in special important energy regions.

V.8. Results of the S_N-calculations

In order to get a reliable value for the calculated multiplication factor which can be compared with the corresponding experimental one, we have to apply certain corrections to the multiplication factor resulting from calculations using diffusion theory for the homogenized material composition of the different zones of the assembly. An essential correction is the transport- or S_N-correction which takes into account the difference between an appropriate treatment of the neutron transport process and the usual diffusion approximation for this process. Although some of the transport corrections are given in the literature and were partially applied in our study, we wanted to have an independent check of these data. Therefore we evaluated for most of the assemblies that we have studied S_N-corrections by means of our own nuclear data and code. All calculations have been done in one-dimensional geometry with the code DTK [70], the Karlsruhe version of the well known DTF-IV-code [71, 72], using the 26 group SNEAK-set as nuclear data basis.* We have taken the original S_N constants as published in [71] on pages 135 up to 138.

Having had not much experience with the code at the beginning of the present work, first of all some studies have been undertaken to become more familiar with it. Mainly we have been interested in the question how to choose mesh-size and the order N of the S_N-calculations which are necessary to get a desired accuracy. The essential results of these studies are given in the section entitled "Comments on the S_N-calculations".

By using the results specified in the section mentioned above, we have done the calculations reported on in the section entitled "S_N-corrections for various assemblies".

Assuming that the one-dimensional S_N-corrections for the various space directions could be added up to give the final S_N-corrections, we also compare in this section the added up value with the S_N-correction for the equivalent spherical model of the assembly.

---

*) The calculations have been done on an IBM 360/65 with an Operating System providing multiprogramming with a variable number of tasks (MVT).

Comments on the S_N-calculations

First we will give some general remarks about the dimension and the numeration of zones. Unless otherwise stated the zone dimensions used by DTK-calculations are identical with those used in one dimensional diffusion calculations. Usually the zone denoted as zone 1 corresponds to the lower or inner part of the assembly.

We have assumed in this chapter that the reader is somewhat familiar with the notations used in the DTF-IV-code and therefore we will not explain all notations used here.

Before considering the influence of mesh size on the multiplication factor k_{eff}, we will discuss an effect, which in some circumstances can make the DTK calculated value not a good approximation for the real k_{eff}. The code determines k_{eff} in a sequence of eigenvalues from which the last one is assumed to be identical with k_{eff}, of course within the desired accuracy. In this sequence the new eigenvalue is obtained from the old one by multiplication of the latter one with a variable factor called λ. For illustration see table V-10a and table V-10b. The eigenvalue within a row has been determined by multiplicating the factor λ in the same row with the eigenvalue in the row above. The iteration process is stopped if $|\lambda-1|$ is less than or equal to ε, with ε being specified in the input by the user of the code.

After termination of the iteration process there is done a final step in which one more eigenvalue is calculated using the above described method. In most cases λ for this final step is closer to unity than the previous one. This non-oscillating convergence [*] of λ being the usual one is shown in table V-10a; ε has been specified to 10^{-5} so that the $|\lambda-1| \leq \varepsilon$ condition has been fulfilled after 10 outer iterations with $|\lambda-1| = 0.5 \cdot 10^{-5}$. The value of λ used in the final step is closer to unity than the previous one. In this case and if some other conditions, which will be discussed later, are also fulfilled, we can have much confidence that the last eigenvalue is a good approximation for k_{eff}.

But thereare some other cases; one of these is shown in table V-10b. The $|\lambda-1| \leq \varepsilon$ condition has been satisfied after 3 outer iterations because $|1-1.000\ 05| = 0.5 \cdot 10^{-4}$

---

[*] Non-oscillating means non-oscillating at the end and some steps before the end of the iteration process. For example, if you take the values of table V-10a, $|1-\lambda|$ converges monotonously to zero only after the third outer iteration.

is less than 10^{-4}, but using the last λ, $|\lambda-1|$ becomes greater than ε ($|\lambda-1| = 4.13\cdot10^{-4}>10^{-4}$). It is evident that in this case the last eigenvalue is not a good approximation for k_{eff} and we must check all results on the appearance of this effect.

Meanwhile DTK has been improved. In a first step there was given a detailed printing of the number of inner iterations for each energy group. If at the iteration break off the distribution of the inner iterations over the energy groups oscillates not too much and if in addition the number of iterations for one group is low, we may take this also as an indication that the last eigenvalue is a good approximation for k_{eff}. In a second step the possibility has been provided to use

a) Tschebyscheff extrapolation and

b) an improved guess for the source distribution.

Using Tschebyscheff extrapolation causes the effect that the convergence of λ is oscillating * so that the iteration may be terminated without having reached the desired accuracy for the eigenvalue. To exclude this possibility a new iteration break off condition of the form

$$\frac{1}{1.4}\{|1-\lambda_i| + |1-\lambda_{i-1}|\} < \varepsilon$$

with i being the outer iteration number has been introduced by the authors of /70/.

Besides ε, which is responsible for the accuracy of k_{eff}, it is possible to fix EPSA in the input of the code to determine the fluxes with a certain accuracy. But being primarily interested in k_{eff} we have not taken advantage of this possibility.

The following investigations on the influence of mesh size on the accuracy of k_{eff} were motivated by two reasons: a small number of mesh points saves computing time on the one hand and reduces possible numerical effects, e.g. round off errors, on the other hand. We have made our investigations for SUAK U1B respectively for SUAK UH1B. The results are shown in table V-11a and table V-11b and plotted in figure 6A and figure 6B. In figure 6A we have plotted the

*) We have seen that this may also be true if Tschebyscheff extrapolation is not used.

variation of k_{eff} versus the number of mesh intervals in zone 3, because this zone is identical with the core and the number of mesh intervals used in the other zones containing no fissionable material is changed most times proportional to the corresponding change in the core region.
Looking at table V-11a and figure 6A we can see that k_{eff} is increasing with rising mesh interval number. But the increment is small if we have more than 30 mesh intervals in zone 3.
Doing the same calculations in spherical geometry using the assembly SUAK UH1B (see table V-11b respectively figure 6B) one remarks only two facts different from the preceding results shown in table V-11a and figure 6A:

a) The part of the curve with small changes has a decreasing tendency *
   and
b) This part of the curve starts at about 20 mesh intervals.

The first difference is due to changed geometry whereas the second one is less significant as explained below. In the case of figures V-11a and V-11b we have taken in slab geometry in z-direction the total size of the assembly for the calculations because the configuration is not symmetric, whereas in spherical geometry only the radius of the sphere has been used. In order to have a correspondence between the two cases we would have to take in slab geometry only half the core height, so that the mesh interval number is halved and the part of the curve with small changes starts in figures 6A and 6B at the same number of mesh intervals. To overcome this difficulty we must not relate to the mesh interval number but to the mesh interval size.
To obtain a general rule for fixing the mesh interval size valid for all cases investigated here, we use the transport mean free path λ_{tr}. We have given the mesh interval axis in figures 6A and 6B a second notation measured in units of λ_{tr} divided by the mesh size. If this quantity has a value of about 3 there are only small changes in k_{eff}, if we increase the number of mesh intervals, so that a mesh interval size of about one third of λ_{tr} seems to be an appropriate value, at least if the assembly to be investigated is similar to SUAK U1B or SUAK UH1B. This rule has been confirmed by the negative results of all spot checks which we have made additionally.

---

*) Looking at table V-11b one may argue that this tendency is not true for higher mesh interval number. But the changes showing the opposite tendency are only of the order 10^{-5} which is less than the accuracy $\varepsilon=10^{-4}$ thereby used.

Having spherical or cylindrical geometry, one may suspect k_{eff} not bein quite correct because of the different size of volume elements at different radial positions * supposing an equal mesh spacing. In order to check this we divided the one zone homogenized SUAK U1B spherical core into 4 zones and varied the number of mesh intervals in this zones. The result of these investigations - listed in table V-12a - indicates that fortunately our suspicion has not proved right. Taking the same total number of mesh intervals k_{eff} remains unchanged within the first four digits although the largest volume elements in the various cases differ by a factor of 2, with the ratio of largest to smallest volume element being about 270. Only by increasing the total number of intervals (case 4 in table V-12a) we got an effect of the order 10^{-4}, but this can be understood if we remember figure V-11b: for spherical geometry an increase of the number of mesh intervals results at a certain point in a small decrease of k_{eff}.

We have done the investigations described above for cylindrical geometry too. The results - listed in table V-12b - also lead to the statement that the size of a volume element has no influence on the accuracy of k_{eff} if we only choose the mesh size properly, e.g. about one third of the transport mean free path.

Finally, we have studied the dependence of k_{eff} on the order N of the S_N-calculations. We have done this for various assemblies in different geometries. The results are listed in table V-13a upt to table V-13l and plotted in figure 7A up to figure 7L. Looking at the figures one may observe some general tendencies. If we compare all calculations done in slab geometry we recognize that k_{eff} computed with a quadrature order N=2 ($k_{eff}(S_2)$) is always considerably smaller than the rest of the values. Furthermore one can see that $k_{eff}(S_8)$, $k_{eff}(S_{12})$ and $k_{eff}(S_{16})$ are not much different from $k_{eff}(S_6)$, so that a quadrature order N=6 would have been sufficient**.

---

*) In our calculations the volume of inner and outer elements differ by a factor of up to 1000.

**) This statement of course is valid only for slab geometry and assemblies resembling those investigated in this report.

Comparing all calculations done in spherical and cylindrical geometry one remarks that $k_{eff}(S_2)$ is always much larger than the other values of k_{eff}. In addition $k_{eff}(S_N)$ is not becoming constant rapidly for higher orders of N, but still decreases slightly. If we exclude numerical effects we come to the conclusion that it is necessary to calculate with the highest possible quadrature order allowed by our present code in spherical and cylindrical geometry if k_{eff} should be determined with high accuracy.
Because computing time increases very rapidly for high order S_N-calculations, an improved version of DTK has been established by the authors of [70] by which we can calculate the high quadrature order $k_{eff}(S_N)$ within a small fraction of the time needed by the old version *. This is done by using

a) Tschebyscheff extrapolation and
b) the possibility to use the flux of a former case to get a reasonable guess for the source distribution of a successive calculation for example with increased order of N.

There are some values in tables V-13a to V-13l which have been determined in this manner. They are characterized by the small number of outer iterations. The effect of the reduction of computing time is remarkable; for example (see table V-13i) all given values of k_{eff} starting with $k_{eff}(S_2)$ up to $k_{eff}(S_{16})$ have been obtained within 8 minutes and 16 seconds, whereas using the previously applied method to compute only $k_{eff}(S_{12})$ has taken 10 minutes and 12 seconds. More examples for computing times are given in the tables V-13a to V-13l and if possible, comparisons between computing times obtained with the old and new version of the code.
We have compared our results with those given in [73] finding good agreement especially with respect to the dependence of k_{eff} on the quadrature order N for spherical and cylindrical geometry. There is given in [73] no calculation referring to slab geometry and the mesh interval dependence starts at 13 mesh intervals and is only given for cylindrical geometry so that a detailed comparison with respect to these items is not possible.

---

*) This improved version has been mentioned earlier in connection with the iteration break off condition.

On page 30 of [71] there has been made the statement "..., diffusion calculations are often more accurate than S_2-calculations". With respect to the assemblies analized in this report this statement is not valid for all geometries. If one looks at table V-14 one can see that only in spherical geometry the k_{eff}(diff)-value is closer to the $k_{eff}(S_N)$-value than the $k_{eff}(S_2)$-value. In cylindrical and especially in slab geometry the $k_{eff}(S_2)$-value is much more accurate than the diffusion calculated value of k_{eff}.

Summary

If we take into account only assemblies similar to those investigated here, we have to choose for the mesh size about one third of λ_{tr} to get a k_{eff} with sufficient accuracy. For slab geometry a quadrature order of N=6 is sufficient, whereas in spherical and cylindrical geometry N=6 may be sufficient when only three digits are important. If higher accuracy is desired higher quadrature order must be used for these two geometries. The different size of volume elements in non-slab geometry with equal mesh spacing has found to have practically no influence on the accuracy of k_{eff}. Other effects reported here have been taken into account by improvements in the code for example with respect to the convergence condition and the saving of computing time for higher order S_N-calculations.

S_N-corrections for various assemblies

The S_N-corrections for the assemblies ZPR-III-10, ZPR-III-25, ZPR-III-48, ZEBRA 6A, SNEAK 3A1, SNEAK 3A2, SUAK U1B and SUAK UH1B are given in table V-15a up to V-15h.

Before discussing the results we will make two remarks about mesh size and quadrature order. Not in all cases we have given the mesh size a value of about one third of λ_{tr}, because some of these calculations have been done before the first section of this report has been finished. But all mesh sizes are situated in such a range that the possible errors in k_{eff} are only about 0.0001 (see table V-11a and V-11b together with table V-15a to table V-15h).

As for the quadrature order we have taken in cylindrical and spherical geometry the maximal values allowed by the code *. In some cases we have computed S_{16}-values for k_{eff} also in slab geometry, but usually we have taken the S_6-values.

By table V-15a to table V-15h one can see that a S_N-correction has been necessary for all assemblies if one aims to come to an accuracy for the criticality of more than $1.0 \cdot 10^{-3}$. The S_N-corrections on k_{eff} decreases if the size of the assemblies increases. This statement agrees with the results given in [73].

In the part of this report entitled "Comments on the S_N-calculations", we have made the assumption that the one-dimensional S_N-corrections on k_{eff} for slab and cylindrical geometry - respectively at SUAK for slab geometry in all three space directions - could be added up to give the final S_N-correction. Comparing the added up values with the corresponding spherical values (all given in tables V-15a to V-15h) we see that our assumption is doubtful. It is true that there is agreement in the case of the assembly ZPR-III-25 but otherwise there are differences in the S_N-corrections between 8% and 21% even up to 60% for the SUAK-assemblies. The agreement in the ZPR-III-25 case may be fortuitous because due to calculating accuracy all k_{eff}-values are uncertain by one unit in the last digit given.

We tried to find a reason for the disagreement mentioned above. Our suspicion has been that an inappropriate boundary condition is used in the diffusion calculations especially in spherical geometry. To get an idea of the influence of the boundary condition we calculated k_{eff} for SUAK U1B with one-dimensional diffusion theory in spherical and slab geometry using two different boundary conditions: the first of these has been the ususally used condition

$$\frac{\phi'(a)}{\phi(a)} = -\frac{1}{0.7104 \cdot \lambda_{tr}}$$

and the second one has been

$$\phi(a+d) = 0$$

with $$d = 0.7104 \cdot \lambda_{tr}$$

*) N=8 for cylindrical and N=16 for spherical geometry.

The results listed in table V-16 demonstrate the correctness of our suspicion. There is little difference for the slab values (0.17%) but large difference for the spherical values (1.6%). If we take into account the uncertainty in the boundary condition the relative error between the added up value and the spherical value for SUAK U1B is reduced considerably. One may expect that the differences for the other assemblies will be reduced correspondingly.

The uncertainty in the boundary condition effects very much the criticality for the SUAK assemblies because these assemblies are small with respect to the other ones and are unreflected in two space directions so that differences in the extrapolated end point have a larger effect on k_{eff}.

Summary

We have to take into account for all assemblies studied here the S_N-corrections on k_{eff}, if we want to obtain an accuracy of better than 10^{-3}. The calculation of the S_N-corrections for spherical models may lead to values which differ from those obtained by adding up the corresponding one-dimensional S_N-corrections determined by using the assumption of separability of the flux in different space directions. But the difference can be attributed to a large extent to the uncertainty in the boundary condition for the diffusion calculation especially for spherical geometry.

Outer iteration number	Eigenvalue	Lambda
0	0.8810000	
1	0.8996826	0.8996818
2	0.8939858	0.9936674
3	0.8940460	1.000067
4	0.8944250	1.000423
5	0.8946577	1.000259
6	0.8947753	1.000131
7	0.8948326	1.000064
8	0.8948585	1.000029
9	0.8948715	1.000014
10	0.8948761	1.000005
11	0.8948799	1.000004

Assembly	SUAK UH1B
Geometry	sphere
Quadrature Order	6
Number of Zones	1
Number of Intervals	98
ε	10^{-5}

Table V-10a: Variation of Eigenvalues during outer iterations. Non-oscillating convergence of λ to 1 at the end of the iteration process.

Outer iteration number	Eigenvalue	Lambda
0	0.8810000	
1	0.8996648	0.8996638
2	0.8938476	0.9936436
3	0.8939926	1.000050
4	0.8943624	1.000413

Assembly	SUAK UH1B
Geometry	sphere
Quadrature Order	6
Number of Zones	1
Number of Intervals	98
ε	10^{-4}

Table V-10b: Variation of Eigenvalues during outer iterations. Oscillating convergence of λ to 1 at the end of the iteration process.

Number of mesh intervals total	Zone 1	Zone 2	Zone 3	Zone 4	k_{eff}	Outer iteration number	Last λ	Δk_{eff}
8	1	1	5	1	0.833436	11	1.000001	
								0.003176
16	2	2	10	2	0.836612	13	1.000003	
								0.000575
24	3	3	15	3	0.837187	14	1.000000	
								0.000198
32	4	4	20	4	0.837385	14	1.000003	
								0.000093
40	5	5	25	5	0.837478	14	1.000003	
								0.000048
48	6	6	30	6	0.837526	14	1.000001	
								0.000031
56	7	7	35	7	0.837557	14	1.000003	
								0.000033
63	6	6	45	6	0.837590	14	1.000003	
								0.000031
130	10	10	100	10	0.837621	13	1.000003	

Assembly	SUAK U1B
Geometry	plane in z-direction
Quadrature Order	8
ε	10^{-5}

Table V-11a: Variation of k_{eff} with the number of mesh intervals. Zone 3 is identical with the core.

Number of mesh intervals	k_{eff}	Outer iteration number	Last λ	Δk_{eff}
3	0.889086	10	0.9999713	
				0.003637
4	0.892723	10	0.9999589	
				0.001084
5	0.893807	10	0.9999659	
				0.000516
6	0.894323	10	0.9999690	
				0.000380
8	0.894703	9	0.9999572	
				0.000130
10	0.894833	9	0.9999662	
				0.000101
15	0.894934	8	0.9999708	
				0.000007
20	0.894941	7	0.9999794	
				-0.000057
25	0.894884	6	0.9999876	
				-0.000035
30	0.894819	6	1.000016	
				-0.000023
50	0.894796	7	1.000044	
				-0.000008
60	0.894788	7	1.000049	
				+0.000012
80	0.894805	8	1.000032	

Assembly	SUAK UH1B
Geometry	sphere
Quadrature Order	6
ε	10^{-4}

Table V-11b:
Variation of k_{eff} with the number of mesh intervals.

Zone	Right boundary [cm]	Number of intervals	Smallest volume element [cm^3]	Largest volume element [cm^3]	Total number of intervals	k_{eff}	Outer iteration number	Last λ
1	8.000	5	17.157	1046.592				
2	13.000	15	279.408	689.908				
3	16.000	40	160.199	240.145				
4	19.364	50	217.329	315.896	110	0.836799	14	1.000004
1	8.000	5	17.157	1046.592				
2	13.000	10	427.780	1021.541				
3	16.000	40	160.198	240.145				
4	19.364	55	197.474	287.271	110	0.836801	14	1.000004
1	8.000	10	2.145	581.202				
2	13.000	20	207.410	520.784				
3	16.000	35	183.233	274.264				
4	19.364	45	241.564	350.875	110	0.836772	14	1.000004
1	8.000	20	0.268	305.881				
2	13.000	30	136.853	349.432				
3	16.000	80	79.867	120.353				
4	19.364	100	108.389	158.188	230	0.836704	14	1.000004

Geometry	sphere
Quadrature Number	8
ε	10^{-5}

Table V-12a: SUAK U1B. Varying size of volume elements in spherical geometry.

Mesh intervals in Zone					Smallest and largest volume element in zone				$k_{eff}(S_N)$	Outer iteration number	Last λ
1	2	3	4	5	2	3	4	5			
10	21	9	31	19	40.322 88.998	217.298 323.467	127.139 185.301	306.498 399.387	0.970423	3	1.000007
10	19	11	29	21	44.708 98.223	176.803 265.643	135.977 198.002	277.084 361.582	0.970446	3	1.000004
10	17	13	27	23	50.164 109.585	149.024 225.354	146.139 212.582	252.818 330.301	0.970485	3	1.000001
10	15	15	25	25	57.133 123.915	128.786 195.672	157.941 229.486	232.467 304.004	0.970559	5	0.9999862
10	13	17	23	27	66.346 142.556	113.388 172.902	171.815 249.297	215.145 281.586	0.970423	3	1.000011
10	11	19	21	29	79.091 167.794	101.277 154.875	188.361 272.856	200.217 262.244	0.970419	3	1.000009
10	9	21	19	31	97.871 203.876	91.502 140.252	208.436 301.336	187.240 245.404	0.970418	3	1.000011

Smallest and largest volume element in zone 1	
3.14159	59.69019

Table V-12b: Varying size of volume elements in cylindrical geometry.
All volumes are given in cm^3.

Assembly	ZEBRA 6A
Geometry	cylinder
Quadrature Order	6
ε	10^{-4}
Right boundaries of zones /cm/	
10.00 23.07 36.15 53.37 70.59	
Total number of mesh intervals	90

Order N of S_N-calculation	k_{eff}	Outer iteration number	Last λ
2	0.832344	13	1.000002
4	0.838085	14	1.000002
6	0.837627	14	1.000001
8	0.837590	14	1.000003
12	0.837633	14	1.000003
16	0.837679	14	1.000001

Assembly	SUAK U1B
Geometry	slab in z-dir.
ε	10^{-5}
Zone	Mesh intervals
1	6
2	6
3 core	45
4	6

Table V-13a: Variation of k_{eff} with the quadrature order.

Order N of S_N-calculation	k_{eff}	Outer iteration number	Last λ
2	0.961550	16	1.000009
4	0.960804	4	1.000048
6	0.960128	5	0.9999885
8	0.959984	4	0.9999909

Assembly	ZPR-III-48
Geometry	cylinder
ε	10^{-4}
Zone	Mesh intervals
1	40
2	20

Total DTK computing time for all k_{eff} values (with improved code):
5 min 59 sec

Table V-13b: Variation of k_{eff} with the quadrature order.

Order N of S_N-calculation	k_{eff}	Outer iteration number	Last λ
2	0.971194	12	1.000038
4	0.961985	12	1.000032
6	0.961506	12	1.000034
8	0.961363	12	1.000034
12	0.961175	12	1.000032
16	0.961096	12	1.000035

Assembly	ZPR-III-48
Geometry	sphere
ε	10^{-4}
Zone	Mesh intervals
1	10
2	30
3	20

Table V-13c: Variation of k_{eff} with the quadrature order.

Order N of S_N-calculation	k_{eff}	Outer iteration number	Last λ
2	0.977436	13	1.000038
4	0.979326	13	1.000047
6	0.979125	13	1.000047
8	0.979111	13	1.000048
12	0.979116	13	1.000047
16	0.979127	13	1.000046

Assembly	ZPR-III-10
Geometry	slab
ε	10^{-4}
Zone	Mesh intervals
1	10
2	13
3	27

Table V-13d: Variation of k_{eff} with the quadrature order.

Order N of S_N-calculation	k_{eff}	Outer iteration number	Last λ
2	0.985757	17	1.000008
4	0.985199	4	1.000037
6	0.984156	5	0.9999980
8	0.983928	4	0.9999895

Assembly	ZPR-III-10
Geometry	cylinder
ε	10^{-4}
Zone	Mesh intervals
1	10
2	20
3	30

Computing times	
old method S_2 and S_4	improved method S_2 and S_4 and S_6 and S_8
5 min 12 sec	5 min 43 sec

Table V-13e: Variation of k_{eff} with the quadrature order.

Order N of S_N-calculation	k_{eff}	Outer iteration number	Last λ
2	1.000214	8	1.000001
4	0.988320	7	1.000015
6	0.987458	5	1.000007
8	0.987207	4	0.9999957
12	0.986970	7	1.000021
16	0.986848	3	0.9999930

Assembly	ZPR-III-10
Geometry	sphere
ε	10^{-4}
Zone	Mesh intervals
1	10
2	25
3	25

Computing time for S_2 up to S_{16}:

5 min 46 sec

Table V-13f: Variation of k_{eff} with the quadrature order.

Order N of S_N-calculation	k_{eff}	Outer iteration number	Last λ
2	0.970277	17	1.000053
4	0.970814	17	1.000058
6	0.970746	17	1.000057
8	0.970750	17	1.000057
12	0.970750	17	1.000058
16	0.970751	17	1.000058

Assembly	ZPR-III-25
Geometry	slab
ε	10^{-4}
Zone	Mesh intervals
1	8
2	24
3	18

Table V-13g: Variation of k_{eff} with the quadrature order.

Order N of S_N-calculation	k_{eff}	Outer iteration number	Last λ
2	0.972167	19	1.000061
4	0.971906	19	1.000060
6	0.971592	19	1.000058
8	0.971546	19	1.000058

Assembly	ZPR-III-25
Geometry	cylinder
ε	10^{-4}
Zone	Mesh intervals
1	8
2	30
3	22

Table V-13h: Variation of k_{eff} with the quadrature order.

Order N of S_N-calculation	k_{eff}	Outer iteration number	Last λ
2	0.976101	17	1.000038
4	0.972702	8	1.000006
6	0.972421	4	0.9999971
8	0.972380	3	0.9999982
12	0.972336	3	0.9999973
16	0.972320	3	0.9999968

Assembly	ZPR-III-25
Geometry	sphere
ε	10^{-4}
Zone	Mesh intervals
1	15
2	45
3	30

Computing time for S_2 up to S_{16}	
Old Method	Improved Method
46 min.	8 min. 16 sec.

Table V-13i: Variation of k_{eff} with the quadrature order.

Order N of S_N-calculation	k_{eff}	Outer iteration number	Last λ
2	0.965114	11	1.000023
4	0.967606	11	1.000026
6	0.967313	11	1.000026
8	0.967293	11	1.000027
12	0.967290	11	1.000024
16	0.967305	11	1.000026

Assembly	ZEBRA 6A
Geometry	slab
ε	10^{-4}
Zone	Mesh intervals
1	25
2	20

Table V-13j: Variation of k_{eff} with the quadrature order.

Order N of S_N-calculation	k_{eff}	Outer iteration number	Last λ
2	0.972010	12	1.000032
4	0.971387	12	1.000026
6	0.970364	12	1.000027
8	0.970182	12	1.000027

Assembly	ZEBRA 6A
Geometry	cylinder
ε	10^{-4}
Zone	Mesh intervals
1	6
2	40
3	30

Table V-13k: Variation of k_{eff} with the quadrature order.

Order N of S_N-calculation	k_{eff}	Outer iteration number	Last λ
2	0.985999	12	1.000032
4	0.973833	12	1.000028
6	0.973125	12	1.000025
8	0.972899	12	1.000025
12	0.972625	12	1.000026
16	0.972510	12	1.000026

Assembly	ZEBRA 6A
Geometry	sphere
ε	10^{-4}
Zone	Mesh intervals
1	8
2	32
3	20

Table V-131: Variation of k_{eff} with the quadrature order.

Assembly	Geometry	$k_{eff}(S_N)-k_{eff}(diff)$	N	$k_{eff}(S_2)-k_{eff}(S_N)$
ZPR-III-48	cylinder	0.0050	8	0.0016
	sphere	0.0061	16	0.0101
ZPR-III-10	slab	0.0039	16	-0.0017
	cylinder	0.0087	8	0.0019
	sphere	0.0116	16	0.0134
ZPR-III-25	slab	0.0008	16	-0.0005
	cylinder	0.0015	8	0.0007
	sphere	0.0023	16	0.0038
ZEBRA 6A	slab	0.0043	16	-0.0022
	cylinder	0.0072	8	0.0018
	sphere	0.0095	16	0.0135

Table V-14: Comparing diffusion calculated k_{eff} values with S_N calculated k_{eff} values for various assemblies and different geometries.

Assembly: ZPR-III-10				λ_{tr} = 3.663 cm			
Geometry and Buckling	k_{eff} (one-dim.diff.)	Zone	Mesh Interval	Right Boundary (cm)	Mesh Size (cm)	Quadrature order and k_{eff} (S_N)	Increase
		1	10	10.0	1.000	N=16	
slab	0.9752	2	13	22.95	0.996		
$57.534 \cdot 10^{-4}$		3	27	55.95	1.222	0.9791	0.0039
		1	10	10.0	1.000	N=8	
cylinder	0.9752	2	20	22.11	0.606		
$23.839 \cdot 10^{-4}$		3	30	63.59	1.383	0.9839	0.0087
		1	10	10.0	1.000	N=16	
sphere	0.9752	2	25	25.011	0.600		
-		3	25	62.011	1.480	0.9868	0.0116

Increase(sphere)	increase (slab) + increase (cylinder)	Difference	Relative error
0.0116	0.0126	0.0010	7.9%

Table V-15a: S_N-Corrections for ZPR-III-10.

Assembly: ZPR-III-25				λ_{tr} = 3.267 cm			
Geometry and Buckling	k_{eff} (one-dim.diff.)	Zone	Mesh Intervals	Right Boundary (cm)	Mesh size (cm)	Quadrature order and k_{eff} (S_N)	Increase
		1	8	10.0	1.25	N=16	
slab		2	24	38.175	1.174		
$20.981 \cdot 10^{-4}$	0.9700	3	18	68.675	1.694	0.9708	0.0008
		1	8	10.0	1.25	N=8	
cylinder		2	30	42.6	1.087		
$10.744 \cdot 10^{-4}$	0.9700	3	22	83.4	1.855	0.9715	0.0015
		1	15	10.0	0.667	N=16	
sphere		2	45	45.753	0.795	0.795	
-	0.9700	3	30	82.753	1.233	0.9723	0.0023

Increase (sphere)	Increase (slab) + increase (cylinder)	Difference	Relative error
0.023	0.0023	0.0000	0.0%

Table V-15b: S_N-Corrections for ZPR-III-25.

Assembly: ZPR-III-48				λ_{tr} = 4.741 cm			
Geometry and Buckling	k_{eff} (one-dim.diff.)	Zone	Mesh Intervals	Right Boundary (cm)	Mesh Size (cm)	Quadrature order and k_{eff} (S_N)	Increase
slab		1	30	38.180		N=6	
$18.132 \cdot 10^{-4}$	0.9549	2	20	68.660		0.9576	0.0027
cylinder		1	40	41.58	1.040	N=8	
$8.8832 \cdot 10^{-4}$	0.9550	2	20	71.58	1.500	0.9600	0.0050
		1	10	10.00	1.000	N=16	
sphere		2	35	45.213	1.006		
-	0.9550	3	15	75.213	1.500	0.9611	0.0061

Increase (sphere)	Increase (slab) + increase (cylinder)	Difference	Relative error
0.0061	0.0077	0.0016	20.8%

Table V-15c: S_N-corrections for ZPR-III-48.

Assembly: ZEBRA 6A				λ_{tr} = 4.810 cm			
Geometry and Buckling	k_{eff} (one-dim.diff.)	Zone	Mesh Intervals	Right Boundary (cm)	Mesh Size (cm)	Quadrature order and $k_{eff}(S_N)$	Increase
slab		1	25	30.08	1.203	N=16	
22.178	0.9630	2	20	60.50	1.521	0.9673	0.0043
		1	6	10.0	1.667	N=8	
cylinder		2	40	36.15	0.654		
12.418	0.9630	3	30	70.59	1.148	0.9702	0.0072
		1	8	10.0	1.250	N=16	
sphere	0.9630	2	32	38.203	0.881		
-		3	20	72.643	1.722	0.9725	0.0095

Increase (sphere)	Increase (slab) + increase (cylinder)	Difference	Relative error
0.0095	0.0115	0.0010	8.7%

Table V-15d: S_N-corrections for ZEBRA 6A.

Assembly: SNEAK 3A1				λ_{tr} = 4.230 cm			
Geometry and Buckling	k_{eff} (one-dim.diff.)	Zone	Mesh Intervals	Right Boundary (cm)	Mesh Size (cm)	Quadrature order and $k_{eff}(S_N)$	Increase
slab		1	30	40.27	1.342	N=6	
$13.540 \cdot 10^{-4}$	0.9902	2	20	70.77	1.525	0.9917	0.0015
		1	4	5.000	1.250		
		2	21	32.900	1.329	N=8	
cylinder		3	15	51.200	1.220		
$8.4696 \cdot 10^{-4}$	0.9902	4	25	80.859	1.186	0.9925	0.0023
		1	30	39.231	1.308	N=16	
sphere		2	10	52.684	1.345		
-	0.9911	3	22	82.343	1.348	0.9942	0.0031

Increase (sphere)	Increase (slab) + increase (cylinder)	Difference	Relative error
0.0031	0.0038	0.0007	18.4%

Table V-15e: S_N-corrections for SNEAK 3A1.

Assembly: SNEAK 3A2				λ_{tr} = 4.173 cm			
Geometry and Buckling	k_{eff} (one-dim.diff.)	Zone	Mesh intervals	Right Boundary (cm)	Mesh Size (cm)	Quadrature order and $k_{eff}(S_N)$	Increase
slab		1	35	40.27	1.151	N=6	
$16.949 \cdot 10^{-4}$	0.9827	2	20	70.77	1.525	0.9842	0.0015
		1	4	5.000	1.250		
cylinder		2	25	33.760	1.150	N=8	
		3	8	44.660	1.363		
$8.5998 \cdot 10^{-4}$	0.9828	4	30	80.859	1.207	0.9856	0.0028
sphere		1	30	40.094	1.336	N=16	
		2	8	48.315	1.028		
-	0.9837	3	30	84.515	1.207	0.9875	0.0038

Increase (sphere)	Increase (slab) + increase (cylinder)	Difference	Relative error
0.0038	0.0043	0.0005	11.6%

Table V-15f: S_N-corrections for SNEAK 3A2.

Assembly: SUAK U1B				λ_{tr} = 3.567 cm			
Geometry and Buckling	k_{eff} (one-dim.diff.)	Zone	Mesh intervals	Right Boundary (cm)	Mesh Size (cm)	Quadrature order and $k_{eff}(S_N)$	Increase
		1	3	3.0	1.000		
slab in z-dir.		2	4	6.5	0.875	N=6	
		3	36	41.6	0.975		
$139.601 \cdot 10^{-4}$	0.8237	4	3	44.6	1.000	0.8376	0.0139
slab in x-dir. $128.097 \cdot 10^{-4}$	0.8238	1	33	32.3	0.979	N=6 0.8324	0.0086
sphere	0.8237	1	18	19.364	1.076	0.8361 N=16	0.0124

Increase (sphere)	Increase (slab z-dir.) + increase (slab x-dir.)	Difference	Relative error
0.0124	0.0311	0.0187	60.1%

Table V-15g: S_N-corrections for SUAK U1B.

Assembly: SUAK UH1B				λ_{tr} = 3.358 cm			
Geometry and Buckling	k_{eff} (one-dim.diff.)	Zone	Mesh Intervals	Right Boundary (cm)	Mesh Size (cm)	Quadrature order and $k_{eff}(S_N)$	Increase
		1	3	3.0	1.000		
slab in z-dir.		2	4	6.5	0.875	N=6	
$141.314 \cdot 10^{-4}$		3	34	39.55	0.972		
	0.8807	4	3	42.55	1.000	0.8942	0.0135
slab in x-dir. $134.681 \cdot 10^{-4}$	0.8808	1	32	32.3	1.009	N=6 0.8891	0.0083
sphere	0.8808	1	18	19.087	1.060	0.8937 N=16	0.0129

Increase (sphere)	Increase (slab z-dir.) + 2·increase (slab x-dir.)	Difference	Relative error
0.0129	0.0301	0.0172	57.1%

Table V-15h: S_N-corrections for SUAK UH1B.

Geometry	Boundary Condition	k_{eff}	Difference
sphere	(1) a = 19.364 cm	0.823752	-0.015595
	(2) d = 2.534 cm	0.808157	
slab in x-direction	(1) a = 16.15 cm	0.824127	0.001661
	(2) d = 2.534 cm	0.822466	

Assembly	SUAK U1B
Boundary conditions	
(1) $\phi'(a)/\phi(a) = -1/(0.7104 \cdot \lambda_{tr})$	
(2) $\phi(a+d) = 0$	
a = boundary of the assembly	
$d = 0.7104 \cdot \lambda_{tr}$	

Table V-16: k_{eff} determined by diffusion calculations with various boundary conditions.

VI. GENERAL DISCUSSION AND CONCLUSIONS

Most of the criticality changes observed during the present study are smaller than 0.01 as can be seen from table V-1 and table V-4. This means that some modifications of the nuclear data can totally, others at least for a number of assemblies partially be regarded simply as an inclusion of more recent improved microscopic cross section information into our group sets. Of course these less important modifications provide valuable information on the sensitivity of integral parameters on changes in the differential microscopic data.

The detailed information contained in table V-4 has been summarized in table VI-1. In this table the mean deviation between the measured and best available calculated criticality values for the 12 assemblies studied is given for each of the different group sets used. The corresponding root mean square or standard deviation is also given in table VI-1. This table gives immediately a general impression of the capability of the different group sets to predict correctly the criticality of the variety of assemblies studied. It shows that at least with respect to criticality the MØXTØT-set is preferable to all the other group sets which have been established during this study, a result which of course could have been obtained also by looking at the results of table V-4.

In this general discussion the important effects of the changes in the nuclear data will be summarized. At first the situation at the beginning of the present study that means the results obtained with our reference-set, the so-called SNEAK-set, will be analysed. The most obvious fact is that with this set all assemblies are calculated underreactive. The region of deviation extends from approximately zero to -3% with the exception of ZPR III-55 with an underprediction of criticality by more than 4%. The mean criticality deviation amounts to 1.7% as can be seen from table VI-1. The small assemblies fuelled with U235, i.e. SUAK U1B and ZPR III-10 are well predicted, the subcriticality being less than 0.5%. The hydrogen containing assembly SUAK UH1B represents one exception which is probably caused by insufficient calculational methods, the other exception is the

larger assembly ZPRIII-25 with its relatively large U238 content. As has been known before [2] the SNEAK-3A assemblies, that means large U235 fuelled systems with soft neutron spectra, are calculated slightly underreactive, 3A1 by 0.6% and 3A2 by 1.1%. For the mixed fuelled assembly SNEAK 3B2 an even larger underprediction of 1.6% has been obtained which is an indication that the worth of Pu239 compared to that of U235 is underpredicted by the SNEAK-set. The same tendency is shown by the normal Pu-fuelled assemblies ZEBRA 6A, ZPR III-48 and ZPR III-48B which have been calculated 2-3% underreactive. Out of the two k_∞-experiments ZPR III-55 is predicted more subcritical, SNEAK 5C less subcritical than the normal Pu-fuelled systems. With respect to the latter experiment it seems very probable that the heterogeneity correction is calculated too large. Therefore the result is rather doubtful and should not be taken too seriously.

As a first change of the nuclear data we included the so-called PMB-data that means between 10 - 500 keV the lower capture data for U238 and the low fission and capture data for U235 as given by PÖNITZ and others. Our results with the SNEPMB-set confirmed the conclusions of similar earlier studies [2] namely:
Because of the lower U238 capture data the reactivity of the Pu-fuelled assemblies increases. This effect is particularly pronounced for ZPR III-55. For the U235-fuelled assemblies the reactivity decreases. This result indicates that the effect of the reduction of U235 fission overcompensates the effect of the reduction of U238 capture. It is most pronounced for the assemblies with hard neutron spectra.
With the SNEPMB-set most of the assemblies are calculated about 1%-2% underreactive. Following the conclusions presented in [2] we then decided to keep only the low U238 capture data and to return from the low PÖNITZ to the higher WHITE U235 fission and capture data. This led to the SNEAPM-set which predicts the criticality of U235-fuelled systems rather well. A drastic decrease of the mean criticality deviation and a considerable decrease of the root mean square criticality deviation can be seen in table VI-1.

In the next step we improved the α(Pu) values by including the Pu-α-measurements of GWIN et al. into our group set (PU9SCP-set). As expected, this change caused an increased underprediction of the criticality for the Pu-

systems, especially for the k_∞-experiments.

In the SCTALO-set new data are used for the inelastic scattering matrix of most isotopes which have been calculated by ourselves using the data of the KEDAK-file and evaporation spectra (see Appendix I). The spectra of the inelastically scattered neutrons are in general somewhat softer than the ABN-spectra used before. The criticality changes obtained are generally small. Only for ZPR III-25 and ZPR III-55 the effect is more pronounced due to the special energy dependence of the adjoint flux for these assemblies (see chapter III).

The next two changes have a rather small effect on criticality. The changes in the LA fission data for U235, U238 and Pu239 above 2 MeV leading to the UPUCOR-set cause a general reduction of criticality by only about 0.3% - 0.4%. Also the new cross sections for the higher plutonium isotopes in the PUO2RE-set which replace the old Russian ABN-data used up to now result in rather small criticality changes of about 0.3%.

As expected, a rather large effect is caused by the inclusion of the MOXON-data for the U238 capture cross section. The replacement has been done in two steps. The effect on criticality of the replacement of the previously used Pönitz values in the groups 9-11, i.e. from 10 to 100 keV (MØX911-set) is generally of the order of +1%. The assemblies with high U238 content, namely ZPR III-25 and ZPR III-55 show an even larger reactivity increase. The additional replacement of the U238 capture data below 10 keV by the Moxon data (MØXTØT-set) causes for assemblies with hard neutron spectra a negligible reactivity effect, for assemblies with somewhat softer spectra the criticality increases by 0.5 to 1%. For the k_∞-experiments studied here with still softer spectra the increase is about 1.5%.

It seems worthwhile to mention that the inclusion of the low U238 capture data resulted in an overestimation of the criticality at least for U-fuelled assemblies.

Let us now analyse the situation with the MØXTØT-set which is the final cross section set considered in this study. All assemblies are within a ±2% region of deviation between calculated and measured criticality. The mean criticality deviation of 0.0022 and the root mean square a criticality deviation of 0.0125 given in table VI-1 are the most favourable results obtained in the present study. Furthermore it is encouraging that there is nearly a clear

separation in the k_{eff}-results for U- and Pu-fuelled assemblies, Pu<1.0, U>1.0, the exceptions (SUAK UH1B and SNEAK 5C) being most probably due to deficiencies in the calculational methods. This means that according to the fissile material used, it will be possible to predict the probable deviation between calculated and measured criticality for reactors whose composition and neutron spectrum are similar to the presently studied assemblies. The remaining uncertainty will be in most cases far less than the ±2% deviation mentioned above.

With respect to the calculational methods two facts are of major concern and need an improved treatment: (1) For the assembly SUAK UH1B the anisotropic scattering of hydrogen and a more appropriate weighting spectrum for the generation of group constants for the elastic slowing down should be taken into account. (2) For SNEAK-5C, the corrections applied are rather large (about 9%). The largest part is due to heterogeneity, about 7%, and should be further investigated both experimentally and theoretically. In addition, the rather large REMO-correction of about 2% suggests to study whether a more appropriate weighting spectrum should be used for the generation of group constants for the elastic moderation especially below 1 keV. For this soft spectrum system a considerable part of the neutrons has energies below 1 keV; here the REMO-correction cannot be applied with the presently available code. In the near future the correctness of diffusion calculations using 26 energy groups for the criticals studied here will be checked by P1-calculations using about 200 groups. Major attention will then be given to the determination of the diffusion constant for 26 groups which usually can be calculated only in an approximate manner as explained in [4].

With respect to the nuclear data basis the following conclusions can be drawn for the MØXTØT-set:

(1) The fuel-mixture PU239-U238 is predicted underreactive whereas for the U235-U238 fuel mixture the criticality is overestimated. These facts whose consequences are discussed more extensively later on in this chapter almost obviously lead to the very probable conclusion that Pu239 is underreactive. A too low Pu239 fission cross section is also indicated by the underprediction of both the central material worth ratios and the ratios of the central fission rates of Pu239 to U235 in ZPR III-48 and 48B (table V-7 and V-9). The Pu239 α-data of

GWIN cannot be considered final at the present time but it seems that only minor changes in the α-data will have to be expected in the near future. The α-values presently used require a change in the resonance parameters compared to the parameters used before. This means that we have still to determine new resonance self-shielding factors (f-factors) for Pu239 based on resonance parameters compatible with the Gwin α-values.

For U235 the situation seems not to be so unequivocal. The overestimation of the criticality of U235-U238 fuel mixtures can be caused either by too large U235 fission cross sections or by too small U238 capture cross sections. Very probably our decision will be not to change the U235 fission data at the present time because the uncertainty in the U238 capture data is still too large so that some changes (slight increase) of these data will be sufficient to diminish the present discrepancy in the criticality prediction for the U235-U238 fuelled systems without any change in the U235 fission data. Pu-fuelled systems will then become even more under-reactive. In the preceding work [2] it was already indicated that the measurements of de Saussure for the γ-values of U235 below 300 eV should be included. Since the effect for the assemblies studied here is expected to be of minor importance (perhaps with the exception of the steam density coefficient for the SNEAK-3A-series), this change together with the corresponding changes in the f-factors has been postponed to the future work.

For U238 the situation is still more complicated. As explained in chapter II there are some doubts as to the reliability of the absolute magnitude of the MOXON-data for U238 capture. They are lower than most of the available 30 and 65 keV measurements. Furthermore in the region between 100 and 800 keV the MØXTØT set still contains the Pönitz data which are lower than the Barry data in this range and do not join smoothly to the Barry data used above 800 keV.

In any case it seems to be quite evident that the capture cross section used for the SNEAK-set is too large and has to be reduced; it may be that this has been slightly overdone by the inclusion of the MOXON-data. Besides the indication from the criticality of U-fuelled assemblies this can be deduced by comparing the experimental results for the ratio σ_c U238/σ_f U235 for ZPR III-48 and SNEAK 3A2 and the material worth ratio of U238 to U235 for ZPR III-48 and SNEAK 3A1 with the corresponding theoretical results obtained

with the MØXTØT-set. Therefore it seems probable that in a further step the U238 capture data will be changed slightly. Hopefully such a change which will be based essentially on differential data will lead to a slight increase of the capture rate of U238 compared to the result with the MØXTØT-set but will not be so marked as to bring about a result as large as that obtained with the SNEAK-set.

In any case the change in the capture cross section corresponds to a change in the resonance parameters. Therefore it will be necessary in a further step to determine new f-factors using resonance parameters which are in accordance with the capture cross section of U238.

The influence of cross section uncertainties of the higher Pu-isotopes on the criticality of the systems studied is not very pronounced. Even by comparing k_{eff} for ZPR III-48 with that for ZPR III-48B which has an inner zone with considerably larger Pu240-concentration one is not able to draw firm conclusions on the correctness of the nuclear data for Pu240 because this inner zone is still too small. This fact has also been observed by PITTERLE [74]. One should mention, however, that the inclusion of the new data has brought the prediction of the material worth of Pu240 for both assemblies in agreement with measurement within the admittedly large range of experimental uncertainty (tables V-7 and V-9). Using the old ABN-data the calculated value was lower by a factor of about 4. With our new data we attained a considerable improvement but it is obvious that the criticality of presently available plutonium fuelled assemblies does not provide a check which allows a definite conclusion on the correctness of the unclear data for the higher Pu-isotopes. For this purpose more specific precise experiments have to be performed. The measurements of OOSTERKAMP reported in [40] (see also [48]) can be considered as an example of this sort of experiments.

In our opinion the correctness of the data for the inelastic scattering cannot be judged definitely on the basis of the presently available information. Criticality of the assemblies studied in this work provides no sufficient information. Other experimental information e.g. reaction rates of materials with a fission threshold cannot be considered very reliable because the chamber measurements cannot be compared easily with calculations which are mostly done for homogeneous mixtures. Furthermore

the foil measurements for the U235 fission rate traverse within a cell cannot be well predicted by the heterogeneity code ZERA; it may be that this disagreement is not caused by the nuclear data used in the group sets, but is due to reasons inherent to the code itself. Since the heterogeneous U235 fission rate has to be used for the determination of the fission rate ratio of U238 to U235 the theoretical result is somewhat doubtful. A thorough examination of the ZERA-code would be helpful in this respect.
Further detailed investigations of the neutron energy spectrum might help to check the correctness of the nuclear data for inelastic scattering.

In conclusion it is expected that by the future changes and improvements mentioned before the uncertainty region for the criticality prediction which is now ±2% can be narrowed hopefully to ±1%.
Certain improvements in the calculational methods are indicated e.g. the anisotropy of the elastic slowing down of hydrogen should be taken into account in the S_N-calculations and the influence of an appropriate weighting spectrum on the removal group constants should be considered for SUAK UH1B and SNEAK 5C. As has been stated before a reinvestigation of the ZERA-code for heterogeneous calculations seems to be necessary. This will be essential for the more correct determination (1) of the criticality for SNEAK 5C, (b) of heterogeneous reaction rates in this assembly and e.g. in SNEAK 3A2, (c) of bunching experiments in SNEAK 3A1 and SNEAK 3A2, (d) rather probably also of the steam density coefficient for the SNEAK-3A-series.
For the quantities which have been studied besides the criticality the following items seem to be important:

(α) For the calculation of material worth more refined codes than the usually used first order perturbation theory should be applied which take into account the effect of sample size (see e.g. [64]) or the effect of the heterogeneous structure of the environment (see e.g. [48].

(β) For the calculation of central reaction rates an improved heterogeneity code should be available as indicated just before.

(γ) For the calculation of reaction rate traverses especially in the blanket transport theory should be used. At present the agreement between theory and experiment can be considered fairly good when the MØXTØT-set and transport theory are used. Perhaps slight modifications of the transport or total cross section of U238 or of the structural materials in the energy region 200 keV - 2 MeV will help ro reduce the existing rather small discrepancies.

(δ) With respect to the neutron importance more experimental information and perhaps more appropriate calculational methods seem to be necessary.

The important results and conclusions of the heterogeneity- and S_N-calculations have already been summarized at the end of the corresponding paragraphs in the preceding chapter V and will not be repeated here.

VII. APPENDIX I

Documentation of the new group constants

I.1 Modified group cross sections

Table AI-1 SNEAPM-set

Group	ΔE	$\sigma_\gamma(U^{238})$(b) SNEAK	SNEAPM
6	400 - 800 KeV	0.134	0.121
7	200 - 400	0.138	0.127
8	100 - 200	0.190	0.164
9	46.5- 100	0.286	0.282
10	21.5- 46.5	0.471	0.457
11	10.0- 21.5KeV	0.728	0.630

Table AI-2 SNEPMB-set

Group	ΔE	$\sigma_f(U^{235})$(b) SNEAK	SNEPMB	$\sigma_\gamma(U^{235})$(b) SNEAK	SNEPMB
7	200 - 400 KeV	1.32	1.154	0.227	0.199
8	100 - 200	1.53	1.337	0.375	0.322
9	46.5- 100	1.80	1.667	0.569	0.531
10	21.5 46.5KeV	2.22	2.150	0.794	0.772

Table AI-3 PU9SCP-set

Group	ΔE	$\alpha(Pu^{239})$ SNEAK	PU9SCP	$\sigma_\gamma(Pu^{239})$(b) SNEAK	PU9SCP
11	10.0 - 21.5 KeV	0.420	0.413	0.791	0.775
12	4.65 - 10.0	0.490	0.604	1.20	1.480
13	2.15 - 4.65	0.537	0.905	1.76	2.957
14	1.0 - 2.15	0.593	0.892	2.33	3.504
15	0.465- 1.0 KeV	0.640	0.846	4.70	6.218

Table AI-4 UPUCØR-set

Group	ΔE	$\sigma_f(U^{235})$(b)		$\sigma_f(U^{238})$(b)		$\sigma_f(Pu^{239})$(b)	
		SNEAK	UPUCØR	SNEAK	UPUCØR	SNEAK	UPUCØR
1	6.5 - 10.5MeV	1.65	1.53	0.967	0.934	2.19	2.05
2.	4.0 - 6.5	1.19	1.07	0.584	0.540v	1.86	1.65
3	2.5 - 4.0MeV	1.28	1.17	0.572	0.572	1.97	1.82

Group	ΔE	$\bar{\nu}(Pu^{239})$	
		SNEAK	UPUCØR
1	6.5 - 10.5 MeV	4.02	4.175
2	4.0 - 6.5 MeV	3.60	3.660

Table AI-5 PUO2RE-set (see next pages)

Table AI-6 MØX911, MØXTØT-sets

Group	ΔE	$\sigma_\gamma(U^{238})$(b)		
		SNEAK	SNEAPM SNEAPMB	MØX911 MØXTØT
9	46.5 - 100 KeV	0.286	0.282	0.245
10	21.5 - 46.5	0.471	0.457	0.405
11	10.0 - 21.5	0.728	0.630	0.576
12	4.65- 10.0	1.034	=SNEAK	0.790
13	2.15- 4.65	1.237		1.18
14	1.0 - 2.15	1.590		1.72
15	0.465- 1.0 KeV	3.107	=SNEAK	2.91

Table AI-5 PUO2RE-set

Group	ΔE	Pu^{240} σ_T(b)	σ_f(b)	σ_γ(b)	σ_{el}(b)	Pu^{241} σ_T(b)	σ_f(b)	σ_γ(b)	σ_{el}(b)	Pu^{242} σ_T(b)	σ_f(b)	σ_γ(b)	σ_{el}(b)
26	0.0252	177.2	0.0327	175.4	1.72	1082.3	779.5	291.0	11.77	25.04	0	16.21	8.83
25	0.215-0.465 eV	164.6	0.0306	164.0	0.532	925.0	561.0	348.3	15.17	18.52	0	10.02	8.49
24	0.465-1.0 eV	1637.9	0.294	1570.2	67.42	66.59	44.70	12.03	9.87	17.40	0	9.50	7.90
23	1.0 -2.15 eV	7253.9	1.25	6734.0	518.7	36.08	24.39	2.58	9.11	25.40	0	19.97	5.42
22	2.15 -4.65 eV	22.82	0.0025	7.84	14.97	204.0	126.3	69.20	8.50	1312.4	0	1208.6	103.8
21	4.65 -10.0 eV	11.14	0.00107	0.676	10.47	262.5	214.5	37.25	10.78	11.80	0	0.606	11.20
20	10.0 -21.5 eV	49.01	0.934	35.77	12.31	183.9	125.6	42.21	16.10	11.44	0	1.57	9.87
19	21.5 -46.5 eV	149.9	0.506	77.47	71.94	81.60	60.24	10.53	10.84	12.45	0	3.98	8.47
18	46.5 -100 eV	102.50	0.726	37.96	63.81	73.20	39.27	19.89	14.04	90.13	0	22.95	67.18
17	100 -215 eV	46.94	0.448	18.37	28.12	54.51	29.10	13.66	11.74	26.76	0	10.33	16.43
16	215 -465 eV	29.88	0.0639	6.62	23.20	41.38	20.03	8.88	12.48	33.60	0.00821	7.93	25.67
15	465 -1000 eV	24.30	0.0177	3.79	20.50	31.62	14.23	5.59	11.79	26.63	0.0100	4.55	22.07
14	1.0 -2.15 keV	25.65	0.155	2.48	23.01	24.55	9.38	3.10	12.07	21.47	0.0100	2.81	18.65
13	2.15 -4.65 keV	21.26	0.142	1.51	19.61	20.53	6.06	1.97	12.50	18.22	0.0100	1.94	16.27
12	4.65 -10.0 keV	18.89	0.104	1.02	17.77	16.97	4.47	1.50	11.01	16.09	0.0100	1.48	14.60
11	10.0 -21.5 keV	17.05	0.105	0.730	16.22	15.44	3.55	1.13	10.76	14.70	0.0100	1.11	13.58
10	21.5 -46.5 keV	15.51	0.108	0.494	14.91	14.15	2.91	0.805	10.38	13.55	0.0100	0.758	12.78
9	46.5 -100.0keV	13.90	0.0845	0.287	13.39	12.75	2.42	0.538	9.44	12.90	0.0100	0.487	12.27
8	0.1 -0.2 MeV	11.98	0.0986	0.209	11.08	11.73	2.04	0.314	8.77	12.06	0.0203	0.297	11.03
7	0.2 -0.4 MeV	9.84	0.133	0.148	8.37	10.10	1.72	0.188	7.39	10.25	0.0636	0.222	8.89
6	0.4 -0.8 MeV	8.02	0.548	0.142	5.79	8.35	1.51	0.104	5.82	7.91	0.344	0.199	6.02
5	0.8 -1.4 MeV	7.00	1.43	0.105	4.08	7.24	1.59	0.0487	4.65	6.98	1.32	0.153	4.43

Table AI-5 PUO2RE-set (continued)

		Pu^{240}				Pu^{241}				Pu^{242}			
Group	ΔE	σ_T(b)	σ_f(b)	σ_γ(b)	σ_{el}(b)	σ_T(b)	σ_f(b)	σ_γ(b)	σ_{el}(b)	σ_T(b)	σ_f(b)	σ_γ(b)	σ_{el}(b)
4	1.4 - 2.5MeV	7.35	1.48	0.0586	4.17	7.23	1.74	0.0245	4.63	7.34	1.46	0.0666	3.90
3	2.5 - 4.0MeV	7.93	1.51	0.0268	4.74	7.94	1.54	0.0109	5.31	7.92	1.51	0.0306	4.72
2	4.0 - 6.5MeV	7.76	1.51	0.0118	4.63	7.96	1.54	0.00614	4.94	7.81	1.51	0.0130	4.64
1	6.5 -10.5MeV	6.54	1.89	0.00666	3.56	6.87	2.09	0.00349	3.79	6.53	1.89	0.00753	3.55

I.2 The calculation of the inelastic scattering matrices

The general expression for the probability of inelastic scattering out of any energy group i to any group h is given by Yiftah, Okrent and Moldauer [91] in the following form

$$\sigma_{n'i,K} = \frac{\int_{E_{KL}}^{E_{KH}} dE' \int_{E_{iL}}^{E_{iH}} dE\, \sigma_{n'}(E)\, \phi(E)\, P(E \to E')}{\int_{E_{iL}}^{E_{iH}} \phi(E) dE} \qquad \text{(AI-1)}$$

Here E is the incident neutron-energy and E' the energy of the scattered neutron. The indices L and H indicate the lower and higher energy-limits respectively of any group. $\phi(E)$ represents the energy-dependent neutron flux. $P(E \to E')$ represents the transition probability of the inelastically scattered neutrons. For its determination one has to distinguish between the range of resolved levels of the residual nucleus and the so-called continuum range in which the levels of the residual nucleus are undistinguishable.

I.2a Energy groups with discrete excitation levels for inelastic scattering

For given incident neutron energies E in group i and outgoing neutron energies E' in group K inelastic scattering can occur only to those excitation levels for which

$$E' = E - E_j$$

where E_j is the energy of the jth level.
The transition probability therefore is a δ-function which has the value one, if the above condition is fulfilled and zero, if not. Thus we have

$$\sigma_{n'}(E)\, P(E \to E') = \sum_{j=1}^{N} \sigma_{n'}^{Ej}(E)\, P_j(E \to E') = \sum_{j=1}^{N} \sigma_{n'}^{Ej}(E)\, \delta(E - E' - E_j) \qquad \text{(AI-2)}$$

where N is the number of excitation levels of the isotope considered. P_j the probability of the transition to the jth level of the residual nucleus and $\sigma_{n'}^{Ej}$ the inelastic excitation cross section of the jth level. With this special form of the transition-probability the double integration in (AI-1) can be reduced to a single one over the energy group K to which the scattering occurs.

$$\sigma_{n'i,K} = \frac{\sum_j \int_{E_{KL}}^{E_{KH}} dE' \, \sigma_{n'}^{E_j}(E'+E_j)\,\phi(E'+E_j)}{\int_{E_{iL}}^{E_{LH}} \phi(E)dE} \qquad \text{(AI-3)}$$

with the transformation $E'+E_j \rightarrow E$ it follows:

$$\sigma_{n'i,K} = \frac{\sum_j \int_{E_{KL}+E_j}^{E_{KH}+E_j} dE \, \sigma_{n'}^{E_j}(E)\,\phi(E)\,\chi(E_{iL} \leq E \leq E_{iH})}{\int_{E_{iL}}^{E_{iH}} \phi(E)dE} \qquad \text{(AI-4)}$$

By the distribution-function χ it was taken into account that the incident neutron-energy E should be contained in a 26-group i. On the other hand it must be of course $E_{KL}+E_j \leq E \leq E_{KH}+E_j$ because of the integration over this range. The integration therefore has to be extended only over the interval $[E_u, E_o]$ with the following definition

$$E_u = \begin{cases} E_{iL} & \text{if } E_{KL}+E_j < E_{iL} \\ E_{KL}+E_j & \text{if } E_{KL}+E_j \geq E_{iL} \end{cases} \quad \text{and} \quad E_o = \begin{cases} E_{iH} & \text{if } E_{KH}+E_j > E_{iH} \\ E_{KH}+E_j & \text{if } E_{KH}+E_j \leq E_{iH} \end{cases} \qquad \text{(AI-5)}$$

Instead of the neutron flux the collision density in the special form of the SNEAK-3A spectrum was taken as weighting spectrum. Reasons for preferring the collision density to the neutron flux for weighting purposes are outlined in [4]. The integral was solved numerically by use of the trapezoidal rule. The inelastic excitation cross sections were taken from the KEDAK-tape [27].

I.2b Energy groups with unresolved excitation levels for inelastic scattering

In the energy region, where the excitation levels of the residual nucleus are not experimentally resolved, the energy distribution of the inelastically scattered neutrons is described by an evaporation model. The transition probability for neutrons from energy E to energy E' by inelastic scattering is then given by

$$P(E \rightarrow E') = NE'\exp(-E'/\theta(E)); \quad (E' \leq E) \qquad \text{(AI-6)}$$

Here N is a normalization constant and θ is the so-called nuclear temperature of the residual nucleus, which Weißkopf [41] derived as

$$\theta(E) = \sqrt{\frac{E}{\nu A}} \quad [\text{MeV}] \quad \begin{pmatrix} E \text{ in MeV} \\ \nu \text{ in MeV}^{-1} \end{pmatrix} \qquad \text{(AI-7)}$$

Here again E is the energy of the incident neutron, A is the atomic mass number of the residual nucleus and ν is an adjustable parameter. For a given value of E P(E→E') has its maximum at E'=θ(E). Yiftah,Okrent and Moldauer [91] chose $\nu = 0.096\ \text{MeV}^{-1}$ for all nuclei. We took the ν-value recommended by Swarcbaum et al. [42], which is $\nu = 0.16\ \text{MeV}^{-1}$ for all nuclei.
Swarcbaum et al. adjusted more recently nuclear temperatures for materials from Al to U^{238} in the energy region between 2.5 and 7.0 MeV and found that over this whole region ν=0.16 gives an acceptable overall fit for the energy distribution of inelastically scattered neutrons.

Inserting (AI-6) into(AI-1) the cross section for inelatic scattering from energy group i to energy group K is calculated from:

$$\sigma_{n'i,K} = \frac{\int_{E_{KL}}^{E_{KH}} dE' \int_{E_{iL}}^{E_{iH}} dE\ \sigma_{n'}(E)\ \phi(E)\ NE' \exp(-E'/\theta(E))}{\int_{E_{iL}}^{E_{iH}} \phi(E)dE} \qquad \text{(AI-8)}$$

Following Yiftah et al. [91] and Swarcbaum et al. [42] we replaced θ(E) by an average θ_i value for each group i. This was necessary because only a limited amount of computer core storage was available for our program, which is part of the whole MIGRØS-system and was developed originally for the IBM 7074 computer. For the same reason we had to find a very simple expression for θ_i. We chose

$$\theta_i = \sqrt{\frac{E_{iH}+E_{iL}}{2\nu A}}$$

instead of the flux-averaged value taken by Yiftah et al. and Swarcbaum et al. This procedure may be justified if one considers that formula (AI-7) already is an approximation for θ(E).
With the introduction of an averaged θ the energy integrations over the groups i and K can be separated. The E'-integration can be carried out analytically.

The result is

$$\sigma_{n'i,K} = \sigma_{n'i}\, N \left[\theta_i^2 \exp\left(-\frac{E_{KL}}{\theta_i}\right)\left(\frac{E_{KL}}{\theta_i}+1\right) - \theta_i^2 \exp\left(-\frac{E_{KH}}{\theta_i}\right)\left(\frac{E_{KH}}{\theta_i}+1\right)\right] \qquad \text{(AI-9)}$$

$$= \sigma_{n'i}\, N\, \tilde{P}\,(\Delta E_i \to \Delta E_K)$$

The normalization constant N is determined by the requirement

$$\sum_{K \geq i} \tilde{P}(\Delta E_i \to \Delta E_K) N = 1 \quad \text{and} \qquad \text{(AI-10)}$$

$$P(\Delta E_i \to \Delta E_K) = \frac{\tilde{P}(\Delta E_i \to \Delta E_K)}{\sum_{K \geq i} P(\Delta E_i \to \Delta E_K)}$$

I.2c Energy groups, where the excitation levels are partly resolved and and partly unresolved

For nearly all materials the energy of the last discrete excitation level lies within a 26-group, so that the lower part of the group has to be treated by the discrete level method and the upper part by the evaporation model. The results for each part are linked together as follows. Let ΔE^i_d be the energy range of group i, where discrete excitation levels are known, and ΔE^i_c the energy range, where the excitation levels are unresolved. Then for a group with both discrete and "continuous" levels the transition probability of inelastic scattering is calculated according to the formula

$$P(\Delta E_i \to \Delta E_K)_{d,c} = d_i\, P(\Delta E^i_d \to \Delta E_K) + c_i\, P(\Delta E^i_c \to \Delta E_K) \qquad \text{(AI-11)}$$

In (AI-11) $P(\Delta E^i_d \to \Delta E_K)$ is the transition probability to group K of neutrons whose incident energy lies in the range of resolved excitation levels of the residual nucleus within group i. $P(\Delta E^i_d \to \Delta E_K)$ is given by $\sigma_{n'i,K}/\sigma_{n'i}$ where $\sigma_{n'i,K}$ follows from equation (AI-4). $P(\Delta E^i_c \to \Delta E_K)$ is the corresponding quantity for neutrons with energies in the range of unresolved levels of the residual levels of the residual nucleus within group i. $P(\Delta E^i_d \to \Delta E_K)$ and $P(\Delta E^i_c \to \Delta E_K)$ are

both normalized to $\sum_{K\geq 1} P(\Delta E_1 \rightarrow \Delta E_K)=1$.

The relative contributions of resolved and unresolved levels d_i and c_i are given by

$$d_i = \frac{\int_{\Delta E_d^i} \sigma_{n'}(E)\ \phi(E)dE}{\int_{E_{iL}}^{E_{iH}} \phi(E)dE} \quad ; \quad c_i = \frac{\int_{\Delta E_c^i} \sigma_{n'}(E)\ \phi(E)dE}{\int_{E_{iL}}^{E_{iH}} \phi(E)dE} \qquad \text{(AI-12)}$$

$$(\Delta E_d^i + \Delta E_c^i = \Delta E_i)$$

Of course (AI-6) and (AI-7) are simplified formulas. Taking the same value of ν for all nuclei and distinguishing between them by their atomic mass numbers only means neglecting individual nuclear properties. The use of an averaged nuclear temperature instead of performing the double integration is another source of error.

I.2d Transition probabilities for (n,2n) reactions

So far we did not calculate transition probabilities for (n,2n) reactions of our own. In energy groups, where (n,2n) reactions occur, the inelastic transition probabilities of the ABN 26-group set [20], $W(\Delta E_i \rightarrow \Delta E_K)$ were used. The inelastic matrix was then calculated according to

$$\sigma_{n'+n,2n;i,K} = (\sigma_{n'i} + 2\sigma_{n,2ni})\ W(\Delta E_i \rightarrow \Delta E_K) \qquad \text{(AI-13)}$$

I.2e Discussion

The scattering matrices were obtained by multiplication of the transition probabilities with the total 26 group-cross sections for inelastic scattering. Contrary to the ABN-set [20] the scattering matrices have been calculated for scattering into all energy groups $K \leq 26$; no cut because of the smallness of the following matrix-elements was made at any K. Our new transition probabilities in general show a softer spectrum than the matrices of the ABN-set as well in the "continuum" as in the range of discrete levels. For the most

important case of U^{238} the main reasons for this fact are the following:
The inelastic scattering to higher levels especially to the levels between 0.7 and 1 MeV has been underestimated in the ABN-set. Moreover we have taken into account a wider resolved energy range than in the ABN-set.
In the continuum region one reason for the softer spectrum quite clearly is the use of the value of 0.16 for ν, which results in a rather small nuclear temperature and therefore shifts the maximum of the energy distribution of the inelastically scattered neutrons to smaller energies compared to the results obtained with ν=0.096 for example.
ABN also applied an evaporation model in the energy range of unresolved excitation levels. For U^{238} they used experimental values of the nuclear temperature, from which a value of ν=0.11 is obtained. The resulting inelastic scattering matrix was then still modified in the following way. Calculations carried out with this matrix should give the correct value for the total number of fissions in an infinite slab of U^{238}.
For nearly all other materials individual corrections were applied in the ABN-set. This should be kept in mind by someone who wants to compare our matrices to these of Abagjan et al.

The new scattering matrices are given in table AI-7 on the following pages.

Table AI-7

Inelastic scattering matrices $\sigma_{n'i,K}$

Explanation of material names used in the following tables:

AL270 = $^{27}_{13}Al$

C^b120 = $^{12}_{6}C$

CR520 = Cr

FE560 = Fe

MO960 = Mo

NA230 = $^{23}_{11}Na$

NI590 = Ni

O^b160 = $^{16}_{8}O$

PU390 = $^{239}_{94}Pu$

PU400 = $^{240}_{94}Pu$

PU410 = $^{241}_{94}Pu$

PU420 = $^{242}_{94}Pu$

U2350 = $^{235}_{92}U$

U2380 = $^{238}_{92}U$

AL270

I= 1										
K: 1 - 10	3.19E-02	1.28E-01	2.07E-01	2.41E-01	1.42E-01	7.56E-02	2.39E-02	6.73E-03	1.87E-03	4.18E-04
K: 11 - 20	9.04E-05	1.97E-05	4.28E-06	9.14E-07	1.98E-07	4.29E-08	9.15E-09	1.98E-09	4.30E-10	9.15E-11
K: 21 - 26	1.98E-11	4.30E-12	9.16E-13	1.98E-13	4.31E-14	8.62E-15				
I= 2										
K: 2 - 11	5.98E-02	1.91E-01	2.82E-01	1.94E-01	7.38E-02	2.52E-02	6.18E-03	1.73E-03	3.90E-04	8.47E-05
K: 12 - 21	1.85E-05	4.02E-06	8.58E-07	1.86E-07	4.03E-08	8.59E-09	1.86E-09	4.03E-10	8.55E-11	1.86E-11
K: 22 - 26	4.03E-12	8.19E-13	1.86E-13	4.03E-14	9.22E-15					
I= 3										
K: 3 - 8	4.82E-02	2.23E-01	1.19E-01	1.15E-01	2.80E-02	2.43E-04				
I= 4										
K: 4 - 9	1.79E-02	1.49E-01	1.17E-01	5.14E-03	1.83E-04	1.28E-05				
I= 5										
K: 5 - 10	0.0	1.51E-02	5.17E-02	2.31E-02	8.16E-03	2.76E-04				

CR520

I= 1										
K: 1 - 10	9.03E-03	7.93E-02	2.16E-01	3.62E-01	2.71E-01	1.67E-01	5.79E-02	1.70E-02	4.84E-03	1.10E-03
K: 11 - 20	2.39E-04	5.21E-05	1.13E-05	2.42E-06	5.25E-07	1.14E-07	2.43E-08	5.25E-09	1.14E-09	2.43E-10
K: 21 - 26	5.25E-11	1.14E-11	2.43E-12	5.25E-13	1.14E-13	2.02E-14				
I= 2										
K: 2 - 11	4.10E-02	1.68E-01	3.78E-01	3.43E-01	2.38E-01	8.85E-02	2.71E-02	7.83E-03	1.79E-03	3.92E-04
K: 12 - 21	8.57E-05	1.87E-05	3.99E-06	8.65E-07	1.88E-07	4.00E-08	8.65E-09	1.88E-09	4.00E-10	8.66E-11
K: 22 - 26	1.88E-11	4.00E-12	8.66E-13	1.88E-13	3.76E-14					
I= 3										
K: 3 - 12	4.01E-02	3.57E-01	3.91E-01	1.30E-01	5.95E-02	2.34E-02	5.69E-03	8.28E-04	1.81E-04	3.98E-05
K: 13 - 22	8.68E-06	1.86E-06	4.02E-07	8.73E-08	1.86E-08	4.02E-09	8.73E-10	1.86E-10	4.02E-11	8.73E-12
K: 23 - 26	1.86E-12	4.03E-13	8.76E-14	2.27E-14						
I= 4										
K: 4 - 13	2.56E-02	2.04E-01	2.40E-01	9.42E-02	3.70E-02	1.54E-02	5.14E-03	1.70E-03	3.95E-04	8.59E-05
K: 14 - 23	1.83E-05	3.97E-06	8.62E-07	1.84E-07	3.97E-08	8.62E-09	1.84E-09	4.00E-10	8.49E-11	1.73E-11
K: 24 - 26	4.26E-12	6.09E-13	2.03E-13							
I= 5										
K: 5 - 11	7.19E-04	2.56E-02	2.98E-02	1.06E-02	4.24E-03	6.63E-04	1.15E-05			
I= 6										
K: 6 - 11	0.0	1.07E-03	3.03E-03	1.53E-03	6.51E-04	2.32E-04				

C 120

I= 1						
K: 1 - 6	0.0	5.20E-02	1.55E-01	8.65E-02	2.48E-04	1.24E-05
I= 2						
K: 2 - 7	0.0	0.0	3.86E-02	2.00E-02	5.50E-03	8.26E-05

MO960

I= 1										
K: 1 - 10	1.60E-03	3.73E-02	1.92E-01	5.10E-01	5.16E-01	3.82E-01	1.48E-01	4.63E-02	1.35E-02	3.11E-03
K: 11 - 20	6.82E-04	1.49E-04	3.26E-05	6.97E-06	1.51E-06	3.28E-07	6.98E-08	1.51E-08	3.28E-09	6.99E-10
K: 21 - 26	1.51E-10	3.28E-11	6.99E-12	1.51E-12	3.27E-13	7.59E-14				
I= 2										
K: 2 - 11	1.27E-02	1.11E-01	4.35E-01	5.66E-01	4.91E-01	2.10E-01	6.88E-02	2.07E-02	4.82E-03	1.06E-03
K: 12 - 21	2.33E-04	5.10E-05	1.09E-05	2.36E-06	5.13E-07	1.09E-07	2.36E-08	5.13E-09	1.09E-09	2.36E-10
K: 22 - 26	5.13E-11	1.09E-11	2.37E-12	5.13E-13	1.27E-13					
I= 3										
K: 3 - 12	4.53E-02	3.05E-01	5.63E-01	6.10E-01	2.99E-01	1.05E-01	3.28E-02	7.79E-03	1.73E-03	3.82E-04
K: 13 - 22	8.37E-05	1.79E-05	3.88E-06	8.43E-07	1.80E-07	3.89E-08	8.44E-09	1.80E-09	3.89E-10	8.44E-11
K: 23 - 26	1.80E-11	3.89E-12	8.44E-13	2.17E-13						
I= 4										
K: 4 - 13	6.63E-02	5.63E-01	7.13E-01	2.22E-01	6.21E-02	1.76E-02	4.07E-03	9.04E-04	1.99E-04	4.36E-05
K: 14 - 23	9.34E-06	2.02E-06	4.39E-07	9.37E-08	2.03E-08	4.40E-09	9.37E-10	2.03E-10	4.38E-11	9.25E-12
K: 24 - 26	2.06E-12	4.10E-13	1.11E-13							
I= 5										
K: 5 - 14	5.53E-02	3.37E-01	2.73E-01	6.91E-02	1.31E-02	2.19E-03	1.39E-04	8.33E-06	1.82E-06	3.90E-07
K: 15 - 24	8.46E-08	1.84E-08	3.92E-09	8.48E-10	1.84E-10	3.92E-11	8.49E-12	1.83E-12	3.85E-13	8.70E-14
K: 25 - 26	1.65E-14	4.63E-15								
I= 6										
K: 6 - 15	6.44E-02	7.10E-02	1.17E-02	2.23E-03	4.66E-04	1.50E-04	2.14E-05	3.13E-06	6.70E-07	1.45E-07
K: 16 - 25	3.16E-08	6.73E-09	1.46E-09	3.16E-10	6.74E-11	1.46E-11	3.16E-12	6.74E-13	1.47E-13	3.11E-14
K: 26 - 26	8.20E-15									
I= 7										
K: 7 - 14	0.0	2.66E-02	9.94E-03	2.64E-03	6.59E-04	1.25E-04	1.57E-05	3.90E-07		

FE560

I= 1										
K: 1 - 10	8.00E-03	7.77E-02	2.25E-01	3.97E-01	3.07E-01	1.93E-01	6.75E-02	2.00E-02	5.69E-03	1.29E-03
K: 11 - 20	2.81E-04	6.14E-05	1.34E-05	2.86E-06	6.19E-07	1.34E-07	2.86E-08	6.19E-09	1.34E-09	2.86E-10
K: 21 - 26	6.19E-11	1.34E-11	2.86E-12	6.20E-13	1.35E-13	2.87E-14				
I= 2										
K: 2 - 11	3.11E-02	2.67E-01	3.79E-01	4.14E-01	2.02E-01	4.83E-02	1.23E-02	3.23E-03	7.26E-04	1.59E-04
K: 12 - 21	3.47E-05	7.56E-06	1.62E-06	3.50E-07	7.60E-08	1.62E-08	3.50E-09	7.60E-10	1.62E-10	3.50E-11
K: 22 - 26	7.60E-12	1.62E-12	3.50E-13	7.56E-14	1.72E-14					
I= 3										
K: 3 - 12	1.26E-01	5.44E-01	1.11E-01	1.29E-01	7.11E-02	2.50E-02	5.33E-03	6.46E-04	1.10E-04	2.41E-05
K: 13 - 22	5.25E-06	1.12E-06	2.43E-07	5.27E-08	1.12E-08	2.43E-09	5.27E-10	1.12E-10	2.44E-11	5.19E-12
K: 23 - 26	1.06E-12	2.60E-13	3.72E-14	1.24E-14						
I= 4										
K: 4 - 10	1.43E-01	3.53E-01	1.94E-01	1.02E-02	2.54E-03	6.29E-04	3.35E-05			
I= 5										
K: 5 - 11	0.0	5.86E-02	1.24E-01	8.79E-02	2.89E-02	1.74E-02	1.52E-03			

NA230

I= 1										
K: 1 - 10	4.56E-02	1.56E-01	2.26E-01	2.45E-01	1.38E-01	7.12E-02	2.21E-02	6.17E-03	1.70E-03	3.80E-04
K: 11 - 20	8.22E-05	1.79E-05	3.89E-06	8.30E-07	1.80E-07	3.90E-08	8.31E-09	1.80E-09	3.90E-10	8.31E-11
K: 21 - 26	1.80E-11	3.90E-12	8.31E-13	1.80E-13	3.95E-14	9.19E-16				
I= 2										
K: 2 - 11	1.01E-01	1.96E-01	2.59E-01	1.66E-01	9.30E-02	3.03E-02	8.67E-03	2.43E-03	5.45E-04	1.18E-04
K: 12 - 21	2.58E-05	5.61E-06	1.20E-06	2.59E-07	5.62E-08	1.20E-08	2.59E-09	5.62E-10	1.20E-10	2.59E-11
K: 22 - 26	5.62E-12	1.20E-12	2.60E-13	5.62E-14	1.41E-14					
I= 3										
K: 3 - 9	1.75E-01	2.38E-01	7.59E-02	9.30E-02	3.94E-02	8.39E-03	6.72E-05			
I= 4										
K: 4 - 9	3.31E-01	2.42E-01	8.04E-04	6.46E-03	2.75E-03	1.23E-04				
I= 5										
K: 5 - 7	8.11E-02	3.48E-01	4.12E-02							
I= 6										
K: 6 - 11	0.0	1.05E-01	3.04E-02	5.55E-03	7.18E-04	7.82E-06				

NI590

I= 1										
K: 1 - 10	4.92E-03	5.13E-02	1.56E-01	2.85E-01	2.25E-01	1.43E-01	5.06E-02	1.50E-02	4.30E-03	9.76E-04
K: 11 - 20	2.12E-04	4.64E-05	1.01E-05	2.16E-06	4.68E-07	1.02E-07	2.16E-08	4.68E-09	1.02E-09	2.16E-10
K: 21 - 26	4.68E-11	1.02E-11	2.16E-12	4.68E-13	1.02E-13	2.44E-14				
I= 2										
K: 2 - 11	2.78E-02	1.30E-01	3.24E-01	3.13E-01	2.26E-01	8.61E-02	2.66E-02	7.76E-03	1.78E-03	3.90E-04
K: 12 - 21	8.54E-05	1.86E-05	3.98E-06	8.62E-07	1.87E-07	3.99E-08	8.63E-09	1.87E-09	3.99E-10	8.63E-11
K: 22 - 26	1.87E-11	3.99E-12	8.62E-13	1.87E-13	4.24E-14					
I= 3										
K: 3 - 12	1.35E-02	4.47E-01	3.33E-01	1.33E-01	5.33E-02	1.45E-02	2.79E-03	2.05E-05	1.26E-06	2.77E-07
K: 13 - 22	6.05E-08	1.29E-08	2.80E-09	6.08E-10	1.30E-10	2.80E-11	6.08E-12	1.30E-12	2.80E-13	6.08E-14
K: 23 - 26	1.30E-14	2.80E-15	6.08E-16	1.56E-16						
I= 4										
K: 4 - 13	0.0	1.16E-01	1.77E-01	8.50E-02	3.31E-02	8.57E-03	1.30E-03	2.82E-04	6.15E-05	1.34E-05
K: 14 - 23	2.86E-06	6.19E-07	1.34E-07	2.86E-08	6.19E-09	1.34E-09	2.86E-10	6.23E-11	1.32E-11	2.69E-12
K: 24 - 26	6.63E-13	9.48E-14	3.16E-14							
I= 5										
K: 5 - 11	0.0	0.0	0.0	0.0	3.97E-04	1.95E-04	1.03E-05			

O 160

I= 1						
K: 1 - 6	0.0	0.0	4.40E-02	6.66E-02	3.91E-02	1.45E-02

PU390

I= 1										
K: 1 - 10	0.0	0.0	7.26E-02	2.72E-01	4.72E-01	5.81E-01	3.27E-01	1.27E-01	5.45E-02	1.82E-02
I= 2										
K: 2 - 11	2.95E-04	1.26E-02	1.59E-01	4.34E-01	6.08E-01	3.49E-01	1.34E-01	4.35E-02	1.06E-02	2.38E-03
K: 12 - 21	5.27E-04	1.16E-04	2.48E-05	5.37E-06	1.17E-06	2.49E-07	5.38E-08	1.17E-08	2.49E-09	5.38E-10
K: 22 - 26	1.17E-10	2.49E-11	5.38E-12	1.17E-12	3.05E-13					
I= 3										
K: 3 - 12	2.22E-03	6.43E-02	2.92E-01	5.73E-01	4.05E-01	1.73E-01	5.96E-02	1.49E-02	3.40E-03	7.59E-04
K: 13 - 22	1.67E-04	3.58E-05	7.78E-06	1.69E-06	3.60E-07	7.80E-08	1.69E-08	3.61E-09	7.80E-10	1.69E-10
K: 23 - 26	3.61E-11	7.80E-12	1.69E-12	4.57E-13						
I= 4										
K: 4 - 13	1.36E-02	1.18E-01	3.61E-01	3.35E-01	1.65E-01	6.15E-02	1.60E-02	3.72E-03	8.39E-04	1.85E-04
K: 14 - 23	3.98E-05	8.65E-06	1.88E-06	4.01E-07	8.68E-08	1.88E-08	4.01E-09	8.68E-10	1.88E-10	4.01E-11
K: 24 - 26	8.68E-12	1.81E-12	5.04E-13							
I= 5										
K: 5 - 14	3.57E-02	2.16E-01	3.04E-01	1.88E-01	7.91E-02	2.20E-02	5.26E-03	1.20E-03	2.67E-04	5.76E-05
K: 15 - 24	1.25E-05	2.73E-06	5.81E-07	1.26E-07	2.73E-08	5.82E-09	1.26E-09	2.73E-10	5.82E-11	1.26E-11
K: 25 - 26	2.73E-12	6.61E-13								
I= 6										
K: 6 - 15	2.85E-01	2.44E-01	1.51E-01	5.87E-02	1.64E-02	4.08E-03	9.19E-04	1.98E-04	4.28E-05	9.33E-06
K: 16 - 25	2.03E-06	4.33E-07	9.38E-08	2.03E-08	4.34E-09	9.38E-10	2.03E-10	4.34E-11	9.38E-12	2.03E-12
K: 26 - 26	5.41E-13									
I= 7										
K: 7 - 16	4.14E-01	9.27E-02	1.34E-02	4.26E-03	9.57E-04	2.46E-04	5.82E-05	1.25E-05	2.71E-06	5.89E-07
K: 17 - 26	1.26E-07	2.72E-08	5.90E-09	1.26E-09	2.72E-10	5.90E-11	1.26E-11	2.74E-12	5.91E-13	1.53E-13
I= 8										
K: 8 - 17	2.92E-01	7.70E-02	5.19E-03	1.92E-04	5.28E-05	1.27E-05	2.74E-06	5.96E-07	1.29E-07	2.76E-08
K: 18 - 26	5.98E-09	1.30E-09	2.76E-10	5.98E-11	1.30E-11	2.76E-12	6.01E-13	1.28E-13	3.36E-14	
I= 9										
K: 9 - 18	2.05E-01	5.91E-02	4.40E-03	1.02E-03	2.22E-04	4.71E-05	1.03E-05	2.25E-06	4.81E-07	1.04E-07
K: 19 - 26	2.26E-08	4.82E-09	1.04E-09	2.26E-10	4.82E-11	1.04E-11	2.26E-12	6.15E-13		
I= 10										
K: 10 - 11	1.50E-01	8.16E-02								
I= 11										
K: 11 - 14	5.79E-02	8.68E-02	3.38E-02	1.65E-03						
I= 12										
K: 12 - 21	0.0	0.0	1.21E-02	4.01E-03	9.83E-04	2.14E-04	4.68E-05	1.02E-05	2.18E-06	4.71E-07
K: 22 - 26	1.02E-07	2.18E-08	4.71E-09	1.02E-09	2.78E-10					

PU400

I= 1										
K: 1 - 9	0.0	0.0	6.32E-02	2.53E-01	3.79E-01	4.05E-01	2.15E-01	7.59E-02	2.53E-02	
I= 2										
K: 2 - 11	2.64E-04	1.14E-02	1.45E-01	3.97E-01	5.58E-01	3.21E-01	1.23E-01	4.00E-02	9.72E-03	2.19E-03
K: 12 - 21	4.85E-04	1.06E-04	2.28E-05	4.94E-06	1.07E-06	2.29E-07	4.95E-08	1.07E-08	2.29E-09	4.95E-10
K: 22 - 26	1.07E-10	2.29E-11	4.95E-12	1.07E-12	2.76E-13					
I= 3										
K: 3 - 12	2.28E-03	6.66E-02	3.03E-01	5.98E-01	4.24E-01	1.81E-01	6.24E-02	1.56E-02	3.57E-03	7.96E-04
K: 13 - 22	1.75E-04	3.76E-05	8.16E-06	1.77E-06	3.78E-07	8.17E-08	1.77E-08	3.78E-09	8.18E-10	1.77E-10
K: 23 - 26	3.78E-11	8.18E-12	1.77E-12	4.79E-13						
I= 4										
K: 4 - 13	2.05E-02	1.79E-01	5.49E-01	5.11E-01	2.53E-01	9.40E-02	2.45E-02	5.70E-03	1.28E-03	2.84E-04
K: 14 - 23	6.10E-05	1.32E-05	2.88E-06	6.14E-07	1.33E-07	2.88E-08	6.14E-09	1.33E-09	2.88E-10	6.14E-11
K: 24 - 26	1.33E-11	2.85E-12	7.80E-13							
I= 5										
K: 5 - 14	4.36E-01	4.35E-01	3.15E-01	1.28E-01	5.00E-02	1.31E-02	3.06E-03	6.91E-04	1.53E-04	3.29E-05
K: 15 - 24	7.14E-06	1.55E-06	3.31E-07	7.17E-08	1.55E-08	3.31E-09	7.17E-10	1.56E-10	3.31E-11	7.18E-12
K: 25 - 26	1.55E-12	3.94E-13								
I= 6										
K: 6 - 15	1.12E 00	3.49E-01	4.79E-02	1.59E-02	4.24E-03	8.66E-04	1.71E-04	3.73E-05	7.99E-06	1.73E-06
K: 16 - 25	3.76E-07	8.02E-08	1.74E-08	3.76E-09	8.02E-10	1.74E-10	3.76E-11	8.02E-12	1.75E-12	3.71E-13
K: 26 - 26	9.77E-14									
I= 7										
K: 7 - 16	8.32E-01	3.30E-01	2.24E-02	8.26E-04	1.38E-04	1.88E-05	4.15E-06	8.93E-07	1.94E-07	4.22E-08
K: 17 - 26	9.00E-09	1.95E-09	4.22E-10	9.00E-11	1.95E-11	4.23E-12	9.00E-13	1.96E-13	4.16E-14	1.10E-14
I= 8										
K: 8 - 17	3.59E-01	2.32E-01	4.78E-03	7.67E-04	6.11E-05	1.06E-05	2.29E-06	4.99E-07	1.08E-07	2.31E-08
K: 18 - 26	5.01E-09	1.09E-09	2.32E-10	5.01E-11	1.09E-11	2.32E-12	5.04E-13	1.07E-13	2.82E-14	
I= 9										
K: 9 - 12	4.78E-02	8.10E-02	1.24E-02	1.03E-03						

PU410

I= 1										
K: 1 - 10	0.0	8.88E-03	4.44E-02	2.22E-01	3.73E-01	4.79E-01	3.02E-01	1.24E-01	3.55E-02	8.88E-03
I= 2										
K: 2 - 11	2.61E-04	1.13E-02	1.45E-01	4.00E-01	5.64E-01	3.25E-01	1.25E-01	4.06E-02	9.86E-03	2.22E-03
K: 12 - 21	4.92E-04	1.08E-04	2.31E-05	5.01E-06	1.09E-06	2.32E-07	5.02E-08	1.09E-08	2.32E-09	5.02E-10
K: 22 - 26	1.09E-10	2.32E-11	5.03E-12	1.09E-12	2.89E-13					
I= 3										
K: 3 - 12	1.46E-03	4.30E-02	1.97E-01	3.90E-01	2.77E-01	1.18E-01	4.08E-02	1.02E-02	2.33E-03	5.21E-04
K: 13 - 22	1.15E-04	2.46E-05	5.34E-06	1.16E-06	2.47E-07	5.35E-08	1.16E-08	2.47E-09	5.35E-10	1.16E-10
K: 23 - 26	2.47E-11	5.35E-12	1.16E-12	3.07E-13						
I= 4										
K: 4 - 13	1.03E-02	9.06E-02	2.79E-01	2.60E-01	1.29E-01	4.80E-02	1.25E-02	2.91E-03	6.55E-04	1.45E-04
K: 14 - 23	3.11E-05	6.76E-06	1.47E-06	3.13E-07	6.78E-08	1.47E-08	3.13E-09	6.78E-10	1.46E-10	3.13E-11
K: 24 - 26	6.78E-12	1.41E-12	3.94E-13							
I= 5										
K: 5 - 14	3.94E-02	2.41E-01	3.41E-01	2.12E-01	8.93E-02	2.48E-02	5.95E-03	1.36E-03	3.02E-04	6.52E-05
K: 15 - 24	1.42E-05	3.08E-06	6.58E-07	1.42E-07	3.09E-08	6.58E-09	1.42E-09	3.09E-10	6.58E-11	1.42E-11
K: 25 - 26	3.09E-12	7.73E-13								
I= 6										
K: 6 - 15	1.84E-01	3.49E-01	2.15E-01	1.29E-01	3.24E-02	7.45E-03	1.58E-03	3.49E-04	7.53E-05	1.64E-05
K: 16 - 25	3.57E-06	7.62E-07	1.65E-07	3.58E-08	7.62E-09	1.65E-09	3.58E-10	7.63E-11	1.65E-11	3.57E-12
K: 26 - 26	9.18E-13									
I= 7										
K: 7 - 16	5.46E-01	2.29E-01	1.53E-02	7.33E-03	1.50E-03	3.36E-04	7.42E-05	1.59E-05	3.46E-06	7.52E-07
K: 17 - 26	1.60E-07	3.47E-08	7.53E-09	1.61E-09	3.47E-10	7.53E-11	1.61E-11	3.49E-12	7.42E-13	1.95E-13
I= 8										
K: 8 - 17	3.58E-01	2.29E-01	1.09E-02	1.24E-03	2.01E-04	2.18E-05	4.68E-06	1.02E-06	2.21E-07	4.72E-08
K: 18 - 26	1.02E-08	2.22E-09	4.72E-10	1.02E-10	2.22E-11	4.72E-12	1.03E-12	2.18E-13	5.75E-14	
I= 9										
K: 9 - 18	1.39E-01	1.67E-01	4.01E-02	3.97E-06	2.01E-05	4.36E-06	9.50E-07	2.07E-07	4.41E-08	9.55E-09
K: 19 - 26	2.07E-09	4.42E-10	9.56E-11	2.07E-11	4.42E-12	9.56E-13	2.07E-13	5.64E-14		
I= 10										
K: 10 - 19	0.0	2.82E-02	2.92E-02	6.52E-03	1.19E-03	1.50E-04	1.13E-05	2.41E-06	5.22E-07	1.13E-07
K: 20 - 26	2.42E-08	5.23E-09	1.13E-09	2.42E-10	5.23E-11	1.13E-11	3.08E-12			

PU420

I= 1										
K: 1 - 10	0.0	8.93E-03	6.25E-02	2.59E-01	4.02E-01	4.29E-01	2.23E-01	8.93E-02	2.68E-02	8.93E-03
I= 2										
K: 2 - 11	2.66E-04	1.17E-02	1.50E-01	4.16E-01	5.88E-01	3.40E-01	1.30E-01	4.24E-02	1.03E-02	2.32E-03
K: 12 - 21	5.14E-04	1.13E-04	2.42E-05	5.25E-06	1.14E-06	2.43E-07	5.26E-08	1.14E-08	2.43E-09	5.26E-10
K: 22 - 26	1.14E-10	2.43E-11	5.26E-12	1.14E-12	3.06E-13					
I= 3										
K: 3 - 12	2.20E-03	6.54E-02	3.01E-01	5.96E-01	4.25E-01	1.82E-01	6.28E-02	1.57E-02	3.59E-03	8.01E-04
K: 13 - 22	1.76E-04	3.78E-05	8.21E-06	1.78E-06	3.80E-07	8.23E-08	1.78E-08	3.80E-09	8.23E-10	1.78E-10
K: 23 - 26	3.80E-11	8.23E-12	1.79E-12	4.70E-13						
I= 4										
K: 4 - 13	2.33E-02	2.06E-01	6.38E-01	5.96E-01	2.96E-01	1.10E-01	2.88E-02	6.68E-03	1.51E-03	3.33E-04
K: 14 - 23	7.15E-05	1.55E-05	3.38E-06	7.20E-07	1.56E-07	3.38E-08	7.20E-09	1.56E-09	3.37E-10	7.20E-11
K: 24 - 26	1.56E-11	3.29E-12	9.17E-13							
I= 5										
K: 5 - 14	3.06E-01	3.32E-01	2.29E-01	1.46E-01	4.87E-02	1.11E-02	2.58E-03	5.84E-04	1.29E-04	2.78E-05
K: 15 - 24	6.05E-06	1.31E-06	2.80E-07	6.07E-08	1.32E-08	2.81E-09	6.07E-10	1.32E-10	2.81E-11	6.08E-12
K: 25 - 26	1.31E-12	3.30E-13								
I= 6										
K: 6 - 15	9.92E-01	3.19E-01	1.80E-02	8.89E-03	2.98E-03	8.04E-04	2.03E-04	4.44E-05	9.50E-06	2.06E-06
K: 16 - 25	4.47E-07	9.53E-08	2.06E-08	4.47E-09	9.53E-10	2.06E-10	4.47E-11	9.53E-12	2.07E-12	4.41E-13
K: 26 - 26	1.16E-13									
I= 7										
K: 7 - 16	7.07E-01	3.40E-01	2.65E-02	1.05E-03	2.56E-04	5.76E-05	1.27E-05	2.73E-06	5.93E-07	1.29E-07
K: 17 - 26	2.75E-08	5.95E-09	1.29E-09	2.75E-10	5.95E-11	1.29E-11	2.75E-12	5.99E-13	1.27E-13	3.35E-14
I= 8										
K: 8 - 17	4.07E-01	2.96E-01	7.63E-03	2.05E-03	5.22E-04	1.42E-04	3.80E-05	8.30E-06	1.80E-06	3.85E-07
K: 18 - 26	8.33E-08	1.81E-08	3.85E-09	8.34E-10	1.81E-10	3.85E-11	8.39E-12	1.78E-12	4.69E-13	
I= 9										
K: 9 - 14	3.77E-02	7.13E-02	1.42E-02	3.37E-03	8.46E-04	1.15E-04				
I= 10										
K: 10 - 17	0.0	0.0	0.0	0.0	1.69E-03	9.26E-04	1.14E-04	2.83E-06		

U2350

I= 1										
K: 1 - 10	0.0	9.92E-03	4.96E-02	2.48E-01	4.26E-01	5.55E-01	3.47E-01	1.39E-01	3.97E-02	9.92E-03
I= 2										
K: 2 - 11	3.99E-04	1.64E-02	2.02E-01	5.43E-01	7.53E-01	4.30E-01	1.64E-01	5.32E-02	1.29E-02	2.90E-03
K: 12 - 21	6.43E-04	1.41E-04	3.02E-05	6.56E-06	1.42E-06	3.04E-07	6.57E-08	1.43E-08	3.04E-09	6.57E-10
K: 22 - 26	1.43E-10	3.04E-11	6.57E-12	1.42E-12	3.68E-13					
I= 3										
K: 3 - 12	3.16E-03	8.84E-02	3.93E-01	7.61E-01	5.34E-01	2.27E-01	7.80E-02	1.95E-02	4.45E-03	9.92E-04
K: 13 - 22	2.18E-04	4.68E-05	1.02E-05	2.21E-06	4.71E-07	1.02E-07	2.21E-08	4.71E-09	1.02E-09	2.21E-10
K: 23 - 26	4.71E-11	1.02E-11	2.21E-12	5.95E-13						
I= 4										
K: 4 - 13	8.82E-02	6.32E-01	6.55E-01	1.77E-01	5.77E-02	1.76E-02	4.30E-03	9.47E-04	2.08E-04	4.55E-05
K: 14 - 23	9.72E-06	2.11E-06	4.57E-07	9.75E-08	2.11E-08	4.58E-09	9.75E-10	2.12E-10	4.53E-11	9.36E-12
K: 24 - 26	2.21E-12	3.67E-13	1.13E-13							
I= 5										
K: 5 - 14	3.75E-01	7.69E-01	2.23E-01	2.72E-02	7.89E-03	1.88E-03	4.17E-04	9.19E-05	2.01E-05	4.30E-06
K: 15 - 24	9.33E-07	2.02E-07	4.32E-08	9.34E-09	2.03E-09	4.32E-10	9.39E-11	2.00E-11	4.06E-12	1.00E-12
K: 25 - 26	1.43E-13	4.77E-14								
I= 6										
K: 6 - 15	7.33E-01	3.45E-01	3.45E-02	6.58E-03	1.45E-03	3.16E-04	7.01E-05	1.54E-05	3.30E-06	7.16E-07
K: 16 - 25	1.55E-07	3.31E-08	7.17E-09	1.56E-09	3.31E-10	7.17E-11	1.56E-11	3.31E-12	7.21E-13	1.53E-13
K: 26 - 26	4.04E-14									
I= 7										
K: 7 - 16	5.26E-01	2.09E-01	8.05E-03	7.36E-04	4.25E-05	9.10E-06	2.01E-06	4.31E-07	9.36E-08	2.03E-08
K: 17 - 26	4.34E-09	9.38E-10	2.04E-10	4.34E-11	9.39E-12	2.04E-12	4.34E-13	9.44E-14	2.01E-14	5.28E-15
I= 8										
K: 8 - 11	3.21E-01	1.20E-01	9.84E-03	6.01E-04						
I= 9										
K: 9 - 11	1.29E-01	2.32E-02	6.67E-05							
I= 10										
K: 10 - 11	1.47E-02	4.07E-03								
I= 11										
K: 11 - 11	9.00E-06									

U2380

I= 1										
K: 1 - 10	0.0	1.06E-02	1.17E-01	4.36E-01	6.92E-01	7.98E-01	4.58E-01	1.70E-01	5.32E-02	2.13E-02
I= 2										
K: 2 - 11	4.43E-04	1.87E-02	2.35E-01	6.41E-01	8.95E-01	5.14E-01	1.96E-01	6.38E-02	1.55E-02	3.49E-03
K: 12 - 21	7.73E-04	1.70E-04	3.63E-05	7.88E-06	1.71E-06	3.65E-07	7.89E-08	1.71E-08	3.65E-09	7.89E-10
K: 22 - 26	1.71E-10	3.65E-11	7.90E-12	1.71E-12	4.50E-13					
I= 3										
K: 3 - 12	3.72E-03	1.07E-01	4.82E-01	9.44E-01	6.66E-01	2.84E-01	9.78E-02	2.45E-02	5.58E-03	1.25E-03
K: 13 - 22	2.74E-04	5.88E-05	1.28E-05	2.77E-06	5.91E-07	1.28E-07	2.78E-08	5.91E-09	1.28E-09	2.78E-10
K: 23 - 26	5.91E-11	1.28E-11	2.78E-12	7.43E-13						
I= 4										
K: 4 - 13	6.83E-02	5.06E-01	1.33E 00	7.21E-01	2.07E-01	5.89E-02	1.40E-02	3.17E-03	7.07E-04	1.56E-04
K: 14 - 23	3.34E-05	7.25E-06	1.57E-06	3.36E-07	7.27E-08	1.58E-08	3.36E-09	7.28E-10	1.57E-10	3.33E-11
K: 24 - 26	7.34E-12	1.45E-12	4.14E-13							
I= 5										
K: 5 - 14	9.73E-01	6.38E-01	4.63E-01	2.51E-01	6.36E-02	1.23E-02	2.65E-03	5.38E-04	1.03E-04	1.86E-05
K: 15 - 24	3.59E-06	7.79E-07	1.66E-07	3.60E-08	7.80E-09	1.66E-09	3.61E-10	7.73E-11	1.60E-11	3.77E-12
K: 25 - 26	6.29E-13	1.90E-13								
I= 6										
K: 6 - 15	1.34E 00	3.83E-01	2.32E-02	1.59E-02	5.72E-03	1.35E-03	3.10E-04	6.81E-05	1.46E-05	3.16E-06
K: 16 - 25	6.85E-07	1.46E-07	3.16E-08	6.86E-09	1.46E-09	3.16E-10	6.86E-11	1.46E-11	3.18E-12	6.76E-13
K: 26 - 26	1.78E-13									
I= 7										
K: 7 - 16	8.11E-01	3.84E-01	2.95E-02	1.14E-03	2.48E-04	5.26E-05	1.16E-05	2.49E-06	5.41E-07	1.18E-07
K: 17 - 26	2.51E-08	5.42E-09	1.18E-09	2.51E-10	5.43E-11	1.18E-11	2.51E-12	5.46E-13	1.16E-13	3.05E-14
I= 8										
K: 8 - 17	4.66E-01	3.68E-01	8.06E-03	1.83E-03	4.03E-04	8.93E-05	1.92E-05	4.18E-06	9.09E-07	1.94E-07
K: 18 - 26	4.20E-08	9.11E-09	1.94E-09	4.20E-10	9.11E-11	1.94E-11	4.22E-12	8.97E-13	2.36E-13	
I= 9										
K: 9 - 14	6.23E-02	1.36E-01	3.63E-02	8.80E-03	1.54E-03	7.57E-05				
I= 10										
K: 10 - 17	0.0	0.0	0.0	0.0	1.44E-04	4.33E-05	5.35E-06	1.32E-07		

VIII. APPENDIX II

Documentation of the assembly characteristics used in the calculations and of the integral data used for the comparison between theory and experiment

It seems necessary or at least very useful to have a fairly complete documentation of the data used as input data in this work. Such a documentation provides the necessary information on the basis of our work, helps in comparing our results with those of similar studies, eases a continuation of this work by ourselves or other people and serves as a sufficiently detailed basis to which to refer in further studies. Most of the information is provided as tables of a fixed forme. The abbreviations and symbols used in these tables are explained in table AII-1.

SUAK U1B

The data for the material and geometric composition have been taken from /-59-7
Other data from the same reference are:

$k_{eff} = 0.86 \pm 0.01$

$\Delta k_{het} \approx 0$ (heterogeneity correction negligible)

The fundamental mode buckling has been determined such as to give agreement for k_{eff} with the one-dimensional calculations. The bucklings used in the one-dimensional calculations have been obtained in an analogous manner by an iteration procedure.

The assembly is symmetric in X and Y-direction. The first data for the one-dimensional SLAB-geometry refer to this X- respectively Y-direction. The second data for the one-dimensional SLAB-geometry refer to the Z-direction (vertical direction). The radius of the equivalent sphere has been determined such as to give the same k_{eff} as that obtained by the other one-dimensional calculations.

The REMO-correction and the S_N-correction have been determined during this study to be -0.0001 and +0.031 respectively. The S_N-correction has been obtained by adding up the individual S_N-corrections for the three directions of the cube. All correction calculations mentioned here have been done using the SNEAK-set.

No reflector has been assumed in the spherical calculations because in reality

4 of the 6 sides of the cube are unreflected.
The calculations mentioned have been done in diffusion approximation with the exception of the S_N-calculations.

SUAK UH1B

The data for the material and geometric composition have been taken from [59]
Ohter data from the same reference are:

$k_{eff} = 0.945 \pm 0.01$
$\Delta k_{het} \approx 0$ (heterogeneity correction negligible)
$\Delta k_{aniso} = +0.007$ (correction for the anisotropic downscattering of hydrogen)

The fundamental mode buckling has been determined such as to give agreement for k_{eff} with the one-dimensional calculations. The bucklings used in the one-dimensional calculations have been obtained in the analogous manner by an iteration procedure.
The assembly is symmetric in X- and Y-direction. The first data for the one-dimensional SLAB-geometry refer to this X- respectively Y-direction. The second data for the one-dimensional SLAB-geometry refer to the Z-direction (vertical direction). The radius of the equivalent sphere has been determined such as to give the same k_{eff} as that obtained by the other one-dimensional calculations.
The REMO-correction and the S_N-correction have been determined during this study to be +0.0003 and +0.030 respectively. The S_N-correction has been obtained by adding up the individual S_N-corrections of the three directions of the cube. All calculations mentioned here have been done using the SNEAK-set.
No reflector has been assumed in the spherical calculations because in reality 4 of the 6 sides of the cube are unreflected.
The calculations mentioned have been done in diffusion approximation with the exception of the S_N-calculations.

ZPR III-10

The data for the material composition have been taken from [75]. The data for the geometrie configuration have been taken from [76]. They are in rather good agreement with those given in [77]. The S_N-correction of +0.013 has also been taken from [75]. It is in very good agreement with that calculated by ourselves of +0.0127. The heterogeneity correction of +0.0105 has been de-

termined from the corresponding data given in table II of [77].
The REMO-correction has been calculated by ourselves to be -0.0008.
The fundamental mode buckling has been determined such as to give agreement for k_{eff} with the one-dimensional calculations. The bucklings used in the one-dimensional calculations have been obtained in an analogous manner by an iteration procedure. The radius of the equivalent sphere has been determined such as to give the same k_{eff} as that of the other one-dimensional calculations leading to a shape factor of 0.9297. The thickness of the blanket of 37 cm for the spherical calculations has been chosen as a guessed average of the real axial and radial blanket thicknesses. Except for the S_N-calculations all calculations mentioned here have been done in diffusion approximation using the SNEAK-set.

ZPR-III-25

The data for the material composition have been taken from [75]. The data for the geometric configuration have been taken from [78]. They are in rather good agreement with those given in [77]. The S_N-correction of +0.002 has been taken also from [75]. It is in very good agreement with that calculated by ourselves of +0.0023.
The heterogeneity correction of +0.0085 has been determined from the corresponding data given in table II of [77]. The REMO-correction has been calculated by ourselves to be -0.0013.
The fundamental mode buckling has been determined such as to give agreement for k_{eff} with the one-dimensional calculations. The bucklings used in the one-dimensional calculations have been obtained in an analogous manner by an iteration procedure. The radius of the equivalent sphere has been determined such as to give the same k_{eff} as that of the other one-dimensional calculations leading to a shape factor of 0.92166. The thickness of the blanket of 37 cm for the spherical calculations has been chosen as a guessed weighted average of the real axial and radial blanket thicknesses.
Except for the S_N-calculations all calculations mentioned here have been done in diffusion approximation using the SNEAK-set.

ZPR III-48

The data for the material and geometric composition of the assembly have essentially been taken from [74], Vol. I, pp. 95-96. Other information is available from [79] and [80]. The mixture number 4 of table AII-6 is used for the blanket in the spherical calculation. Its composition has also been taken from [74] and, as explained there, represents a weighted average of the axial and radial blanket compositions.

The fundamental mode buckling has been determined such as to give agreement for k_{eff} with the one-dimensional calculations. The bucklings used in the one-dimensional calculations have been obtained in an analogous manner by an iteration procedure. The radius of the equivalent sphere has been determined such as to give the same k_{eff} as that of the other one-dimensional calculations leading to a shape factor of 0.933456. Our value of 45.213 cm compares favourably well with that of 45.15 cm given in [74]. In agreement with [74] we have chosen the thickness of the spherical blanket to be equal to that of the radial blanket.

In [74] a S_N-correction of +0.0053 is reported. This represents the difference in k_{eff} for spherical diffusion theory and S_4 transport theory calculations. In our own calculations we found for the same case a value of +0.0065

and a value of +0.0076 by adding up the S_N-corrections for the axial and radial directions, which shows a 15% increase compared to the correction for the spherical case. The finally applied value of +0.006 is based on the value 0.0053 but takes into account the 15% increase just mentioned before. The heterogeneity correction of +0.014 has been taken from [74]. It is in between other published values for the same assembly of +0.013 by Edison [81] and +0.016 by Broomfield. The REMO-correction of +0.0046 has been calculated by ourselves. All our calculations referred to here have been done using the SNEAK-set. Except for the S_N-calculations the diffusion approximation has been applied.

The experimental results for the central reaction rate ratios and for the material worths relative to that of U235 have been taken from [74]. Almost all of these values are also given in [79]. It is known that there exists a general difficulty in calculating the absolute worth of materials correctly even for such important reactor materials as U235 or Pu239. Furthermore there is a discrepancy in the conversion factor from inhours to $\Delta k/k$ for ZPR III-48: 1002 inhours $\triangleq 1\%\Delta k/k$ is published in [79] and 942 inhours $\triangleq 1\%\Delta k/k$ is used in [74]. If one assumes that the reson for the present difficulties in calculating the correct absolute

material worth, as is presently supposed, is due to a normalization effect, for example in β_{eff}, one may avoid these difficulaties by comparing the theoretical and experimental data for the material worths relative to the material worth of U235. This has been done in the present work.

ZPR III-48B

The assembly ZPR III-48B is very similar to ZPR III-48. The only difference, apart from a small change in core radius, is the central plutonium zone. The plutonium isotopic mixture of this zone contains a larger amount of higher plutonium isotopes, especially of Pu240. The composition of this inner zone has been taken from [83]. The data for the real core geometry are those reported in [74]. The core radii for the equivalent spherical model have been derived by ourselves applying a shape factor of 0.933456 which we derived for the similar assembly ZPR III-48. The equivalent spherical core radius of 45.7045 is in good agreement with the value of 45.67 published in [74]. The thickness of the spherical blanket has been chosen to be 30.0 cm, the same as that for ZPR III-48, in close agreement with the actual reactor axial and radial blanket thicknesses.

The S_N- and heterogeneity-corrections have been taken the same as the corresponding values for ZPR III-48. The REMO-correction of +0.0047 has been calculated for the spherical model of the assembly by ourselves. As usually the SNEAK-set and diffusion approximation have been used for this calculation.

The central fission ratios are taken from [83] p. 65, the data for the central material worths from [74] p. 57. The same arguments as for ZPR III-48 are adopted in using the material worth relative to that of U235 for the comparison between theory and experiment.

A median fission energy of 223.1 keV has been obtained for ZPR III-48B in an analogous manner to that used for the determination of the values given in table 1.

ZEBRA-6A

The data for the material and geometric composition have been taken from [84]. The S_N-correction of +0.010 has been taken from [75]. It is almost the same as that of +0.011 reported in [84]. Our own value of +0.0117 is in reasonable agreement with the above values. The heterogeneity correction has to be taken as zero since the real heterogeneous assembly has been transformed into a homogeneous model for the calculations using an experimentally determined correction for the

heterogeneity. The REMO-correction of +0.0040 has been determined by ourselves.

The fundamental mode buckling has been determined such as to give agreement for k_{eff} with the one-dimensional calculations. The bucklings used in the one-diemensional calculations have been obtained in an analogous manner by an iteration process. The radius of the equivalent sphere has been determined such as to give the same k_{eff} as that of the other one-dimensional calculations, leading to a shape factor of 0.9456. The shape factor given in [84] is 0.935. We have chosen for the thickness of the spherical blanket the same value as that for the real radial blanket thickness, since leakage in radial direction is more important than in axial direction.

The experimental values for the central reaction rate ratios have also been taken from [84].

All our calculations mentioned here have been done using the SNEAK-set. Except for the S_N-calculations the diffusion approximation has been applied.

SNEAK 3A1

The assembly SNEAK 3A1 has first been described in [66]. A comprehensive description of the experiments in the SNEAK-3A assemblies with the exception of SNEAK 3A1 has been compiled by SEHRÖDER [67]. The material compositions chosen for our work have been taken from this study [67], since it is based on a more refined (compared to [66]) evaluation of the experiments. The C- and H-concentrations of the mixtures 1 and 2 have been taken from [66]. The blanket composition, mixture 3, has been the same for SNEAK 3A1 and SNEAK 3A2. Mixture 4 has also essentially been taken from SNEAK 3A2 except for the C- and H- concentration. The H-concentration has been determined as volume-average of the H-concentration of the two core zones containing mixture 1 and mixture 2 respectively. The C-concentration then has been adjusted assuming that for polyethylene the hydrogen content is twice that of carbon (CH_2). This way of determining the C-concentration seems more appropriate for the calculation of the so-called steam density coefficient and its comparison with the experiment. Mixture 4 has been used in the fundamental mode and one-dimensional axial calculations. With respect to the data on geometry the height of the axial zones has been taken from [66]. The outer dimension of the assembly has also been taken from [67] since these data seem to be more reliable and the outer dimensions of the assembly have not been changed during the SNEAK-3A-experiments [85]. The radii of the inner and

outer core zone have been taken from [66].
The S_N-correction of +0.003 has been taken from [66]. It is in reasonable agreement with the value calculated by ourselves of +0.0038. The heterogeneity-correction of +0.003 has also been taken from [66]. The REMO-correction of -0.0006 has been calculated by ourselves.
The fundamental mode buckling has been determined such as to give agreement for k_{eff} with the one-dimensional calculations. The bucklings used in the one-dimensional calculations have been obtained in an analogous manner by an iteration procedure. The outer core radius of the equivalent sphere has been determined such as to give the same k_{eff} as that of the other one-dimensional calculations leading to a shape factor of 0.92347. Using this shape factor and the given volume of the inner core zone the radius of the inner core zone has been derived. This value is only of minor importance since both core zones have very similar compositions. We have chosen for the thickness of the spherical blanket the same value as that for the real radial blanket thickness since leakage in radial direction is more important than that in axial direction. Furthermore the thicknesses of the radial and axial blanket are nearly equal 29.66 cm and 30.5 cm respectively.
The SNEAK-set and diffusion approximation have been used in all cases except those where other information is mentioned explicitly.

SNEAK 3A2

The data for the material and geometric composition have been taken from [67]. One should mention that the composition of mixture 4 has been obtained as a volume-average of the compositions of mixture 1 and mixture 2 which are present in the inner and outer core zone respectively. Mixture 4 has been used in the fundamental mode and one-dimensional axial calculations.
The S_N-correction of +0.004 has been published in [2], p. 29. It is in good agreement with the value of +0.0041 calculated by ourselves. The heterogeneity correction of +0.004 is given in [2] p. 29 for a calculation using the so-called H2OPMB-set [2], which is a modified SNEAK-set very similar to the SNEPMB-set used in our present study. The same value is reported in [57], p. 14. Using the SNEAK-set a slightly different value of +0.003 has been obtained in [2]. The small difference of 0.001 in k, however, is not important with respect to the final conclusion to be drawn from the comparison between theory and experiment because the differences observed are most times in the order of 1%. The REMO-correction of -0.0006 has been determined by ourselves. It is rather small but

has a different sign compared to the values obtained in [2] for the SNEAK- and H2OPMB-sets. A possible explanation for this difference is the fact that in the present study the REMO correction is applied to all regions of the assembly including the blanket whereas in the previous study [2] the REMO-correction has been applied to the core region only.
The fundamental mode buckling has been determined such as to give agreement for k_{eff} with the one-dimensional calculations. The bucklings used in the one-dimensional calculations have been obtained in an analogous manner by an iteration procedure. The outer core radius of the equivalent sphere has been determined such as to give the same k_{eff} as that of the other one-dimensional calculations leading to a shape factor of 0.93613. Using this shape factor and the given volume of the inner core zone the radius of the inner core zone has been derived. This value is only of minor importance since both core zones have very similar compositions. We have chosen for the thickness of the spherical blanket the same value as that for the real radial blanket thickness since leakage in radial direction is more important than that in axial direction.

The SNEAK-set and diffusion approximation have been used in all cases except those where other information is mentioned explicitly.

SNEAK 3B2

Experiments and various calculations for the Uranium-Plutonium fuelled assembly SNEAK 3B2 have been described in [68]. Our calculations are based on the same data for the material and geometric composition as reported in that paper.
For the calculation of the axial buckling we have used an axial saving of 13.81 cm which has been obtained at an early stage of the present calculations for SNEAK 3A2. The final correct value of 13.29 cm is not too different from the preliminary value used here. The adoption of the SNEAK 3A2 saving for the assembly SNEAK 3B2 seems to be reasonable because the core-geometry and composition are very similar.

The S_N-correction of +0.004 is assumed to be the same as that for the similar SNEAK 3A2 assembly. The heterogeneity-correction of +0.003 is taken from [68].

The REMO-correction, calculated in the usual manner, is found to be +0.0008. In all calculations mentioned here the SNEAK-set and diffusion approximation have been used.

A median fission energy of 81.81 keV has been obtained for SNEAK 3B2 in an analogous manner to that used for the determination of the values given in table 1.

SNEAK-5C

In SNEAK assembly 5 a series of experiments was carried out to determine k_∞ and reaction rate ratios. The most important of these experiments is that labelled SNEAK-5C. The composition of its inner most zone was chosen to render a k_∞ close to unity. The composition given in table AII-12 has been provided by MEISTER [86]. It should be considered as preliminary but it is to be expected that the final composition which will be published in a comprehensive report on these experiments [62] will not differ very much from that given in table In this report additional detailed information especially on the driver zone will be published.
The heterogeneity-correction of +0.071 has been determined by FISCHER [87] as preliminary result. Meanwhile a somewhat smaller value of +0.068 has been calculated by ourselves. But it seems to us that even this value is probably too large. The REMO-correction of +0.016 has been calculated by ourselves using diffusion approximation. All calculations mentioned here have been done using the group constants of the SNEAK-set.

ZPR III-55

The main incentive for the ZPRIII-55 experiment was to measure the α-value of Pu239 by means of a k_∞ experiment ($\alpha=\sigma_c/\sigma_f$). The composition of the k_∞-zone has been taken from [88]. More recent information is published in [89]. The heterogeneity-correction of +0.010 has been reported by JOURDAN [90]. The REMO-correction of +0.011 has been calculated by ourselves using diffusion approximation. All calculations mentioned here have been done using the SNEAK-set.

SNEAK-series

In our work we have included the so-called SNEAK-series which refers to a series of SNEAK assemblies namely, 3A0, 3A1, 3A2, 3A3 carried out to get information on the steam-density and steam-void coefficient. The assemblies SNEAK 3A1 and SNEAK 3A2 have been described above. SNEAK 3A0 refers to a core composition

where the polyethylene foils have been removed completely so that the hydrogen concentration is zero; the carbon concentration is reduced by the corresponding amount. In SNEAK 3A3 the hydrogen concentration of the core has been doubled by doubling the thickness of the polyethylene foils; the carbon concentration is increased by the corresponding amount. The experiments have been evaluated in [57] by assuming that the core compositions of the different hydrogen contents (and the correspondingly different carbon contents) are placed into the core geometry of the assembly SNEAK 3A2. All experimental and theoretical results therefore are normalized relative to SNEAK 3A2. Especially the calculated criticality is adjusted so that by adding or subtracting a small amount to the k_{eff} of all 4 assemblies the adjusted value for k_{eff} of SNEAK 3A2 is equal to unity.

The core geometry has been simplified for our calculations since it would take too much computer time to take into account the geometry assumed for the evaluation of the experiments and since we expected that fundamental mode calculations would be sufficiently accurate for a comparison of the theoretical and experimental results for the steam-density and steam void coefficient. The bucklings used in the fundamental mode calculations are given in table AII-14. They have been obtained in the following manner. For SNEAK 3A2 the reflector savings of the axial and radial blankets have been determined from the bucklings given in tables AII-9 and AII-10 and the real core geometry also given in these tables.

For the determination of the savings for SNEAK-3A0 by one-dimensional calculations we placed the composition used in the fundamental mode calculations for this assembly into the core geometry of SNEAK 3A2, because 3A0 can be considered as the voided version of 3A2 (see [57]). The savings for SNEAK 3A3 have been obtained by placing the composition used in the fundamental mode calculations into the whole core of the SNEAK 3A3 experiment. In the real 3A3 configuration this composition of high hydrogen concentration was contained only in an inner zone of 18.7 cm whereas the core radius was 42.2 cm as given in [67]. The outer core zones in the real SNEAK 3A3 experiment were the same as in SNEAK 3A2.

The core geometry chosen for the determination of the savings is not a crucial point because according to our experience the savings depend more strongly on the core composition (and eventually on the blanket composition if it is changed) than on the core geometry. Furthermore the core geometry does not change drastically for the experiments 3A0, 3A1, 3A2, 3A3. The core height is the same for all 4 experiments and the radius varies between a smallest value of 42.2 cm

and a largest value of 51.2 cm.

The agreement between our values of k_{eff} for the 4 assemblies determined in the indicated manner and the corresponding values given in [57] can be considered as a check of the adequacy of our approximate procedure.

The compositions used in the fundamental mode calculations are derived from mixture 4 given in table AII-10 for SNEAK 3A2. The concentrations of all isotopes or elements are taken the same in all 4 compositions of the fundamental mode calculations with the exception of carbon and hydrogen. The carbon- and hydrogen concentrations used are given in table AII-14.

The S_N-correction for SNEAK 3A0 of +0.003 has been taken the same as that for SNEAK 3A1. The S_N-correction of +0.004 for SNEAK 3A3 has been taken the same as that for SNEAK 3A2. The heterogeneity corrections of +0.001, +0.003, +0.004, +0.007 for the assemblies 3A0, 3A1, 3A2, 3A3 respectively have been taken from [57], p. 14. The REMO-corrections of -0.0015, -0.0006, -0.0006, -0.0009 for the 4 assemblies have been calculated by ourselves. For the assemblies SNEAK 3A0, SNEAK 3A1, and SNEAK 3A2 the spherical appropriate models have been applied in the one-dimensional calculations. For SNEAK 3A0 this means a radius of the inner core zone of 41 cm, a radius of the outer core zone of 48.56 cm and a blanket thickness of 36.2 cm.

For SNEAK 3A3 the REMO-correction has been determined for the one-dimensional radial geometry. The composition used in the whole core is that taken in the corresponding fundamental mode calculation.

Table AII-1

Explanation of the abbreviations and symbols used in tables AII-2 through AII-13

MIXTURE: The mixtures are numbered consecutively in order to refer on the numbers furtheron

MATERIAL: The material means either element (in natural composition) or isotope. One should mention that only for U235, U238 and Pu239 the cross sections are taken at 300°K. For all other materials the cross sections are taken at 900°K or assumed to be independent of the temperature.

Fundamental mode calculations

NG: Number of energy groups

MIXT: Number of mixtures

BUCKo: Buckling used for the fundamental mode calculations

One-dimensional calculations

GEO: Kind of geometry: slab, cylinder or sphere

NG: Number of energy groups

BUCKLING: Buckling used to take into account the leakage into the separated directions

BC: Boundary condition; the first number refers to the left hand side, the second number to the right hand side.

2 ≙ net current = 0, symmetric or reflective boundary condition

3 ≙ usual diffusion boundary condition

$$\phi_B \pm 0.71 \cdot \lambda_{tr} \cdot \phi'_B = 0$$

where ϕ_B and ϕ'_B are the flux and its gradient at the boundary and the plus sign refers to the right hand, the minus sign to the left hand boundary, if the axis is directed to the right hand side.

NZ: Number of zones

NP: Number of mesh points

ZONE IZ: The zones are numbered consecutively from 1-NZ to refer on zone number IZ in the twodimensional case

MIXT: Number of the MIXTURE mentioned above which is present in zone IZ

XL: Left hand abscissa (radius) of zone IZ

INT: Number of mesh intervals used in this zone

XR: Right hand abscissa (radius) of zone IZ

Two-dimensional calculations

GEO: Geometry
1 = XY-Geometry
2 = RZ-Geometry
3 = RΘ-Geometry

NG: Number of energy groups

NP: Total number of mesh points

ROWS: Number of rows

COL: Number of columns

NZ: Number of zones

BCL: Boundary condition at left hand boundary

BCR: Boundary condition at right hand boundary

BCUP: Boundary condition at upper boundary

BCLOW: Boundary condition at lower boundary

2 ≙ net current = 0, symmetric or reflective condition
3 ≙ usual diffusion boundary condition

SPEKTRUM FOR COND: Origin of the spectrum used for the condensation to few group constants (taken from one of the one-dimensional calculations)

NEW GROUP: The new groups are numbered consecutively

IGUP OLD GROUPS: Upper group index of those groups which belong to the new group considered

MIXT: Number of the new mixture used in the two-dimensional calculations. It may be different from the original number of the mixtures in the line MIXTURE because two different condensation spectra are used for the same mixture of the line MIXTURE. Since different few group cross sections arise from this procedure, the new mixtures characterized by MIXT must be distinguished from each other.

MIXTURE: Number of the original mixture from the line MIXTURE.

PHI-1 dim.(IZ) : The spectrum of the zone number IZ of the one-dimensional calculation indicated in SPEKTRUM FOR COND is used for the condensation of the few group constants of the special mixture (MIXT) considered

ZONE: The two-dimensional zones are numbered consecutively

MIXT: MIXTURE used in the special zone considered

RL: Left radius (or abscissa) of the zone considered

INTH: Number of mesh intervals in the horizontal direction of the zone considered

RR: Right radius (or abscissa) of the zone considered

HUP: Upper height (or radius) of the zone considered

INTV: Number of mesh intervals in the vertical direction of the zone considered

HLOW: Lower height (or radius) of the zone considered

Table AII-2

CRITICAL FACILITY: SUAK U1B

Atom-Densities (in 10^{20} atoms/cm^3)

Mixture / Material	1	2	3	4
Al	42.77	438.0	-	600.0
C	-	-	-	-
Fe	-	-	844.0	-
H	-	-	-	-
Ni	6.60	-	-	-
U235	81.50	-	-	-
U238	328.97	-	-	-

Fundamental Mode Calculation:

NG	MIXT	Bucko
26	1	$197.898 \cdot 10^{-4}$ cm^{-2}

One-Dimensional Calculations:

GEO	NG	Buckling	BC	NZ	NP
SLAB	26	$128{,}097 \cdot 10^{-4}$ cm^{-2}	23	1	101

Zone IZ	MIXT	XL /cm/	INT	XR /cm/
1	1	0.	100	16.15

GEO	NG	BUCKLING	BC	NZ	NP
SLAB	26	$139.601 \cdot 10^{-4}\ cm^{-2}$	33	4	116

Zone IZ	MIXT	XL /~cm_7	INT	XR /~cm_7
1	4	0.0	15	3.0
2	3	3.0	10	6.5
3	1	6.5	80	41.6
4	2	41.6	10	44.6

GEO	NG	BUCKLING	BC	NZ	NP
SPHERE	26	-	23	1	101

Zone IZ	MIXT	XL /~cm_7	INT	XR /~cm_7
1	1	0.0	100	19.363968

Table AII-3

CRITICAL FACILITY: SUAK UH1B

Atom-Densities (in 10^{20} atoms/cm^3)

Mixture Material	1	2	3	4
Al	42.77	438.0	-	600.0
C	74.22	-	-	-
Fe	-	54.0	844.0	-
H	148.44	-	-	-
Ni	5.29	-	-	-
U235	65.02	-	-	-
U238	262.37	-	-	-

Fundamental Mode Calculation:

NG	MIXT	Bucko
26	1	$205.338 \cdot 10^{-4}$ cm^{-2}

One-Diemensional Calculations:

GEO	NG	BUCKLING	BC	NZ	NP
SLAB	26	$134.681 \cdot 10^{-4}$ cm^{-2}	23	1	101

ZONE IZ	MIXT	XL /cm/	INT	XR /cm/
1	1	0.	100	16.15

GEO	NG	BUCKLING	BC	NZ	NP
SLAB	26	$141.314 \cdot 10^{-4}$ cm^{-2}	33	4	116

ZONE IZ	MIXT	XL /cm/	INT	XR /cm/
1	4	0.0	15	3.0
2	3	3.0	10	6.5
3	1	6.5	80	39.55
4	2	39.55	10	42.55

GEO	NG	BUCKLING	BC	NZ	NP
SPHERE	26	-	23	1	101

ZONE IZ	MIXT	XL /cm/	INT	XR /cm/
1	1	0.0	100	19.087051

Table AII-4

CRITICAL FACILITY: ZPRIII-10

Atom-Densities (in 10^{20} atoms/cm^3)

Mixture / Material	1	2
Cr	29.6	11.2
Fe	171.1	44.0
Ni	17.8	6.7
U235	56.88	0.91
U238	277.9	399.8

Fundamental Mode Calculation:

NG	MIXT	BUCKo
26	1	$81.373 \cdot 10^{-4}$ cm^{-2}

One-Dimensional Calculations:

GEO	NG	BUCKLING	BC	NZ	NP
SLAB	26	57.534	23	3	113

ZONE IZ	MIXT	XL /~cm_7	INT	XR /~cm_7
1	1	0.	20	10.0
2	1	10.0	26	22.95
3	2	22.95	66	55.95

GEO	NG	BUCKLING	BC	NZ	NP
CYL	26	$23.839 \cdot 10^{-4}$ cm^{-2}	23	3	129

ZONE IZ	MIXT	XL [cm]	INT	XR [cm]
1	1	0.	20	10.0
2	1	10.0	24	22.11
3	2	22.11	84	63.59

GEO	NG	BUCKLING	BC	NZ	NP
SPHERE	26	-	23	3	125

ZONE IZ	MIXT	XL [cm]	INT	XR [cm]
1	1	0.	20	10.0
2	1	10.0	30	25.011
3	2	25.011	74	62.011

Two-Dimensional Calculations:

GEO	NG	NP	ROWS	COL	NZ	BCL	BCR	BCUP	BCLOW	SPECTRUM FOR COND
2	11	1152	32	36	5	2	3	2	3	1-dim. SPHERE

NEW GROUP	1	2	3	4	5	6	7	8	9	10	11
IGUP OLD GROUPS	2	3	4	5	6	7	8	9	15	20	26

MIXT	I	II	III
MIXTURE	1	1	2
PHI-1 dim (IZ)	1	2	3

ZONE	MIXT	RL [cm]	INT	RR [cm]	HUP [cm]	INT	HLOW [cm]
1	I	0.	6	10.0	10.0	6	0.
2	II	10.0	8	22.11	22.95	14	0.
3	II	0.	6	10.0	22.95	8	10.0
4	III	22.11	21	63.59	55.95	31	0.
5	III	0.	14	22.11	55.95	17	22.95

Table AII-5

CRITITCAL FACILITY: ZPRIII-25

Atom-Densities (in 10^{20} atoms/cm^3)

Mixture Material	1	2
Cr	14.0	11.2
Fe	55.5	44.0
Ni	8.4	6.7
U235	34.42	0.91
U238	356.0	399.8

Fundamental Mode Calculation:

NG	MIXT	BUCKo
26	1	$31.725 \cdot 10^{-4}$ cm^{-2}

One-Dimensional Calculations:

GEO	NG	BUCKLING	BC	NZ	NP
SLAB	26	$20.981 \cdot 10^{-4}$ cm^{-2}	23	3	137

ZONE IZ	MIXT	XL / cm /	INT	XR / cm /
1	1	0	20	10.0
2	1	10.0	56	38.175
3	2	38.175	60	68.675

GEO	NG	BUCKLING	BC	NZ	NP
CYL	26	$10.744 \cdot 10^{-4}$ cm^{-2}	23	3	145

ZONE IZ	MIXT	XL / cm /	INT	XR / cm /
1	1	0.	20	10.0
2	1	10.0	64	42.60
3	2	42.60	60	83.40

GEO	NG	BUCKLING	BC	NZ	NP
SPHERE	26	-	23	3	149

ZONE IZ	MIXT	XL /cm/	INT	XR /cm/
1	1	0.	20	10.0
2	1	10.0	70	45.753
3	2	45.753	58	82.753

Two-Dimensional Calculations:

GEO	NG	NP	ROWS	COL	NZ	BCL	BCR	BCUP	BCLOW	SPEKTRUM FOR COND
2	11	1584	36	44	5	2	3	3	2	1 dim. SPHERE

NEW GROUP	1	2	3	4	5	6	7	8	9	10	11
IGUP OLD GROUPS	2	3	4	5	6	7	8	9	11	16	26

MIXT	I	II	III
MIXTURE	1	1	2
PHI-1 dim (IZ)	1	2	3

ZONE	MIXT	RL /cm/	INT	RR /cm/	HUP /cm/	INT	HLOW /cm/
1	I	0.	5	10.0	10.0	5	0.
2	II	10.0	17	42.6	38.175	20	0.
3	II	0.	5	10.0	38.175	15	10.0
4	III	42.6	21	83.4	68.675	35	0.
5	III	0.	22	42.6	68.675	15	38.175

Table AII-6

CRITICAL FACILITY: ZPRIII-48

Atom-Densities (in 10^{20} atoms/cm^3)

Mixture / Material	1	2	3	4
Al	1.09	-	-	-
C	207.67	-	-	-
Cr	26.81	14.81	11.93	12.8
Fe	99.85	55.15	44.44	47.7
Mo	2.06	-	-	-
Na	62.31	-	-	-
Ni	13.30	7.29	5.87	6.3
Pu239	16.45	-	-	-
Pu240	1.06	-	-	-
Pu241	0.11	-	-	-
Pu242	0.004	-	-	-
U235	0.16	0.82	0.83	0.83
U238	74.27	383.77	397.98	393.0

Fundamental Mode Calculation:

NG	MIXT	BUCKo
26	1	27.015 10^{-4} cm^{-2}

One-Dimensional Calculations:

GEO	NG	BUCKLING	BC	NZ	NP
SLAB	26	18.132 10^{-4} cm^{-2}	23	2	91

ZONE IZ	MIXT	XL [cm]	INT	XR [cm]
1	1	0.	60	38.18
2	2	38.18	30	68.66

GEO	NG	BUCKLING	BC	NZ	NP
CYL	26	$8.883\ 10^{-4}\ cm^{-2}$	23	2	91

ZONE IZ	MIXT	XL /cm/	INT	XR /cm/
1	1	0.	60	41.58
2	3	41.58	30	71.58

GEO	NG	BUCKLING	BC	NZ	NP
SPHERE	26	-	23	3	91

ZONE IZ	MIXT	XL /cm/	INT	XR /cm/
1	1	0.	14	10.0
2	1	10.0	46	45.213
3	4	45.213	30	75.213

TWODIMENSIONAL CALCULATIONS:

GEO	NG	NP	ROWS	COL	NZ	BCL	BCR	BCUP	BCLOW	SPEKTRUM FOR COND
2	11	1296	36	36	5	2	3	3	2	1-dim. SPHERE

NEW GROUP	1	2	3	4	5	6	7	8	9	10	11
IGUP OLD GROUPS	3	4	5	6	7	8	9	10	12	16	26

MIXT	I	II	III	IV
MIXTURE	1	1	2	3
PHI-1dim (IZ)	1	2	3	3

ZONE	MIXT	RL [cm]	INT	RR [cm]	HUP [cm]	INT	HLOW [cm]
1	I	0.	4	10.0	10.0	5	0.
2	II	10.0	16	41.58	38.18	20	0.
3	II	0.	4	10.0	38.18	15	10.0
4	III	0.	20	41.58	68.66	15	38.18
5	IV	41.58	15	71.58	68.66	35	0.

Table AII-7

CRITICAL FACILITY: ZPRIII-48B

Atom Densities (in 10^{20} atoms/cm^3)

Mixture / Material	1	2	3	4	5
Al	1.18	1.09	-	-	-
C	207.67	207.67	-	-	-
Cr	51.92	26.81	14.81	11.93	12.8
Fe	102.23	99.85	55.15	44.44	47.7
Mo	2.06	2.06	-	-	-
Na	62.31	62.31	-	-	-
Ni	11.13	13.30	7.29	5.87	6.3
Pu239	14.36	16.45	-	-	-
Pu240	3.11	1.06	-	-	-
Pu241	0.59	0.11	-	-	-
Pu242	0.07	0.004	-	-	-
Si	1.25	-	-	-	-
U235	0.16	0.16	0.82	0.83	0.83
U238	74.05	74.27	383.77	397.98	393.0

GEO	NG	BUCKLING	BC	NZ	NP
SPHERE	26	-	23	3	86

ZONE IZ	MIXT	XL [cm]	INT	XR [cm]
1	1	0.	30	19.758
2	2	19.758	25	45.7045
3	5	45.7045	30	75.7045

Two-Dimensional Calculations:

GEO	NG	NP	ROWS	COL	NZ	BCL	BCR	BCUP	BCLOW	SPEKTRUM FOR COND
2	11	1296	36	36	5	2	3	3	2	1-dim. SPHERE

NEW GROUP	1	2	3	4	5	6	7	8	9	10	11
IGUP OLD GROUPS	3	4	5	6	7	8	9	10	12	16	26

MIXT	I	II	III	IV
MIXTURE	1	2	3	4
PHI-1 dim (IZ	1	2	3	3

ZONE	MIXT	RL /cm/	INTH	RR /cm/	HUP /cm/	INTV	HLOW /cm/
1	I	0.	8	19.0	15.26	7	0.
2	II	19.0	12	42.26	38.18	20	0.
3	II	0.	8	19.0	38.18	13	15.26
4	III	0.	20	42.26	68.66	15	38.18
5	IV	42.26	15	71.58	68.66	35	0.

Table AII-8

CRITICAL FACILITY: ZEBRA-6A

Atom Densities (in 10^{20} atoms/cm^3)

Mixture / Material	1	2
Al	25.04	-
C	295.90	234.10
Cr	12.70	9.13
Cu	8.29	-
Fe	42.55	32.53
Na	44.74	-
Ni	4.43	3.18
Pu239	18.79	-
Pu240	1.44	-
Pu241	0.16	-
U235	0.46	1.94
U238	63.53	268.10

Fundamental Mode Calculation:

NG	MIXT	BUCKo
26	1	$34.596 \cdot 10^{-4}$ cm^{-2}

One-Dimensional Calculations:

GEO	NG	BUCKLING	BC	NZ	NP
SLAB	26	$22.178 \cdot 10^{-4}$ cm^{-2}	23	2	101

ZONE IZ	MIXT	XL /~cm_7	INT	XR /~cm_7
1	1	0.	60	30.08
2	2	30.08	40	60.50

GEO	NG	BUCKLING	BC	NZ	NP
CYL	26	$12.418 \cdot 10^{-4}$ cm^{-2}	23	3	141

ZONE IZ	MIXT	XL /~cm_7	INT	XR /~cm_7
1	1	0.	20	10.0
2	1	10.0	52	36.15
3	2	36.15	68	70.59

GEO NG	BUCKLING	BC	NZ	NP
SPHERE 26	-	23	3	131

ZONE IZ	MIXT	XL /~cm_7	INT	XR /~cm_7
1	1	0.	26	10.0
2	1	10.0	74	38.203
3	2	38.203	30	72.643

Two-Dimensional Calculations:

GEO	NG	NP	ROWS	COL	NZ	BCL	BCR	BCUP	BCLOW	SPEKTRUM FOR COND
2	11	1152	32	36	5	2	3	3	2	1-dim. SPHERE

NEW GROUP	1	2	3	4	5	6	7	8	9	10	11
IGUP OLD GROUPS	3	4	5	6	7	8	9	10	12	16	26

MIXT	I	II	III
MIXTURE	1	1	2
PHI-1 dim (IZ)	1	2	3

ZONE	MIXT	RL [cm]	INTH	RR [cm]	HUP [cm]	INTU	HLOW [cm]
1	I	0.	5	10.0	10.0	5	0.
2	II	10.0	13	36.15	30.08	16	0.
3	II	0.	5	10.0	30.08	11	10.0
4	III	36.15	17	70.59	60.50	31	0.
5	III	0.	18	36.15	60.50	15	30.08

Table AII-9

CRITICAL FACILITY: SNEAK 3A1

Atom-Densities (in $10^{20}/cm^3$)

Mixture / Material	1	2	3	4
Al	129.10	129.36	-	129.211
C	4.12	4.13	0.14	4.063
Cr	36.47[1]	36.32[2]	11.95[3]	36.380
Fe	122.04[4]	121.51[5]	39.55	121.730
H	7.40	7.42	-	7.412
Mg	0.64	0.64	-	0.640
Mo	0.39	0.39	0.19	0.390
Ni	18.54	18.27	9.84	18.424
O	145.29	145.67	-	145.510
Si	1,88	1.86	0.46	1.870
Ti	0.40	0.39	-	0.394
U235	20.31	20.25	1.625	20.270
U238	81.04	81.21	399.414	81.140

Fundamental Mode Calculation:

NG	MIXT	BUCK
26	4	$22.010 \cdot 10^{-4}$ cm^{-2}

One-Dimensional Calculations:

GEO	NG	BUCKLING	BC	NZ	NP
SLAB	26	$13.540 \cdot 10^{-4}$ cm^{-2}	23	2	91

1) includes 1.94 of Mn
2) includes 1.96 of Mn
3) includes 0.87 of Mn
4) includes 0.19 of Co
5) includes 0.18 of Co

ZONE IZ	MIXT	XL /~cm_7	INT	XR /~cm_7
1	4	0.	60	40.27
2	3	40.27	30	70.77

GEO	NG	BUCKLING	BC	NZ	NP
CYL	26	$8.470 \cdot 10^{-4}$ cm^{-2}	23	4	121

ZONE IZ	MIXT	XL /~cm_7	INT	XR /~cm_7
1	1	0.	30	5.0
2	1	5.0	30	32.9
3	2	32.9	30	51.2
4	3	51.2	30	80.86

GEO	NG	BUCKLUNG	BC	NZ	NP
SPHERE	26	-	23	3	147

ZONE IZ	MIXT	XL /~cm_7	INT	XR /~cm_7
1	1	0.	48	39.231
2	2	39.231	48	52.684
3	3	52.684	50	82.344

Two-Dimensional Calculations:

GEO	NG	NP	ROWS	COL	NZ	BCL	BCR	BCUP	BCLOW	SPEKTRUM FOR COND
2	11	1600	40	40	4	2	3	3	2	1 dim - SPHERE

NEW GROUP	1	2	3	4	5	6	7	8	9	10	11
IGUP OLD GROUPS	2	3	4	5	6	7	8	9	11	16	26

MIXT	I	II	III
MIXTURE	1	2	3
PHI-1-dim (IZ)	1	2	3

ZONE	MIXT	RL [cm]	INTH	RR [cm]	HUP [cm]	INTU	HLOW [cm]
1	I	0.	16	32.90	40.27	20	0.
2	II	32.90	9	51.20	40.27	20	0.
3	III	0.	25	51.20	70.77	19	40.27
4	III	51.20	14	80.86	70.77	39	0.

Table AII-10

CRITICAL FACILITY: SNEAK 3A2

Atom-Densities (in 10^{20} atoms/cm^3)

Mixture Material	1	2	3	4
Al	129.10	129.36	-	129.211
C	9.32	9.08	0.14	9.217
Cr	36.47[1]	36.32[2]	11.95[3]	36.380
Fe	122.04	121.51[5]	39.55	121.730
H	17.92	17.45	-	17.719
Mg	0.64	0.64	-	0.640
Ni	18.54	18.27	9.84[*]	18.424
Mo+Nb	0.39	0.39	0.19	0.390
O	145.29	145.67	-	145.510
Si	1.88	1.86	0.46	1.870
Ti	0.40	0.39	-	0.394
U235	20.31	20.25	1.625	20.270
U238	81.04	81.21	399.414	81.140

Fundamental Mode Calculations:

NG	MICT	BUCKo
26	4	$25.549 \cdot 10^{-4}$ cm^{-2}

One-Dimensional Calculations:

GEO	NG	BUCKLING	BC	NZ	NP
SLAB	26	$16.949 \cdot 10^{-4}$ cm^{-2}	23	2	91

1) includes 1.94 of Mn
2) includes 1.96 of Mn
3) includes 0.87 of Mn
4) includes 0.19 of Co
5) includes 0.18 of Co

[*] The number given by R. Böhme and H. Seufert in KFK-811 and in Nuclear Applications & Technology Vol. 7, p. 494, 1969 is in error.

ZONE IZ	MIXT	XL /~cm_7	INT	XR /~cm_7
1	4	0.	60	40.27
2	3	40.27	30	70.77

GEO	NG	BUCKLING	BC	NZ	NP
CYL	26	$8.600 \cdot 10^{-4}$ cm^{-2}	23	4	121

ZONE IZ	MIXT	XL /~cm_7	INT	XR /~cm_7
1	1	0.	30	5.0
2	1	5.0	30	33.76
3	2	33.76	30	44.66
4	3	44.66	30	80.86

GEO	NG	BUCKLING	BC	NZ	NP
SPHERE	26	-	23	3	131

ZONE IZ	MIXT	XL /~cm_7	INT	XR /~cm_7
1	1	0.	83	40.094
2	2	40.094	17	48.315
3	3	48.315	30	84.515

Two-Dimensional Calculations:

GEO	NG	NP	ROWS	COL	NZ	BCL	BCR	BCUP	BCLOW	SPEKTRUM FOR COND
2	11	1600	40	40	4	2	3	3	2	1 dim- SPHERE

NEW GROUP	1	2	3	4	5	6	7	8	9	10	11
IGUP OLD GROUP	3	4	6	7	8	9	10	11	13	15	26

MIXT	I	II	III
MIXTURE	1	2	3
PHI-1 dim (IZ)	1	2	3

ZONE	MIXT	RL [cm]	INTH	RR [cm]	HUP [cm]	INTU	HLOW [cm]
1	I	0.	16	33.76	40.27	20	0.
2	II	33.76	6	44.66	40.27	20	0.
3	III	0.	22	44.66	70.77	19	40.27
4	III	44.66	17	80.86	70.77	39	0.

Table AII-11

CRITICAL FACILITY: SNEAK-3B2

Atom-Densities (in 10^{20} atoms/cm^3)

Mixture Material	1	2	3	4
Al	125.6	129.66	129.47	-
C	9.73	8.76	9.00	0.14
Cr	35.95[1]	36.08[2]	36.28[3]	11.95[4]
Fe	119.84[5]	120.65[6]	121.35[7]	39.55
H	18.49	16.81	17.29	-
Mg	1.31	0.65	0.65	-
Mo	0.38[8]	0.40	0.40	-
Ni	17.55	18.43	18.23	9.84
O	122.2	146.28	145.80	-
Si	2.54	1.84	1.86	0.46
Ti	0.30	0.38	0.39	0.19
U235	0.56	20.404	20.25	1.625
U238	81.86	81.39	81.26	399.414
Pu239	14.76	-	-	-
Pu240	1.33	-	-	-
Pu241	0.11	-	-	-
Pu242	0.06	-	-	-

1) includes 2.23 Mn
2) includes 1.99 Mn
3) includes 1.97 Mn
4) includes 0.87 Mn
5) includes 0.14 Co
6) includes 0.18 Co
7) includes 0.19 Co
8) includes 0.09 Nb

GEO	NG	BUCKLING	BC	NZ	NP
CYL	26	$8.46 \cdot 10^{-4}$ cm^{-2}	23	4	129

ZONE IZ	MIXT	XL /~cm~7	INT	XR /~cm~7
1	1	0.	60	29.910
2	2	29.91	12	36.180
3	3	36.18	16	44.530
4	4	44.53	40	82.120

Two-Dimensional Calculations:

GEO	NG	NP	ROWS	COL	NZ	BCL	BCR	BCUP	BCLOW	SPEKTRUM FOR COND
2	11	1600	40	40	5	2	3	3	2	1 dim- CYL

NEW GROUP	1	2	3	4	5	6	7	8	9	10	11
IGUP OLD GROUPS	3	4	6	7	8	9	10	11	13	15	26

MIXT	I	II	III	IV
MIXTURE	1	2	3	4
PHI-1 dim (IZ)	1	2	3	4

ZONE	MIXT	RL /~cm~7	INTH	RR /~cm~7	HUP /~cm~7	INTU	HLOW /~cm~7
1	I	0.	14	29.91	40.2		0.
2	II	29.91	6	36.18	40.2		0.
3	III	36.18	6	44.53	40.02		0.
4	IV	44.53	13	82.12	40.2		0.
5	IV	0.	40	82.12	70.7		40.2

Table AII-12

CRITICAL FACILITY: SNEAK-5C

Atom Densities (in 10^{20} atoms/cm^3)

Mixture Material	1
Al	0.0145
C	612.1704
Cr	13.1268
Fe	46.7934
Mg	0.0065
Mo	0.1116
Nb	0.0860
Ni	7.5235
O	39.4747
Pu239	4.7656
Pu240	0.4281
Pu241	0.0389
Pu242	0.0020
Si	0.5399
U235	0.3307
U238	50.5434
V [1)]	0.9165

1) Vanadium has been taken instead of manganese

Fundamental Mode Calculation:

NG	MIXT	BUCK o
26	1	0.0

Table AII-13

CRITICAL FACILITY: ZPRIII-55

Atom-Densities (in 10^{20} atoms/cm^3)

Mixture Material	1
Al	1.11
C	372.69
Cr	18.95
Fe	61.77
Ni	8.39
Pu239	10.68
Pu240	0.51
Pu241	0.05
U235	0.33
U238	152.82

Fundamental Mode Calculation:

NG	MIXT	BUCKo
26	1	0.0

Table AII-14

Savings and Bucklings, Carbon- and Hydrogen-Concentrations used in the Fundamental Mode Calculations for SNEAK-series, 3A0, 3A1, 3A2, 3A3

Assembly	S_{ax} [cm]	S_{rad} [cm]	H_c [cm]	R_c [cm]	$B^2_{ax} \cdot 10^4$ [cm^{-2}]	$B^2_{rad} \cdot 10^4$ [cm^{-2}]	$B^2_{tot} \cdot 10^4$ [cm^{-2}]	C-concentration in 10^{20} atoms/cm^3	H-concentrations in 10^{20} atoms/cm^3
3A02	14.1566	14.6162	80.54	44.66	8.329456	16.461494	24.790950	0.36	0.
3A1	13.7045	14.1588	80.54	44.66	8.469593	16.718531	25.188124	4.063	7.412
3A2	13.2944	13.7573	80.54	44.66	8.599800	16.949119	25.548919	9.217	17.719
3A3	12.7101	12.9645	80.54	44.66	8.790509	17.418687	26.209196	18.28	35.84

IX. Literature

[1] E. Kiefhaber et al.: BNES Conf. on the Physics of Fast Reactor Operation and Design, London, June 1969, paper 1.9, p. 94

[2] H. Küsters, J.J. Schmidt et al.: KFK 793 (EUR 3962e, EANDC(E)-113"U") 1968

[3] H. Küsters et al.: IAEA Conf. on Fast Reactor Physics, Karlsruhe 1967, Proceed. Vol. I, p. 167; see also KFK 628, 1967

[4] H. Huschke, KFK 770 (EUR 3953d), 1968

[5] A. Michaudon et al.: CEA-1093, 1959; Geneva Conf. 1958, P/1186, part 4; Proceed. Vol. 16, p. 115

[6] P.H. White, J. Nucl. En., Pts. A/B, Reactor Sci. Techn. 19, 325, 1965; P.H. White et al., IAEA Sympos. on the Physics and Chemistry of Fission, Salzburg, 1965, paper SM-60/14

[7] J.L. Perkin et al., J. Nucl. En., Pts. A/B, Reactor Sci. Techn. 19, 423, 1965

[8] R.K. Smith et al., Bull. Am. Phys. Soc. 2, 196, 1957

[9] G. de Saussure et al., Nucl. Sci. Eng. 23, 45, 1965

[10] Wang-Shi-di et al., IAEA Sympos. on the Physics and Chemistry of Fission, Salzburg, 1965, paper SM-60/86; see also reports R-1761, 1964; R-2024, R-2025, 1965

[11] C.A. Uttley, AERE-M1272 (EANDC(UK)-37"L"), 1963

[12] B.C. Diven et al., Phys. Rev. 120, 556, 1960

[13] L.W. Weston et al., Nucl. Sci, Eng. 20, 80, 1964

[14] C.H. Westcott et al., IAEA Atomic Energy Review 3.1, 1965

[15] J.J. Schmidt, KFK 120/part I, chapter VI 1

[16] J.J. Schmidt, KFK 120/part I, chapter IV 2

[17] J.F. Barry et al., J. Nucl. En., Pts. A/B, Reactor Sci. Techn. 18, 491, 1964

[18] J.J. Schmidt, KFK 120/part I, chapter VI 2

[19] E. Barnard et al., EANDC Conf. on the Study of Nuclear Structure with Neutrons, Antwerp, 1965, P/26;
E.R. Rae et al., Geneva Conf. 1964, P/167

[20] L.P. Abagjan et al., KFK-tr-144, 1964

[21] R.W. Lamphere, Phys. Rev. 104, 1654, 1956

[22] L.M. Bollinger et al., Geneva Conf. 1958, P/687; Proceed. Vol. 15, p. 127

[23] W.R. Kanne et al., Geneva Conf. 1955, P/595; Proceed. Vol. 4, p.315;
J.B. Sampson, D.F. Molino, KAPL-1793,1957;
J.B. Sampson, E.A. Luebke, Nucl. Sci. Eng. 4, 745, 1958

[24] G. de Saussure et al., IAEA Conf. on Nuclear Data for Reactors, Paris, 1966, Proceed. Vol. II, p. 233

[25] J.C. Hopkins, B.C. Diven, Nucl. Sci. Eng. 12, 169, 1962

[26] J.J. Schmidt, KFK 120/part I, chapter VI 3

[27] I. Langner et al., KFK 750 (EANDC(E)-88"U", EUR 3715e), 1968

[28] S.M. Dubrovina, V.A. Shigin, Sov. Phys. Doklaty 9, 579, 1965

[29] G.N. Smirenkin et al., Sov. J. At. En. 13, 974, 1963

[30] W.P. Pönitz et al., KFK 635 (EUR 3679e), 1967;
K.H. Beckurts et al., IAEA Sympos. on Fast Reactor Physics, Karlsruhe, 1967, Proceed. Vol. I, p. 67

[31] H.O. Menlove, W.P. Pönitz, Nucl. Sci. Eng. 33, 24, 1968

[32] K.H. Beckurts, private communication, 1967

[33] W.P. Pönitz, IAEA Conf. on Nuclear Data for Reactors, Paris, 1966, Proceed. Vol. I, p. 277; see also KFK 454, 1966
W.P. Pönitz, J. Nucl. En., Pts. A/B, 20, 825, 1966; see also KFK 505, 1966;
W.P. Pönitz et al., J. Nucl. En. 22, 505, 1968; see also EANDC(E)-84"S", 1968

[34] R. Gwin et al., WASH-1093, 1968, p. 106;
G. de Saussure, private communication, 1968

[35] T.A. Pitterle et al., Second Conf. on Neutron Cross Sections and Technology, Washington, 1968, Proceed. Vol. II, p. 1243

[36] P. Ribon et al., CEA-N-989 (EANDC(EUR)-111), 1968

[37] M.G. Schomberg et al., unpublished, 1968;
E.R. Rae, private communication, 1969

[38] M.G. Schomberg et al., IAEA Conf. on Fast Reactor Physics, Karlsruhe, 1967, paper SM-101/41, Proceed. Vol. I, p. 289

[39] Y.V. Ryabov et al., At. Energy 24, 351, 1968

[40] J.J. Schmidt, KFK 966 (EUR 4172d, EANDC(E)-117"U"), 1969; Atomkernenergie, to be published

[41] J.M. Blatt, V.F. Weißkopf, "Theoretical Nuclear Physics", J.Wiley&Sons, 1952, chapter VIII

[42] G. Szwarcbaum et al., IA-899, 1964

[43] G. Hansen et al., WASH-1074, 1967, p. 77f;
L. Stewart, private communication, 1968

[44] J. Fréhaut et al., EANDC(E)-89"U", 1968, ps. 221, 224

[45] H. Condé et al., J. Nucl. En. 22, 53, 1968

[46] S. Yiftah et al., IAEA Conf. on Fast Reactor Physics, Karlsruhe 1967, Proceed. Vol. I, p. 123

[47] M.G. Cao et al., Second Conf. on Neutron Cross Sections and Technology, Washington, 1968, Proceed. Vol. I, p. 513;
W. Kolar, K.H. Böckhoff, ibidem, p.519;
E.M. Migneco, J.P. Theobald, ibidem p. 527;
H. Weigmann et al., ibidem p. 533

[48] W. Oosterkamp, KFK 1036 (EUR 4309e), 1969

[49] B.C. Diven, LA 3586, 1966

[50] M.C. Moxon et al., to be published;
M.C. Moxon, E.R. Rae, private communication, 1969

[51] M.C. Moxon et al., reported by E.R. Rae et al. in Geneva Conf. 1964, P/167

[52] J.H. Gibbons et al., Phys. Rev. 122, 182, 1961

[53] G. de Saussure et al., ORNL-3360, 1963, p. 62; see also EANDC-33"U", 1963, p. 64f

[54] T.S. Belanova et al., J. Nucl. En. 20, 411, 1966

[55] L.B. Miller, W.P. Pönitz, Nucl. Sci. Eng. 35, 295, 1969

[56] P. Greebler, B.A. Hutchins, R.B. Lindford, B. Wolfe, GEAP-5635, 1968

[57] P. Engelmann et al., KFK 776, EUR 3955d

[58] D. Wintzer, KFK 743, EUR 3725d, 1969

[59] F. Mitzel, K.E. Schroeter, Nukleonik Vol. 12, p. 110, 1969

[60] E. Kiefhaber, KFK-882, EUR 4161e, 1968

[61] H. Späth, KFK 738, 1968

[62] K. Böhnel, H. Meister, KFK-Report to be published

[63] W.W. Little Jr. and R.W. Hardie, Nucl. Sci. and Eng. 36,115, 1969

[64] E.A. Fischer, KFK 995, 1969

[65] R. Böhme, H. Seufert, KFK 811, 1968

[66] D. Stegemann et al., KFK 627, 1967

[67] R. Schroeder, KFK 847, 1968

[68] M. Edelmann et al., BNES-Conference on the Physics of Fast Reactor Operation and Design, London , June 1969, paper 1.11. p.113

[69] D. Wintzer, KFK 633, 1967

[70] C. Günther, W. Kinnebrock, The onedimensional S_N-Program DTK, unpublished data

[71] K.D. Lathrop, DTF-IV, a Fortran-IV-Program for Solving the Multigroup Transport Equation with Anisotropic Scattering, LA-3373, 1965

[72] B.G. Carlson et al., DTF Users Manual, UNC Phys/Math. 3321, Volume II, 1964

[73] L.D. O'Dell, R.W. Hardie, W.W. Little, Jr., A numerical comparison of diffusion and transport (S_N)-codes for selected fast reactor configurations, AEC Research & Development Report, Battelle Memorial Institute Pacific Northwest Laboratory, Richland, Washington 99352, March 1969

[74] T.A. Pitterle, E.M. Page, M. Yamamoto, APDA-216, 1968

[75] A. Baker, ANL-7320, p. 116 ff., 1966

[76] R.A. Porter, private information

[77] W.G. Davey, Nucl. Sci. and Eng. 19, 259, 1964

[78] W.P. Keeney, private information

[79] A.M. Broomfield et al., ANL-7320, p. 205 ff., 1966

[80] ANL-7267, Reactor Development Program, Progress Report, October 1966

[81] G.E. Edison, L.L. Bennett, ANS Trans. Vol. 10, No. 2, 1967

[82] A.M. Broomfield, R.G. Palmer, ANS Trans. Vol. 11, No. 1, 1968

[83] ANL-7349, Reactor Development Program, Progress Report, June 1967

[84] J. Adamson et al., ANL-7320, p. 216 ff. (1966)

[85] R. Schröder, private communication

[86] H. Meister, private communication

[87] E.A. Fischer, private communication

[88] ANL-7527, Reactor Development Program, Progress Report, December 1968

[89] C.E. Till, BNES Conference on the Physics of Fast Reactor Operation and Design, London, June 1969, paper 1.3

[90] G. Jourdan, private communication

[91] S. Yiftah, D. Okrent, P.A. Moldauer, Fast Reactor Cross Sections, Pergamon Press, 1960

Acknowledgement:

The authors would like to thank Dr. H. Küsters for his continuous interest in this work, his encouragement, and many stimulating discussions.

Table 1: Characteristics of Fast Critical Assemblies studied *)

		SUAK U1B	SUAK UH1B	ZPR-III-10	ZPR-III-25	ZPR-III-48	ZEBRA 6A	SNEAK-3A1	SNEAK-3A2	SNEAK-5C	ZPR-III-55
Median fission energy [keV] 1)		611.1	532.1	375.8	365.6	225.0	186.0	100.0	55.77	1.20	143.3
Neutron lifetime $1 \cdot 10^7$ [sec]		0.286	1.788	0.515	0.728	2.776	2.681	2.942	3.725	16.483	4.187
$\sigma_f U238/\sigma_c U238$		0.59	0.36	0.40	0.25	0.21	0.25	0.21	0.21	0.07	0.12
Migration area M^2 [cm^2]		47.7	28.1	64.8	62.7	179.7	170.0	148.2	126.7	144.1	97.5
Geometric buckling $B^2 \cdot 10^{+4}$ [cm^{-2}]		197.9	205.3	81.4	31.7	27.0	34.6	22.0	25.5	0	0
$M^2 \cdot B^2$		0.94	0.58	0.53	0.20	0.49	0.59	0.33	0.32	0	0
Core Volume [liters]		36.6	34.5	70.5	435.3	414.7	247.0	663.3	504.7	-	-
Core fissile mass [kg]		116.4	87.5	156.4	584.6	273.3	188.6	524.7	399.4	-	-
REACTION RATES 2)	Total leakage	0.645	0.468	0.396	0.205	0.415	0.462	0.295	0.293	-	-
	Total fission	0.386	0.394	0.389	0.388	0.340	0.339	0.398	0.399	0.348	0.344
	Total capture	0.187	0.276	0.244	0.422	0.294	0.238	0.321	0.329	0.720	0.727
	Capture in U238	0.136	0.156	0.181	0.378	0.205	0.154	0.204	0.198	0.500	0.623
	Fission in U238	0.081	0.057	0.073	0.093	0.044	0.038	0.043	0.042	0.036	0.074
	Capture in U235	0.051	0.120	0.058	0.060	0.001	0.002	0.099	0.114	0.012	0.003
	Fission in U235	0.305	0.337	0.316	0.295	0.003	0.008	0.355	0.357	0.025	0.010
	Capture in Pu239	-	-	-	-	0.059	0.060	-	-	0.151	0.076
	Fission in Pu239	-	-	-	-	0.285	0.284	-	-	0.281	0.256

*) Taken from fundamental mode homogeneous calculations with the SNEAK-set

1) Determined from one-dimensional calculations

2) Normalized to one fission source neutron in the reactor $\int_0^\infty \nu\Sigma_f(E)\ \phi(E)dE = 1$

Table 2: Influence of the Fission Spectrum

Assembly	SUAK U1B	SUAK UH1B	ZPR III-10	ZPR III-25	SNEAK 3A1	ZEBRA 6A
Actual ν of the assembly	2.59	2.54	2.57	2.56	2.51	2.94
Modified fission spectrum corresponds to ν= of the ABN-set	2.6	2.6	2.6	2.6	2.6	3.0
Δk=k(modified fission spectrum) -k(standard fission spectrum)	-0.002	-0.001	-0.002	-0.003	-0.001	+0.001
Change in $\sigma_f(U238)/\sigma_f(U235)$	-1.2%	-1.2%	-1.2%	-1.2%	-1.2%	+2%
Change in $\phi(1)=\int_{6.5\ MeV}^{10.5MeV}\phi(E)dE$	-6%	-5.5%	-5.5%	-5.5%	-6%	+11%

Table 3: Comparison of central material worths for SNEAK 3A1 calculated in different ways (SNEAK-set has been used)

Material	2-dim.4 groups / 1-dim.sphere 26 groups	2-dim.11 groups / 1-dim.sphere 26 groups
Al	1.005	0.974
B^{10}	0.915	0.959
C	0.025	0.653
Cr	1.071	1.035
Fe	0.968	0.972
H	0.098	0.684
Mg	3.264	1.389
Ni	1.082	1.067
O	0.129	0.784
Mo	0.934	0.967
Pu239	1.043	1.019
U235	1.069	1.030
U238	0.953	0.970

Table V-1: k_{eff} of fundamental mode homogeneous diffusion calculations for the various assemblies with different sets of group contants

Assembly	SNEAK	SNEPMB	SNEAPM	PU9SCP	SCTALØ	UPUCØR	PUO2RE	MØX911	MØXTØT
SUAK U1B	0.8238	0.8087	0.82958	0.82958	0.82759	0.82167	0.82167	0.824531	0.82466
SUAK UH1B	0.8808	0.8782	0.88572	0.88572	0.88883	0.88452	0.88452	0.888290	0.89277
ZPR III-10	0.9752	0.959864	0.98579	0.98579	0.983153	0.97811	0.978110	0.984080	0.984469
ZPR III-25	0.9700	0.95992	0.98932	0.98932	0.978624	0.97389	0.973888	0.986780	0.987716
ZPR III-48	0.95497	0.963581	0.963737	0.955207	0.952548	0.948864	0.951787	0.959456	0.964963
ZEBRA 6A	0.9630	0.969439	0.969780	0.959724	0.95890	0.95490	0.958542	0.964453	0.969320
SNEAK-Series 3A0	0.943	0.934	0.944	0.944	0.944	0.944	0.944	0.946	0.942
SNEAK-Series 3A1	0.969	0.966	0.970	0.970	0.970	0.970	0.970	0.971	0.970
SNEAK-Series 3A2 [1]	1.000	1.000	1.000	1.000	1.000	1.000	1.000	1.000	1.000
SNEAK-Series 3A3	1.036	1.038	1.034	1.034	1.034	1.035	1.035	1.033	1.033
SNEAK 3A1	0.990164	0.981076	1.000428	1.000428	0.999654	0.996736	0.996736	1.006054	1.012547
SNEAK 3A2	0.982758	0.976798	0.991394	0.991394	0.991260	0.988448	0.988448	0.995857	1 003036
SNEAK 5C	0.937010	0.945313	0.945666	0.930798	0.928678	0.926926	0.930885	0.938632	0.952949
ZPR III-55	0.935816	0.953645	0.954084	0.943182	0.93001	0.92646	0.928143	0.944763	0.961705

1) All values of the SNEAK-series normalized so as to give k_{eff}(SNEAK 3A2) = 1

Table V-2: k_{eff} of one- and two-dimensional diffusion calculations for the various assemblies with different sets of group constants

		SNEAK	SNEPMB	SNEAPM	PU9SCP	SCTALO	UPUCØR	PUO2RE	MØX911	MØXTØT
ZPRIII-10	1dim.	0.9752	0.9622	0.9890						0.9863
	2dim.	0.9763	0.9635	0.9904						0.9876
ZPRIII-25	1dim.	0.9700								0.9879
	2dim.	0.9698								0.9878
ZPRIII-48	1dim.	0.9550					0.9478	0.9505		0.9667
	2dim.	0.9522					0.9450	0.9477		0.9639
ZPRIII-48B	1dim.	0.9536					0.9464	0.9597		0.9660
	2dim.	0.9503					0.9432	0.9464		0.9627
ZEBRA6A	1dim.	0.9630					0.9545	0.9577		0.9737
	2dim.	0.9596					0.9512			0.9706
SNEAK3A1	1 dim.	0.9911					0.9973			1.0156
	2dim.	0.9889					0.9950			1.0136
SNEAK3A2	1dim.	0.9837					0.9889			1.0060
	2dim.	0.9820					0.9872			1.0045
SNEAK3B2	1dim.	0.9805	0.9851	0.9906	0.9823	0.9781	0.9749	0.9780	0.9866	0.9942
	2dim.	0.9776		0.9885	0.9804			0.9749		0.9921

Table V-3: Criticality Corrections for the Various Assemblies *)

Assemblies	REMØ Corr.	SN-Corr.	Heterogeneity Corrections	Other Corr.
SUAK U1B	-0.0002	0.031	-	
SUAK UH1B	-0.0004	0.030	-	+0.007
ZPR III-10	-0.0008	0.013	0.0105	
ZPR III-25	-0.0009	0.002	0.0085	
ZPR III-48	+0.0047	0.006	0.014	
ZPR III-48B	+0.0048	0.006	0.014	
ZEBRA 6A	+0.0040	0.010	-	
SNEAK-series 3A0	-0.0015	0.003	0.001	
3A1	-0.0006	0.003	0.003	
3A2	-0.0006	+0.004	0.004	
3A3	-0.0009	0.004	0.007	
SNEAK-3A1	-0.0006	0.003	0.003	
SNEAK-3A2	-0.0006	+0.004	0.004	
SNEAK-3B2	+0.0008	+0.004	0.003	
SNEAK-5C	+0.0185	-	0.071 [1)]	
ZPR III-55	+0.0123	-	0.010	

*) Corrections calculated using SNEAK-set or taken from the literature

1) Heterogeneity correction is probably too large

Table V-4: Best available criticality values for the various assemblies with different sets of nuclear group constants

Assembly	Experimental result for k_{eff}	Theoretical Results: REMO+HET.+SN+other corr.	keff for the different sets of nuclear group constants: SNEAK set	SNEPMB	SNEAPM	PU9SCP	SCTALØ	UPUCØR	PUO2RE	MØX911	MØXTØT
SUAK U1B	0.86 ±0.01	+0.031	0.855	0.840	0.861	0.861	0.859	0.853	0.853	0.856	0.856
SUAK UH1B	0.945±0.01	+0.037	0.918	0.915	0.923	0.923	0.920	0.922	0.922	0.925	0.930
ZPR III-10	1.000	+0.023	0.999	0.986	1.013	1.013	1.010	1.005	1.005	1.011	1.011
ZPR III-25	1.000	+0.010	0.980	0.970	0.999	0.999	0.989	0.984	0.984	0.997	0.998
ZPR III-48	1.000	0.025	0.977	0.986	0.986	0.977	0.975	0.970	0.973	0.983	0.989
ZPR III-48B	1.000	0.025	0.975	0.984	0.984	0.975	0.973	0.968	0.971	0.981	0.987
ZEBRA 6A	1.000	0.014	0.974	0.980	0.981	0.970	0.969	0.965	0.969	0.978	0.985
SNEAK 3A1	1.000	0.005	0.994	0.985	1.004	1.004	1.003	1.000	1.000	1.010	1.019
SNEAK 3A2	1.000	0.007	0.989	0.983	0.997	0.997	0.997	0.994	0.994	1.003	1.012
SNEAK 3B2	1.000	0.006	0.984	0.988	0.995	0.986	0.982	0.979	0.981	0.990	0.998
SNEAK 5C	1.03 ±0.01 [1]	+0.089 [3]	1.026	1.034	1.035	1.020	1.018	1.016	1.020	1.028	1.042
ZPR III-55	1.000	0.022	0.958	0.976	0.976	0.965	0.952	0.948	0.950	0.967	0.984
SNEAK-series 3A0	0.930	-0.005	0.938	0.929	0.939	0.939	0.939	0.939	0.939	0.941	0.937
SNEAK-series 3A1	0.962	-0.002	0.967	0.964	0.968	0.968	0.968	0.968	0.968	0.969	0.968
SNEAK-series 3A2	1.000 [2]	±0.000	1.000	1.000	1.000	1.000	1.000	1.000	1.000	1.000	1.000
SNEAK-series 3A3	1.048	+0.003	1.039	1.041	1.037	1.037	1.037	1.038	1.038	1.036	1.036

[1] Preliminary experimental result

[2] Normalization point for the SNEAK-set

[3] This correction is probably too large

Table V-5: Central material worth- and central reaction rate-ratios for SNEAK 3A1 and SNEAK 3A2 (obtained from homogeneous spherical diffusion calculations)

($\Delta k/k$ per atom of the material considered / $\Delta k/k$ per atom of U235)

Material	Assembly			
	SNEAK 3A1		SNEAK 3A2	
	SNEAK-Set	MOXTOT-Set	SNEAK-Set	MOXTOT-Set
U235	1.0	1.0	1.0	1.0
U238	-0.080	-0.069	-0.082	-0.070
Pu239	+1.419	+1.377	+1.428	+1.374
B10	-1.219	-1.289	-1.759	-1.814
Fe	-0.0087	-0.0079	-0.0097	-0.0089
Cr	-0.0067	-0.0062	-0.0072	-0.0068
Ni	-0.0165	-0.0159	-0.0188	-0.0182
Mo	-0.0691	-0.0709	-0.0931	-0.0944
C	+0.0030	+0.0039	+0.0036	+0.0039
Mg	-0.0007	+0.0003	-0.0001	+0.0005
Al	-0.0027	-0.0021	-0.0022	-0.0017
O	+0.0025	+0.0032	+0.0032	+0.0034
H	+0.1519	+0.1429	+0.1304	+0.1167
$\frac{\sigma_f U238}{\sigma_f U235}$	0.0306	0.0284	0.0292	0.0272
$\frac{\sigma_c U238}{\sigma_f U235}$	0.1435	0.1271	0.1383	0.1237

Table V-6: Reaction rate ratios for SNEAK 3A1 and SNEAK 3A2
(results of fundamental mode homogeneous diffusion calculations)

	$\sigma_f U238/\sigma_f U235$		$\sigma_c U238/\sigma_f U235$	
	Assembly		Assembly	
Group-Set	SNEAK 3A1	SNEAK 3A2	SNEAK 3A1	SNEAK 3A2
SNEAK	0.0305646	0.0291813	0.1435081	0.1383348
SNEPMB	0.0308855	0.0293801	0.1429407	0.13712420
SNEAPM	0.03020257	0.0288892	0.13634168	0.13232973
PU9SCP	0.0302023	0.0288892	0.1363394	0.13232978
SCTALØ	0.02921786	0.02797753	0.13687611	0.13272677
UPUCØR	0.02893525	0.02770097	0.13725308	0.13307827
PUO2RE	0.02893525	0.02770097	0.13725308	0.13307827
MØX911	0.02862756	0.02746573	0.13105388	0.12816419
MØXTØT	0.02841725	0.0272414	0.1270707	0.1237131

Table V-7: Central material worth- and central reaction rate-ratios for ZPR III-48 (obtained from homogeneous spherical diffusion calculations)

Material	Material worth per atom normalized to U235				
	Experiment	SNEAK-Set	UPUCØR-Set	PUO2RE-Set	MØXTØT-Set
U235	1.	1.	1.	1.	
U238	-0.074096±0.00237	-0.07799903	-0.07400296	-0.0743288	-0.0677507
Pu239	+1.3347 ±0.02781	+1.3360672	+1.2851539	+1.28430262	+1.276766
Pu240	+0.2439 ±0.06305	+0.06455886	+0.04834762	+0.2088790	+0.200401
NA	-0.00182 ±0.000107	-0.00391285	-0.00411021	-0.00398746	-0.00374
B10	-1.12219 ±0.02330	-1.038983	-1.0163986	-1.0260348	-1.060586
FE	-0.00876 ±0.000384	-0.0102505	-0.00988528	-0.00984360	-0.0094751
CR	-0.00613 ±0.000334	-0.0085428	-0.00881905	-0.00873844	-0.0084667
NI	-0.013396±0.000305	-0.01655626	-0.01627882	-0.01620403	-0.0161596
MO	-0.05226 ±0.001102	-0.0656266	-0.06350217	-0.06383736	-0.064600
$\frac{\sigma_f U238}{\sigma_f U235}$	0.0307 ±0.0003	0.030994	0.029793	0.029635	0.028852
$\frac{\sigma_f Pu240}{\sigma_f U235}$	0.976 ±0.010	0.913747	0.903357	0.901930	0.894870
$\frac{\sigma_f Pu240}{\sigma_f U235}$	0.243 ±0.002	0.215419	0.203743	0.212505	0.207663
$\frac{\sigma_c U238}{\sigma_f U235}$	0.138 ±0.007	0.146049	0.140746	0.140771	0.130090

Table V-8: Reaction rate-ratios for ZPR III-48
(results of fundamental mode homogeneous diffusion calculations)

	Experiment	SNEAK-Set	SNEPMB	SNEAPM	PU9SCP	SCTALØ	UPUCØR	PUO2RE	MØX911	MØXTØT
$\frac{\sigma_f U\ 238}{\sigma_f U\ 235}$	0.0307±0.0003	0.031022311	0.03186160	0.03065153	0.031170528	0.030143929	0.02983808	0.02967420	0.02928424	0.028992443
$\frac{\sigma_f Pu239}{\sigma_f U\ 235}$	0.976 ±0.010	0.91553033	0.948422475	0.91227088	0.918097626	0.906232658	0.90277856	0.90332037	0.89985206	0.89686276
$\frac{\sigma_f Pu240}{\sigma_f U\ 235}$	0.243 ±0.002	0.21648744	0.22208147	0.21364455	0.21725915	0.20408695	0.204437765	0.21314248	0.21073488	0.20882076
$\frac{\sigma_c U238}{\sigma_f U235}$	0.138 ±0.007	0.14594458	0.14418948	0.13868333	0.13916881	0.14028237	0.14066813	0.14070100	0.13433686	0.12999853

Table V-9: Central material worth- and central reaction rate-ratios for ZPR III-48B
(obtained from homogeneous spherical diffusion calculations)

	Material worth per atom normalized to U235			
		Group-Set		
Material	Experiment	SNEAK-Set	UPUCØR-Set	PUO2RE-Set
U235	1.	1.	1.	1.
U238	-0.07093±0.00295	-0.0779046	-0.7454495	-0.07503325
Pu239	+1.33364±0.03695	+1.3183717	+1.2694856	+1.2649667
Pu240	+0.19997±0.12364	+0.06862482	+0.0516075	+0.20037743
Na	-0.00183±0.00089	-0.00470528	-0.0047630	-0.0045568
B10	-1.08280±0.01918	-0.9992227	-0.98431684	-1.00069404
FE	-0.00932±0.00053	-0.01043646	-0.0100639	-0.00996556
CR		-0.00882984	-0.00906397	-0.00890396
NI		-0.01669868	-0.01637201	-0.01614358
MO		-0.06434499	-0.06256536	-0.06312496
C		-0.00288148	-0.0038271	-0.00367072
AL		-0.00655804	-0.00654037	-0.00646532
$\frac{\sigma_f U238}{\sigma_f U235}$	0.0297 ±0.0005	0.029991	0.0288066	0.0284064
$\frac{\sigma_f Pu239}{\sigma_f U235}$	0.964 ±0.010	0.910871	0.9002064	0.89648053
$\frac{\sigma_f Pu240}{\sigma_f U235}$	0.229 ±0.003	0.210168	0.19858006	0.20600668
$\frac{\sigma_c U238}{\sigma_f U235}$		0.146744	0.14133489	0.1414299

Table VI-1: The mean and root mean square or standard deviation for criticality between experiment and theory with various group sets

Quantity	Group-set								
	SNEAK	SNEPMB	SNEAPM	PU9SCP	SCTALØ	UPUCØR	PUO2RE	MØX911	MØXTØT
$\frac{1}{N}\sum_{i=1}^{N}(k_{eff}\ exp.,i - k_{eff}\ calc.,i)$	0.0173	0.0175	0.0069	0.0123	0.0158	0.0194	0.0179	0.0090	0.0022
$\sqrt{\frac{1}{N}\sum_{i=1}^{N}(k_{eff}\ exp.,i - k_{eff}\ calc.,i)^2}$	0.0270	0.0193	0.0132	0.0189	0.0224	0.0249	0.0232	0.0158	0.0125

i=1,2,... N= index for the various assemblies, N=12

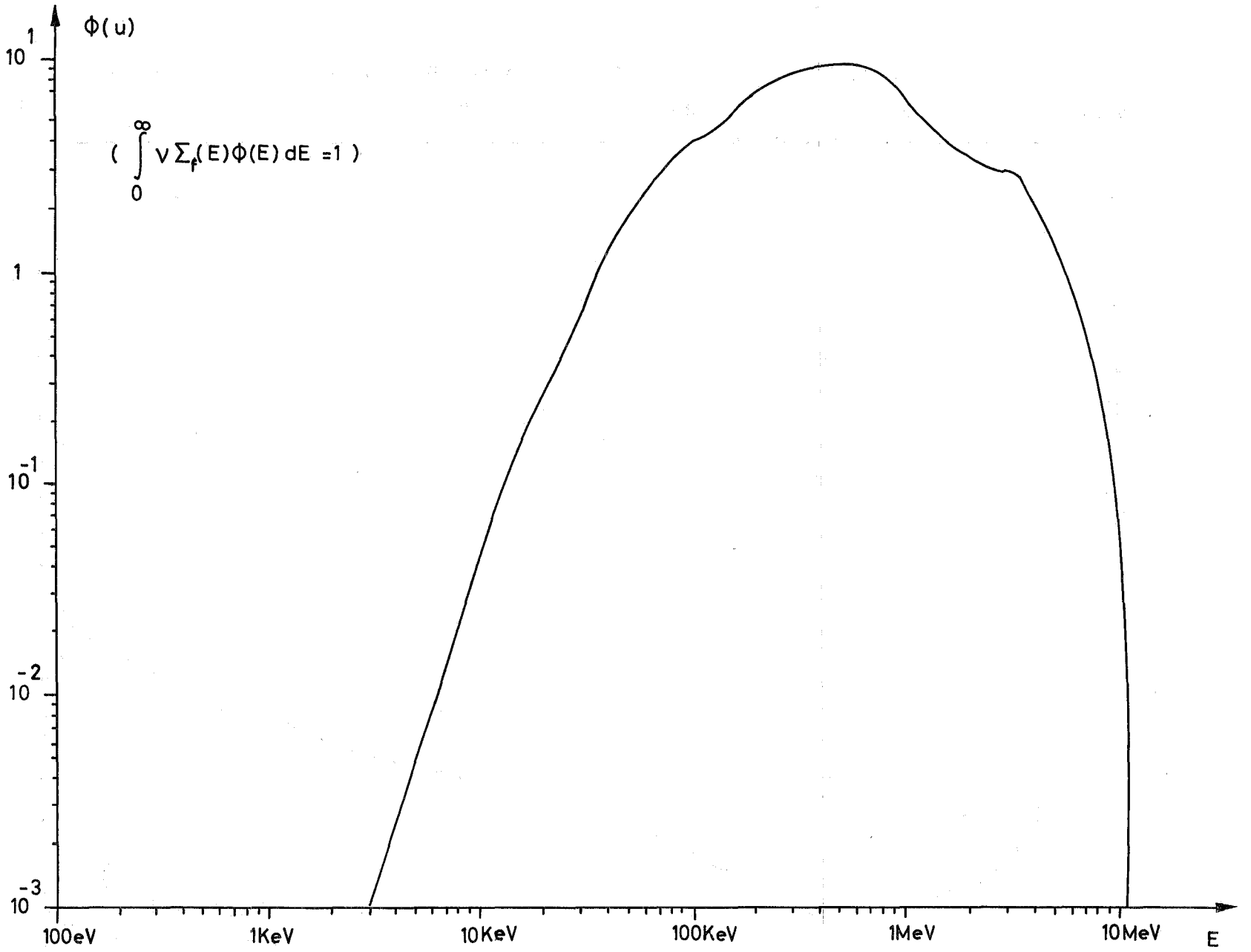

Fig. AII-1 Neutron flux for SUAK U1B

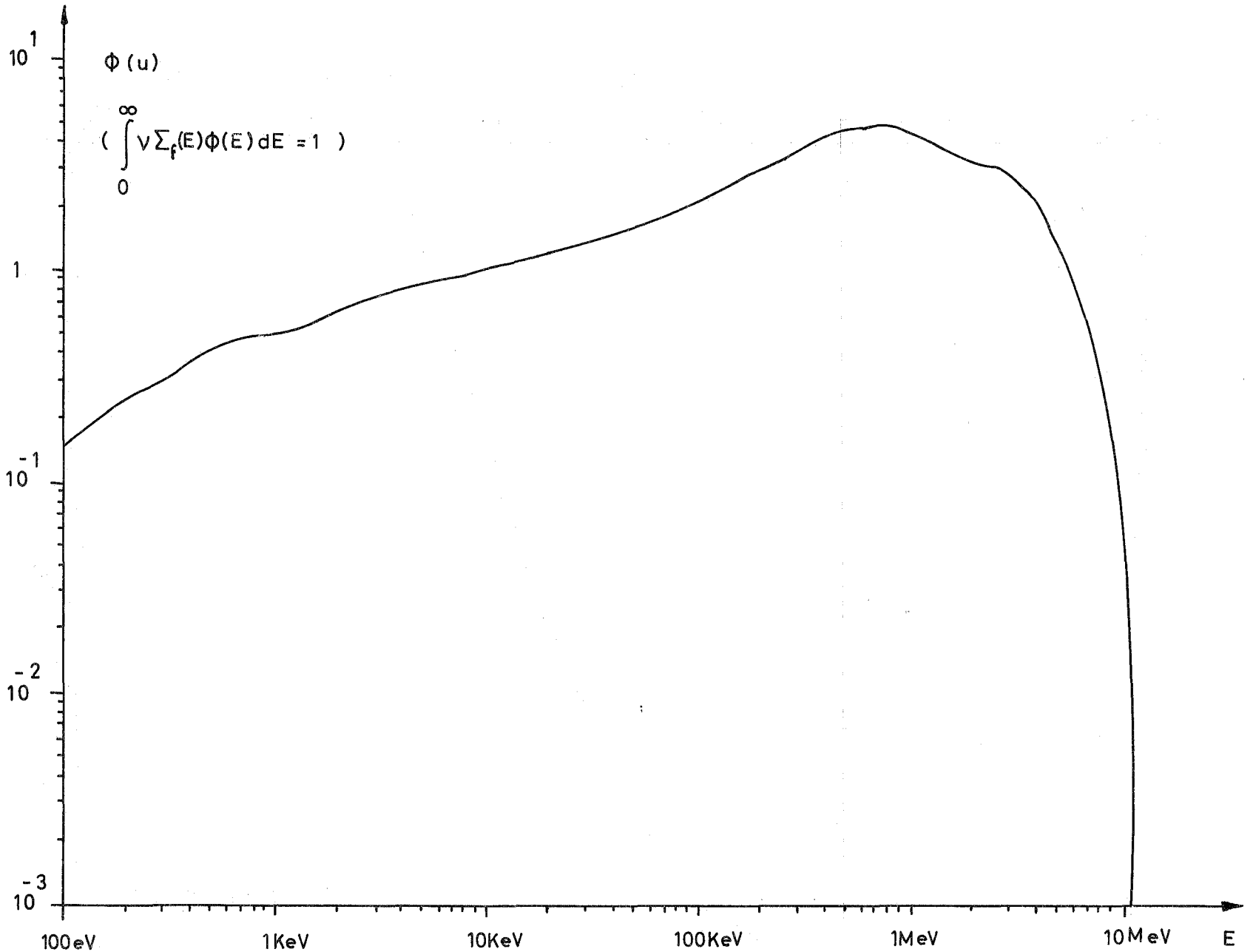

Fig. AII-2 Neutron flux for SUAK UH1B

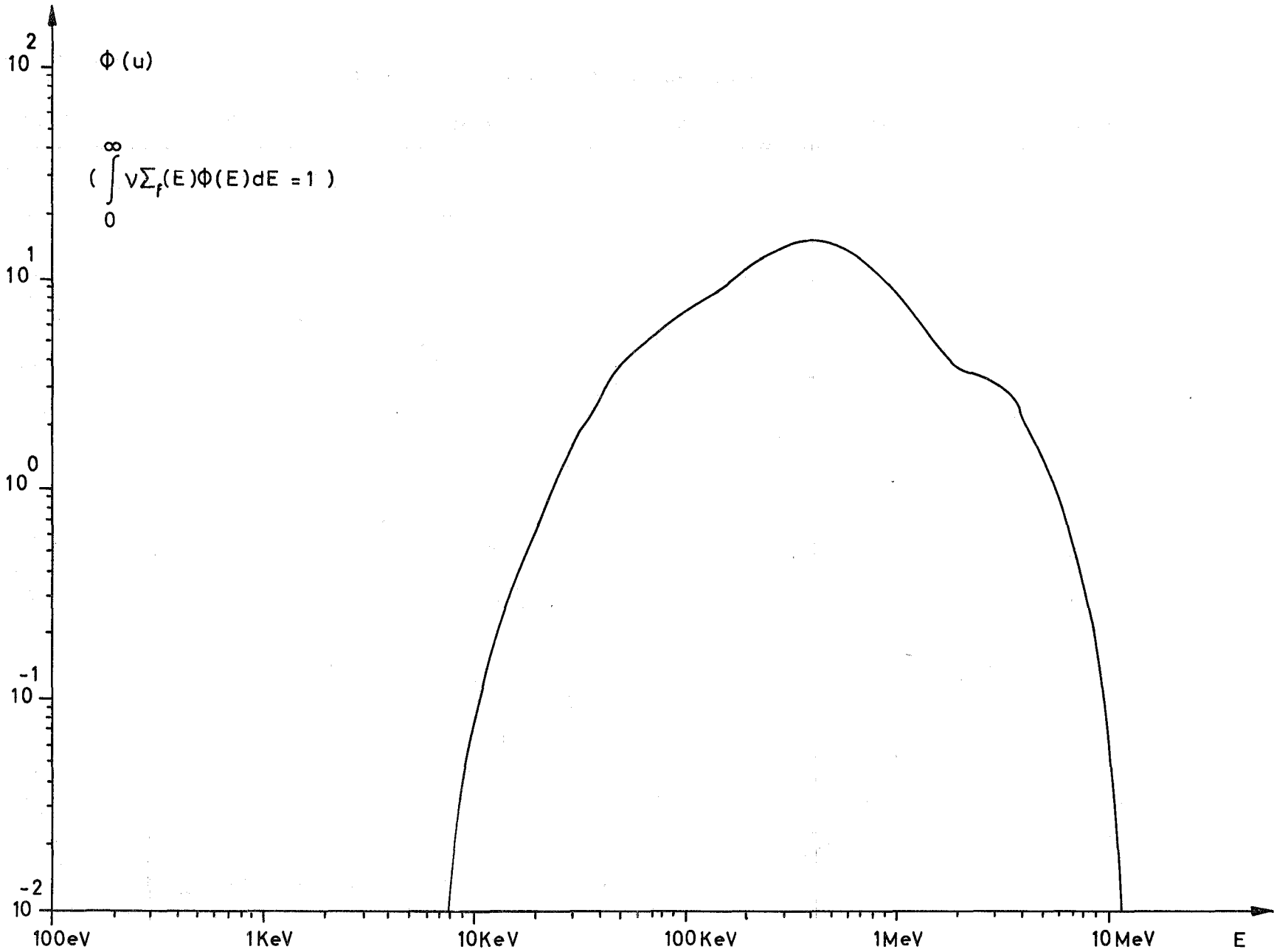

Fig. AII-3 Neutron flux for ZPR-III-10

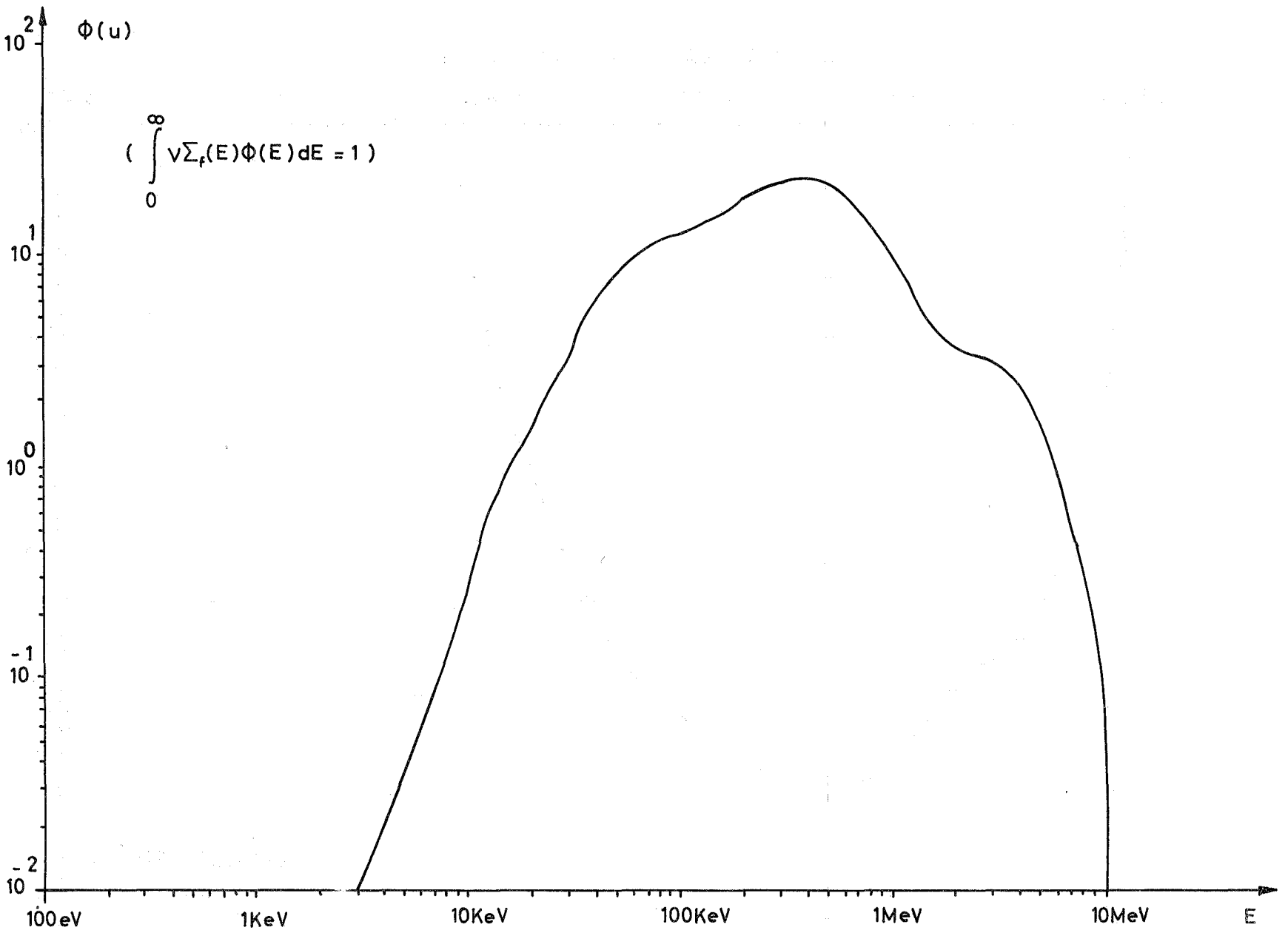

Fig. AII-4 Neutron flux for ZPR-III-25

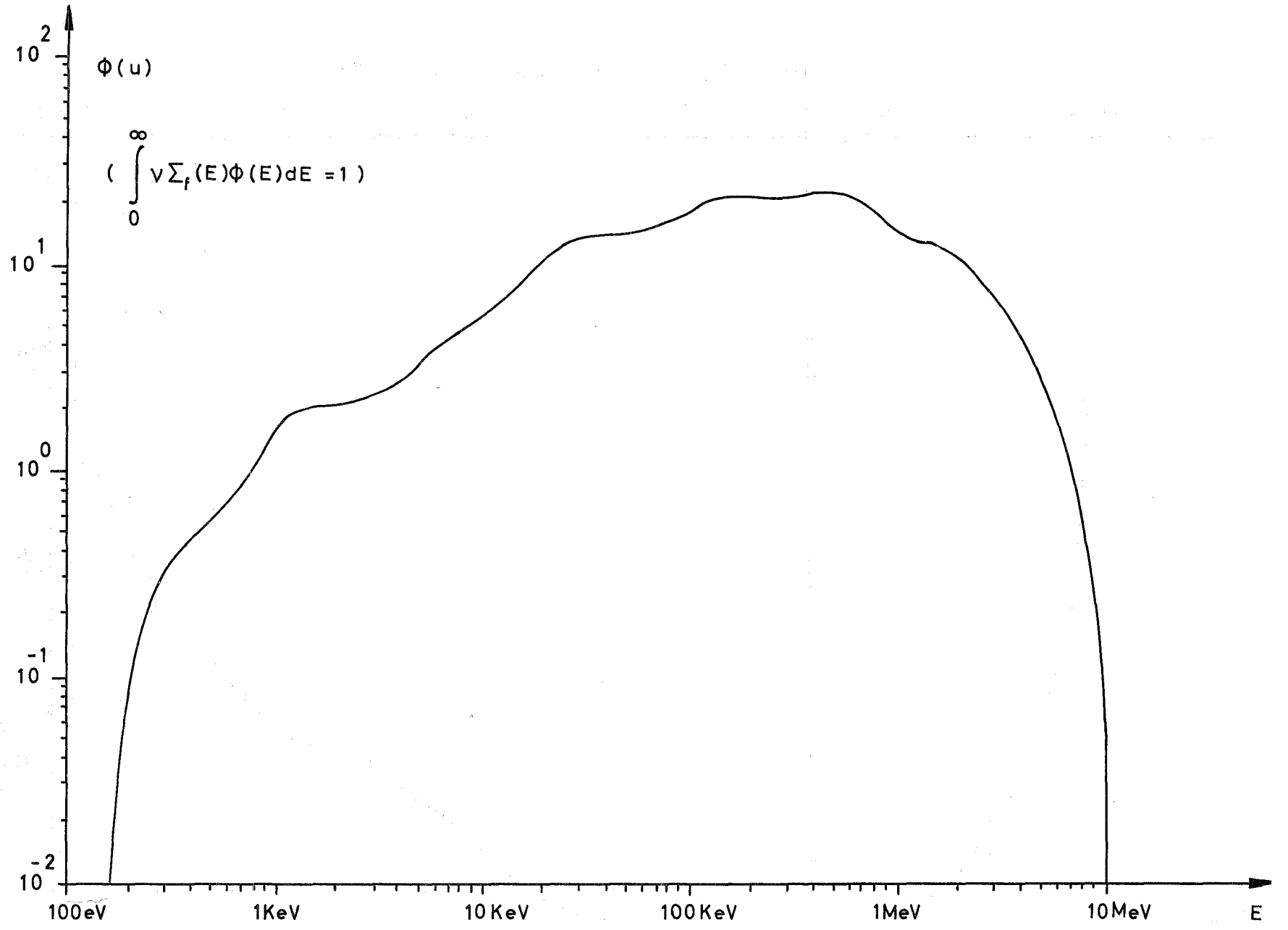

Fig. AII-5 Neutron flux for ZPR-III-48

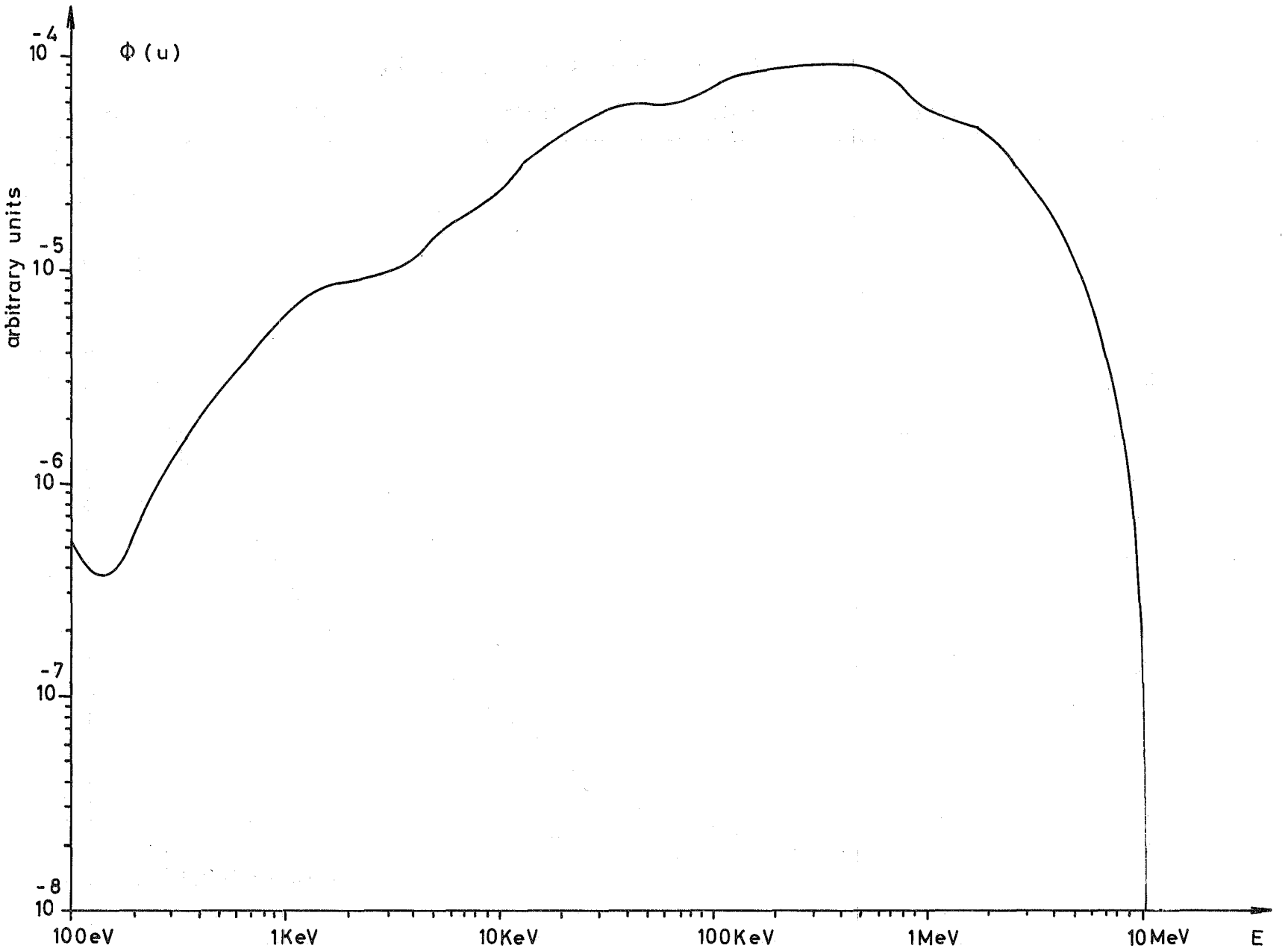

Fig. AII-6 Neutron flux for ZPR-III-48B

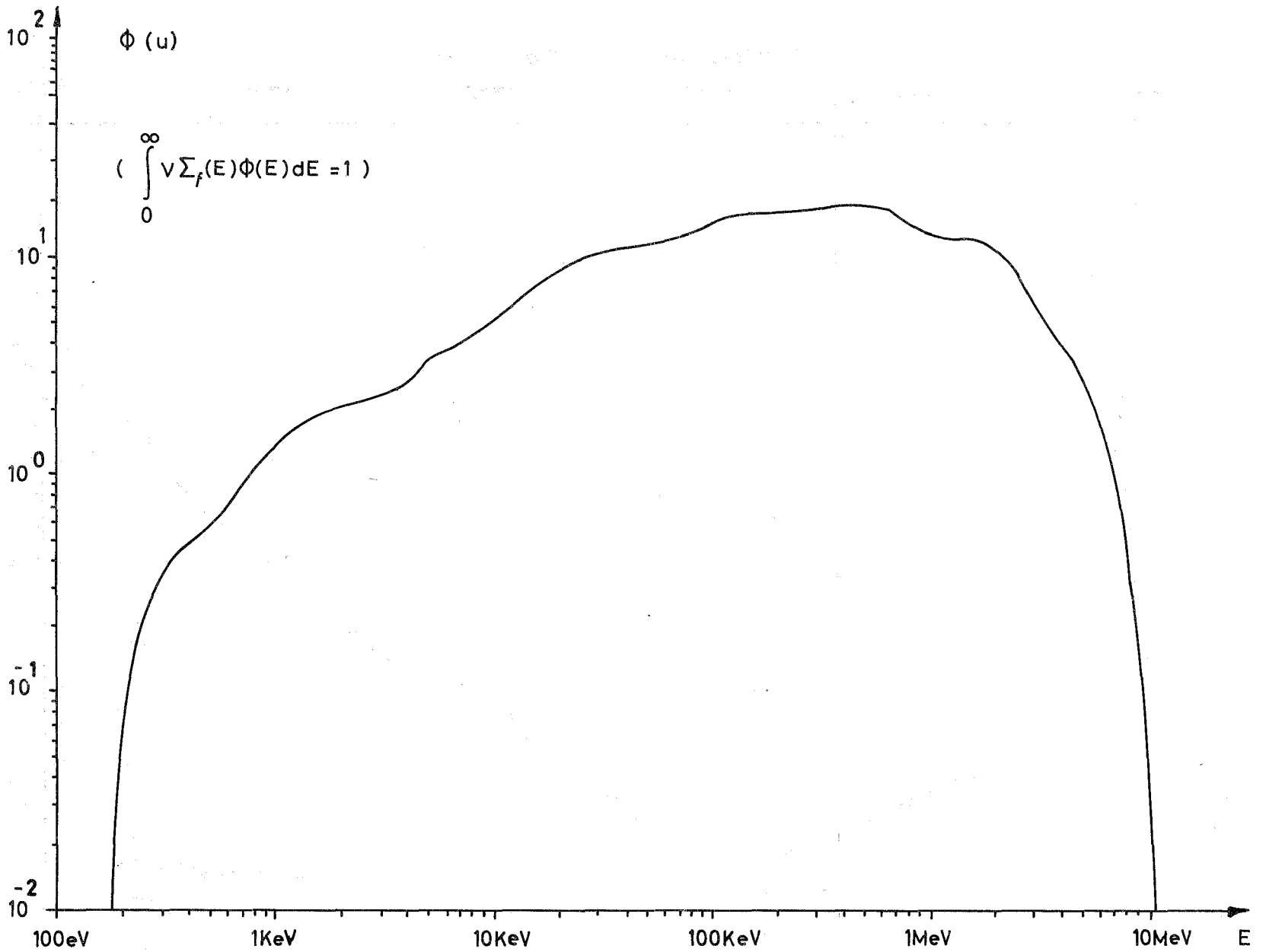

Fig. AII-7 Neutron flux for ZEBRA 6A

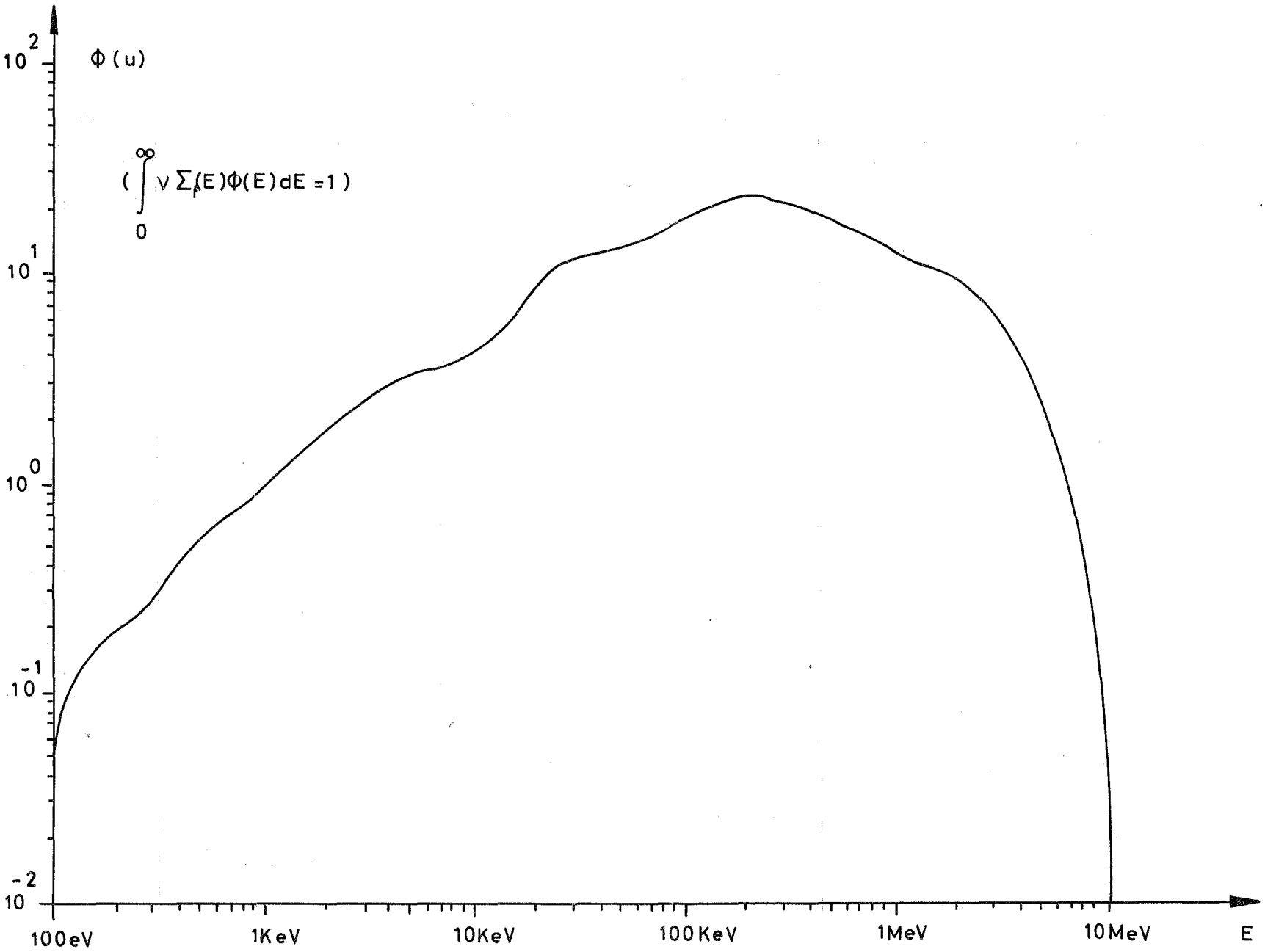

Fig. AII-8 Neutron flux for SNEAK 3 A1

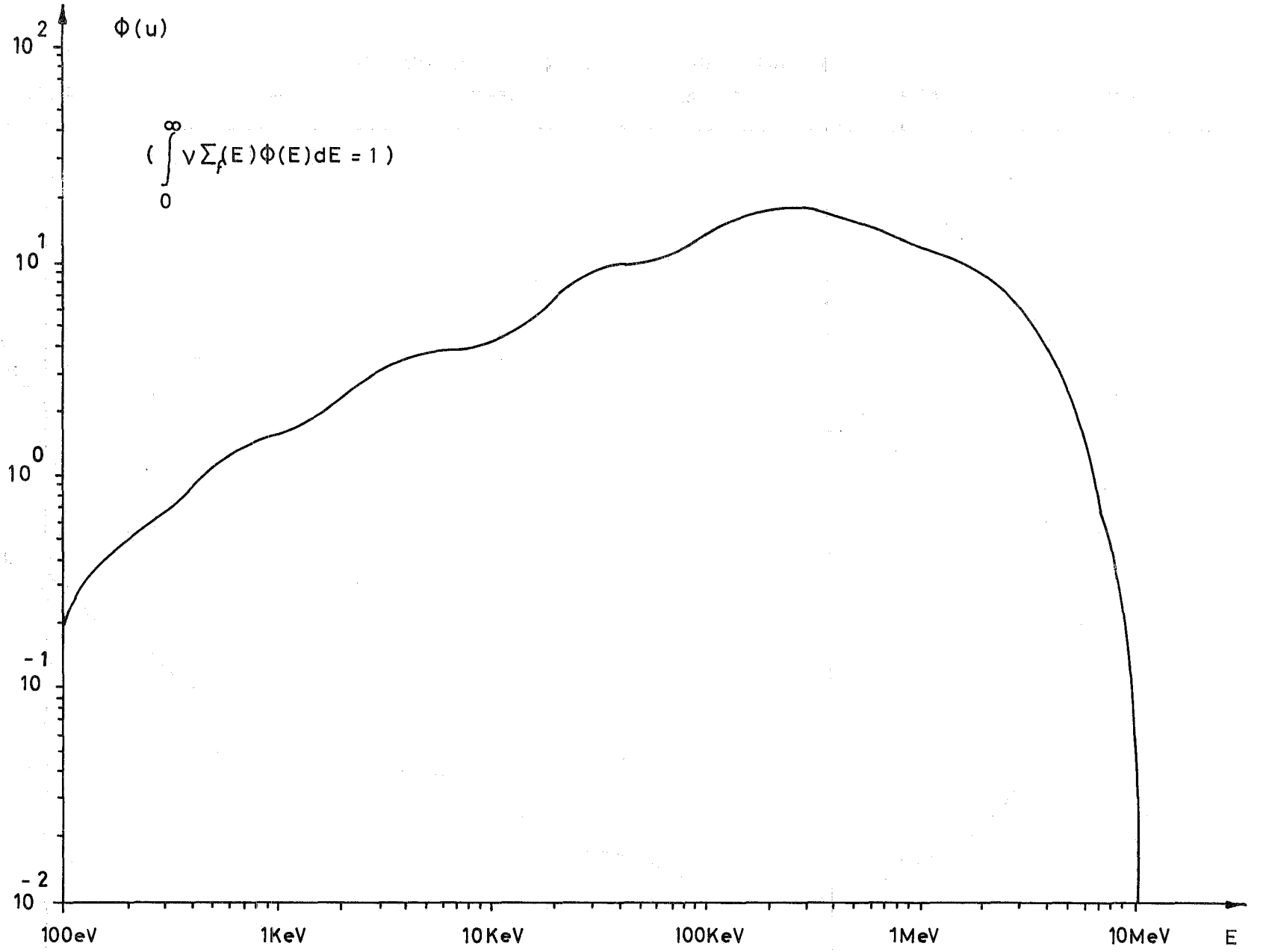

Fig. AII-9 Neutron flux for SNEAK3A2

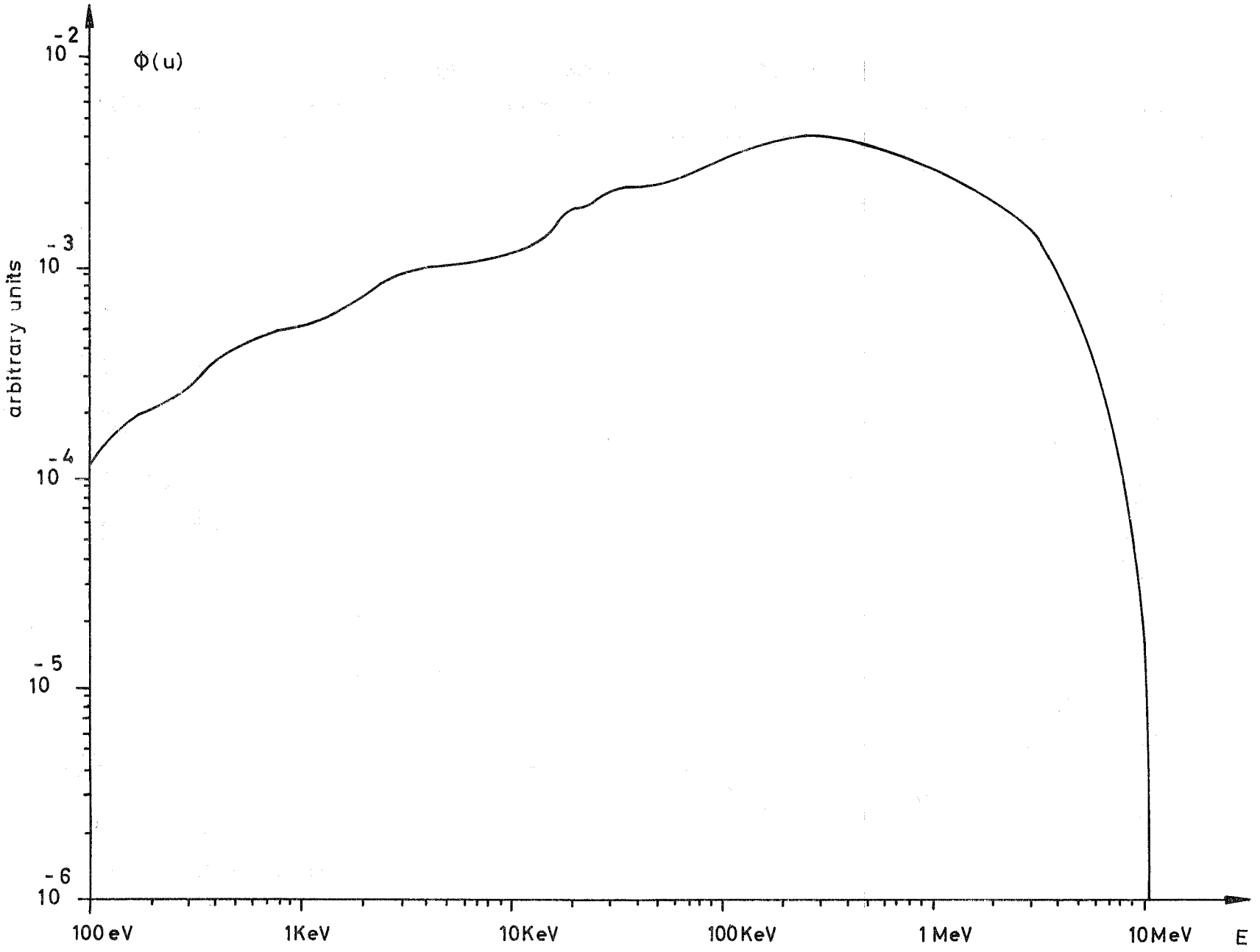

Fig. AII-10 Neutron flux for SEAK 3B2

Fig. AII-11 Neutron flux for SNEAK 5C

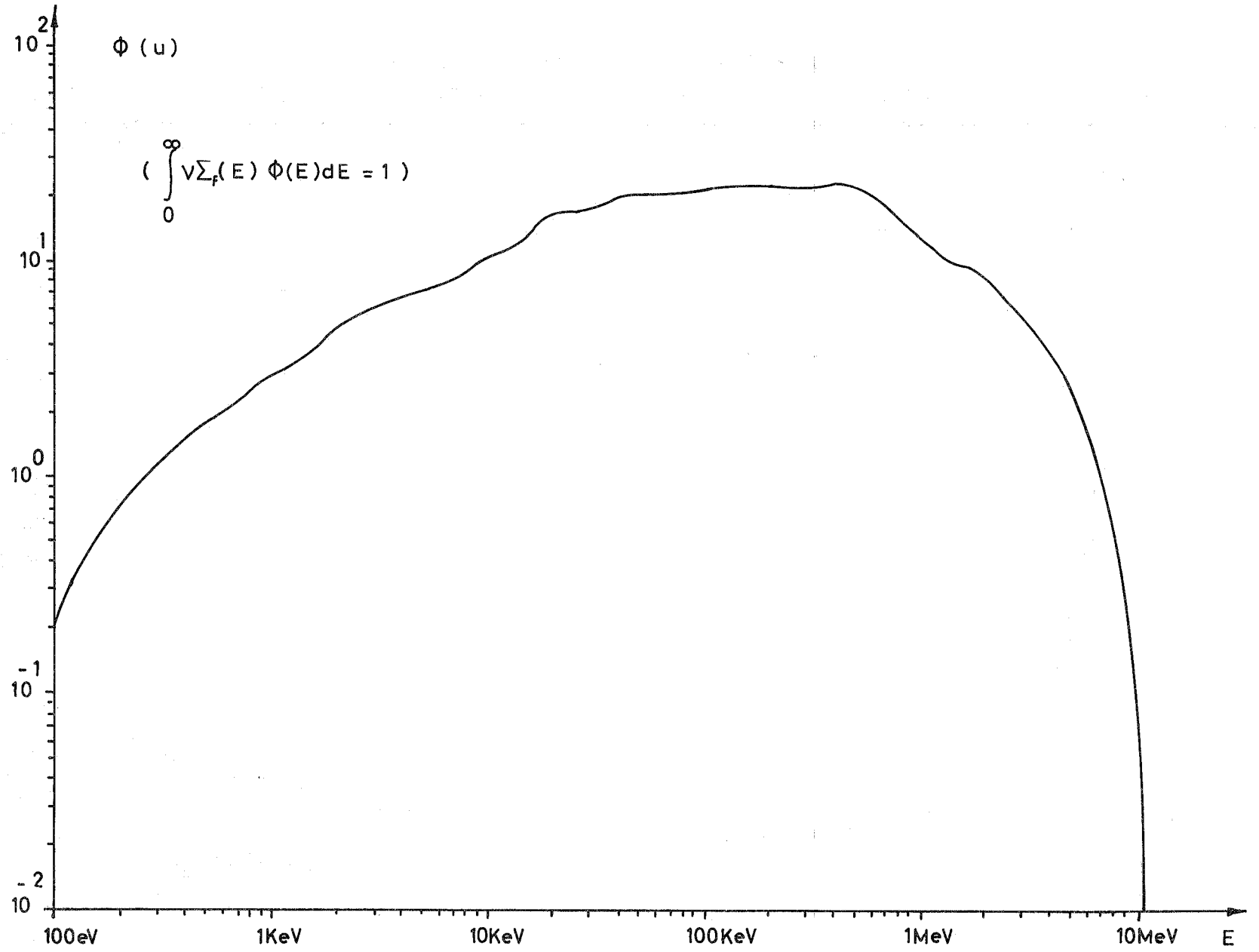

Fig. AII-12 Neutron flux for ZPR-III-55

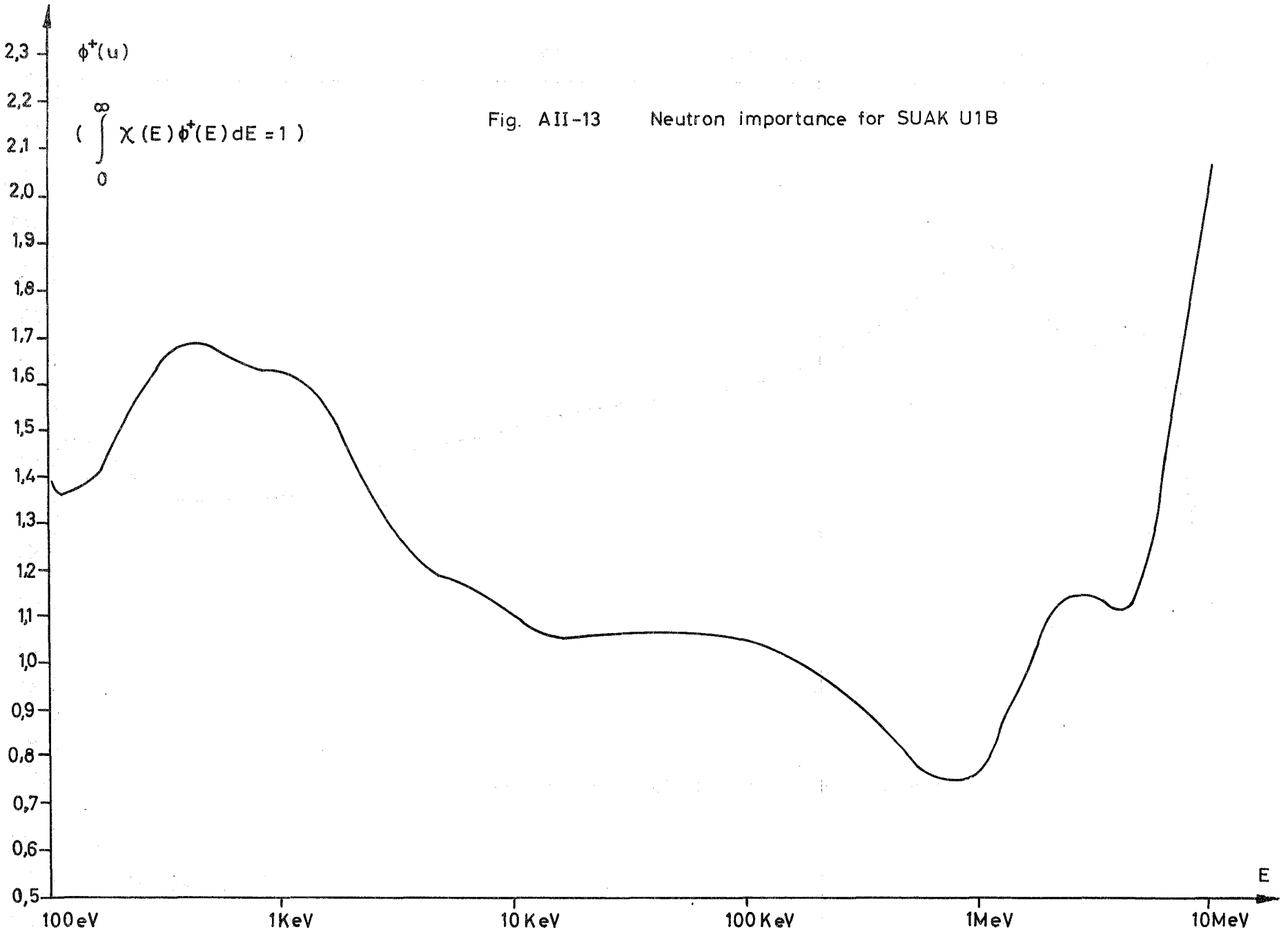

Fig. AII-13 Neutron importance for SUAK U1B

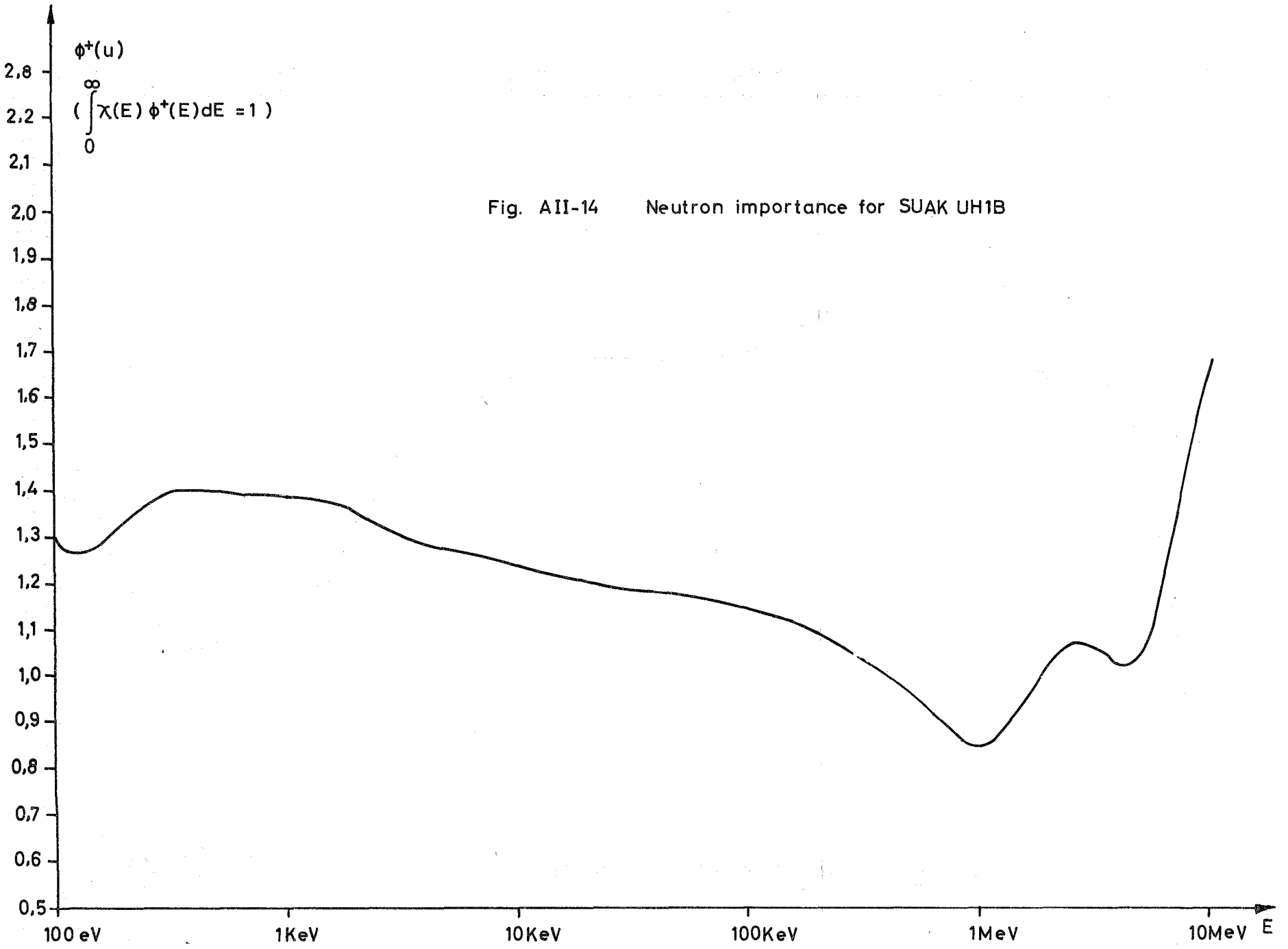

Fig. AII-14 Neutron importance for SUAK UH1B

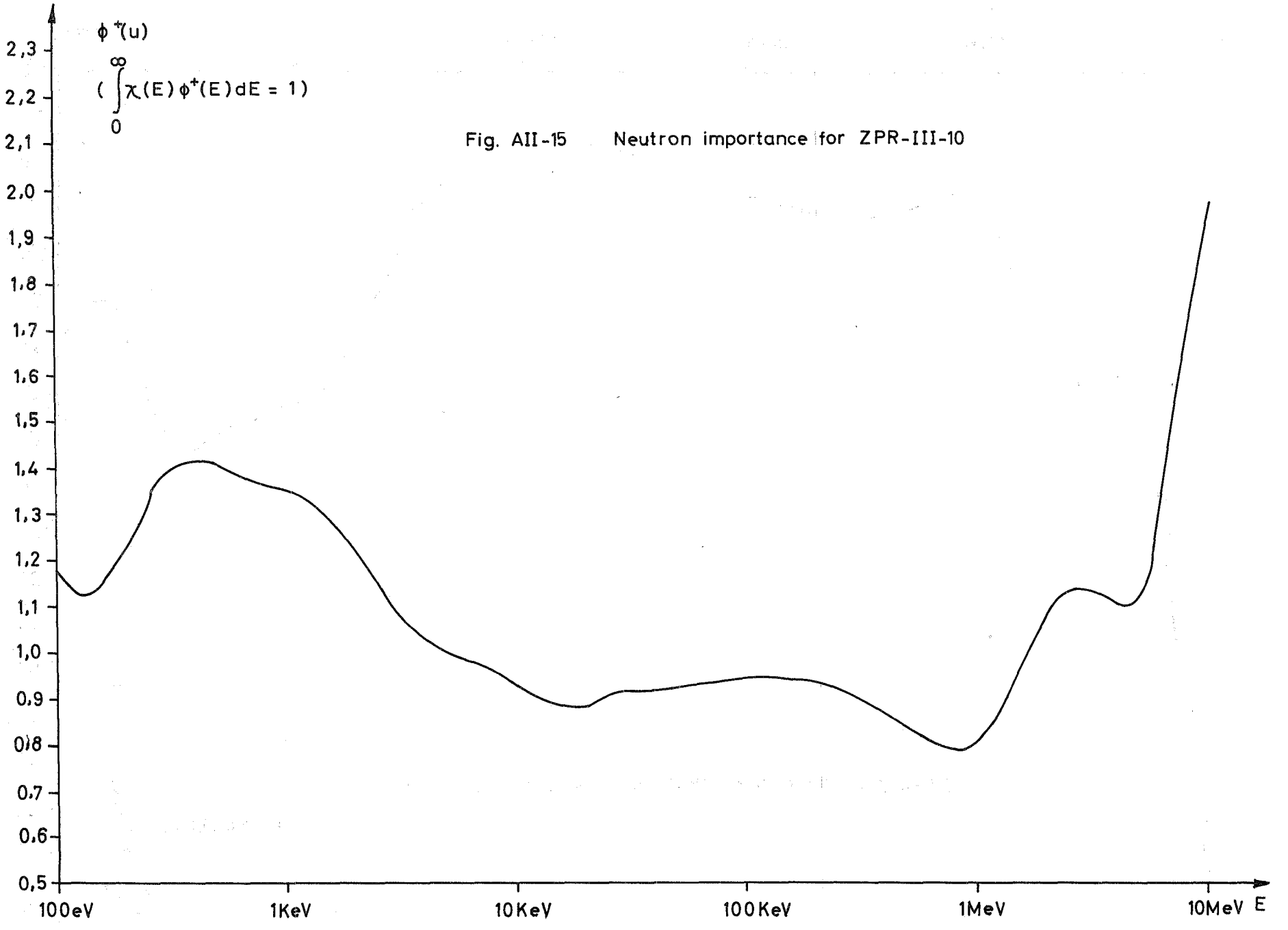

Fig. AII-15 Neutron importance for ZPR-III-10

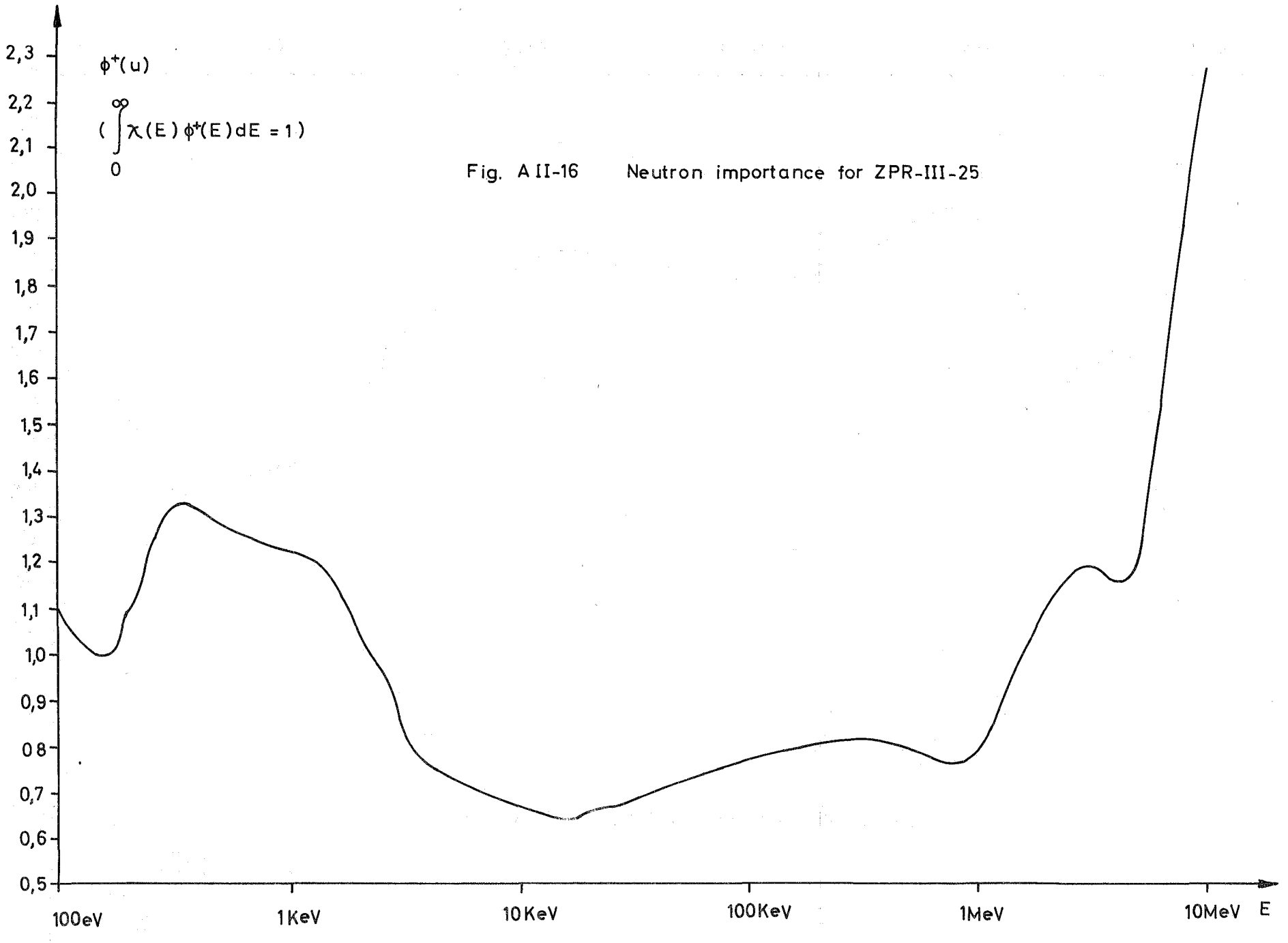

Fig. A II-16 Neutron importance for ZPR-III-25

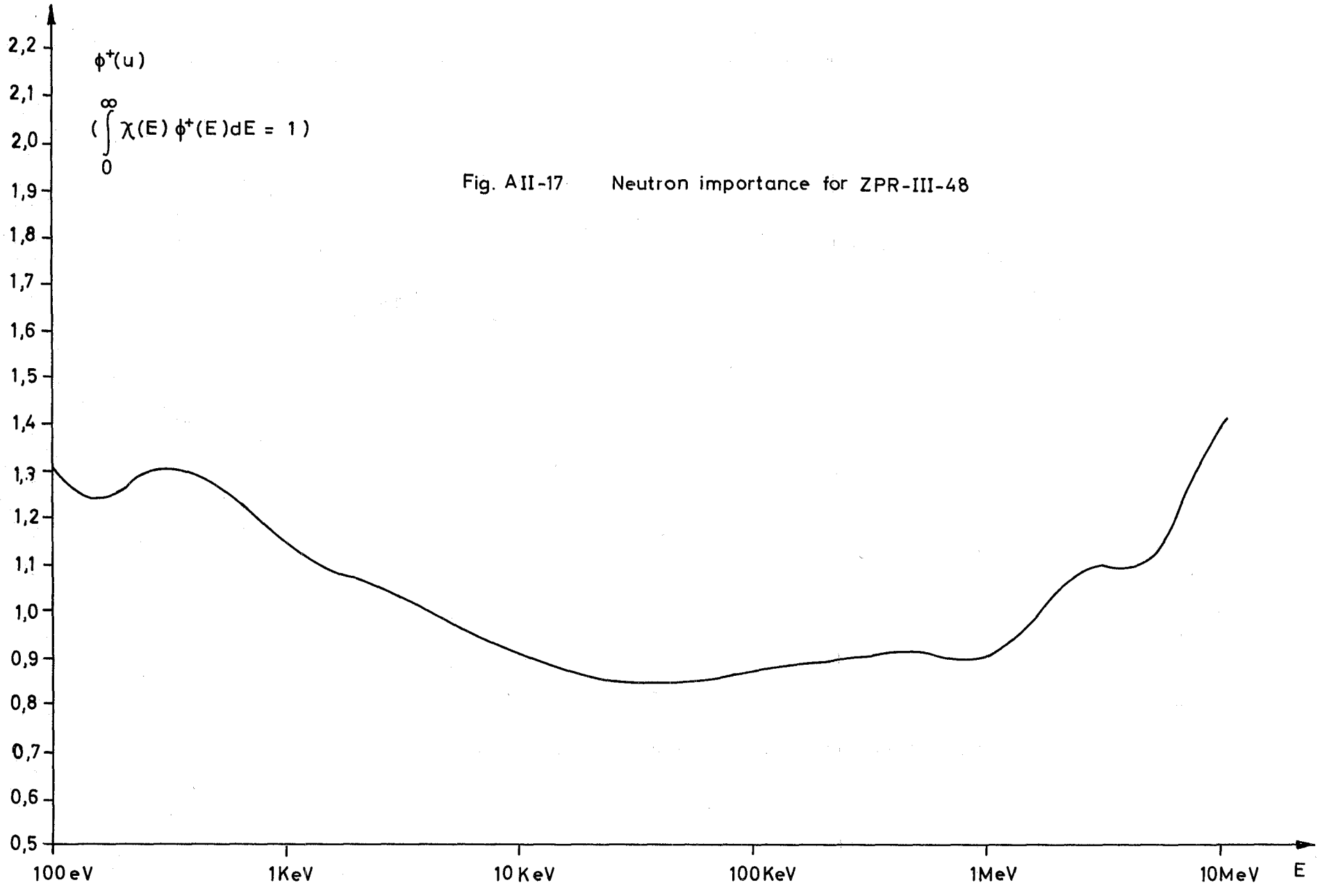

Fig. AII-17 Neutron importance for ZPR-III-48

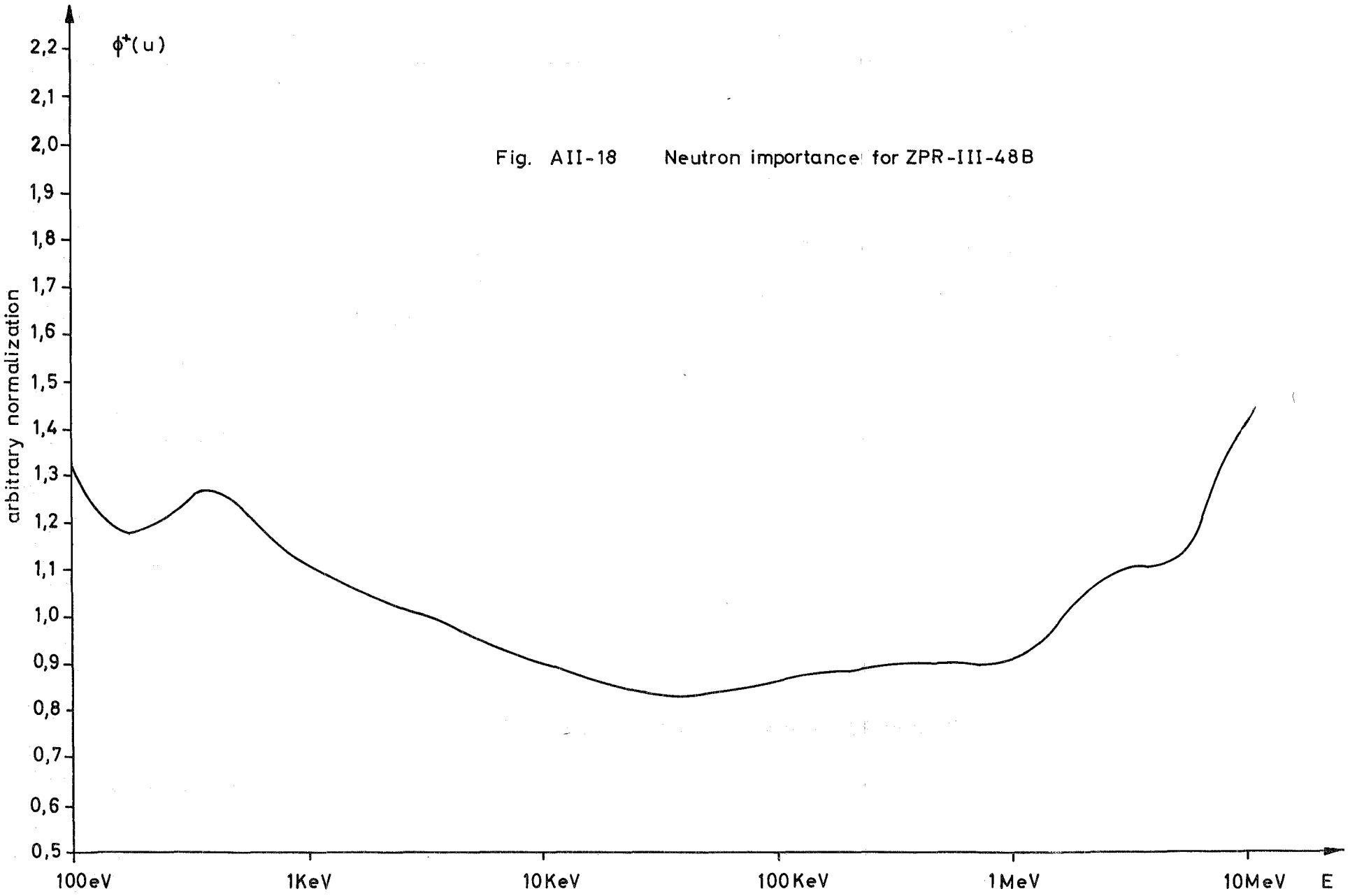

Fig. AII-18 Neutron importance for ZPR-III-48B

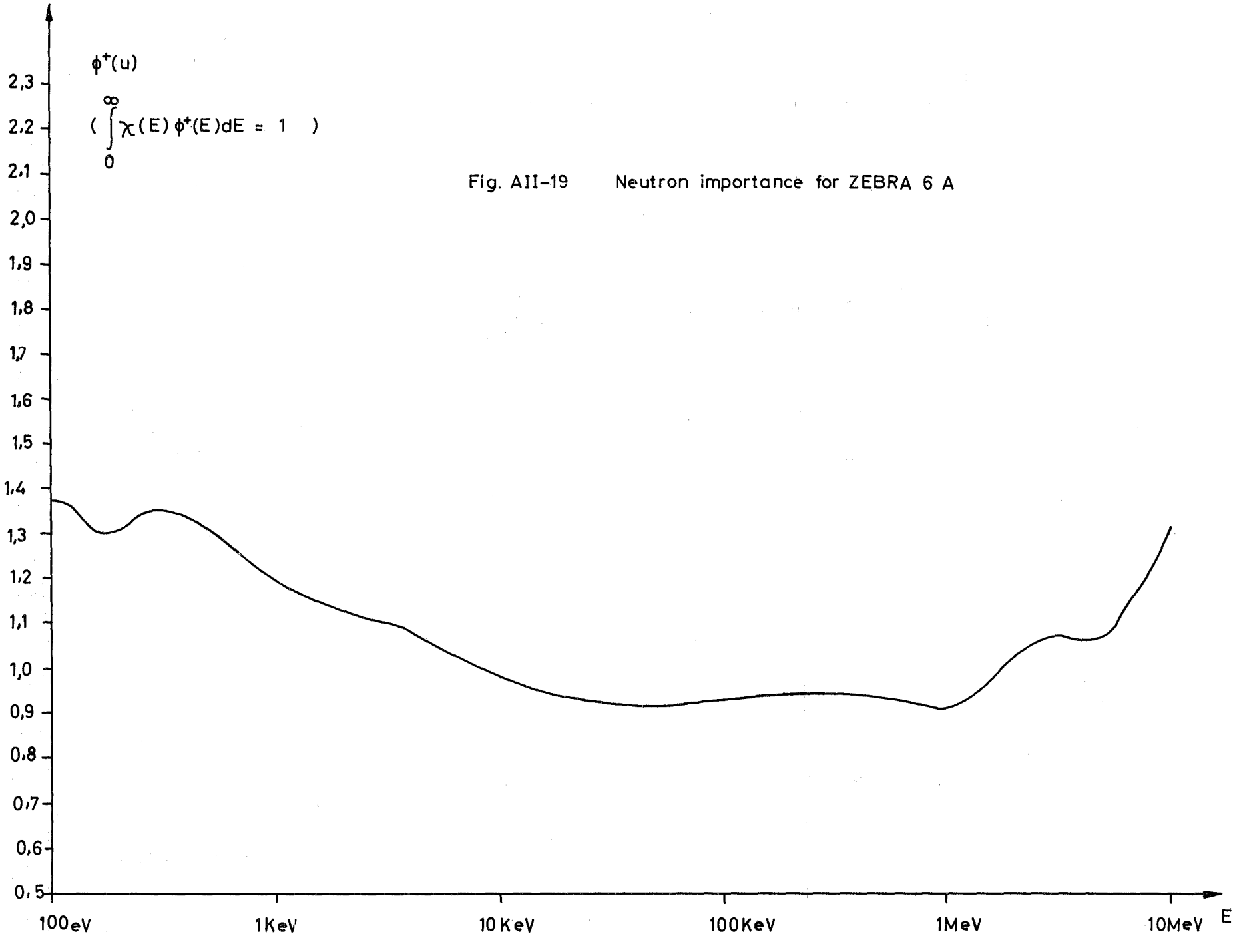

Fig. AII-19 Neutron importance for ZEBRA 6 A

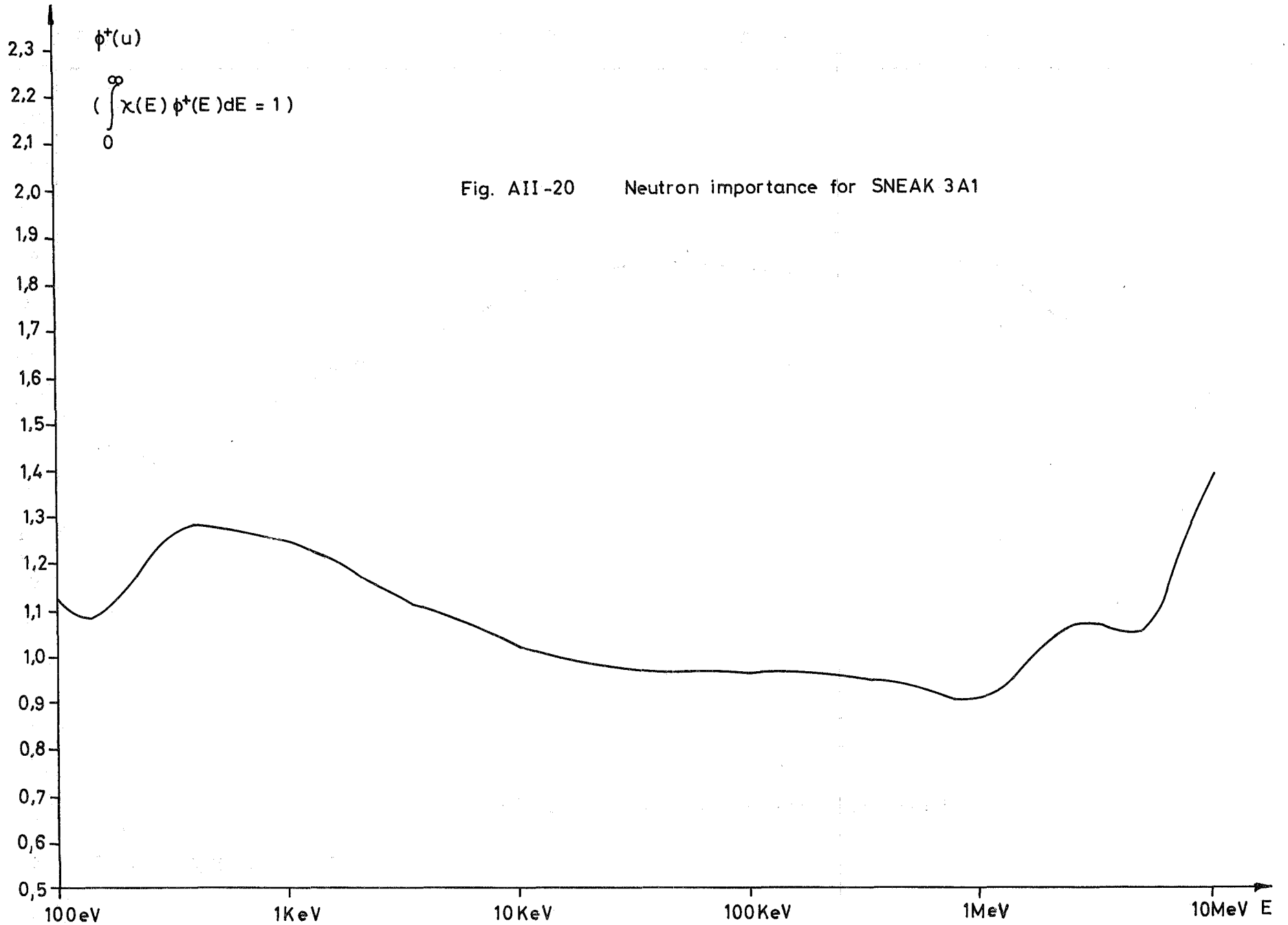

Fig. AII-20 Neutron importance for SNEAK 3A1

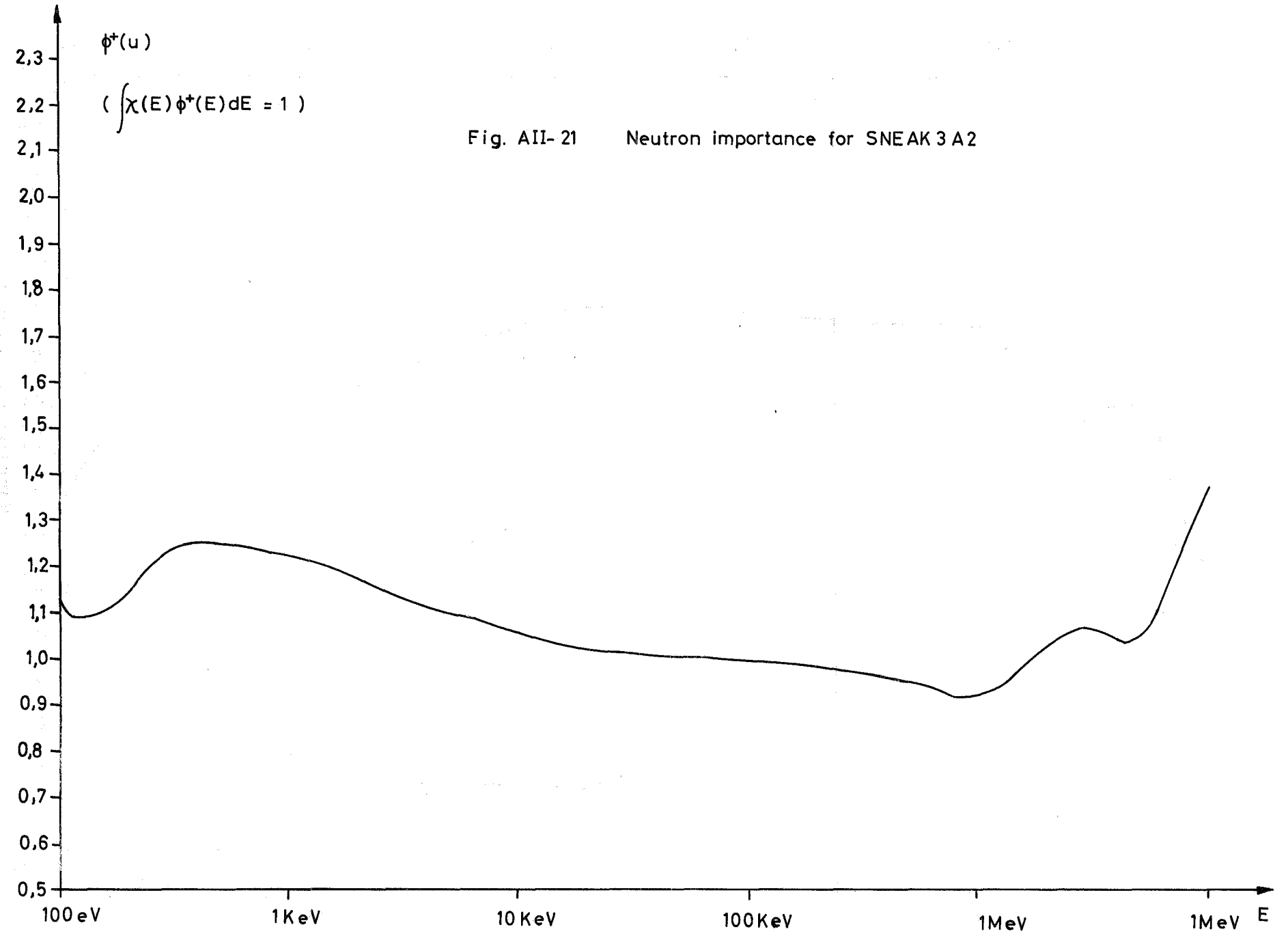

Fig. AII-21 Neutron importance for SNEAK 3A2

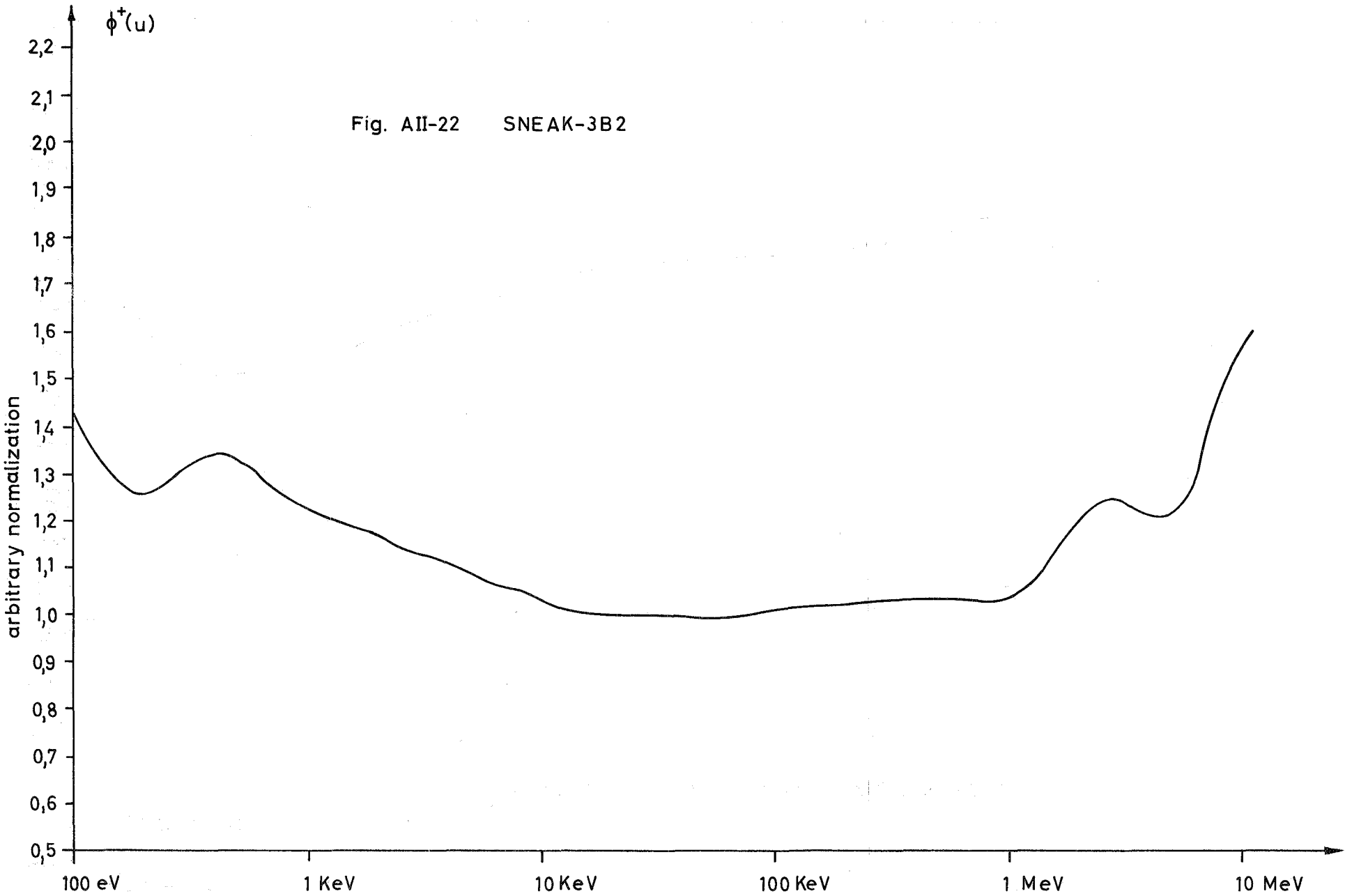

Fig. AII-22 SNEAK-3B2

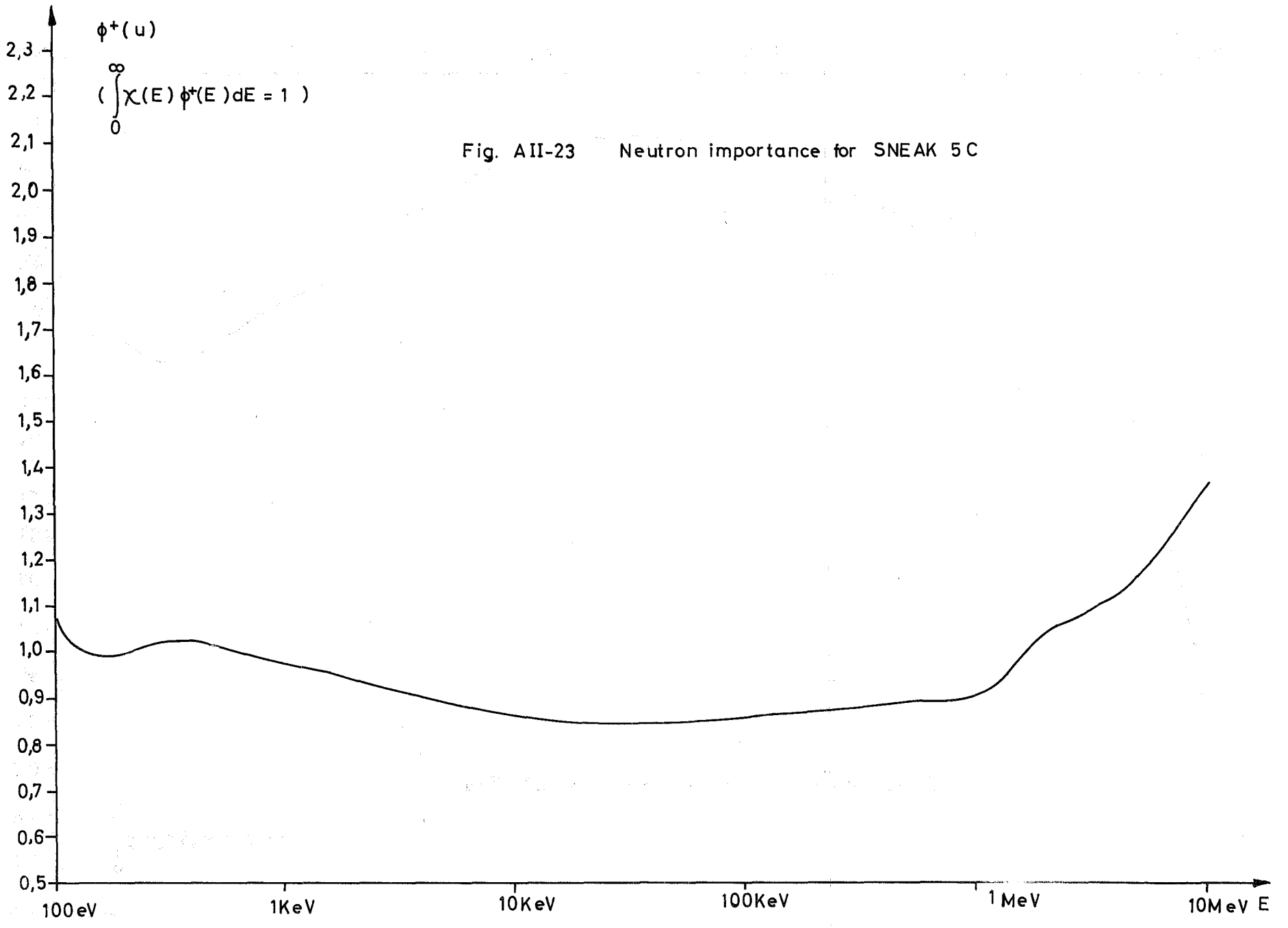

Fig. AII-23 Neutron importance for SNEAK 5C

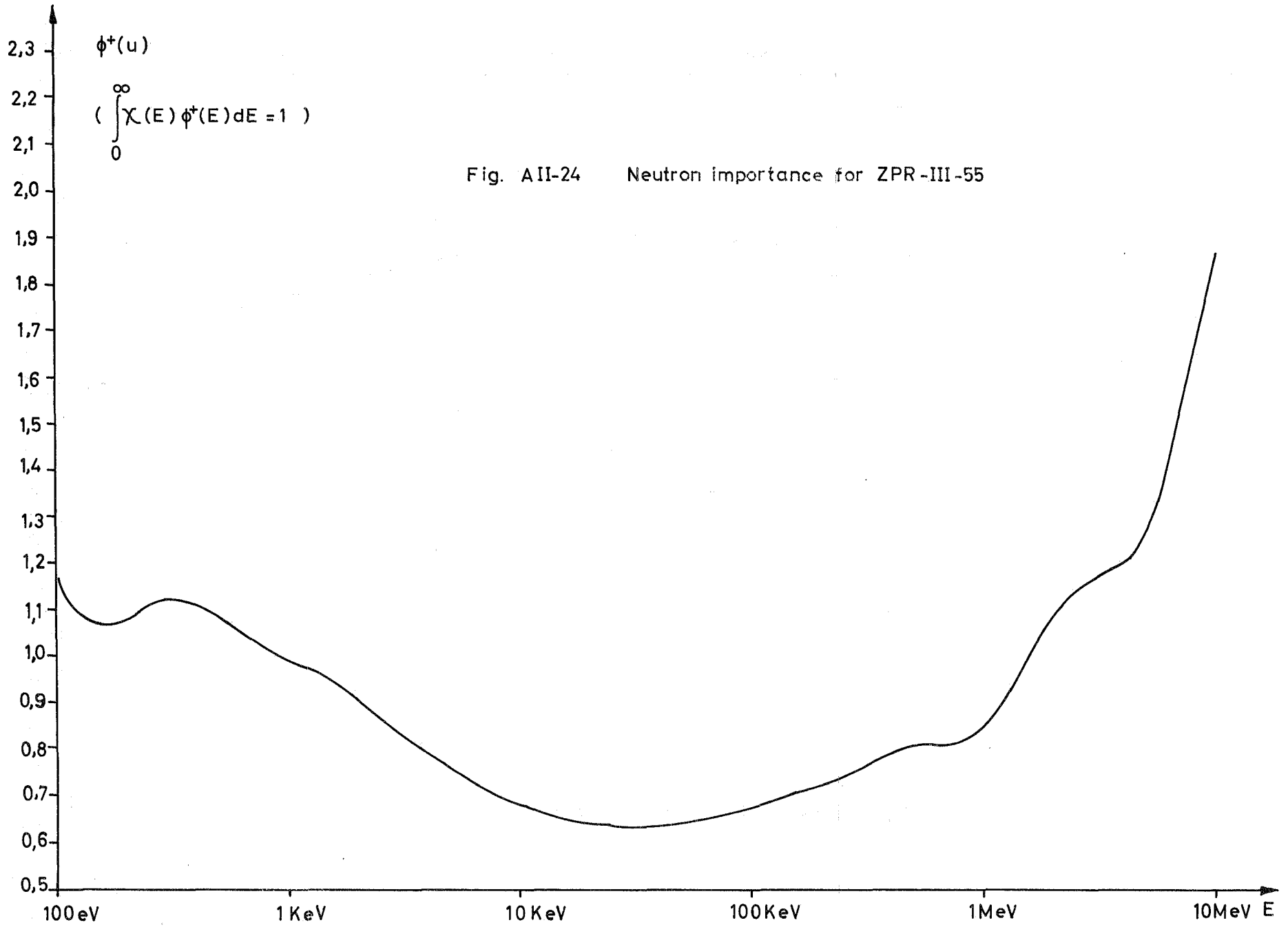

Fig. AII-24 Neutron importance for ZPR-III-55

Fig. AII-25 Collision density for SUAK U1B

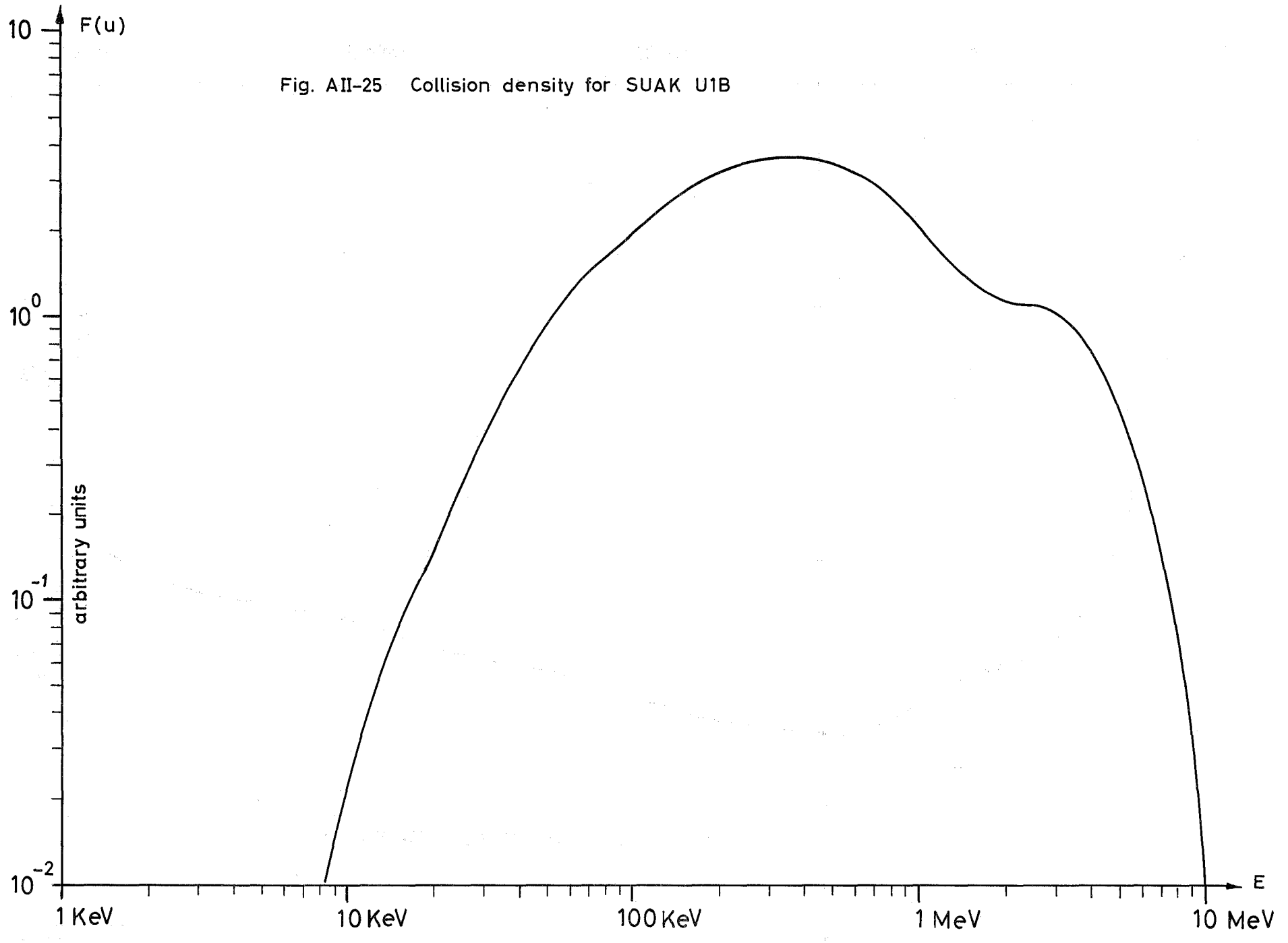

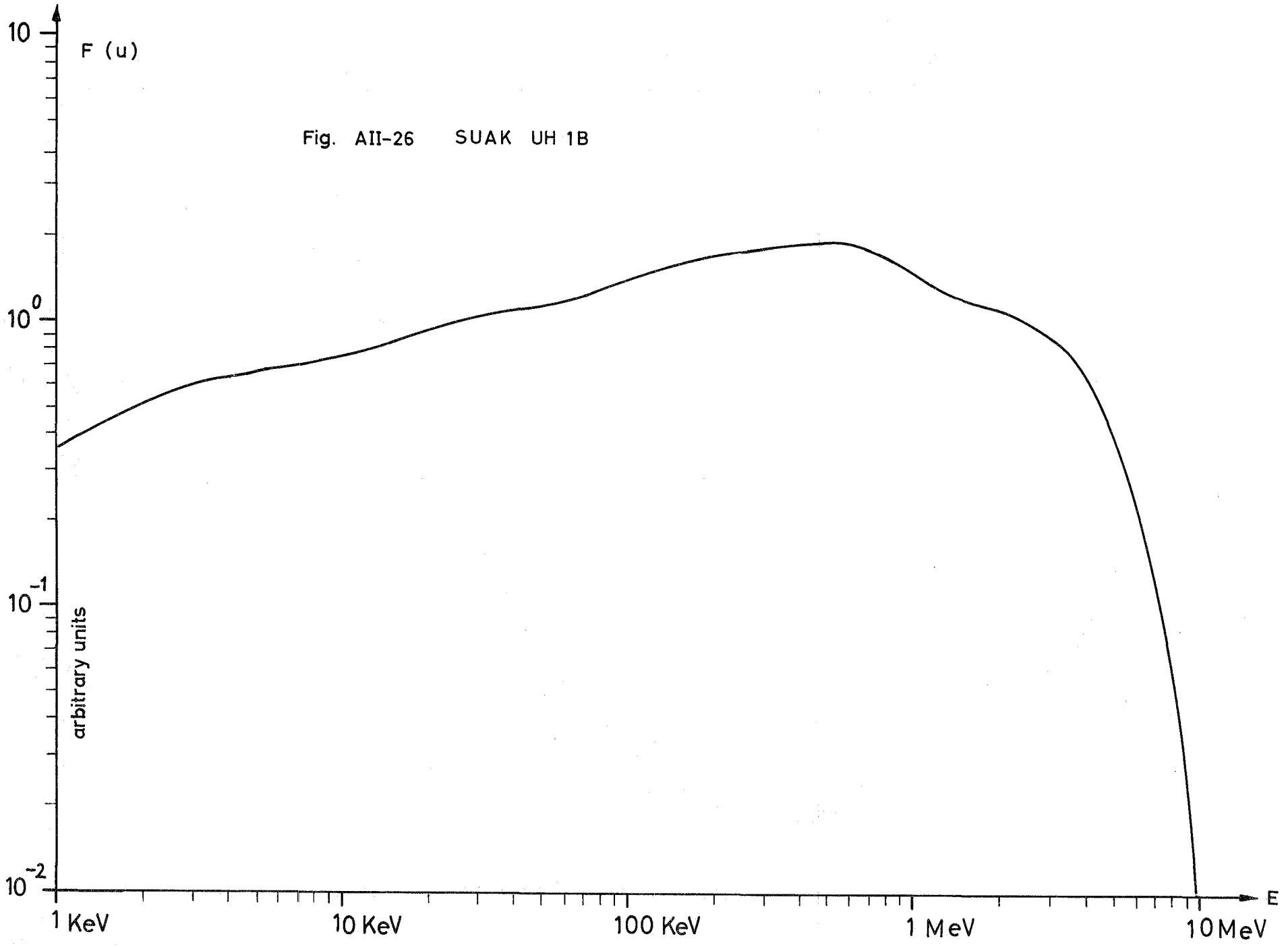

Fig. AII-26 SUAK UH 1B

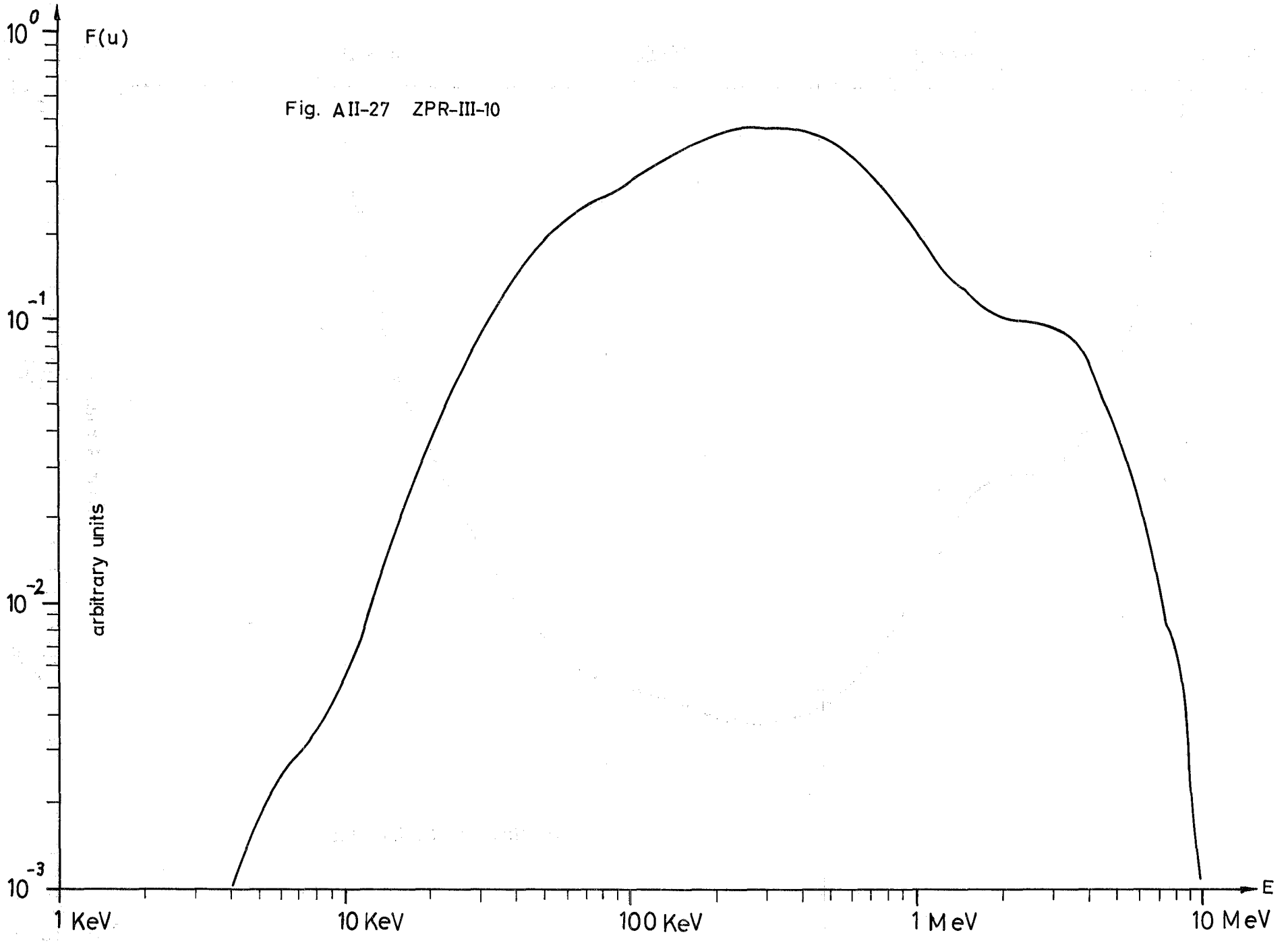
Fig. AII-27 ZPR-III-10
F(u)
arbitrary units
10^{0}
10^{-1}
10^{-2}
10^{-3}
E
1 KeV
10 KeV
100 KeV
1 MeV
10 MeV

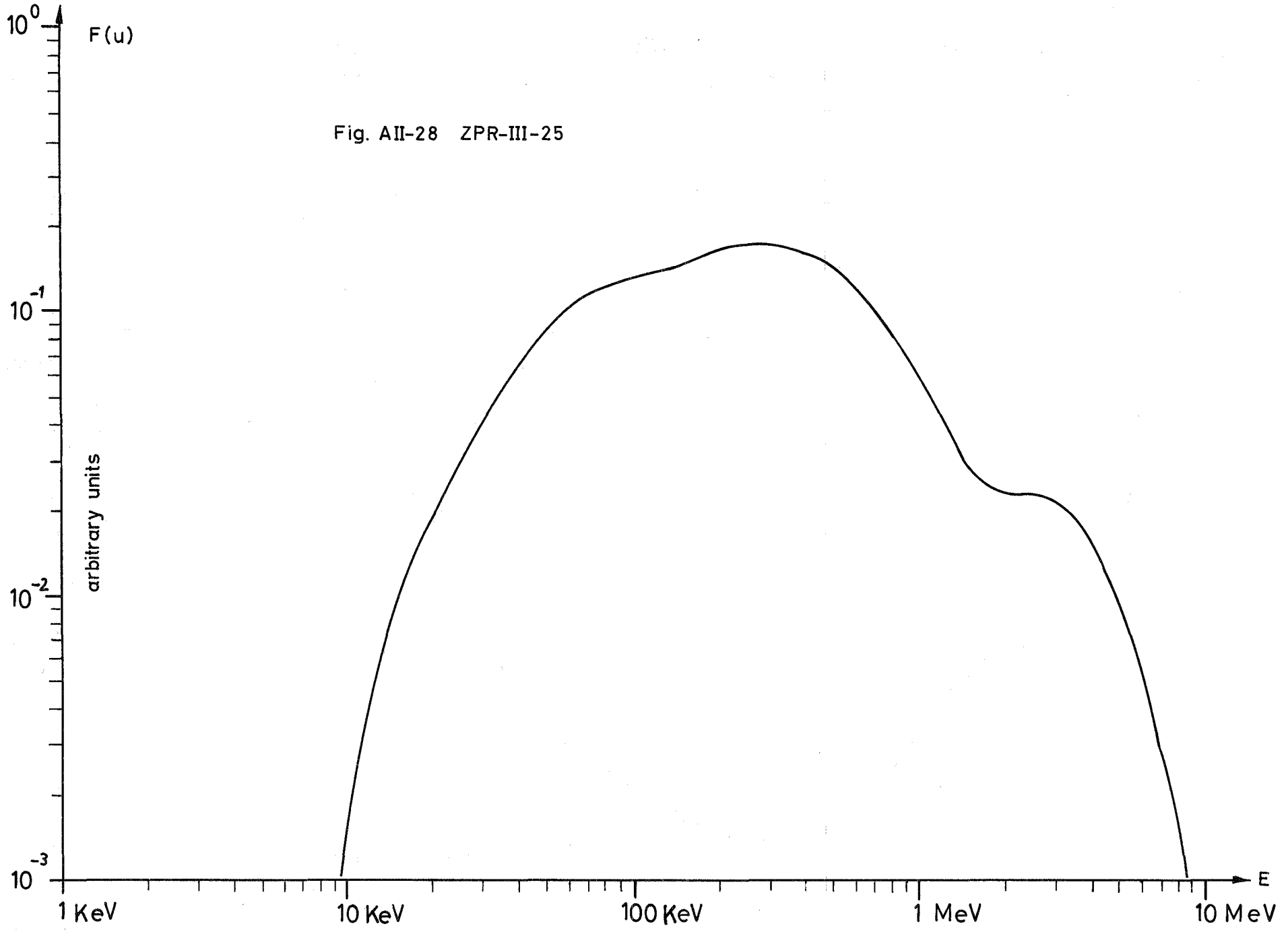

Fig. AII-28 ZPR-III-25

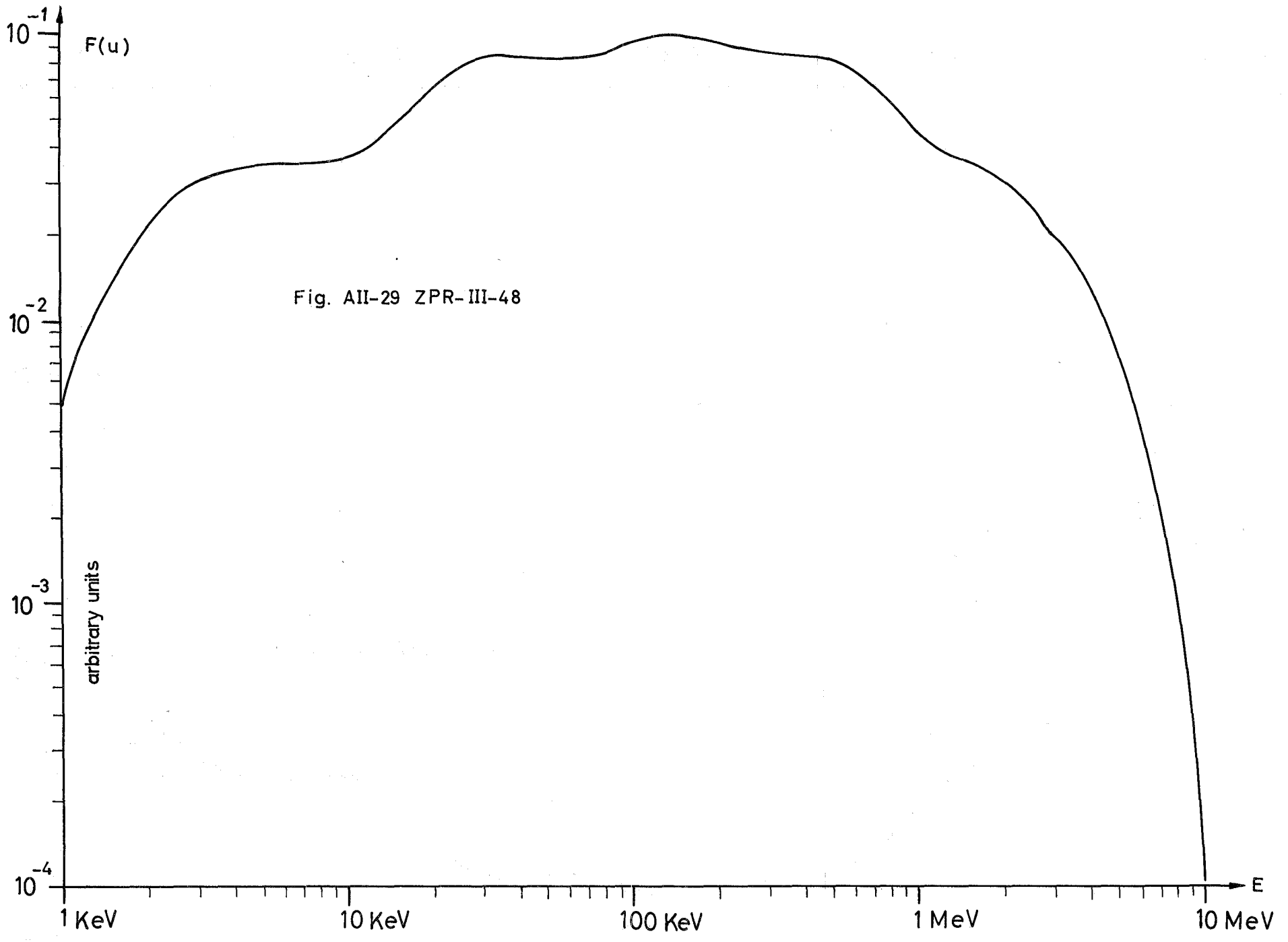

Fig. AII-29 ZPR-III-48

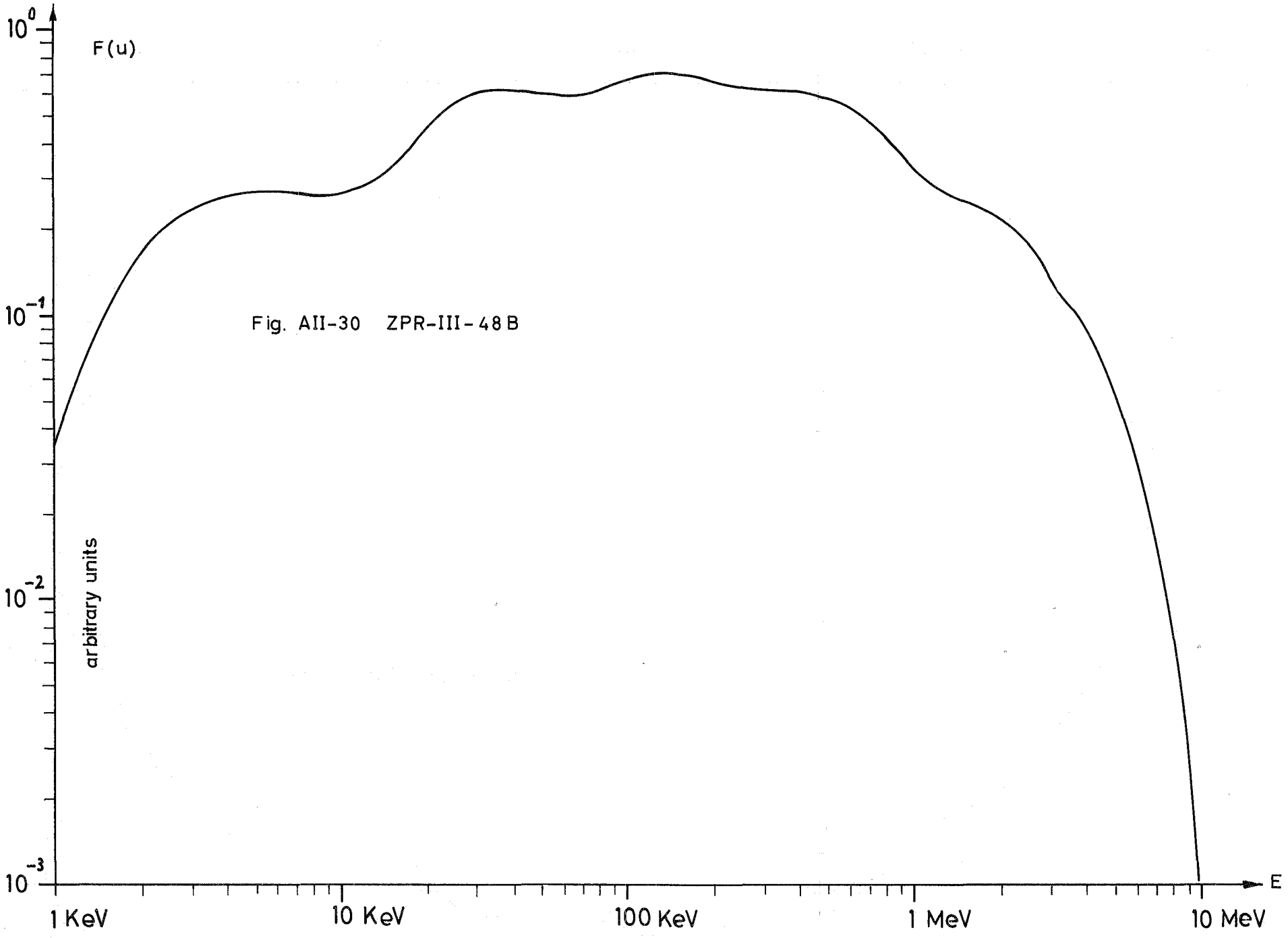

Fig. AII-30 ZPR-III-48B

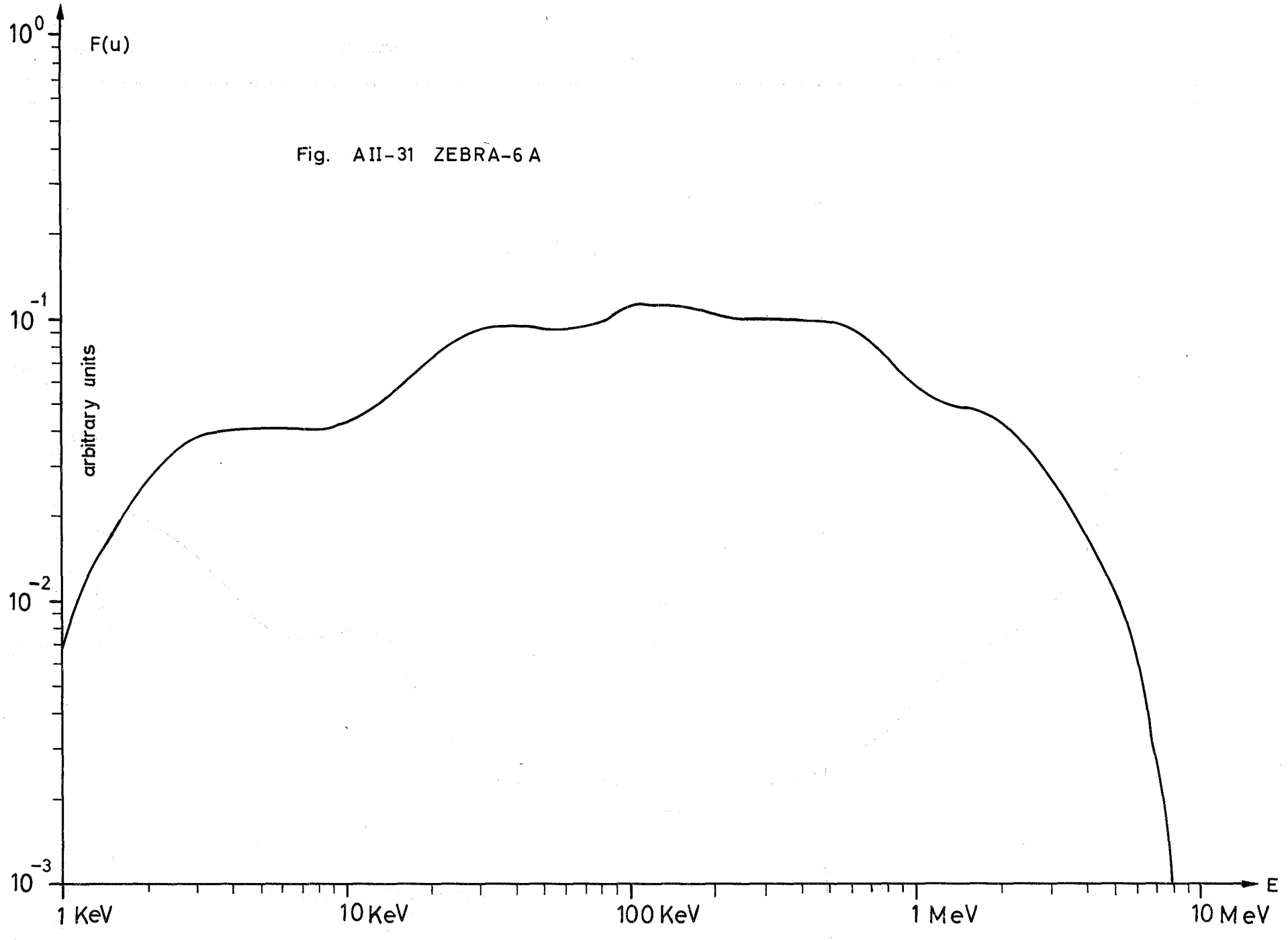

Fig. AII-31 ZEBRA-6 A

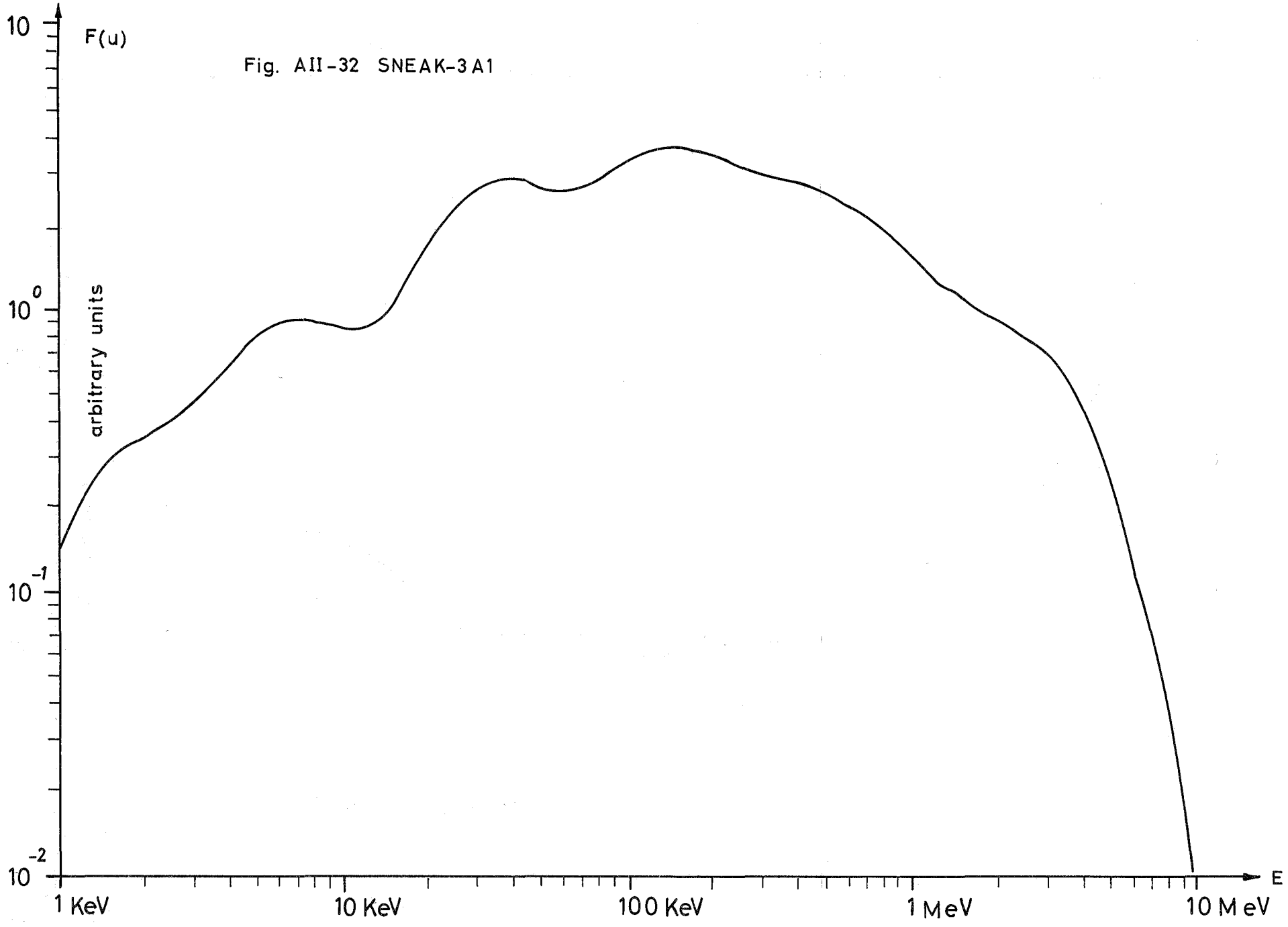
10
F(u)
Fig. AII-32 SNEAK-3A1
arbitrary units
10^0
10^-1
10^-2
E
1 KeV
10 KeV
100 KeV
1 MeV
10 MeV

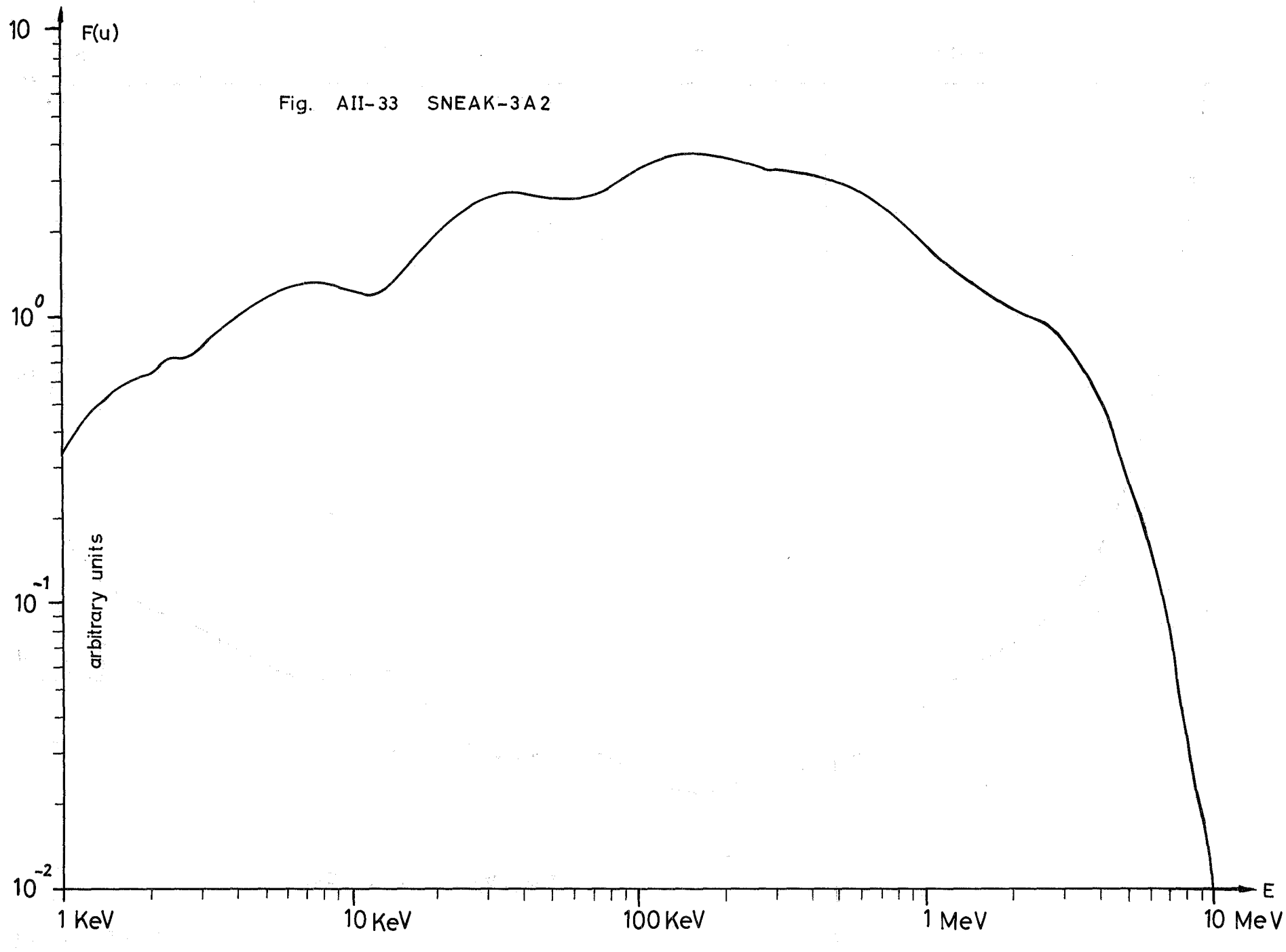
10
F(u)
Fig. AII-33 SNEAK-3A2
10^{0}
10^{-1}
10^{-2}
arbitrary units
E
1 KeV
10 KeV
100 KeV
1 MeV
10 MeV

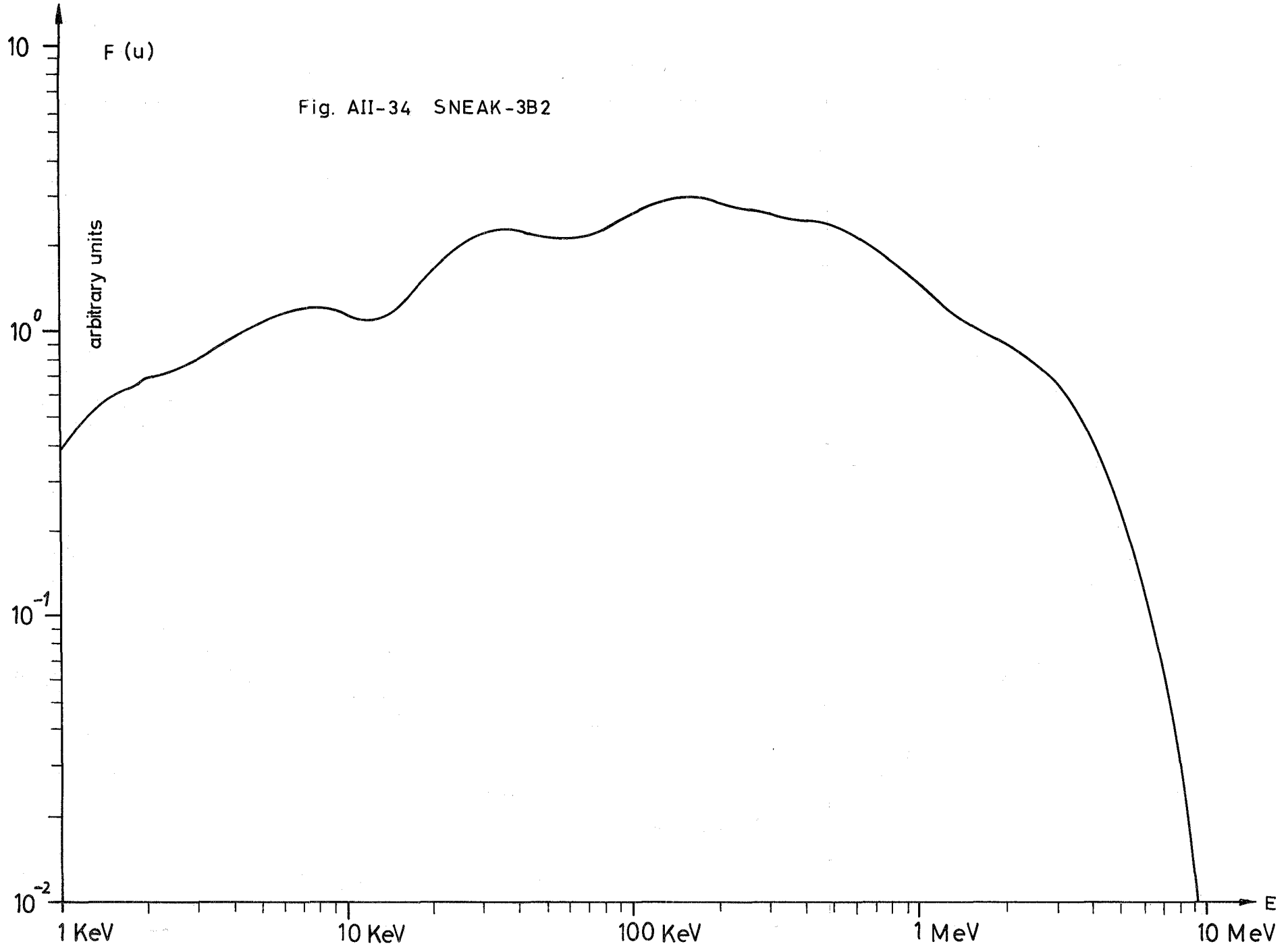

Fig. AII-34 SNEAK-3B2

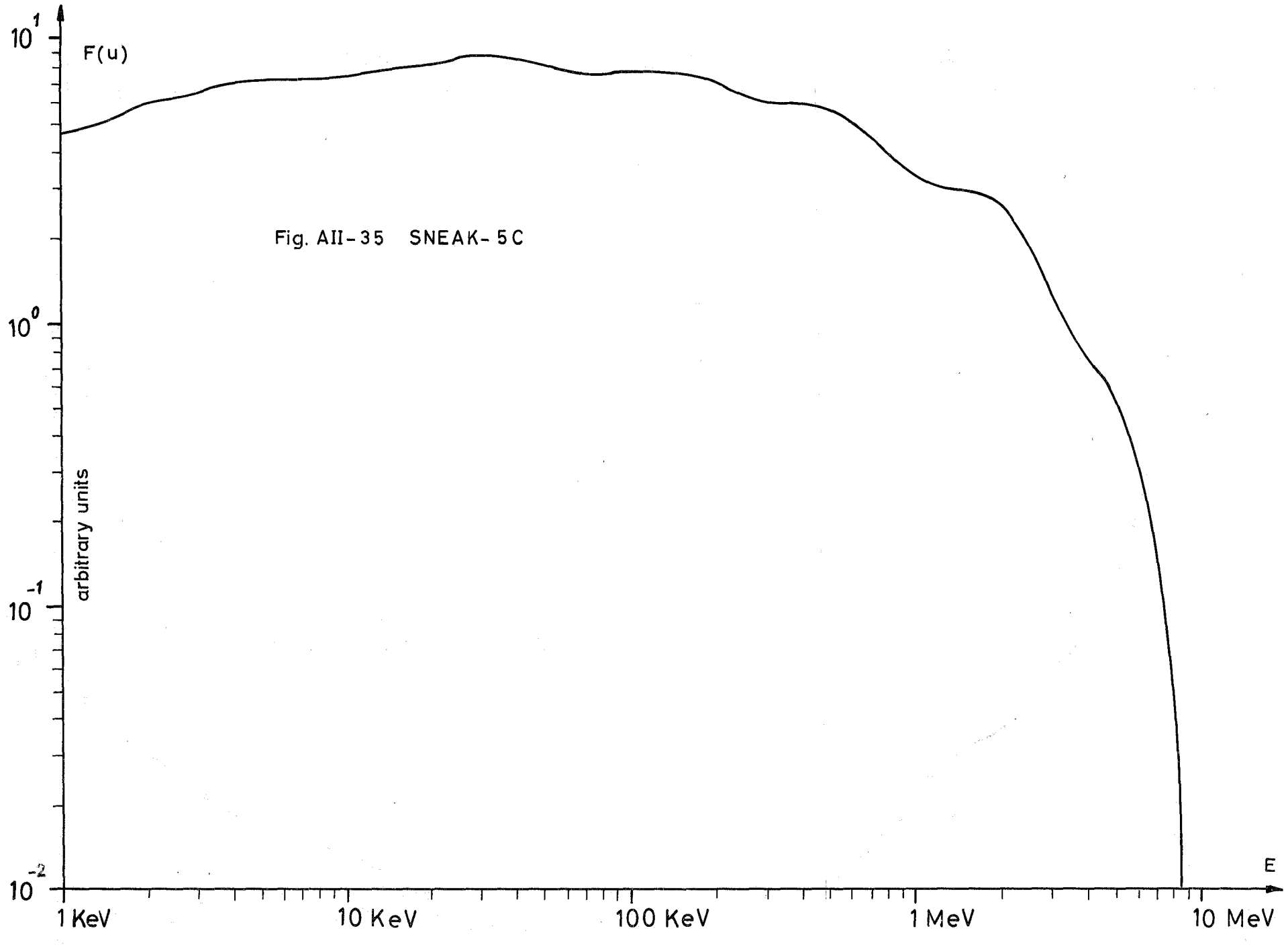

Fig. AII-35 SNEAK-5C

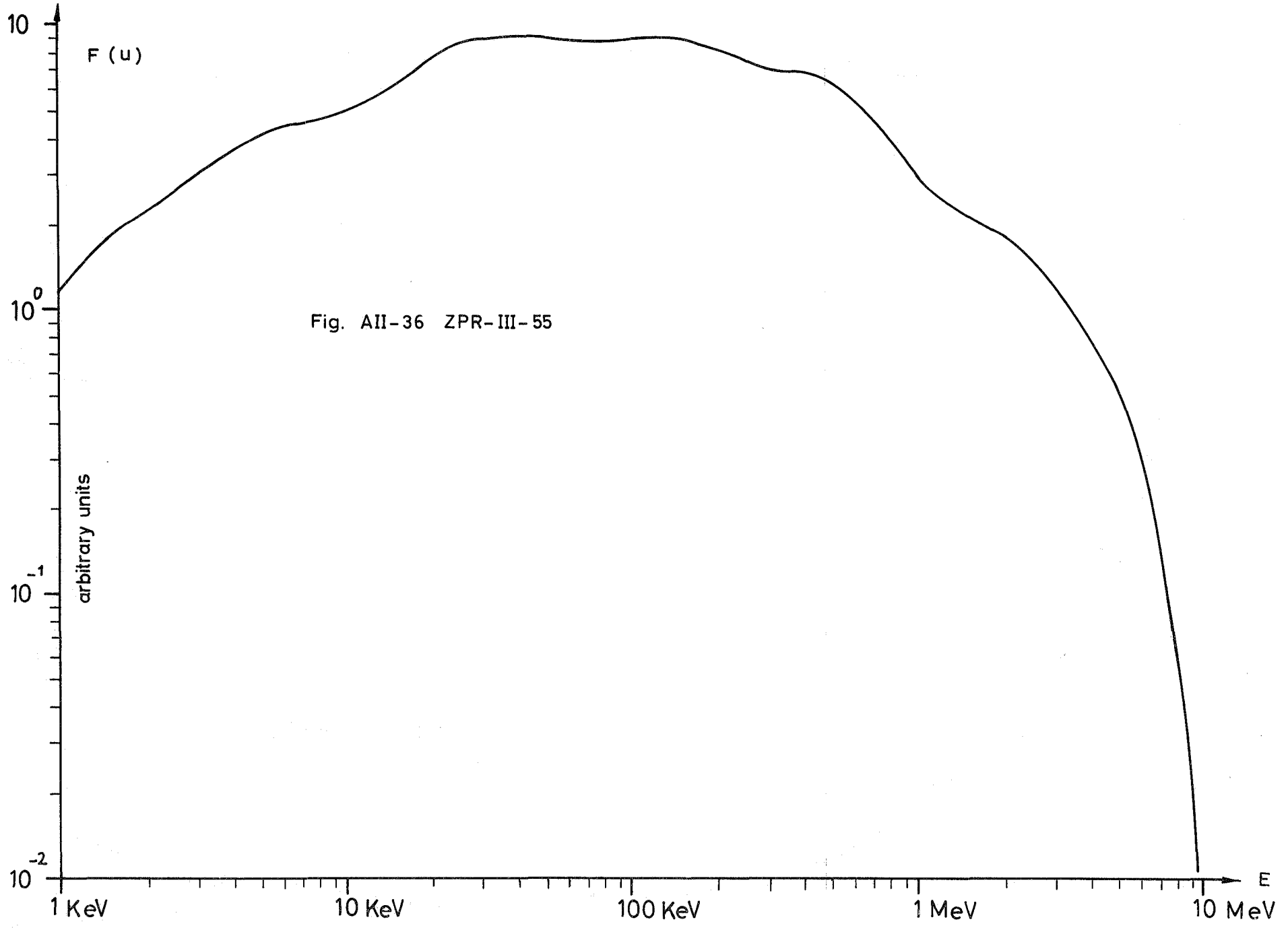

Fig. AII-36 ZPR-III-55

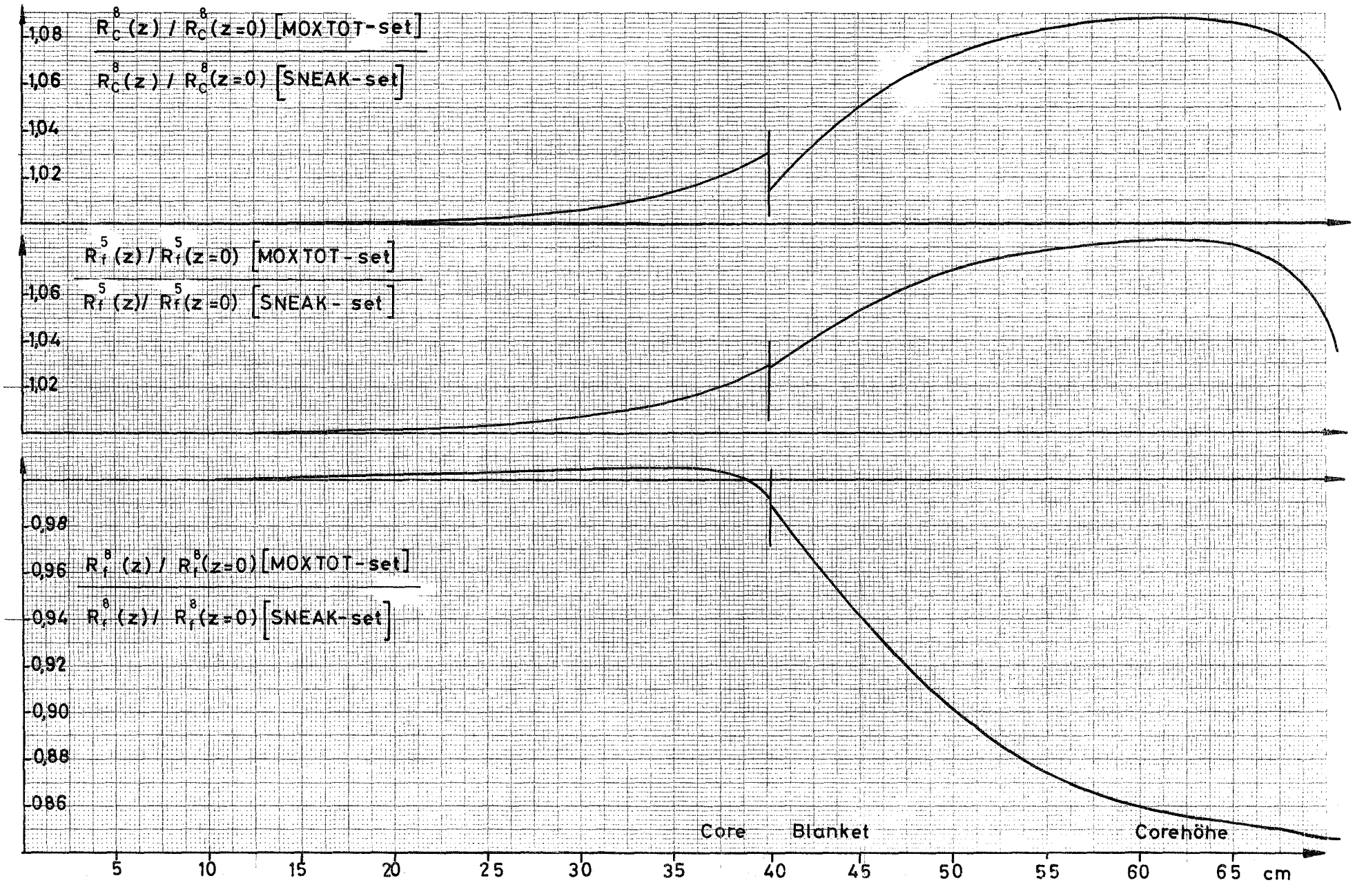

Fig. 1 Comparison of axial reaction rate traverses for SNEAK - 3A2

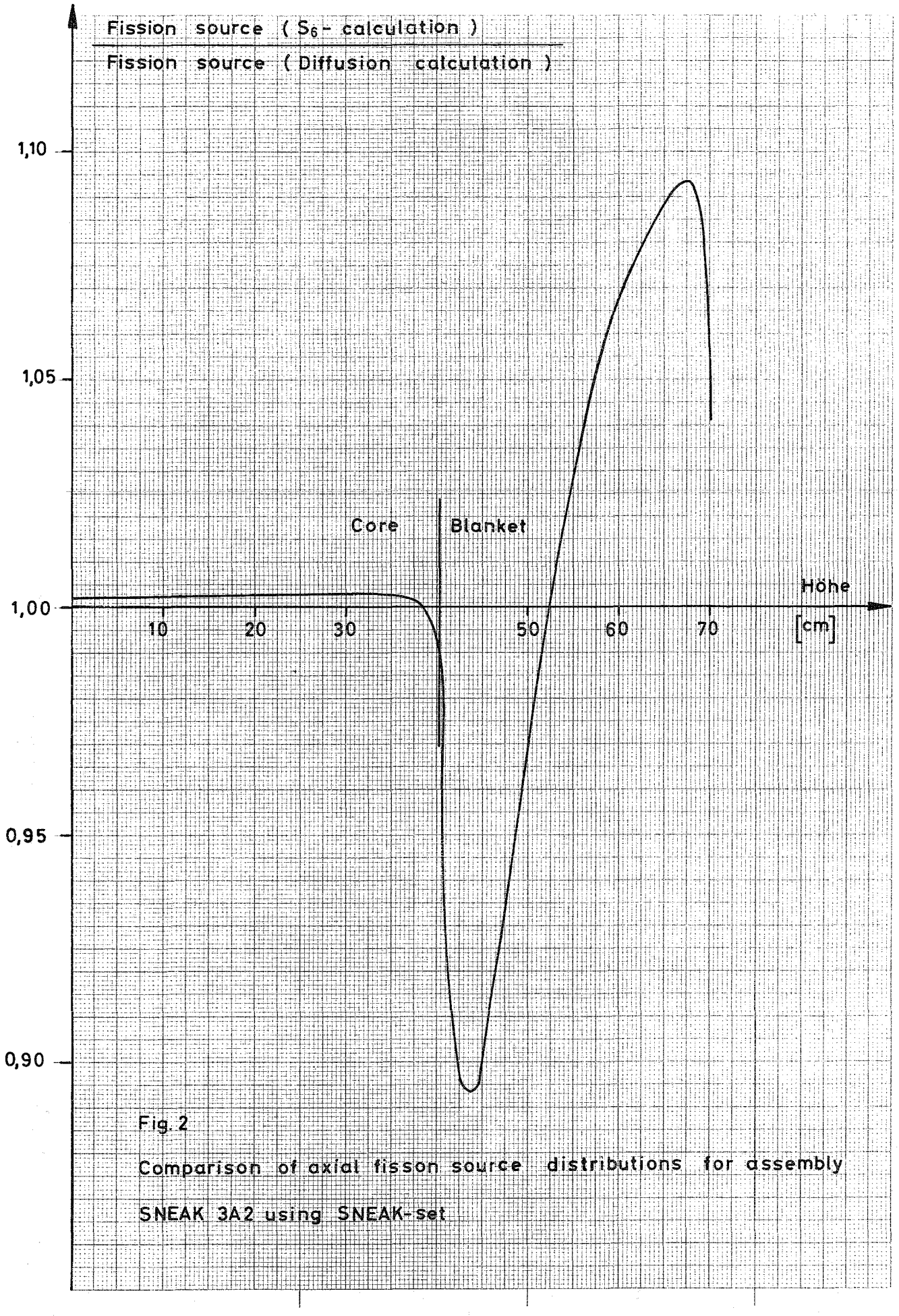

Fig. 2

Comparison of axial fisson source distributions for assembly SNEAK 3A2 using SNEAK-set

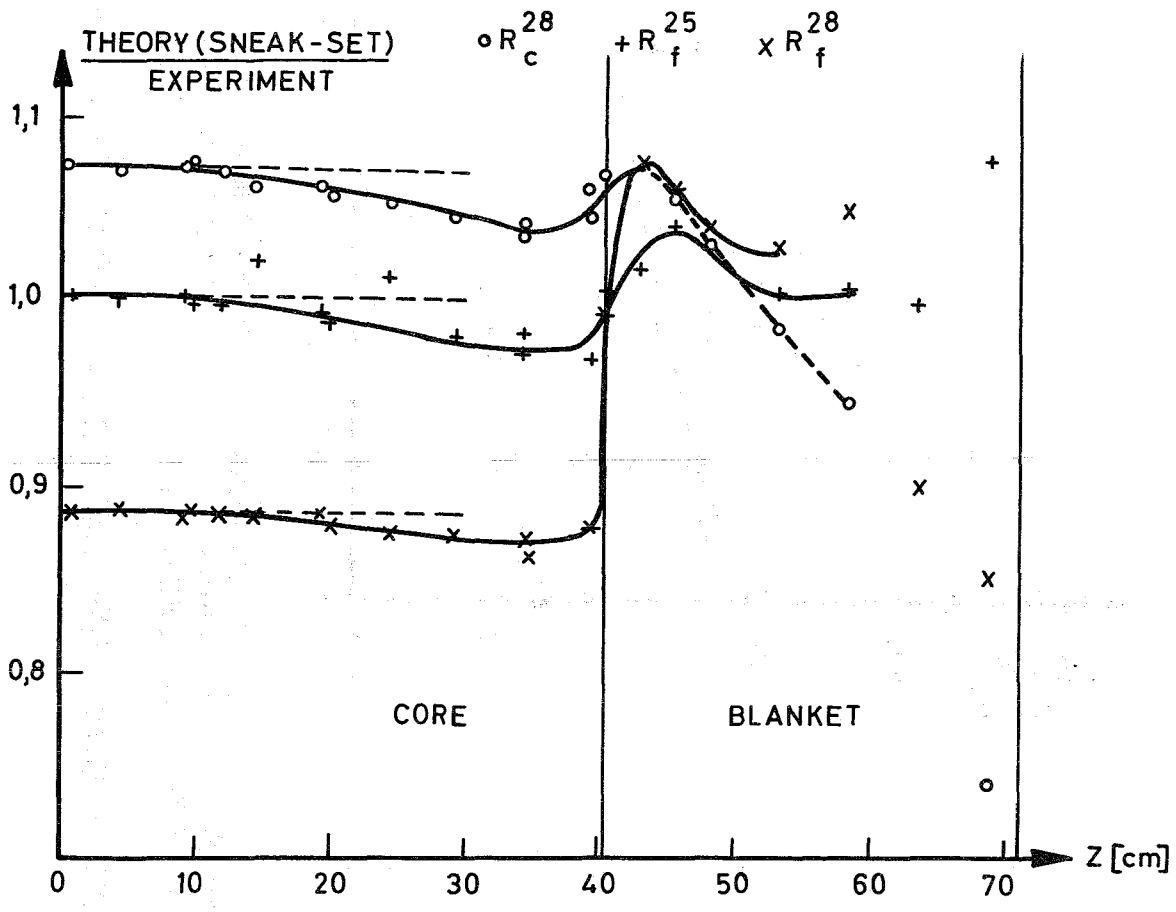

THE RATIO OF CALCULATED TO MEASURED REACTION RATES ALONG THE CENTRAL REACTOR AXIS
(DIFFUSION CALCULATION WITH HETEROGENEITY CORRECTION)

Fig. 3

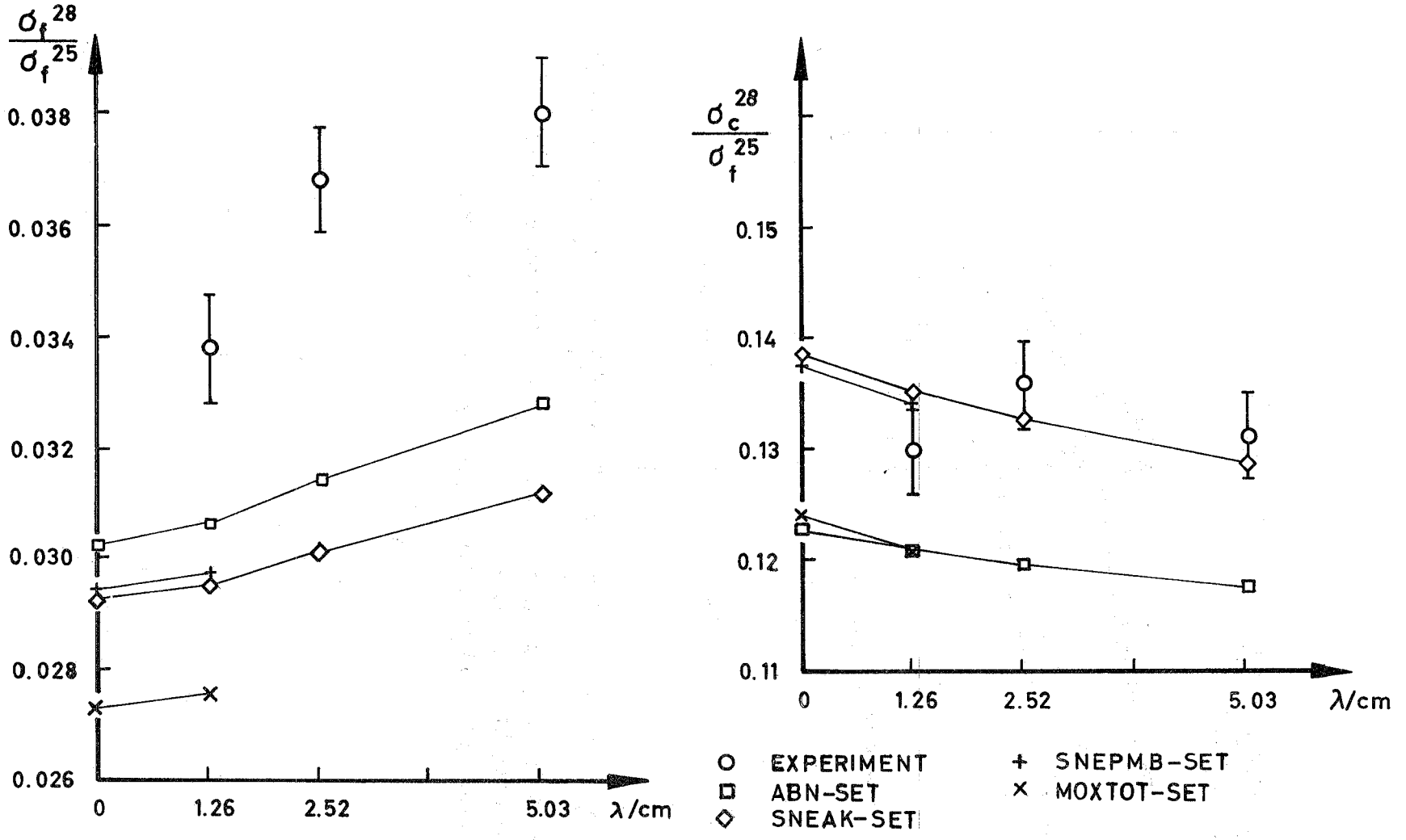

FIG. 4 CENTRAL REACTION RATE RATIOS FOR DIFFERENT DEGREES OF BUNCHING SNEAK 3A-2

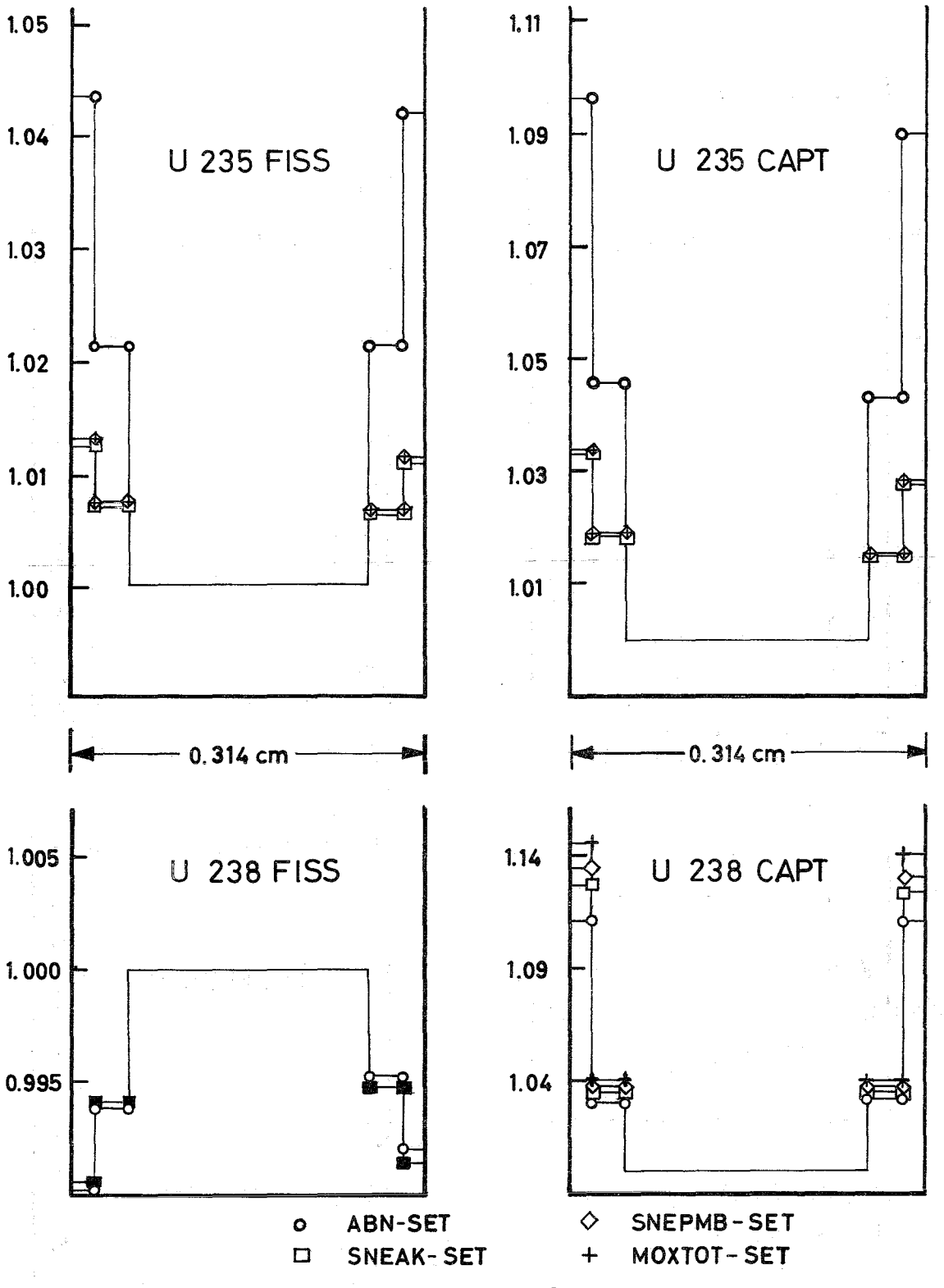

FIG. 5 A RATE DISTRIBUTIONS

FINE STRUCTURE WITHIN THE URANIUM PLATELET OF THE NORMAL UNIT CELL OF CORE ZONE I SNEAK 3A-2

THE RATES ARE NORMALIZED IN THE CENTRAL SUBREGION

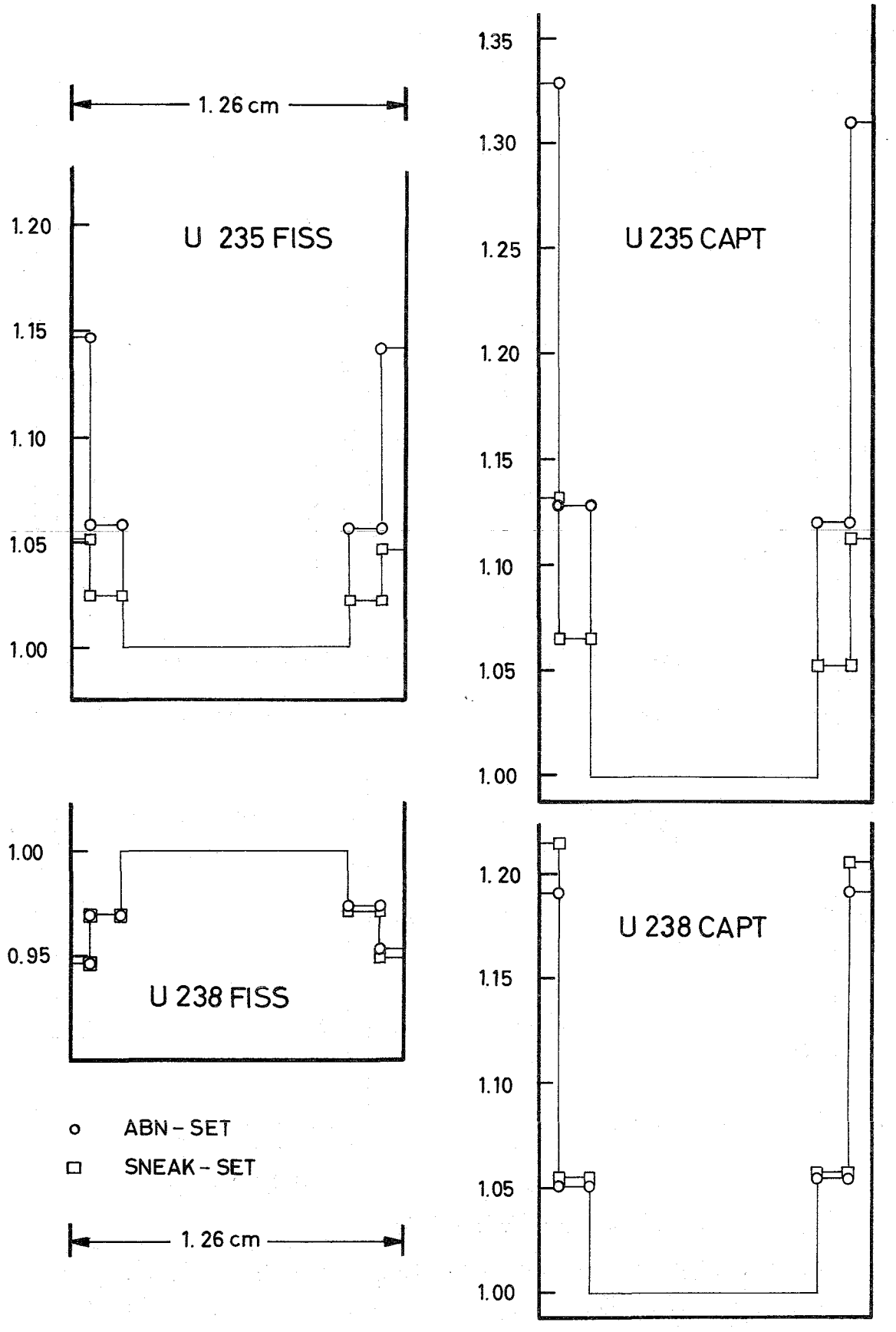

FIG. 5 B RATE DISTRIBUTIONS WITHIN THE URANIUM ZONE OF THE DOUBLE BUNCHED UNIT CELL

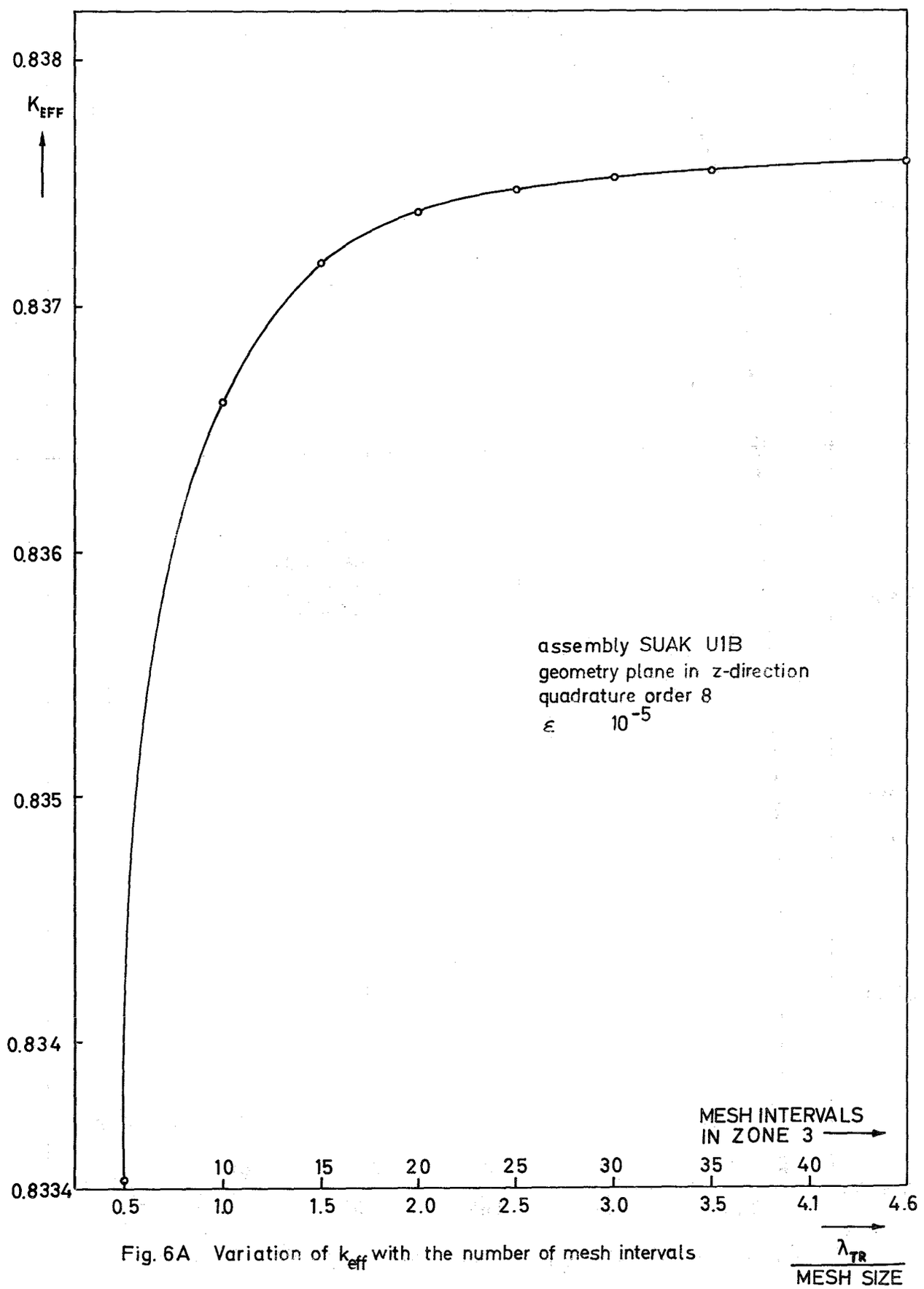

Fig. 6A Variation of k_{eff} with the number of mesh intervals

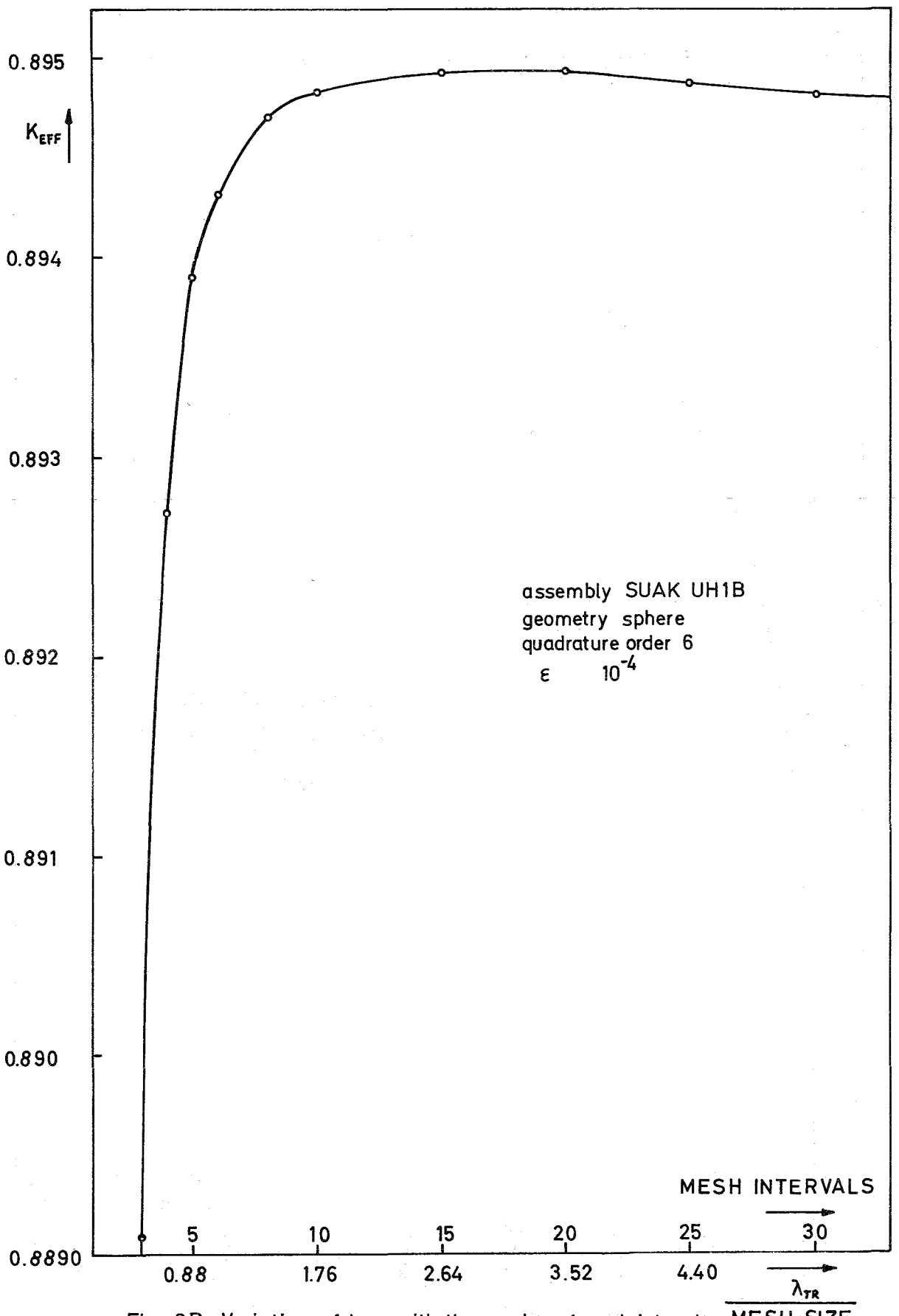

Fig. 6B Variation of k_{eff} with the number of mesh intervals

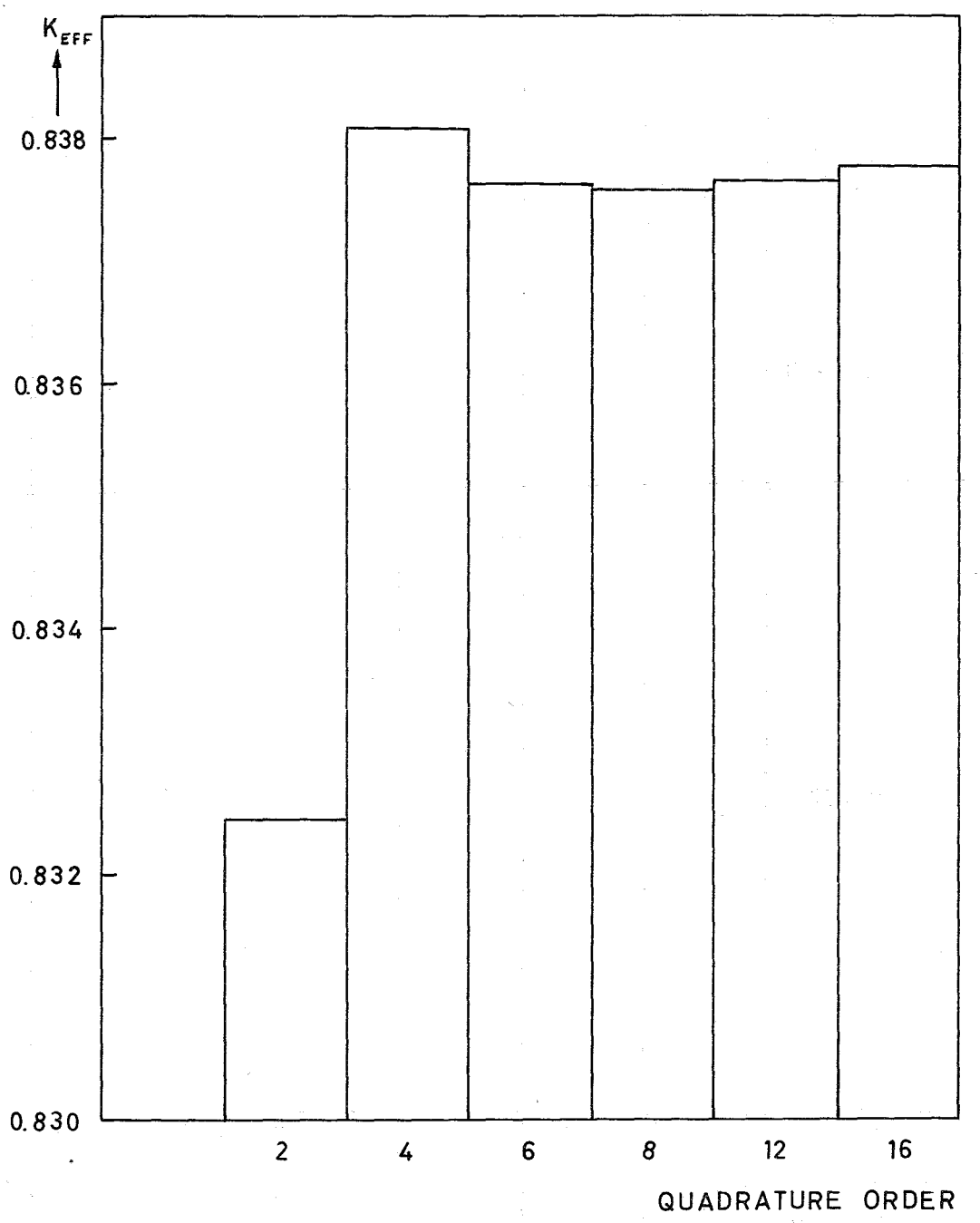

Fig. 7A Variation of k_{eff} with the quadrature order. SUAK U1B, slab geometry. Complete listing of data see table V-13a

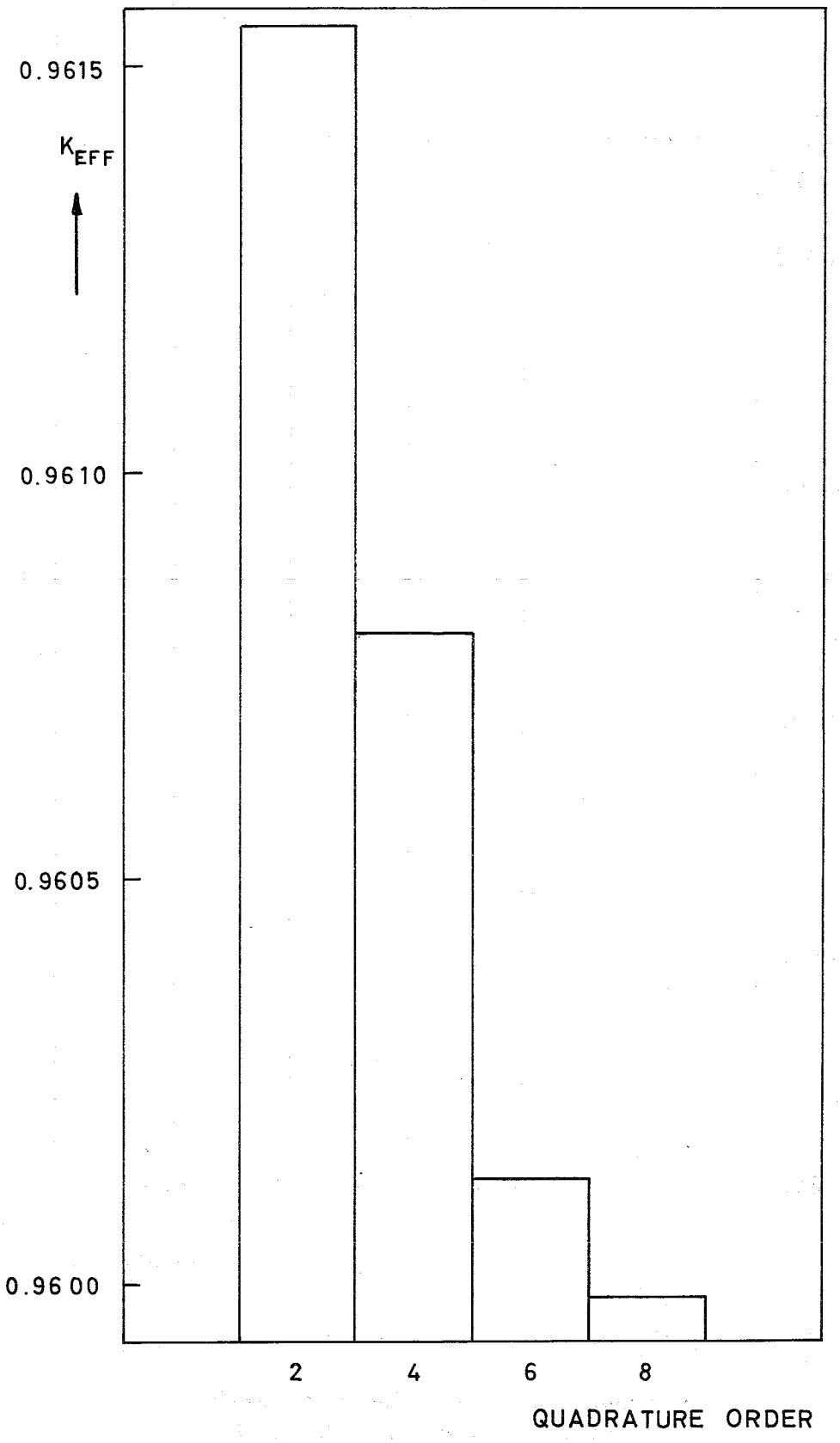

Fig. 7B Variation of k_{eff} with the quadrature order.
Complete listing of data see table V-13 b.
ZPR-III-48, cylindrical geometry.

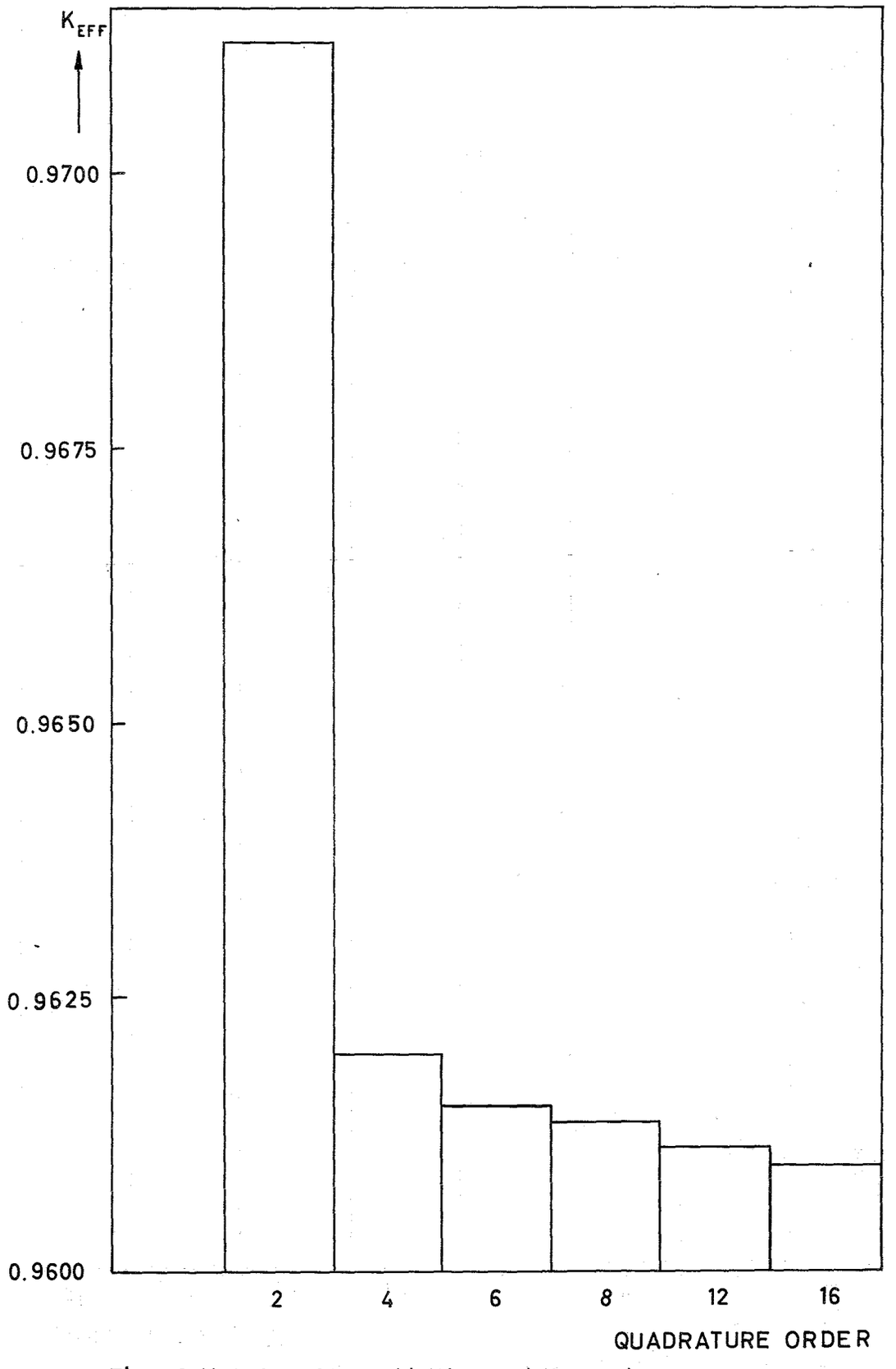

Fig. 7C Variation of k_{eff} with the quadrature order.
Complete listing of data see table V-13c.
ZPR-III-48, spherical geometry.

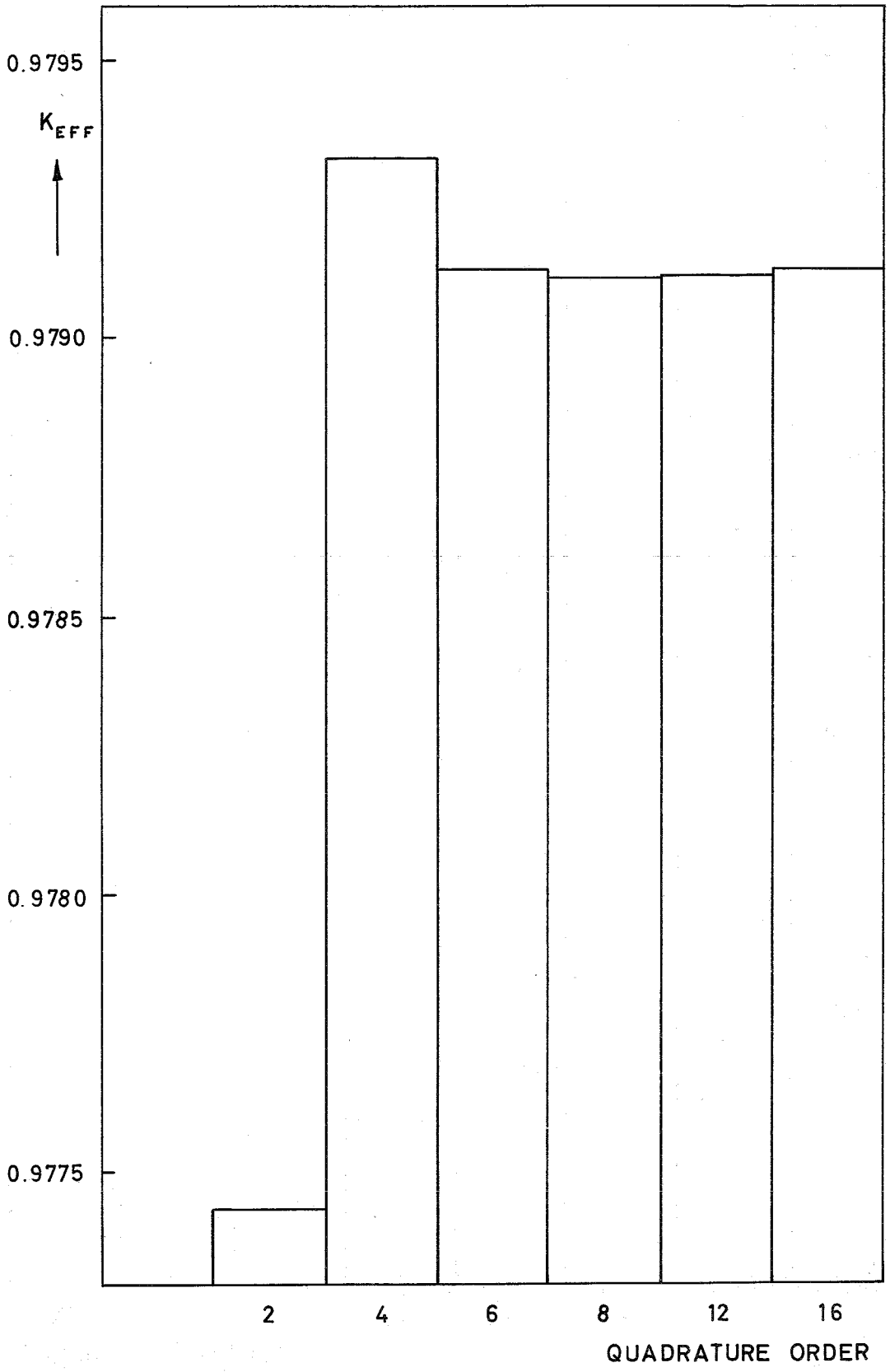

Fig. 7D Variation of k_{eff} with the quadrature order.
Complete listing of data see table V-13d.
ZPR-III-10, slab geometry.

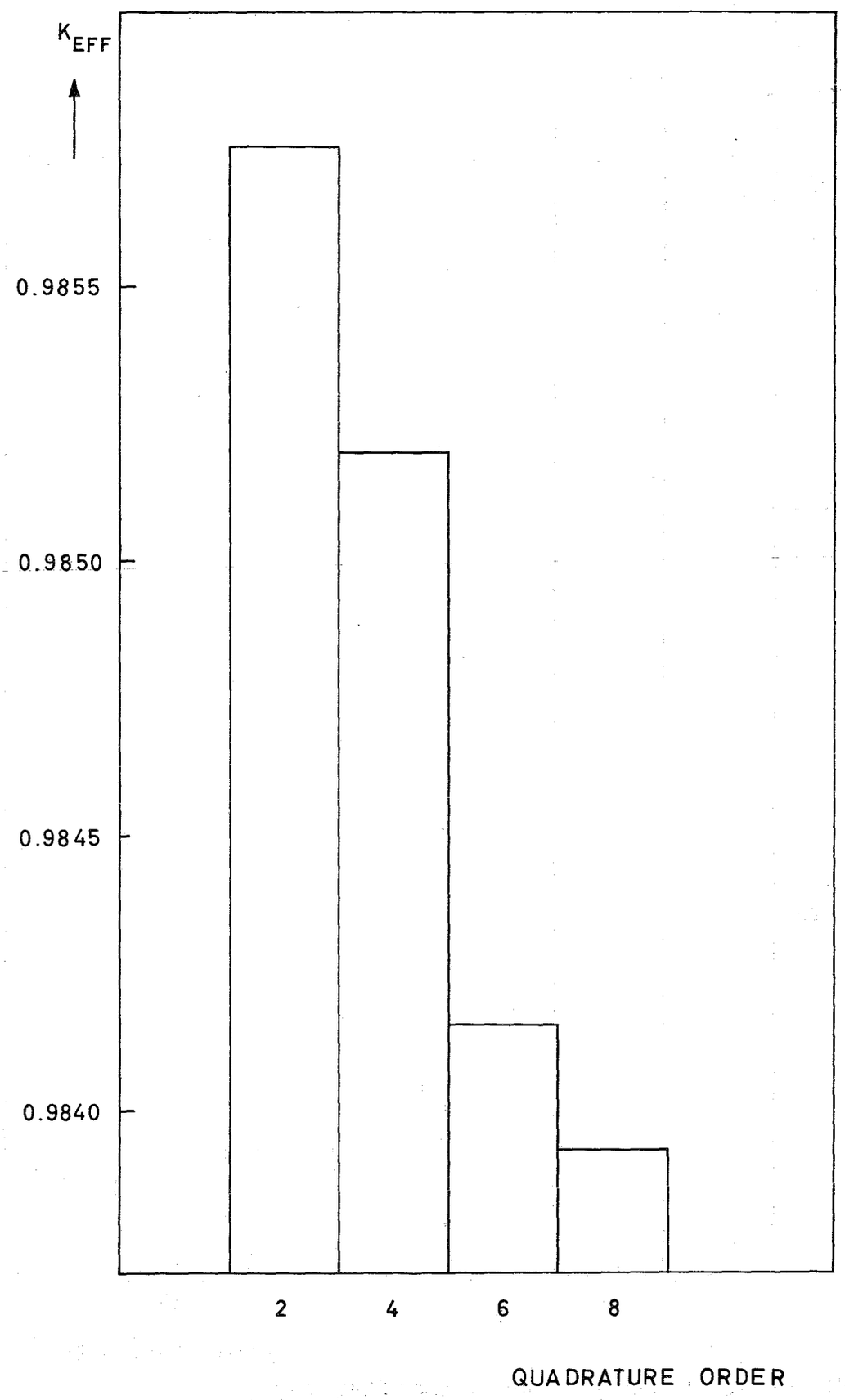

Fig. 7E Variation of k_{eff} with the quadrature order.
Complete listing of data see table V-13e.
ZPR-III-10, cylindrical geometry.

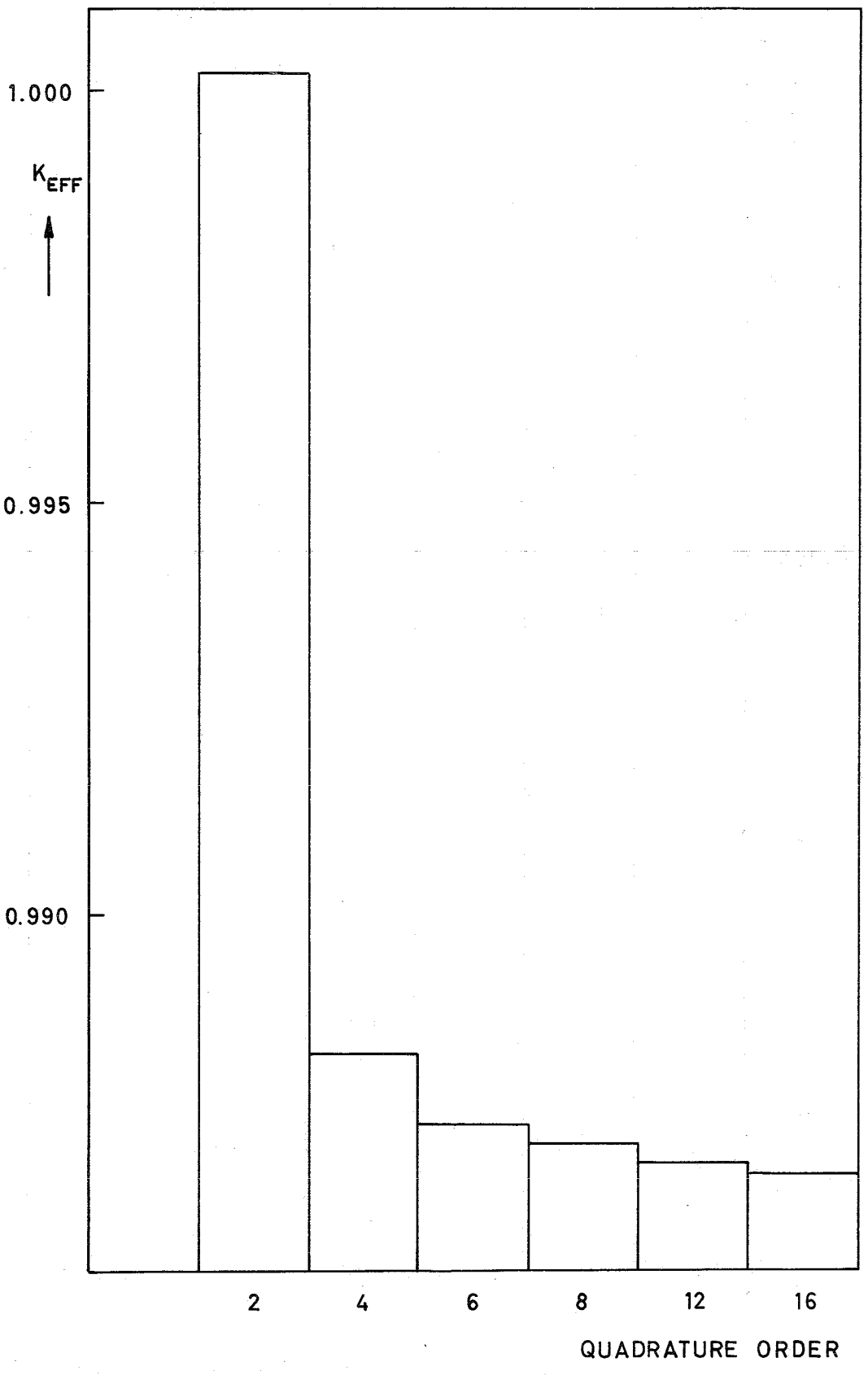

Fig. 7F Variation of k_{eff} with the quadrature order.
Complete listing of data see table V-13f.
ZPR-III-10, spherical geometry.

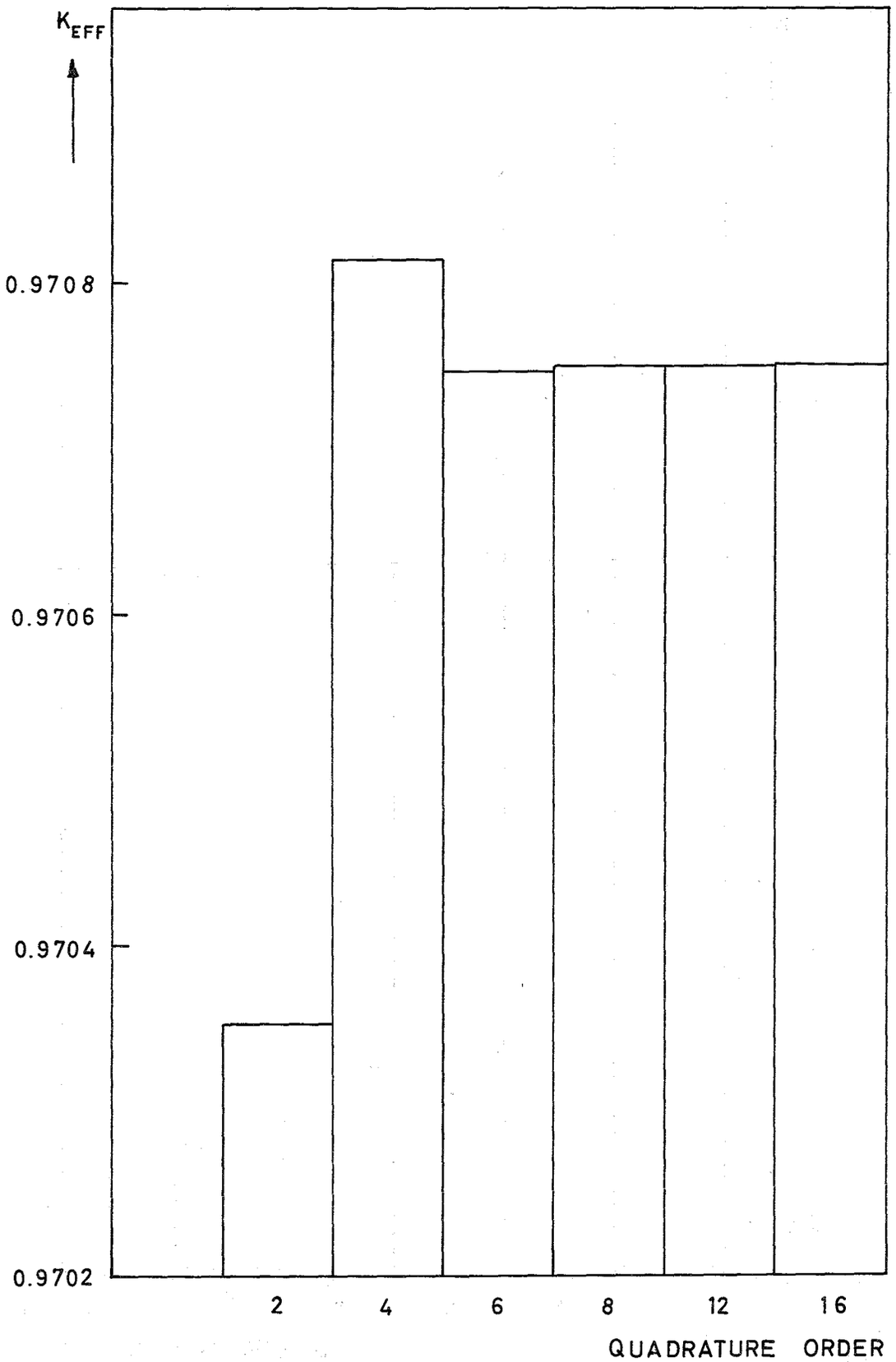

Fig. 7G Variation of k_{eff} with the quadrature order.
Complete listing of data see table V-13g.
ZPR-III-25, slab geometry.

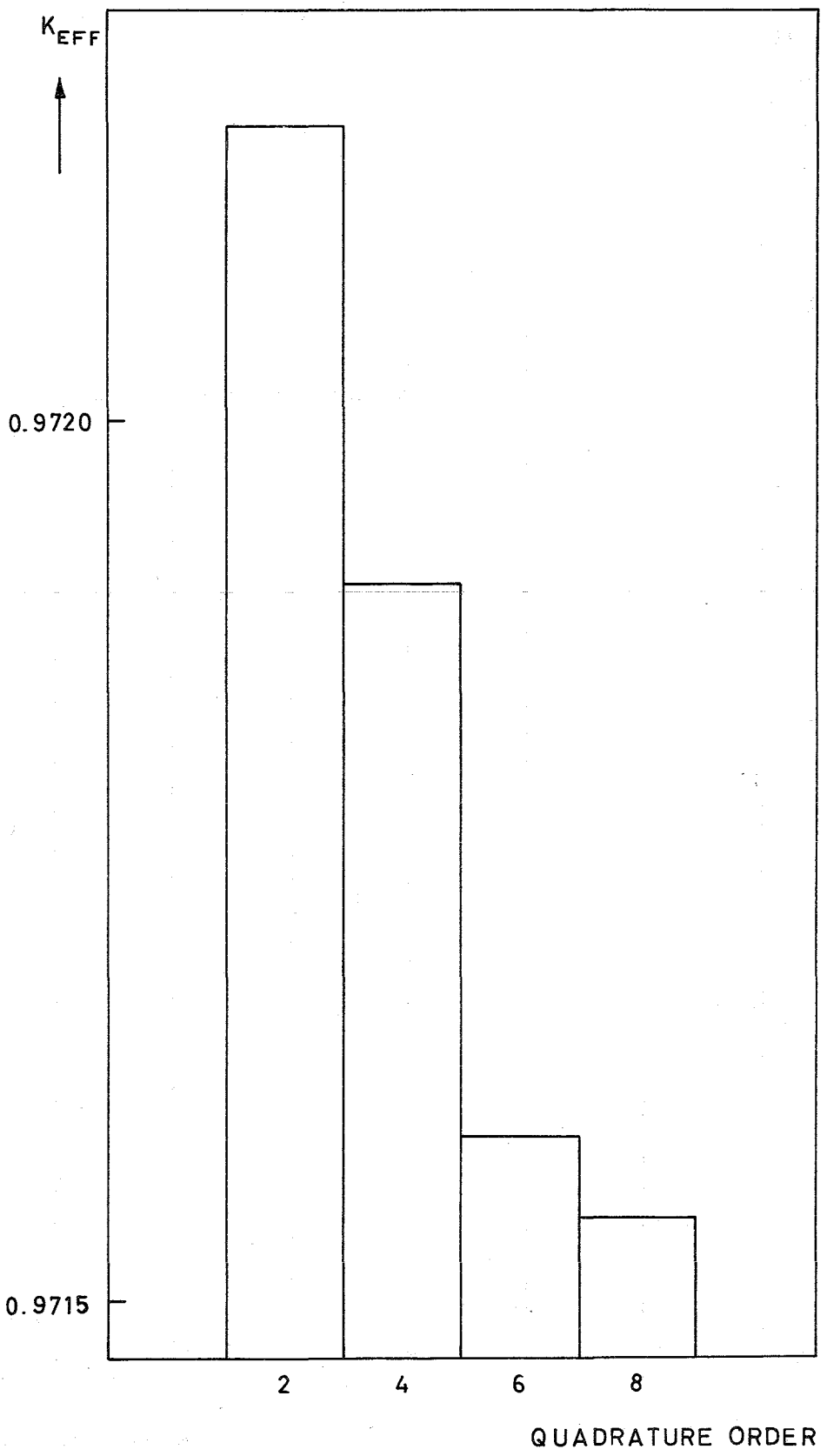

Fig. 7H Variation of k_{eff} with the quadrature order.
Complete listing of data see table V-13h.
ZPR-III-25, cylindrical geometry.

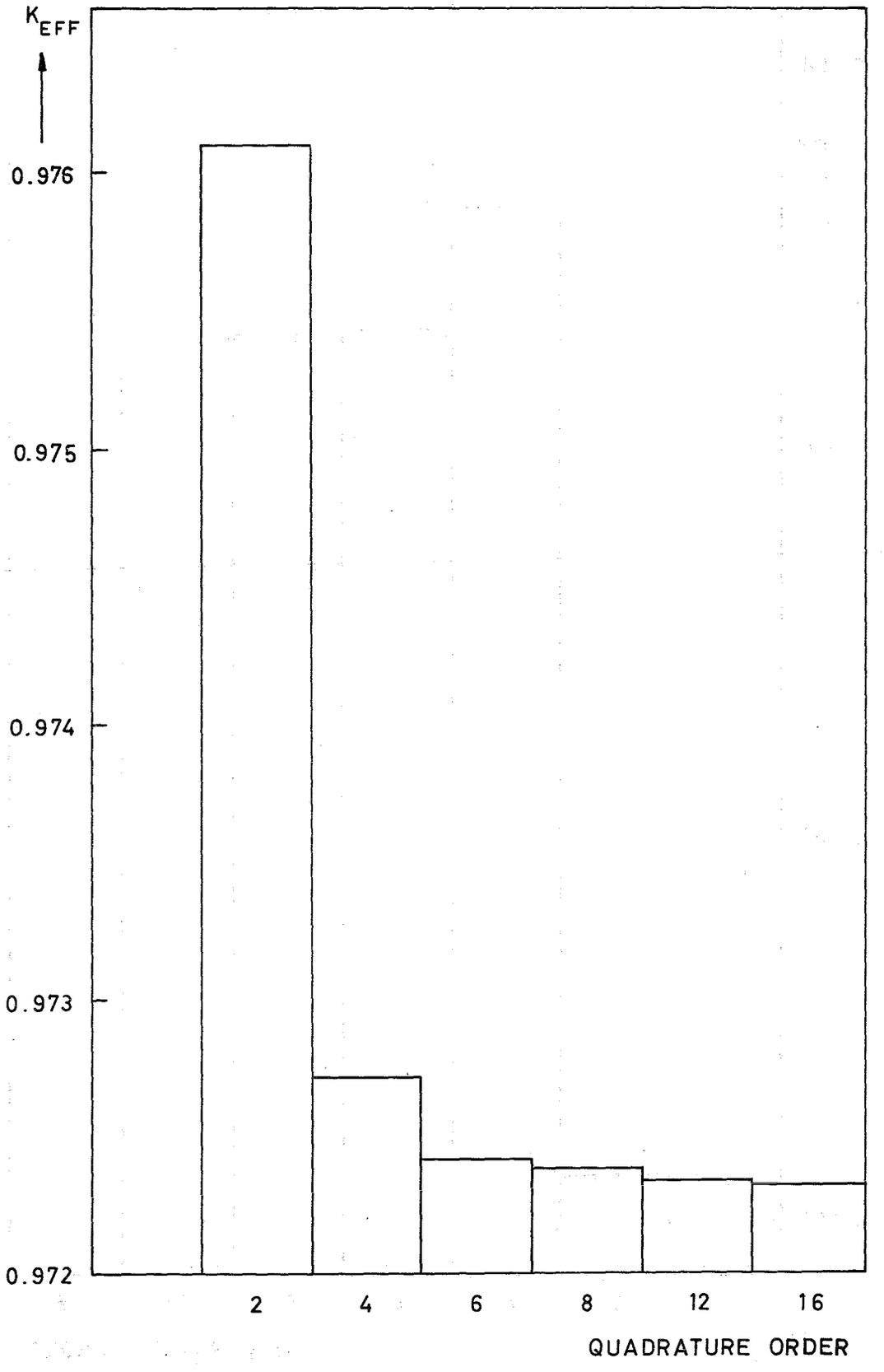

Fig. 71 Variation of k_{eff} with the quadrature order.
Complete listing of data see table V-13i.
ZPR-III-25, spherical geometry.

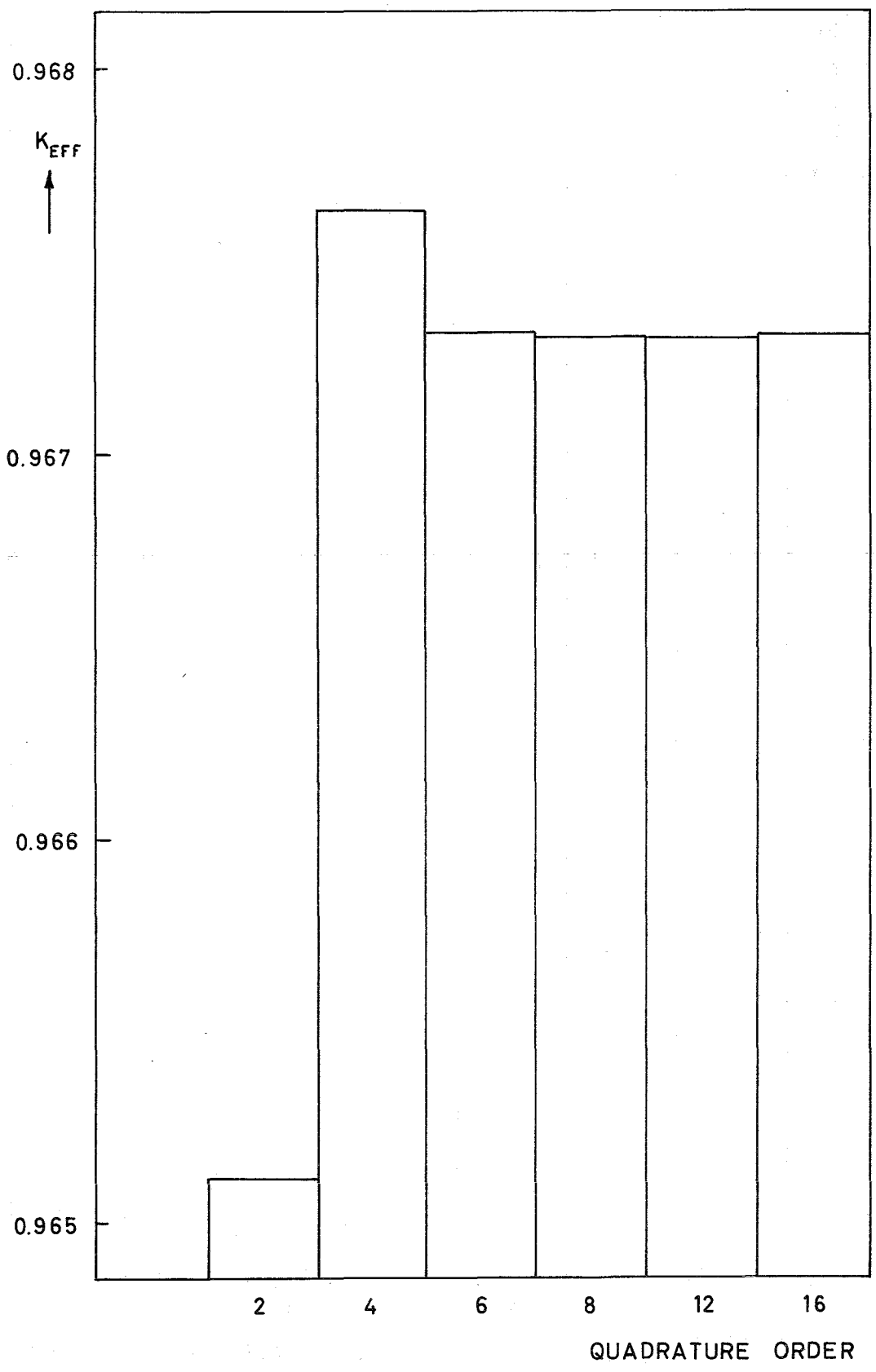

Fig. 7J Variation of k_{eff} with the quadrature order.
Complete listing of data see table V-13 j.
Zebra 6A, slab geometry.

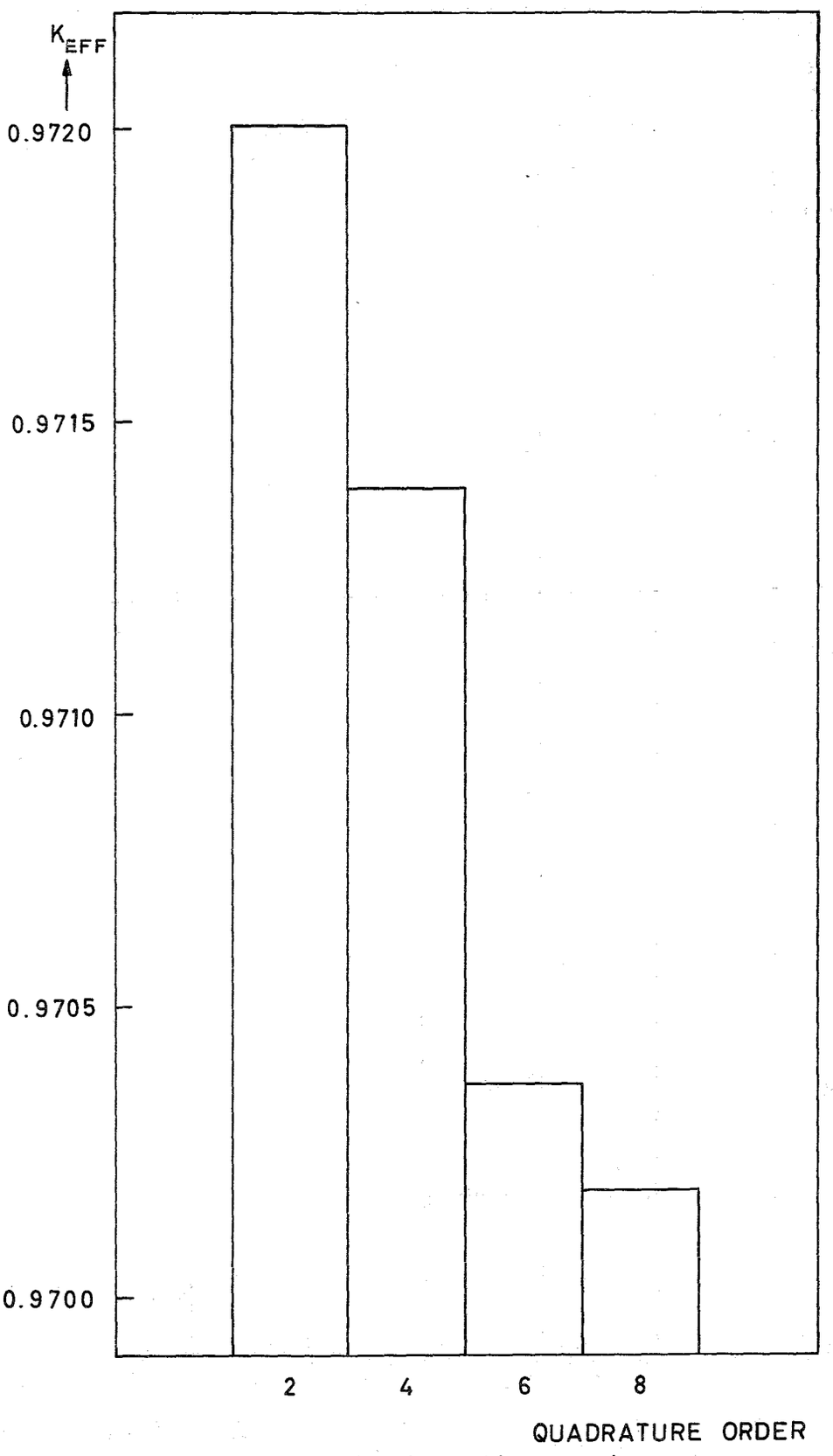

Fig. 7K Variation of k_{eff} with the quadrature order.
Complete listing of data see table V-13 k.
Zebra 6A, cylindrical geometry.

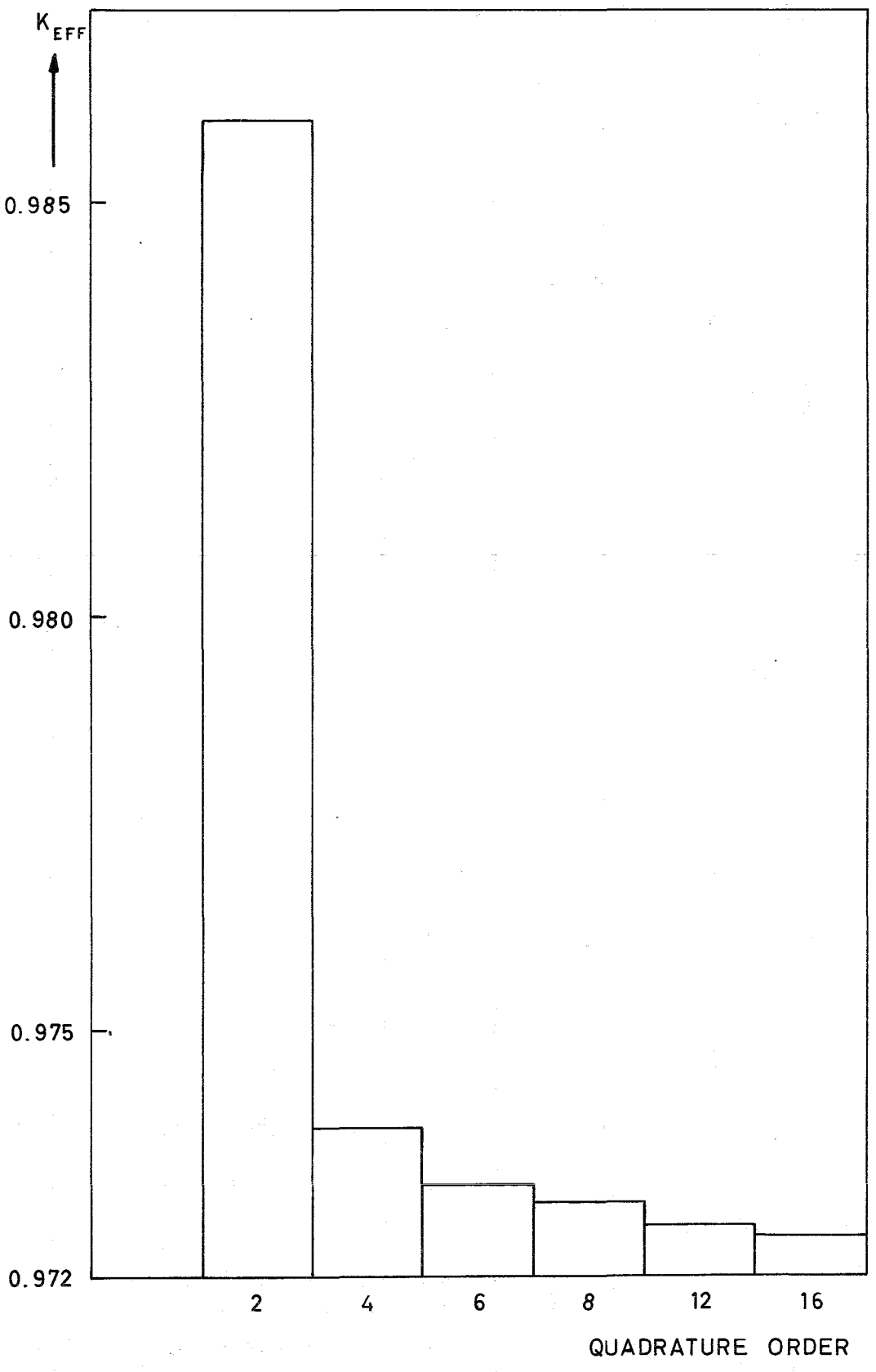

Fig. 7 L Variation of k_{eff} with the quadrature order.
Complete listing of data see table V-13 l.
Zebra 6A, spherical geometry.